

601051

FDL-TDR-64-44 ✓

203 p. 3.5-0

STRUCTURAL DYNAMIC RESPONSE
OF JARCF LOGISTIC V/STOL VEHICLES

TECHNICAL DOCUMENTARY REPORT FDL-TDR-64-44

April 1964



AF Flight Dynamics Laboratory
Research and Technology Division
Air Force Systems Command
Wright-Patterson Air Force Base, Ohio

Project No. 1370 Task No. 137008

(Prepared under Contract No. AF33(657)-8452 by
Sikorsky Aircraft, Division of United Aircraft
Corporation, Stratford, Connecticut; M. J. Rich,
W. D. Jepson, A. C. Buffalano and R. F. Stebbins,
authors)

NOTICES

When Government drawings, specifications, or other data are used for any purpose other than in connection with a definitely related Government procurement operation, the United States Government thereby incurs no responsibility nor any obligation whatsoever; and the fact that the Government may have formulated, furnished, or in any way supplied the said drawings, specifications, or other data, is not to be regarded by implication or otherwise as in any manner licensing the holder or any other person or corporation, or conveying any rights or permission to manufacture, use, or sell any patented invention that may in any way be related thereto.

Qualified requesters may obtain copies of this report from the Defense Documentation Center (DDC), (formerly ASTIA), Cameron Station, Bldg. 5, 5010 Duke Street, Alexandria, Virginia, 22314.

This report has been released to the Office of Technical Services, U.S. Department of Commerce, Washington 25, D. C., for sale to the general public.

Copies of this report should not be returned to the Research and Technology Division, Wright-Patterson Air Force Base, Ohio, unless return is required by security considerations, contractual obligations, or notice on a specific document.

FOREWORD

The research work in this report was performed by Sikorsky Aircraft, Division of United Aircraft Corporation, Stratford, Connecticut, for the Aerospace Dynamics Branch, Vehicle Dynamics Division, AF Flight Dynamics Laboratory, Wright-Patterson Air Force Base, Ohio, under Contract AF 33(657)-8452. This research is part of a continuing effort to provide more rational structural design criteria for the most critical components of large logistic V/STOL aircraft. The investigation is part of the Research and Technology Division, Air Force Systems Command exploratory development program. This work was performed under Project No. 1370 "Dynamic Problems in Flight Vehicles", Task No. 137008, Dynamic Load Design Criteria". Mr. Bernard H. Groomes of the AF Flight Dynamics Laboratory was the Project Engineer. The research was conducted from June 1962 to February 1964 by the Technical Branch of the Engineering Division of Sikorsky Aircraft. Principal Investigator in this study was Mr. M. J. Rich assisted by Messrs. R. F. Stebbins (Structures), W. D. Jepson (Aerodynamics and Configurations Study) and A. C. Buffalano (Dynamics).

ABSTRACT

✓ Preliminary designs are evolved for five large logistic V/STOL configurations. Structural elastic characteristics and mass distributions are calculated. The structural dynamic response is investigated for ground landing, take-off abort, maneuvers, gust penetration and landing conditions. The results of this investigation are tabulated in a matrix showing the degree and relative criticalness for the conditions and the V/STOL configurations. The degree of criticalness is established as the ratio of the peak dynamic loading and/or stress to the values used in the configuration design structural study. The latter structural loads and/or stresses are evolved through the use of existing military specifications or normal design practices. (1) ↖

The most critical structural design condition was found to be the take-off run of the ground handling condition and is analyzed in further detail. The detail analysis consists of analyzing the rigid and elastic body response from a ten inch 1-cosine dip at lift-off speed. Wing bending and torsional loads, nose and main gear loads, and center of gravity accelerations are calculated. Time histories of all loads and accelerations are shown for a dip wave length to landing gear wheel base ratio of 3.0. A parametric study is included for λ/l ratios of 1 to 3.8 to show the effect on the various structural components.

Energy absorbing devices are evolved to reduce the criticalness of towing and to minimize the effects of dips on the aircraft structure.

Conclusions of the contents of this report are reached and recommendations made for further study items.

The report may be used as a guide in the structural dynamic response of large logistic V/STOL aircraft to enable the designer to minimize the structural weight and further increase the efficiency of such type aircraft.

This technical documentary report has been reviewed and is approved.

Walter J. Mykyten
WALTER J. MYKITOW
Asst. for Research & Technology
Vehicle Dynamics Division

TABLE OF CONTENTS

SECTION	PAGE
I. INTRODUCTION	1
II. DESCRIPTION OF V/STOL CONFIGURATIONS	3
A. Fixed Jet	4
B. Tilt Wing	4
C. Extended Flap	5
D. Tilt Prop.	5
E. Buried Fan	5
III. PRELIMINARY STRUCTURAL DYNAMIC RESPONSE INVESTIGATION AND ANALYSIS	37
A. Ground Handling	37
1. Taxiing and Take-Off Run.	37
2. Starting and Stopping While Towing	47
3. Tiedown	54
4. Braking.	57
B. Take-Off Abort (VTOL).	65
C. Maneuvers	69
D. Gust Penetration	75
E. Landing Condition.	82
IV. DETERMINATION OF DEGREE AND RELATIVE CRITICALNESS OF STRUCTURAL RESPONSE	91
V. DETAIL STRUCTURAL RESPONSE ANALYSIS.	94
VI. SPECIAL DESIGN CONSIDERATIONS.	112
A. Towbar Shock Strut	112
B. Shock Absorption for Landing Gear.	116
VII. CONCLUSIONS.	121
VIII. RECOMMENDATIONS FOR FURTHER STUDY.	123
APPENDICES:	
1. Configuration Design Methods and Analysis.	124
2. STOL Performance Methods	148
3. Weight Summary, Panel Point Distribution and Group Weight Statements.	162
4. Normal Mode Method of Analysis	169
REFERENCES.	182

LIST OF ILLUSTRATIONS

FIGURE	PAGE
1. Fixed Jet, Three View	9
2. Tilt Wing, Three View	10
3. Extended Flap, Three View	11
4. Tilt Prop, Three View	12
5. Buried Fan, Three View.	13
6. Wing Section Properties: Fixed Jet	14
7. Wing Section Properties: Tilt Wing	15
8. Wing Section Properties: Extended Flap	16
9. Wing Section Properties: Tilt Prop	17
10. Wing Section Properties: Buried Fan.	18
11. Fuselage Section Properties: Fixed Jet	19
12. Fuselage Section Properties: Tilt Wing	20
13. Fuselage Section Properties: Extended Flap	21
14. Fuselage Section Properties: Tilt Prop	22
15. Fuselage Section Properties: Buried Fan.	23
16. Wing Ultimate Shears, Moments and Torsions: Fixed Jet	24
17. Wing Ultimate Shears, Moments and Torsions: Tilt Wing	25
18. Wing Ultimate Shears, Moments and Torsions: Extended Flap	26
19. Wing Ultimate Shears, Moments and Torsions: Tilt Prop	27
20. Wing Ultimate Shears, Moments and Torsions: Buried Fan.	28
21. Fuselage Ultimate Vertical Shear & Bending Moment Diagram: Fixed Jet.	29
22. Fuselage Ultimate Vertical Shear & Bending Moment Diagram: Tilt Wing.	30
23. Fuselage Ultimate Vertical Shear & Bending Moment Diagram: Extended Flap.	31
24. Fuselage Ultimate Vertical Shear & Bending Moment Diagram: Tilt Prop.	32
25. Fuselage Ultimate Vertical Shear & Bending Moment Diagram: Buried Fan	33
26. Non-Dimensional Spring Rate for V/STOL Main and Nose Gear Oleo	34
27. Non-Dimensional Spring Rate for V/STOL Main and Nose Gear Tire.	35
28. Schematic of Aircraft and Runway Dip Geometry	38
29. Time History of Nose Landing Gear Loads for Preliminary Runway Dip Analysis	43
30. Time History of Main Landing Gear Loads for Preliminary Runway Dip Analysis	44
31. Sinusoidal Towing Input Acceleration	47
32. Schematic of Aircraft Geometry for Towing Condition.	48

FIGURE

PAGE

33. Drag Load Force-Time Gradient	57
34. Schematic of Aircraft Geometry for Braking Condition	58
35. Percent Hovering Power with Forward Speed	67
36. L/W Ratio with Forward Speed After Power Failure.	67
37. H-V Envelope	68
38. Maneuver Acceleration Response.	72
39. Schematic of Maneuver g's.	72
40. Schematic of Vibrating Wing.	73
41. Gust Alleviation Factor vs. Mass Ratio	78
42. Gust Non-Dimensional Rigid Body Load-Time History.	79
43. Gust Acceleration Response.	79
44. Schematic of Landing Gear Loads	87
45. Non-Dimensional Acceleration-Time History for Landing Impact	88
46. Aircraft Model for Detailed Runway Dip Analysis	94
47. Schematic of Nose and Main Landing Gear	95
48. Schematic of Aircraft Deformation	96
49. Schematic of Transformation of Free-Free Modes to Pinned-Pinned Modes.	97
50. Schematic of Aircraft Coordinates for Normal Mode Analysis.	99
51. Tilt Wing Detailed Runway Dip Analysis, Time History of Aircraft Loads, Moments and Accelerations	109
52. Tilt Wing Detailed Runway Dip Analysis, Variation of Loads, Moments and Acceleration vs. Dip Wave- length for Elastic Body Analysis.	111
53. Schematic of Aircraft and Towbar.	112
54. Schematic of Towbar Incorporating Honeycomb Core Safety Device	115
55. Simple Sprung Mass System.	116
56. Spring-Mass System with Load Limiting Device	118
57. Response Factor vs. Time Ratio	120
58. Buried Fan Airfoil Section and Wing Planform	134
59. Fixed Wing Transport Aircraft Parasite Drag Area	139
60. Typical Aerodynamic and Weight Variation of Configuration Solution.	140
61. Variation of Profile Drag with Mach Number.	141
62. Configuration Design Solution for Tilt Wing.	142
63. Configuration Design Solution for Extended Flap.	143
64. Configuration Design Solution for Tilt Prop.	144
65. Configuration Design Solution for Buried Fan	145
66. Airflow Through Propeller Plane	153
67. Wing Local Airflow.	154
68. Mass Flow of Air Affected by Propellers.	154
69. Time Variation of Horizontal and Vertical Accelerations During Transition	157
70. Acceleration Forces vs. Constant Forward Speed.	158
71. Local Wing Angle of Attack.	159
72. Variation of Mass Correction Factor with Thrust Coefficient	161
73. Schematic of Fuselage Panel Points	170

FIGURE	PAGE
74. 1st Three Modes, Symmetrical Fuselage, Coupled Wing Bending-Torsion; Fixed Jet.	174
75. 1st Three Modes, Symmetrical Fuselage, Coupled Wing Bending-Torsion; Tilt Wing.	175
76. 1st Three Modes, Symmetrical Fuselage, Coupled Wing Bending-Torsion; Extended Flap.	176
77. 1st Three Modes, Symmetrical Fuselage, Coupled Wing Bending-Torsion; Tilt Prop.	177
78. 1st Three Modes, Symmetrical Fuselage, Coupled Wing Bending-Torsion; Buried Fan	178
79. Cantilever Fundamental Wing Bending- Torsion Modes.	179

LIST OF TABLES

TABLE	PAGE
1. V/STOL Configuration General Data	36
2. Ground Run Dip Analysis: Maximum Gear Loads.	45
3. Towing Start Analysis: Maximum Landing Gear Loads.	53
4. Tiedown Condition: 60 Knot Wing Root Moments, Torsions and Stresses.	56
5. Braking Condition: Maximum Landing Gear Loads.	64
6. Maneuver Condition: Wing Root Moments, Torsions and Stresses.	74
7. Gust Penetration: Rigid Body Data.	80
8. Gust Penetration: 50 fps Gust Wing Root Moments, Torsions and Stresses.	81
9. Ultimate Design Landing Gear Loads	89
10. Landing Impact: Wing Root Moments, Torsions and Stresses.	90
11. Degree of Criticalness.	93
12. Summary of Critical Pitch Condition.	107
13. Summary of Critical Translation Condition.	107
14. V/STOL Configuration Data	146
15. Panel Point Weights: Fuselage and Contents.	163
16. Panel Point Weights: One-Half Wing and Contents.	164
17. Group Weight Statements.	165
18. Weight Formulae and Assumptions.	166
19. Summary of Vibration Data	181

LIST OF SYMBOLS

A, dip amplitude, in.

AR, wing aspect ratio.

A_p, total propeller disc area, ft²

A₁, major fan diameter, ft.

A₂, minor fan diameter, ft.

a, horizontal distance between nose gear and center of gravity, ft.

a₁, horizontal distance between main gear and center of gravity, ft.

a₂, horizontal distance between main gear and center of gravity for aircraft making a tail down landing, ft.

BHP, engine brake horsepower.

BM, bending moment, in-lbs.

b, wing span, ft.

C, wing chord length, ft.

CG, center of gravity.

CP, center of pressure.

C_D, wing drag coefficient.

C_{DF}, coefficient of aerodynamic cleanness.

C_{DO}, wing profile drag coefficient.

C_F, coefficient of ground friction.

C_L, wing lift coefficient.

C_r, wing root chord, ft.

C_t, wing tip chord, ft.

C₁, nose gear damping coefficient, lb-sec/in.

C₂, main gear damping coefficient, lb-sec/in.

C₃, towbar damping coefficient, lb-sec/in.

DE, dissipative energy per unit time, lb-ft/sec.

DL , disc loading, lbs/ft^2

D_F , fuselage parasite drag, lbs.

D_M , vertical jet engine or lift fan momentum drag, lbs.

D_W , wing drag, lbs.

d , propeller or fan diameter, ft.

E , drop energy absorbed by landing gear, lb-ft.

e_1 , distance from center of fuselage to edge of major fan, ft.

e_2 , distance between edges of major and minor fans, ft.

e' , horizontal distance between center of gravity and center of pressure for aircraft making a tail down landing, ft.

FL , total fuel load, lbs.

F_D , prescribed shear pin force, lbs.

F_H , horizontal forces, lbs.

F_M , vertical load on both main gears, lbs.

\bar{F}_M , average vertical load on both main gears, lbs.

F_{MD} , drag load on both main gears, lbs.

$F_{V \text{ DYN}}$, dynamic vertical load on both main gears, lbs.

$F_{MD \text{ DYN}}$, dynamic drag load on both main gears, lbs.

F_{MS} , vertical static load on both main gears at some forward velocity, lbs.

F_{\angle} , axial compressive load in both main gears for tail down landing, lbs.

$F_{\angle D}$, drag load normal to strut on both main gears for tail down landing, lbs.

F_N , vertical load on nose gear, lbs.

\bar{F}_N , average vertical load on nose gear, lbs.

F_{ND} , drag load on nose gear, lbs.

$F_{N \text{ DYN}}$, dynamic vertical load on nose gear, lbs.

$F_{ND \text{ DYN}}$, dynamic drag load on nose gear, lbs.

F_{NS} , vertical static load on nose gear at some forward velocity, lbs.

F_S , spring force, lbs.

F_V , vertical forces, lbs.

f , equivalent parasite drag area, ft^2

g , acceleration of gravity, ft/sec^2

H , height lost for a resultant contact velocity, ft.

HP, horsepower.

h , vertical distance from center of gravity to center of pressure located along wing chord, ft.

h_F , vertical translation coordinate of fuselage panel points with respect to ground.

h_W , vertical translation coordinate of wing panel points with respect to ground.

$\bar{h}_f(x, y, t)$, fuselage displacement in free-free mode, a function of x , y , and t .

$\bar{h}_w(x, y, t)$, wing displacement in free-free mode, a function of x , y , and t .

h_{TIP} , vertical motion at wing tip.

I , pitching mass moment of inertia about the nose gear, slug-ft^2 .

I_F , fuselage pitching inertia matrix.

I_O , pitching mass moment of inertia about the center of gravity, slug-ft^2 .

I_W , wing pitching inertia matrix.

I_x , moment of inertia, in^4

I_y , moment of inertia, in^4

I_z , moment of inertia, in^4

i_p , thrust incidence angle with respect to the wing chord zero lift line, degrees or radians.

i_w , wing incidence angle with respect to the fuselage reference line, degrees or radians.

J , moment of inertia or torsional rigidity, in^4

W_p , propulsion system weight, lbs.

w_s , wing loading, lbs/ft²

\bar{w}_s , average wing loading, lbs/ft²

w_{fu} , fuselage width, ft.

X , maximum longitudinal input acceleration of towing vehicle, g's.

x , horizontal distance, ft.

x_a , ratio of flap width to chord.

x_i , location of coordinate along x axis.

x_f , flap width, ft.

x_{MO} , main gear static oleo deflection, in.

x_{MT} , main gear static tire deflection, in.

x_{NO} , nose gear static oleo deflection, in.

x_{NT} , nose gear static tire deflection, in.

x_o , horizontal motion of the center of gravity, ft.

x_p , horizontal motion of the arbitrary point P, ft.

x_{root} , coordinate of wing elastic axis.

x_1 , absolute horizontal motion of the nose gear, ft.

\bar{x}_1 , relative horizontal motion between nose gear tire and oleo, ft.

\bar{x}_2 , relative horizontal motion between main gear tire and oleo, ft.

y_i , location of coordinate along y axis.

y_{root} , coordinate of wing root section.

Z , vertical distance, ft.

Z_b , bending section modulus, in³

Z_p , absolute vertical motion of the arbitrary point P, ft.

Z_t , torsion section modulus, in³

M , aircraft mass, slugs.
 M_F , fuselage mass matrix.
 M_M , unsprung mass of both main gears, slugs.
 M_{MO} , mass above main gear oleo, slugs.
 M_{MT} , main gear tire mass, slugs.
 M_N , unsprung mass of nose gear, slugs.
 M_{NO} , mass above nose gear oleo, slugs.
 M_{NT} , nose gear tire mass, slugs.
 M_P , incremental mass at point P, slugs.
 M_W , wing mass matrix.
 M_{ab} , mass tensor.
 M_C , airfoil section critical Mach number.
 M_{cr} , cruise Mach number.
 $M_1, 2, 3, \dots, n$, lumped masses assigned to fuselage stations, slugs.
 N_0 , input factor of acceleration in towing condition.
 N_X , desired limitation on input to aircraft for towing condition.
 N_Z , vertical load factor, g's.
 n , number of props or fans.
 P , arbitrary point on fuselage.
 PE , potential energy, lb-ft.
 PL , payload lbs.
 q , slipstream dynamic pressure, lbs/ft.²
 q (L/D) max., free stream dynamic pressure at the speed for maximum lift to drag ratio, lbs/ft.²
 q_i , fuselage ignorable coordinate.
 q_0 , absolute vertical motion of center of gravity, ft.
 q_∞ , free stream dynamic pressure, lbs/ft.²
 \dot{q}_b , maximum incremental body g's.

\ddot{q}_w , maximum wing acceleration, g's.

q^a , coordinate tensor including translatory and rotory displacements.

q^i , modal shape of the i^{th} coordinate tensor.

$q_1, 2, 3, \dots, n$, absolute fuselage coordinates.

$\bar{q}_1, 2, 3, \dots, n$, relative fuselage coordinates.

q_1 , absolute vertical motion of the nose gear oleo and tire, ft.

q_2 , absolute vertical motion of the main gear oleo and tire, ft.

q_3 , absolute horizontal motion of the nose gear oleo, ft.

R , aircraft range, miles.

RATO, Rocket Assist Take-Off, 115,700 lbs for 4.68 sec., rise time of 0.5 sec.

R_f , structural response factor.

S , wing area, ft^2 .

S_b , bending stress, lbs/in^2 .

S_s , shear stress, lbs/in^2 .

S_u , moment unbalance about nose gear, slug-ft.

s , number of semi-chords.

sfc, specific fuel consumption lbs/BHP/hr .

T , thrust, lbs.

T_M , torsional moment, in-lbs.

T_c , thrust coefficient based on slipstream velocity = $1 - (q_\infty/q)$.

T_{HP} , thrust horsepower.

T_j , vectored jet thrust, lbs.

T_{j0} , static vectored jet thrust, lbs.

T_N , natural period, sec.

T_o , static prop. thrust, lbs.

T_{sfc} , thrust specific fuel consumption, lbs/lb/hr .

T_v , vertical jet thrust, lbs.

t , time, sec.

t_0 , time for ground run, sec.

t_p , critical pulse time, sec.

t_1 , time at the end of transition, controls are positioned for climb-out, sec.

t_{01} , transition interval, sec.

t_{12} , climb-out interval, sec.

t_2 , time at the instant the aircraft reaches the 50 ft. obstacle, sec.

t_3 , time to reach peak gust acceleration, sec.

t_4 , time duration of wheel penetration in runway dip, sec.

U , gust velocity, ft/sec.

UL , useful load, lbs.

V , aircraft forward velocity, ft/sec. or knots.

V_c , horizontal climb velocity, ft/sec.

V_{LO} , aircraft lift-off velocity, ft/sec. or knots.

V_0 , horizontal initial velocity for any part of the flight path, ft/sec.

V_z , aircraft sinking velocity, ft/sec.

v , induced velocity in the propeller plane, ft/sec.

v_e , exit downwash velocity (jet engines), ft/sec.

\dot{v}_t , fully developed induced velocity = $2v$, ft/sec.

W , aircraft design gross weight, take-off weight, lbs.

\bar{W} , average gross weight, lbs.

W_{cr} , crew weight, lbs.

W_E , weight empty, lbs.

W_{fc} , cruise fuel weight, lbs.

W_i , weight at i^{th} coordinate, lbs.

W_0 , maximum or overload STOL weight, lbs.

W_p , propulsion system weight, lbs.

w_s , wing loading, lbs/ft²

\bar{w}_s , average wing loading, lbs/ft²

w_{fu} , fuselage width, ft.

X , maximum longitudinal input acceleration of towing vehicle, g's.

x , horizontal distance, ft.

x_a , ratio of flap width to chord.

x_i , location of coordinate along x axis.

x_f , flap width, ft.

x_{MO} , main gear static oleo deflection, in.

x_{MT} , main gear static tire deflection, in.

x_{NO} , nose gear static oleo deflection, in.

x_{NT} , nose gear static tire deflection, in.

x_o , horizontal motion of the center of gravity, ft.

x_p , horizontal motion of the arbitrary point P, ft.

x_{root} , coordinate of wing elastic axis.

x_1 , absolute horizontal motion of the nose gear, ft.

\bar{x}_1 , relative horizontal motion between nose gear tire and oleo, ft.

\bar{x}_2 , relative horizontal motion between main gear tire and oleo, ft.

y_i , location of coordinate along y axis.

y_{root} , coordinate of wing root section.

Z , vertical distance, ft.

Z_b , bending section modulus, in³

Z_p , absolute vertical motion of the arbitrary point P, ft.

Z_t , torsion section modulus, in³

- \bar{z}_1 , relative vertical motion across nose gear oleo, ft.
 \bar{z}_2 , relative vertical motion across main gear oleo, ft.
 \bar{z}_3 , relative vertical motion of nose gear tire with respect to ground, ft.
 \bar{z}_4 , relative vertical motion of main gear tire with respect to ground, ft.
 \ddot{z} , aircraft vertical acceleration, ft/sec².
 z_M , vertical distance main gear penetrates dip, ft.
 z_N , vertical distance nose gear penetrates dip, ft.
 \ddot{z}_{MG} , vertical acceleration at the main gear, ft/sec².
 \ddot{z}_0 , vertical acceleration of center of gravity, ft/sec².
 $\Delta \dot{z}_{ss}$, change in vertical steady state acceleration, ft/sec².
 α_F , fuselage pitching coordinates with respect to ground.
 $\bar{\alpha}_F(x, y, t)$ fuselage relative pitching, free-free mode, a function of x , y , and t .
 α_f , fuselage angle of attack with respect to the horizontal, degrees.
 α_{f0} , fuselage angle of attack during the ground run phase, degrees.
 α_{f1} , fuselage angle of attack at the end of transition, degrees.
 α_s , angle between resultant slipstream velocity and horizontal, degrees.
 α_W , wing pitching coordinate with respect to ground.
 $\bar{\alpha}_W(x, y, t)$ wing relative pitching, free-free mode, a function of x , y , and t .
 α_w , wing angle of attack, degrees.
 β , airfoil lift slope, radians.
 γ , climb path angle, degrees.
 γ_1 , fan area ratio = A_2/A_1 .
 δ , tow bar useful stroke, ft.
 δ_F , flap deflection, degrees.
 δ_{LG} , average landing gear deflection, ft.

- δ_M , main gear stroke ft.
 δ_N , nose gear stroke, ft.
 δ_w , wing unbalance matrix.
 ϵ , ratio of fan turbine blade length to fan diameter.
 ξ_i , normal mode coordinate of the i^{th} mode.
 η , propulsive efficiency including transmission losses, cruise.
 η_M , main gear efficiency.
 η_N , nose gear efficiency.
 η_o , static propulsive efficiency including transmission losses.
 η_w , wing efficiency factor = .95 to .98 (does not include variations of f with angle of attack).
 θ , angle between the thrust vector and the horizontal, degrees.
 θ_i , fuselage ignorable coordinate.
 θ_o , thrust tilt angle during ground run, degrees.
 θ_y , pitching motion at the center of gravity, degrees.
 θ_1 , thrust tilt angle at the end of transition, degrees.
 Λ , $\frac{1}{4}$ chord sweepback angle, degrees.
 λ , runway dip wavelength, ft.
 λ_1 , wing taper ratio = c_t/c_r .
 λ_M , non-dimensional mass parameter.
 μ , transformation matrix.
 ρ , air density, slugs/ft.³
 ρ_1 , sign of $\dot{x}_1 = |\dot{x}_1|/\dot{x}_1$.
 ρ_2 , sign of $\dot{x}_2 = |\dot{x}_2|/\dot{x}_2$.
 τ , ratio of instantaneous to steady state braking force.
 τ_1 , exponent of equivalent parasite drag function.
 ϕ , angle of inclination of aircraft in tail down landing, degrees.
 ϕ_{Fi} , normalized fuselage bending shape.

ϕ_{w1} , normalized wing bending shape.

$\Phi = C_{fg}$, ft/sec.²

ω , frequency, rad/sec.

ω_n , natural frequency, rad/sec.

Matrix Notation

$\begin{bmatrix} \quad \end{bmatrix}$ matrix array.

$\left\{ \begin{array}{c} \quad \end{array} \right\}$ column matrix.

$\{ \quad \}$ row matrix.

$\begin{bmatrix} \quad \end{bmatrix}'$ prime indicates transpose of a matrix.

I. INTRODUCTION

The purpose of this study is to investigate and determine analytically the critical structural dynamic response conditions and governing parameters for one class of V/STOL aircraft. This information will aid the V/STOL aircraft designer in optimizing the structural configuration and structural weight resulting in a reduced take-off gross weight and power required or an increase in payload.

The particular class of V/STOL aircraft selected was a large logistic transport type capable of carrying 20,000 lbs. of cargo and having a 1800 nautical mile range.

Five configuration types, as described in Section II, were selected so as to provide an examination of the relative structural dynamic response problems involved in the large logistic transport class of V/STOL aircraft.

The initial part of this study is to determine the structural arrangement of the five configuration types through preliminary design procedures. This involves an aerodynamic and weight analysis to resolve the size and performance of the aircraft. The scope of this study permits only a limited type of iterative process in determining the configuration design and is only of sufficient scope to allow a relative structural study. While the results of such a preliminary design do show relative gross weights and performance, it must be emphasized that the purpose of this study is limited to dynamic structural response and is not of sufficient scope for use in overall design evaluation. For the purposes of this study the configuration types are simplified and altered from a basic configuration, only where necessary, to represent each of the particular types in this class of aircraft.

From the preliminary design analysis, which establishes the configuration structural arrangement, the structural and elastic properties of the fuselage and wing are evolved using "static" flight and ground loading conditions. Thus, the basic structural and weight data become available for use in the required structural response studies.

In a parallel effort a review of methods of analysis and the applicability to the particular types of V/STOL aircraft is made. It was decided that for the initial investigation existing methods are of sufficient scope to analyze for structural response and the results of such analyses would point out areas for further consideration and detailed analysis. However, while techniques exist, there is the requirement of assembling the various portions into programs that apply to the specific types of structures used in this study.

The next portion of the study was to review the types of configurations and select the conditions and the aircraft mode (VTOL or STOL) to be investigated. The conditions investigated were selected by anticipating the problems that would be encountered.

In general, discrete types of loadings were selected in order to arrive at the maximum structural response. The particular conditions are (1) Ground Handling, (2) Take-Off Abort, (3) Flight Maneuver, (4) Gust Penetration, and (5) Landing.

The resulting investigation yields a matrix of analyses consisting of eight conditions and five types of V/STOL configurations. The results of the load analyses are the maximum gear loads, maximum wing root loadings, and the ability to land after an aborted take-off. For some of the conditions, such as the take-off abort and the landing condition, the results are relative capabilities or comparisons with other load conditions.

The matrix of analyses that results in comparative loads or capabilities is resolved into a form for direct evaluation in terms of degree of criticalness. The degree of criticalness is established by the ratio of the dynamic and steady state loading or stress to the normal ultimate flight or ground loads used in the preliminary structural design of the aircraft. The degree of criticalness can be relatively assessed by the numerical values for the type of loadings.

The most critical or most pertinent problems were chosen for detail investigation as a result of the matrix of analyses. While many critical results are found, the scope of this study did not permit going further into detail analysis for all critical conditions. The results found from the matrix of analyses shows that the most critical condition is starting and stopping while towing. However, since towing conditions are controllable, in that the initial input acceleration by the vehicle can be limited or a safety device can be incorporated in the towbar (see Section VI, Special Design Considerations), thus, this condition can be eliminated from the critical list.

The next most critical condition, taxiing and take-off run, cannot be legislated out due to the requirements of rough field landing of which the dip analysis represents a first approximation. The structural response will be more critical for the runway dip condition since the wing structures have elastic body frequencies which are very close to their rigid body frequencies. It is, therefore, concluded that the taxi and take-off run condition is the most critical. A detail dip analysis is necessary to ascertain more accurately the loadings and the effects of these loadings on the structure.

From the matrix of analyses for the investigations and the subsequent detail analysis, special design considerations were produced. These involved the use of augmenting or changing the landing gear system to reduce the effects of structural dynamic response and/or to minimize the problem involved in order to provide landing safety.

The recommendations that result from this study are considered necessary to minimize the anticipated problems that were investigated for this class and type of aircraft. However, some of the items may well be associated with other classes and types having similar problems.

II. DESCRIPTION OF V/STOL CONFIGURATIONS

Given below is a discussion of the general features or physical arrangements which are common to all five V/STOL configurations.

The V/STOL aircraft are multi-engine long range transports, having tricycle type landing gears, capable of carrying a 20,000 lb. payload 1800 nautical miles. The fuselages are fabricated from aluminum alloys using semi-monocoque construction and are typical of other transport aircraft in this payload and range classification. The bending and torsional rigidity of the fuselages vary since the gross weights vary, and it was on this basis that rigidity data was calculated and plotted (Ref. Table 1 and Figs. 11, 12, 13, 14, 15). However, the structural arrangements remain essentially unchanged. The fuselage bending and torsional rigidities are obtained by comparing the unit fuselage shears and bending moments of the specific V/STOL with that of the typical aircraft or reference aircraft mentioned previously. In equation form:

$$\text{Bending Stiffness V/STOL} = \text{Bending Stiffness Reference Aircraft times} \\ \frac{(\text{B.M. V/STOL})}{(\text{B.M. Reference Aircraft})}$$

and

$$\text{Torsional Stiffness V/STOL} = \text{Torsional Stiffness Reference Aircraft times} \\ \frac{(\text{Vertical Shear V/STOL})}{(\text{Vertical Shear Reference Aircraft})}$$

Calculations of fuselage mass distribution were determined by assuming 10 panel points along the fuselage length (Ref. Appendix III Table 15). The load distribution of the V/STOL configurations are proportional to that of the reference aircraft and the differences between the mass distribution curves are a result of the differences in the weights of the fuselage and contents.

The tricycle landing gear, designed by a 2g limit load factor, consists of a two-wheel nose gear and tandem main gears which retract into the fuselage. A retractable ramp in the rear of the fuselage provides the means for loading and unloading cargo. Each fuselage is approximately 100 ft. in length and 13.5 ft. in diameter in the cabin or cargo compartment and each configuration contains a fan in the tail section for pitch control for the VTOL mode.

The wings consist of two-spar aluminum alloy construction (the Buried Fan is three-spar) with the spars continuous through the fuselage. The wing structure is designed by a 3g limit load factor produced by a maneuver condition. Bending moments are reacted by the spar caps and stringers while shear loads are resisted in the spar webs and ultimately balanced at the wing-fuselage intersection. Torsional loads are reacted in the skins and webs of the torque cell between spars. From these shear loads and bending moments produced by this maneuver condition wing spars and skins gages were found and this in turn determined the bending and

torsional rigidity of the wing structure (Ref. Figs. 6, 7, 8, 9, 10).

The STOL performance requirement is defined as the ability to clear a 50 ft. obstacle using a 1000 ft. runway at a gross weight greater than the VTOL weight. This take-off distance will vary depending on the configuration and it was subsequently found that the Buried Fan with RATO (Rocket Assist Take-Off) could not meet the 1000 ft. runway STOL specification. In the case of the Tilt Prop and Fixed Jet the use of RATO (Ref. Table 14) is necessary in order to utilize the maximum take-off weight and meet STOL requirements.

The following paragraphs are a brief discussion describing characteristics which are peculiar to each configuration (Ref. Table 14).

A. Fixed Jet

The Fixed Jet has a cruising speed of 400 knots at an altitude of 38,000 ft. and is powered by ten direct lift jets and four vectorable thrust turbofan engines. The design gross weight is 172,000 lbs. in the VTOL mode which includes 52,520 lbs. of fuel, stored in wing tanks between spars both inboard and outboard of the lift pods. The STOL take-off weight is 232,000 lbs.

The wing has 32° of sweep at $\frac{1}{4}$ chord, an area of 1650 ft.², an aspect ratio of 8.0 and a wing span of 115 ft. The root section has a thickness ratio of 18% while outboard of the lift pods a 15% section is used and allowed to taper to 10% at the tip. High lift devices include 20% chord double-slotted flaps and leading edge slats. Because of sweep-back a bending moment distribution of 60-40 is assumed to act on the rear and forward spars respectively near the wing root.

Ten direct lift jets and four vectorable thrust turbofan engines with an installed thrust of 221,000 lbs. provide lift in the VTOL mode. The lift jets are housed, five per side, in a pod on the inboard section of the wing near the wing-fuselage intersection. The vectorable thrust turbofans located under the wing are primarily for use during cruise but contribute 23% of the total vertical thrust.

B. Tilt Wing

The Tilt Wing has a cruising speed of 275 knots at an altitude of 30,000 ft. and is powered by eight turboprop engines. The design gross weight is 223,000 lbs (in the VTOL mode) which includes 68,075 lbs. of fuel, located in wing tanks between spars. The STOL take-off weight is 334,000 lbs.

The wing of this transport has an area of 2365 ft.², an aspect ratio of 9.0, a wing span of 146 ft. and employs a 23021 airfoil. High lift devices include 40% chord double-slotted flaps and full span leading edge slats. A tilting mechanism is provided to rotate the wing from the normal or cruise position to the upright or VTOL position.

The propulsion system with 98,600 installed hp., consists of eight turboprop engines which drive four 33 ft. diameter props. The powerplant installation (2 engines in each wing nacelle) delivers a total of 15,000 lbs. of thrust at cruise conditions.

C. Extended Flap

The Extended Flap has a cruising speed of 275 knots at an altitude of 30,000 ft. and is powered by eight turboprop engines. The design gross weight in the VTOL mode is 263,000 lbs., including 77,500 lbs. of fuel stored in wing tanks between the spars. The STOL take-off weight is 394,000 lbs.

The wing has an aspect ratio of 10.3, an area of 2600 ft.², a span of 164 ft. and utilizes a 23021 airfoil. High lift device include 40% chord double-slotted flaps and full span leading edge slats. A tilting mechanism is installed at the wing-fuselage intersection to rotate the wing upward a maximum of 30° in order to deflect the airstream to the desired angle. Since clearance cannot be maintained between the props and ground the aircraft must land with the wing in this rotated position.

The powerplant installation produces 130,000 hp. to drive four 37.5 ft. diameter props. Each of the four wing nacelles houses two turboprop engines connected by shafting to the props located under the wing forward of the leading edge.

D. Tilt Propeller

The Tilt Propeller has a cruising speed of 300 knots at an altitude of 30,000 ft. and is powered by eight turbojet engines. The design gross weight is 308,000 lbs. (in the VTOL mode) including 108,000 lbs. of fuel, located in wing tanks between spars in the stationary section of the wing and over the fuselage. The STOL take-off weight is 462,000 lbs.

The wing has an aspect ratio of 6.6, an area of 2560 ft.², a span of 130 ft. and uses a 23021 airfoil. High lift devices include 40% chord double-slotted flaps and full span leading edge slats. A mechanism is installed in the wings to rotate the outboard section with the rotors. Due to the large diameter of the rotors the aircraft must land with the rotors inclined or in the VTOL position in order to obtain sufficient ground clearance.

The propulsion system consists of eight turbojet engines located on top of the wings over the fuselage. 152,000 hp is supplied to the two 57.5 ft. diameter rotors by shafting placed in the wing. Under cruise conditions the rotors develop 23,700 lbs. of thrust.

E. Buried Fan

The Buried Fan has a cruising speed of 400 knots at an altitude of 35,000 ft. and is powered by six turbojet engines. The design gross weight in the VTOL mode is 253,000 lbs. including 94,500 lbs. of fuel located in fuselage tanks. While this aircraft has no STOL capabilities within specifications a maximum or STOL weight of 380,000 lbs. was

legislated in those analyses where the use of a maximum weight is warranted.

The wing has an area of 2800 ft.², an aspect ratio of 4.0, a span of 105 ft. and employs a 23015 airfoil with 13° of sweep at $\frac{1}{4}$ chord. The thickness ratio is 15% from the root to a point between the inboard and outboard lift fans and it then tapers to a 10% section. High lift devices include full span leading edge slats and 20% chord double-slotted flaps. Three-spar construction is used with the addition of a "D" spar as the leading edge to assist in taking torsion loads inboard past the fans. The torsional rigidity is greatly reduced in the area of the lift fans since it is assumed that no wing torsion passes through the fans.

The propulsion system consists of six turbojet engines located on top of the wings and four lift fans (15 ft. diameter fan inboard and a 12 ft. diameter fan outboard) placed in the wings. Under cruise conditions, with the lift fans not in use, the six jet engines produce 20,650 lbs. of thrust. In the VTOL mode 147,500 lbs. of thrust are delivered to the fans where 328,000 lbs. of vertical lift is produced.

The analysis and procedures used in determining the configuration design of each aircraft are contained in Appendix I. The analysis estimates a solution meeting design requirements considering the relative importance of such parameters as take-off weight, aspect ratio, STOL capability, wing loading, structural efficiency and dynamic response problems. Since a general solution for all five V/STOL's is not possible the Tilt Wing, Tilt Prop, and Extended Flap, being propeller aircraft, are grouped together while the jet types are considered separately.

The three view drawings of the five V/STOL configurations are contained in Figures 1 thru 5. General data for the configurations is provided in Table 1, giving geometrical data, landing gear spring rates and damping constants based on the static position of the gears, gross weights in VTOL and STOL modes, airfoil lift slopes, lift-off speeds, and other pertinent data.

The wing structural properties are shown in Figures 6 through 10. The structural data shows the section moments of inertia in bending and torsion about the elastic axis of the wing.

The fuselage structural properties are shown in Figures 11 thru 15 and includes section moments of inertia for vertical bending, lateral bending, and torsion.

The wing ultimate shear, bending, and torsion loadings from a 4.5 g maneuver are contained in Figures 16 thru 20. The fuselage ultimate shear and bending for a 4.5 g maneuver are contained in Figures 21 thru 25.

The group weight statement for the configurations is listed in Table 17 which is a portion of Appendix III. The panel point weight distributions of fuselage and wing are listed in Tables 15 and 16.

The landing gear data for spring rates in vertical and drag directions and the damping constants are contained in Table 1. The procedure for determining this data is as follows:

Oleo and Tire Spring Rates

Oleo and tire spring rates for the study were determined by scaling from data for a similar type existing aircraft. Shown in Fig. 26 is a non-dimensional force-deflection curve based on this data. The ordinate, F/F_{static} , is the ratio of the gear force output to the force under static load conditions. The abscissa $\chi/\chi_{\text{static}}$ is the ratio of oleo deflection to corresponding deflection under static load conditions. A non-dimensional linear spring rate in the neighborhood of the static load condition can be calculated and is found to be:

$$\frac{\partial(F/F_{\text{static}})}{\partial(\chi/\chi_{\text{static}})} = 7.2 \quad (1)$$

A dimensional spring rate can be obtained by:

$$\frac{\partial F}{\partial \chi} = 7.2 \frac{F_{\text{static}}}{\chi_{\text{static}}} \quad (2)$$

A summary of linear oleo spring rates and static gear loads and deflections are shown in Table 1 for each aircraft.

Tire spring rates were also obtained by scaling from existing data. Fig. 27 gives non-dimensional tire data for the main and nose gear. Again, calculation of the non-dimensional linear spring rate is possible in the neighborhood of the static load condition. This yields the following constant.

$$\frac{\partial(F/F_{\text{static}})}{\partial(\chi/\chi_{\text{static}})} = 1.4 \quad (3)$$

Again, a dimensional coefficient can be obtained as follows:

$$\frac{\partial F}{\partial \chi} = 1.4 \frac{F_{\text{static}}}{\chi_{\text{static}}} \quad (4)$$

A summary table of tire data is shown in Table 1. Note that there are four tires in the main gear carriage and two tires in the nose gear carriage.

Oleo Damping Coefficients

Values of effective linear damping were chosen for the main and nose gear oleo based on a weight scaling procedure similar to that used for establishing the oleo spring. Original data for scaling was taken from similar type existing aircraft.

Refer to Table 1 for values of damping coefficients used in this analysis.

Fore and Aft Gear Spring Rates

The fore and aft gear spring rates were scaled from linear gear spring rates provided by data on a similar type aircraft. The scaled gear spring rate was arrived at using the following equation .

$$K = \frac{F}{F_{\text{STATIC}}} K_{\text{STATIC}} \quad (5)$$

where

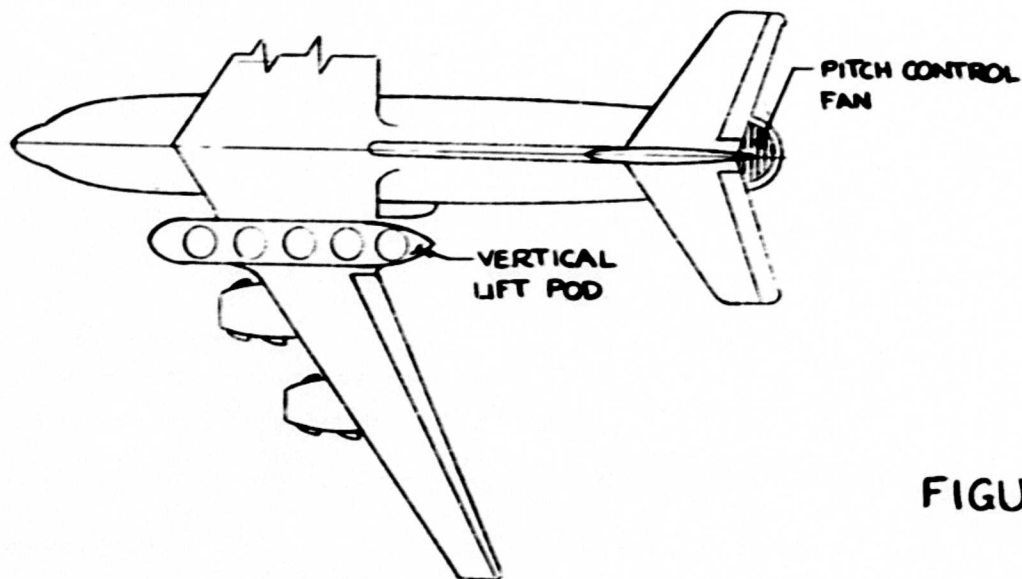
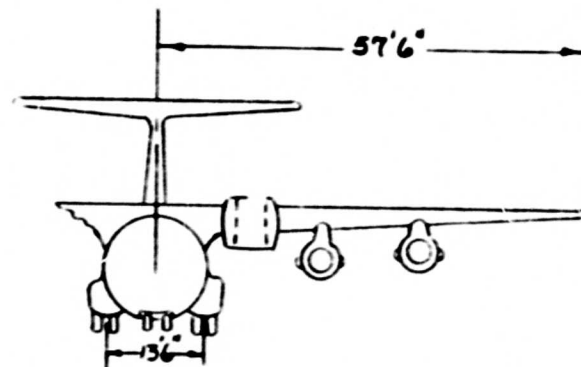
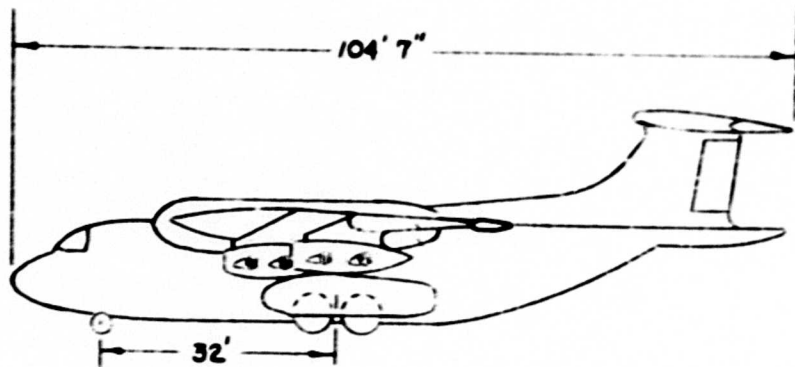
K_{Static} = gear spring rate from a similar type aircraft, lbs/in.

F_{Static} = gear reaction from the similar type aircraft, lbs.

K = gear spring rate used in analysis for a particular configuration, lbs/in.

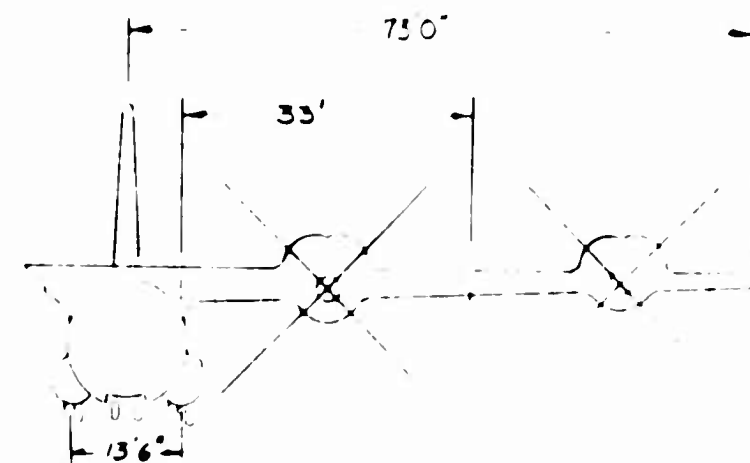
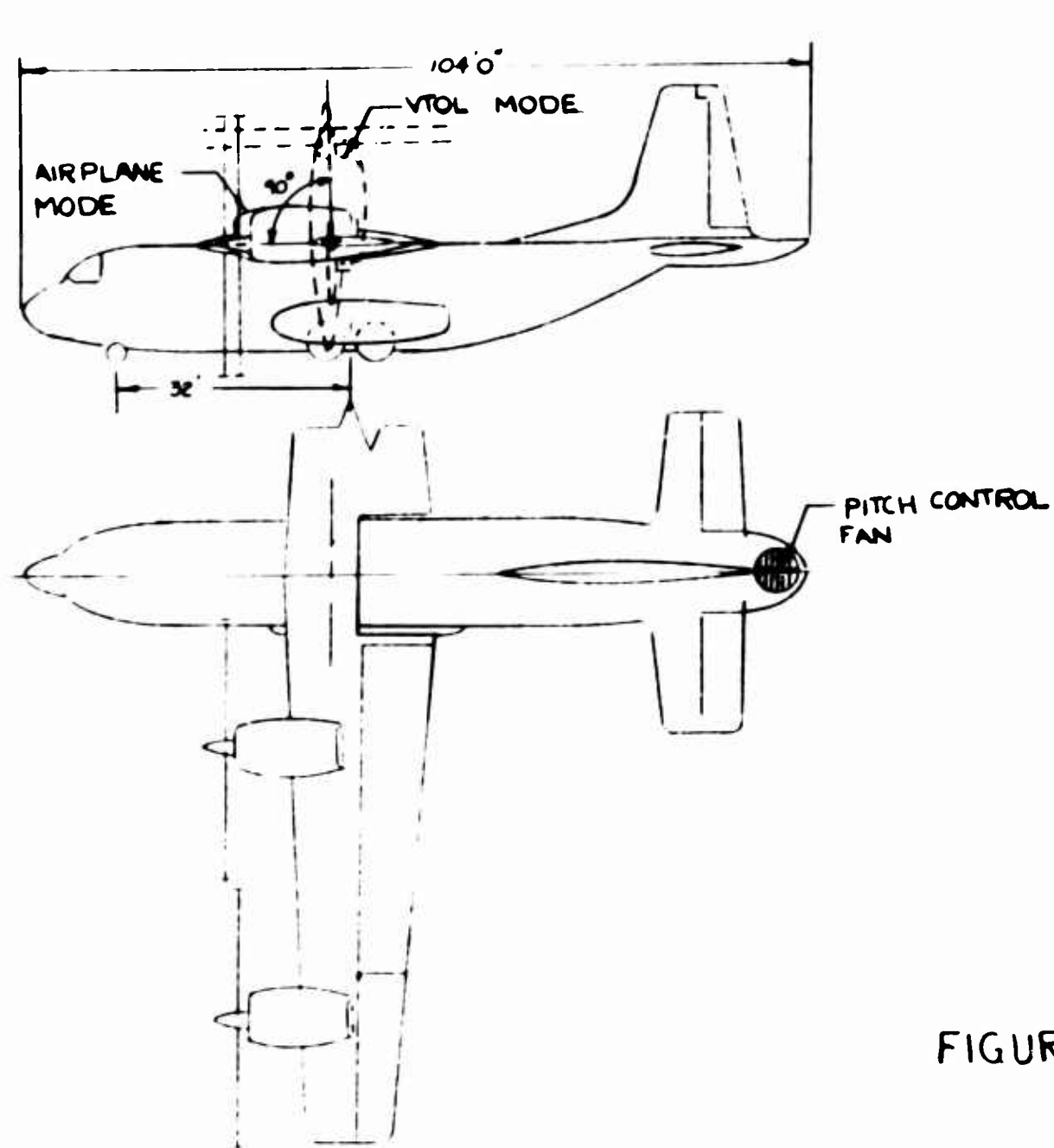
F = gear reaction for that configuration, lbs.

BLANK PAGE



$V_{CR} = 400 \text{ KTS.}$
 $W/S = 86.7 \text{ LBS./FT.}^2$
 $AR = 8.0$
 $B.D.G.W. = 172,000 \text{ LBS. VTOL}$
 $A.D.G.W. = 232,000 \text{ LBS. STOL}$
 $V_{LO} = 108.5 \text{ KTS.}$
 $RATO : THRUST = 231,400 \text{ LBS.}$

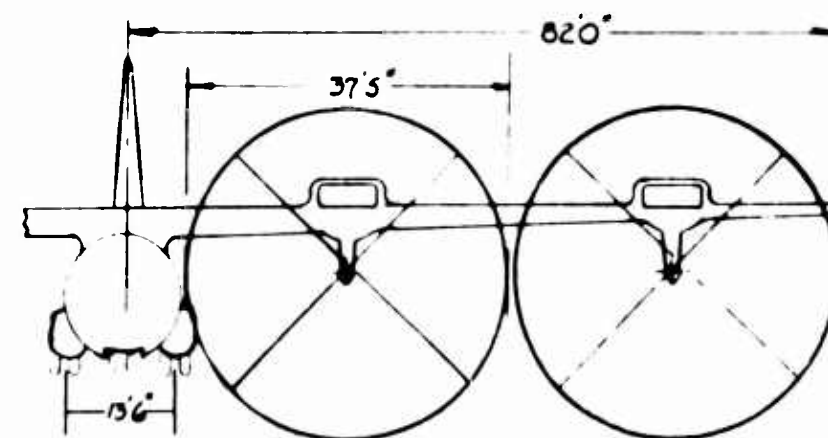
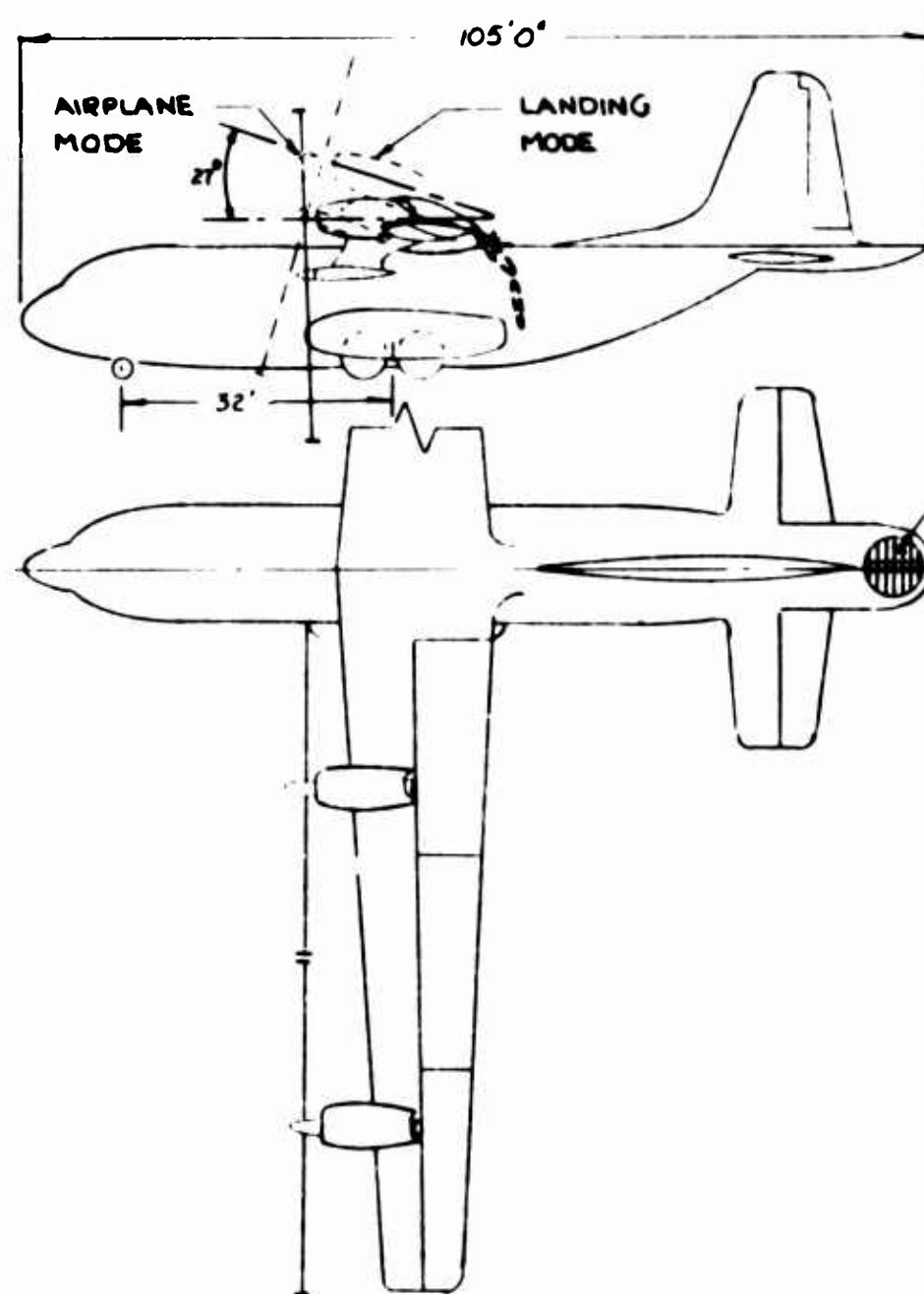
FIGURE 1-FIXED JET 3-VIEW



$V_{CR} = 275 \text{ KTS.}$
 $W/S = 930 \text{ LBS./FT}^2$
 $AR = 9.0$
 $B.D.G.W. = 223,000 \text{ LBS. VTOL}$
 $A.D.G.W. = 334,000 \text{ LBS. STOL}$
 $V_{Lo} = 53.5 \text{ KTS.}$
 $RATO: \text{NONE}$

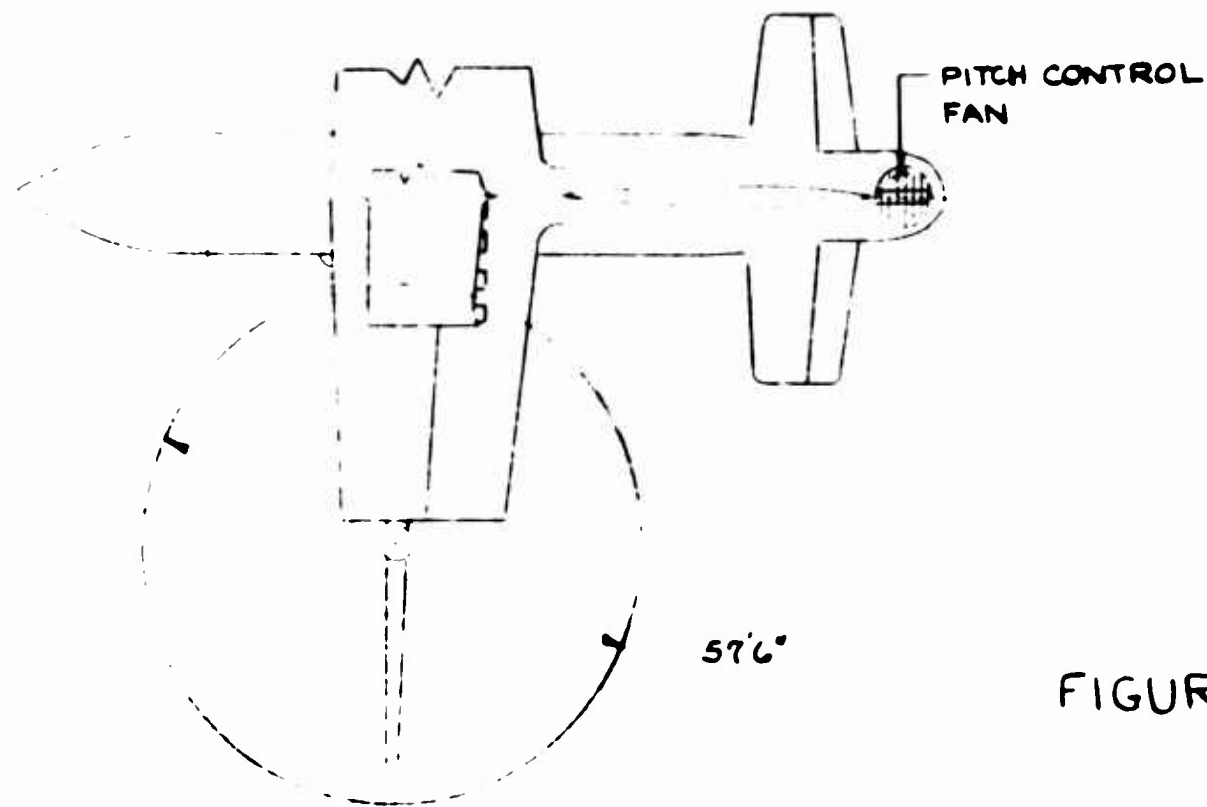
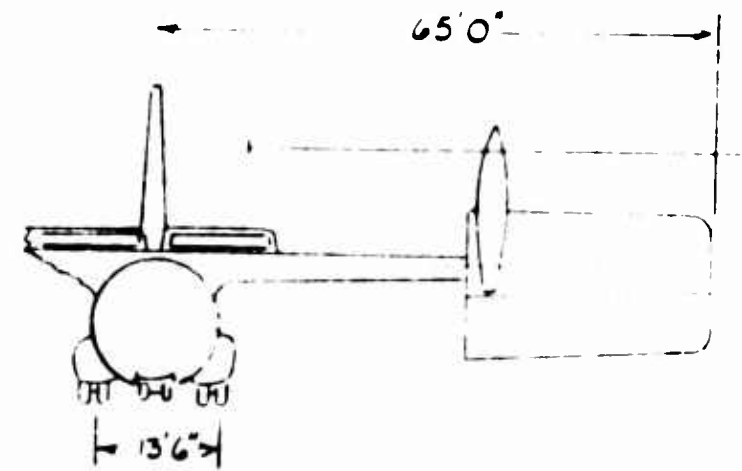
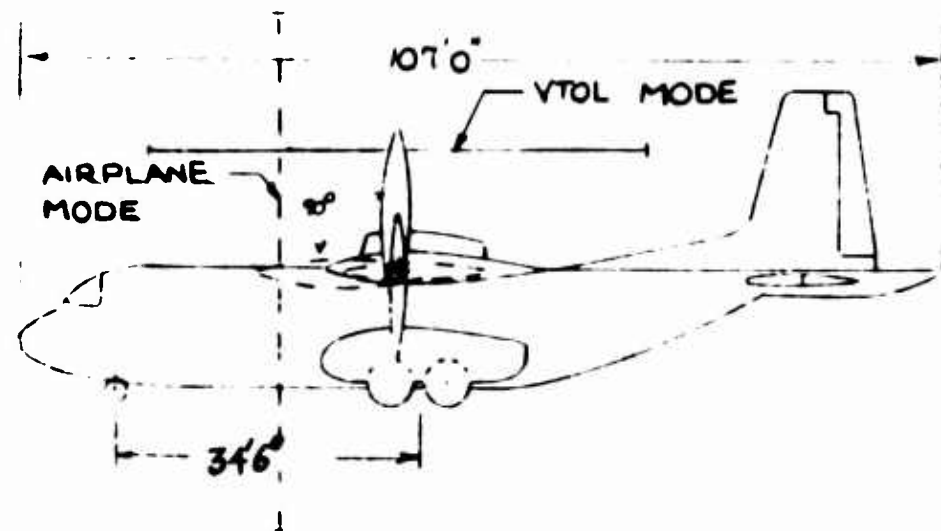
FIGURE 2-TILT WING 3-VIEW

11



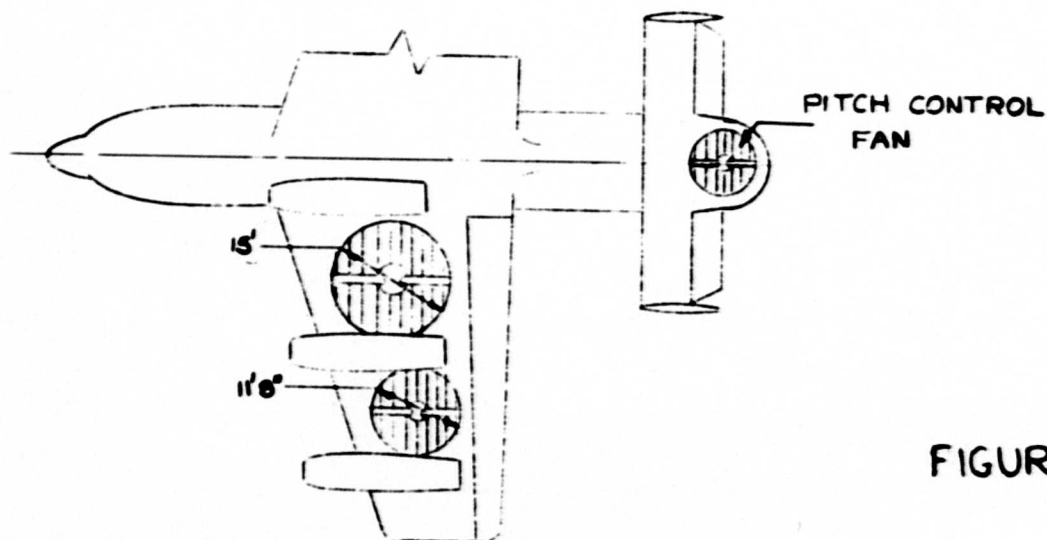
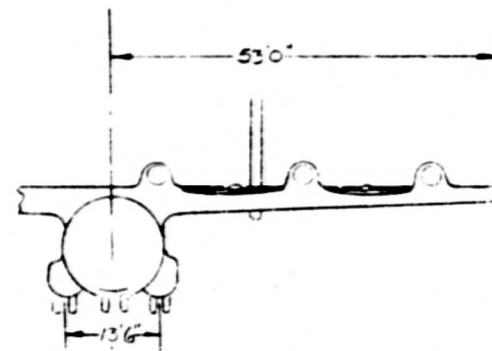
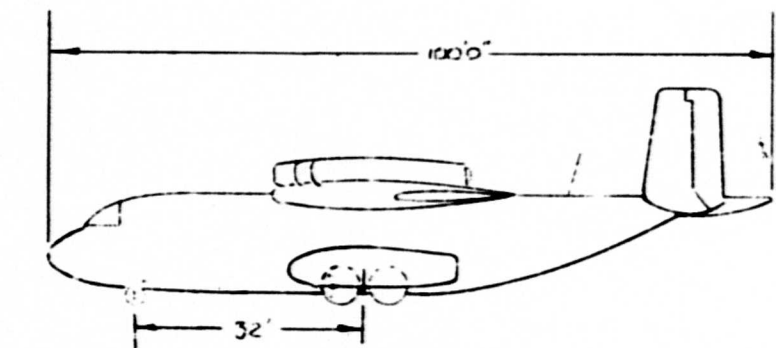
$V_{CR} = 275 \text{ KTS.}$
 $W/S = 100 \text{ LBS./FT}^2$
 $R = 0.3$
 $B.D.G.W. = 263,000 \text{ LBS. VTOL}$
 $A.D.G.W. = 394,000 \text{ LBS STOL}$
 $V_{L0} = 59 \text{ KTS.}$
 $RATO: \text{ NONE}$

FIGURE 3-EXTENDED FLAP 3-VIEW



$V_{CR} = 300 \text{ KTS.}$
 $W/S = 120.0 \text{ LBS./FT}^2$
 $R = 6.6$
 $B.D.G.W. = 308,000 \text{ LBS. VTOL}$
 $A.D.G.W. = 462,000 \text{ LBS. STOL}$
 $V_{L.O.} = 65 \text{ KTS.}$
 $RATO: \text{THRUST} = 115,700 \text{ LBS.}$

FIGURE 4- TILT PROP 3-VIEW



$V_{CR} = 400 \text{ KTS.}$
 $W/S = 74.3 \text{ LBS./FT.}^2$
 $R = 40$
 $B.D.G.W. = 253,000 \text{ LBS. VTOL}$
 $A.D.G.W. = 380,000 \text{ LBS. STOL}$
 $V_{LE} = 114 \text{ KTS.}$
 $RATO: \text{THRUST} = 347,100 \text{ LBS.}$

LEGISLATED VALUE

FIGURE 5 - BURIED FAN 3-VIEW

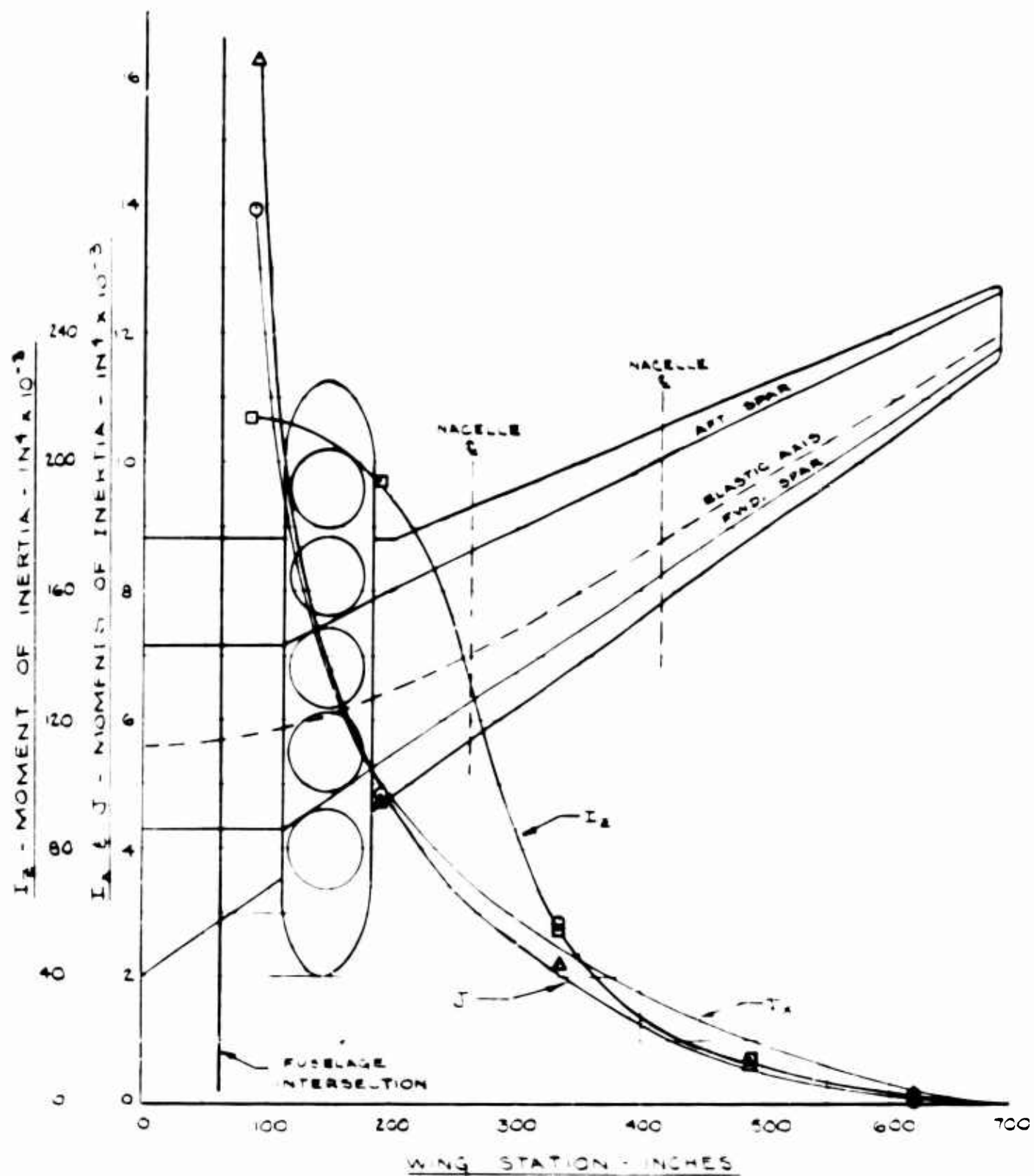


Figure 1. Wing Section Properties

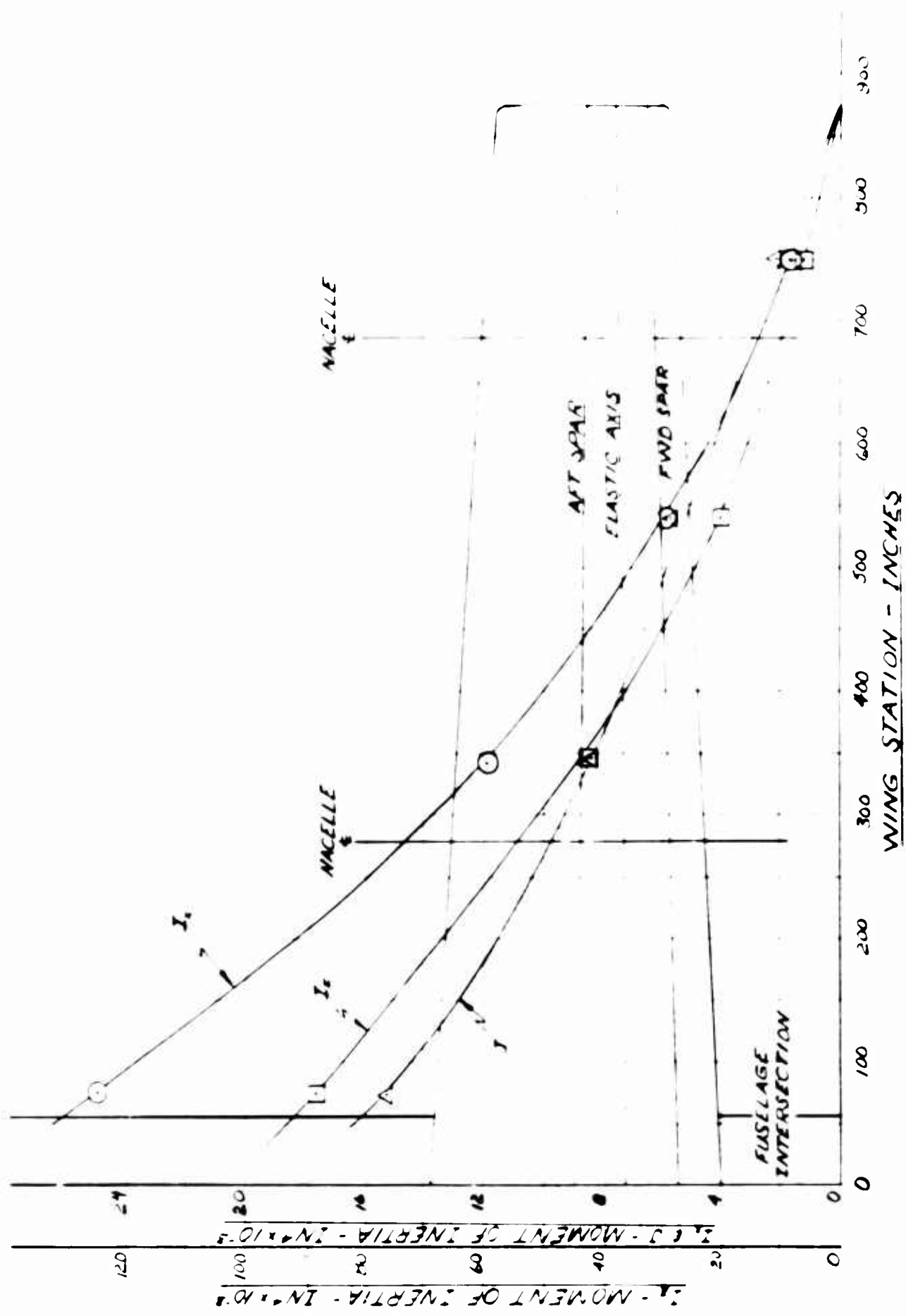


Figure 7 - Wing Section Properties: Tilt Wing

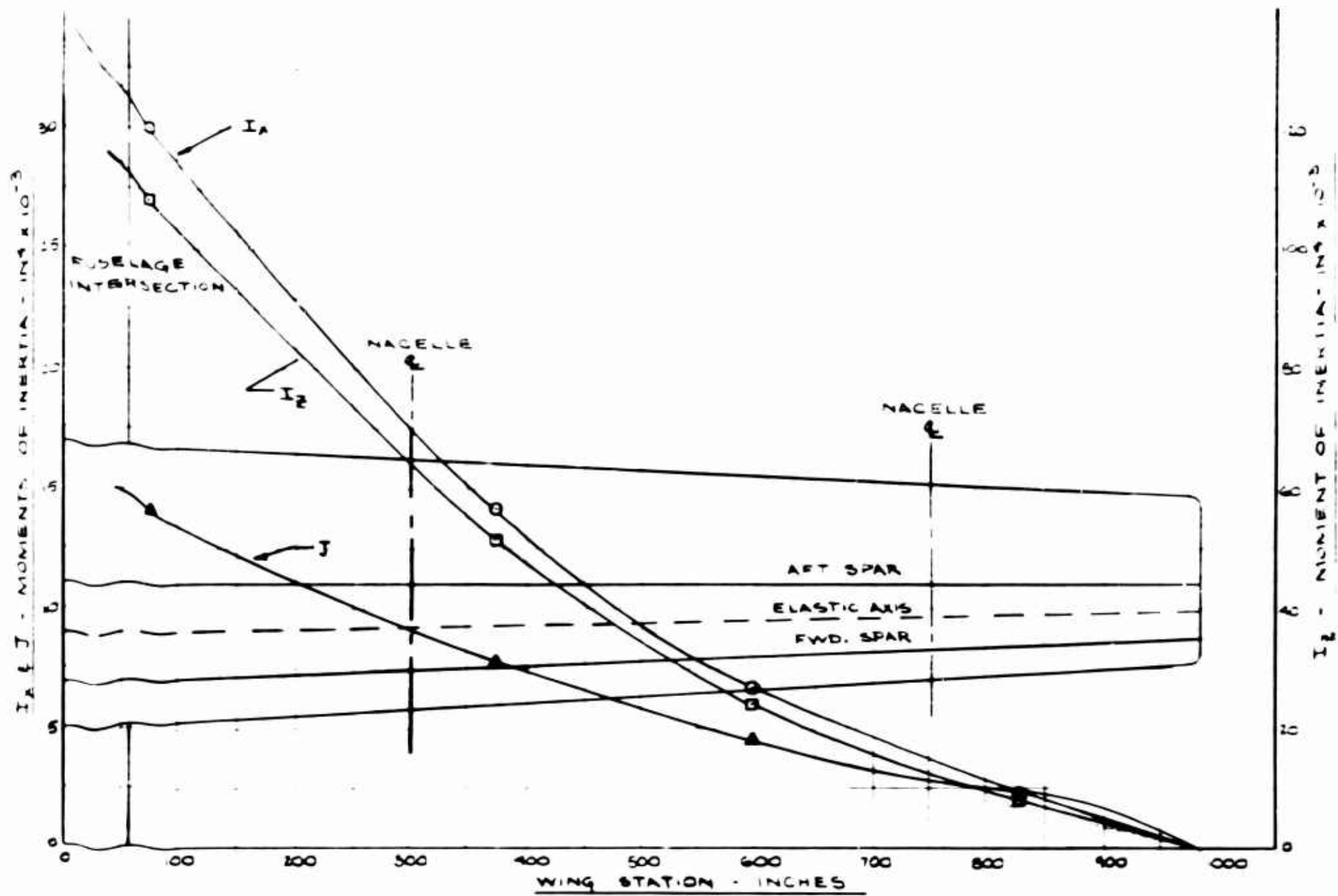


Figure 8 - Wing Section Properties: Extended Plan

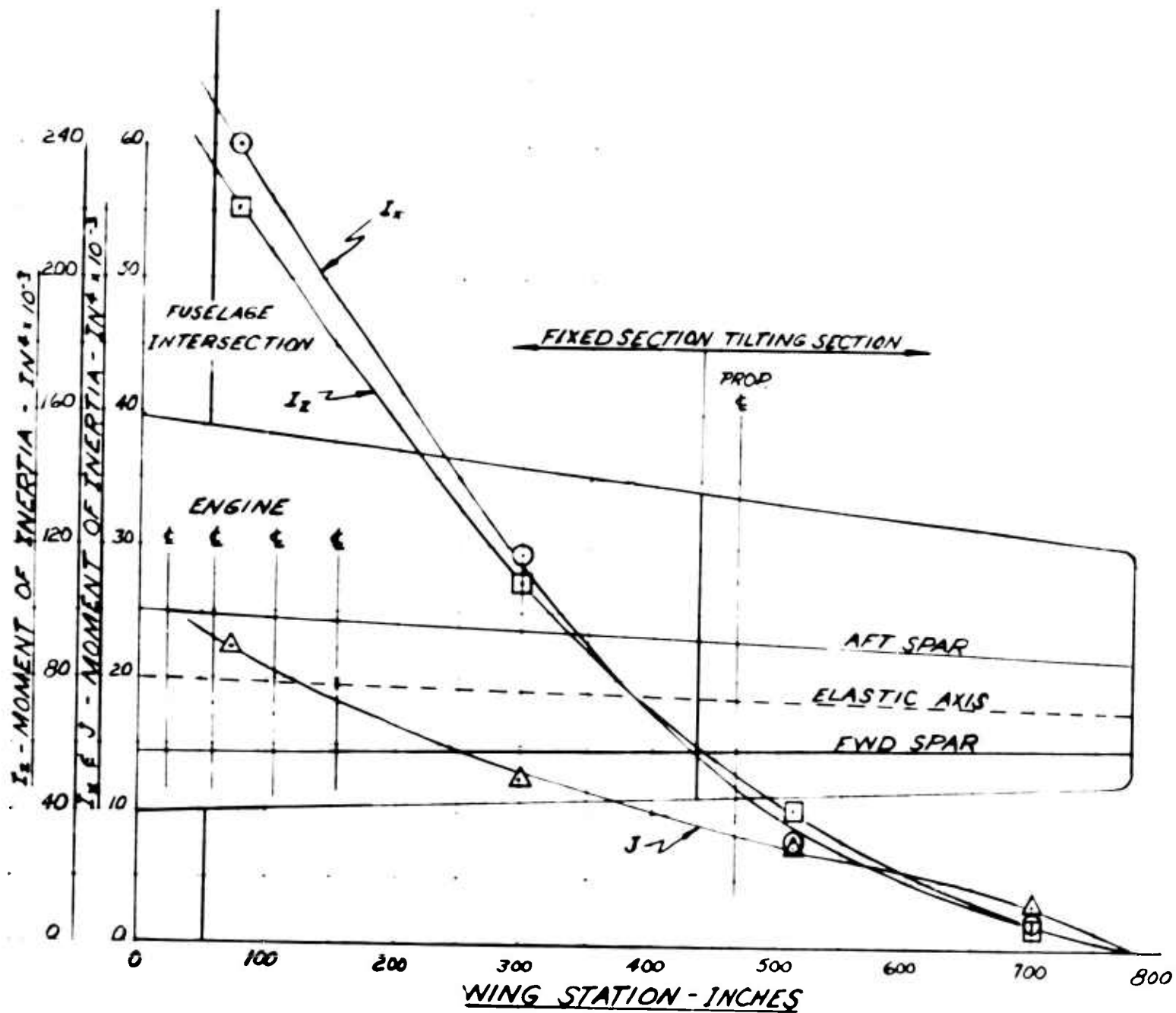


Figure 9 - Wing Section Properties: Tilt Prop

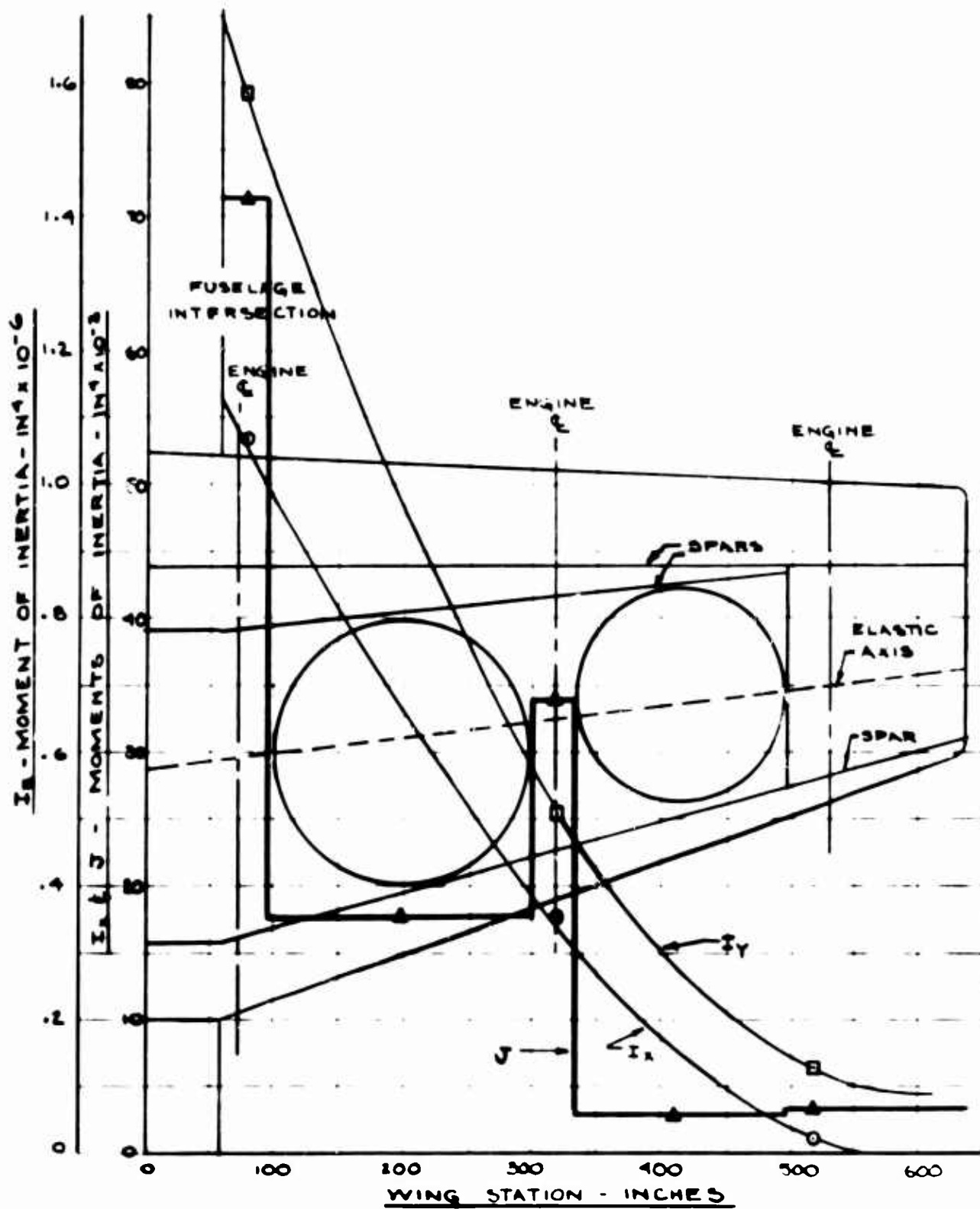


Figure 10 - Wing Section Properties: Buried Fan

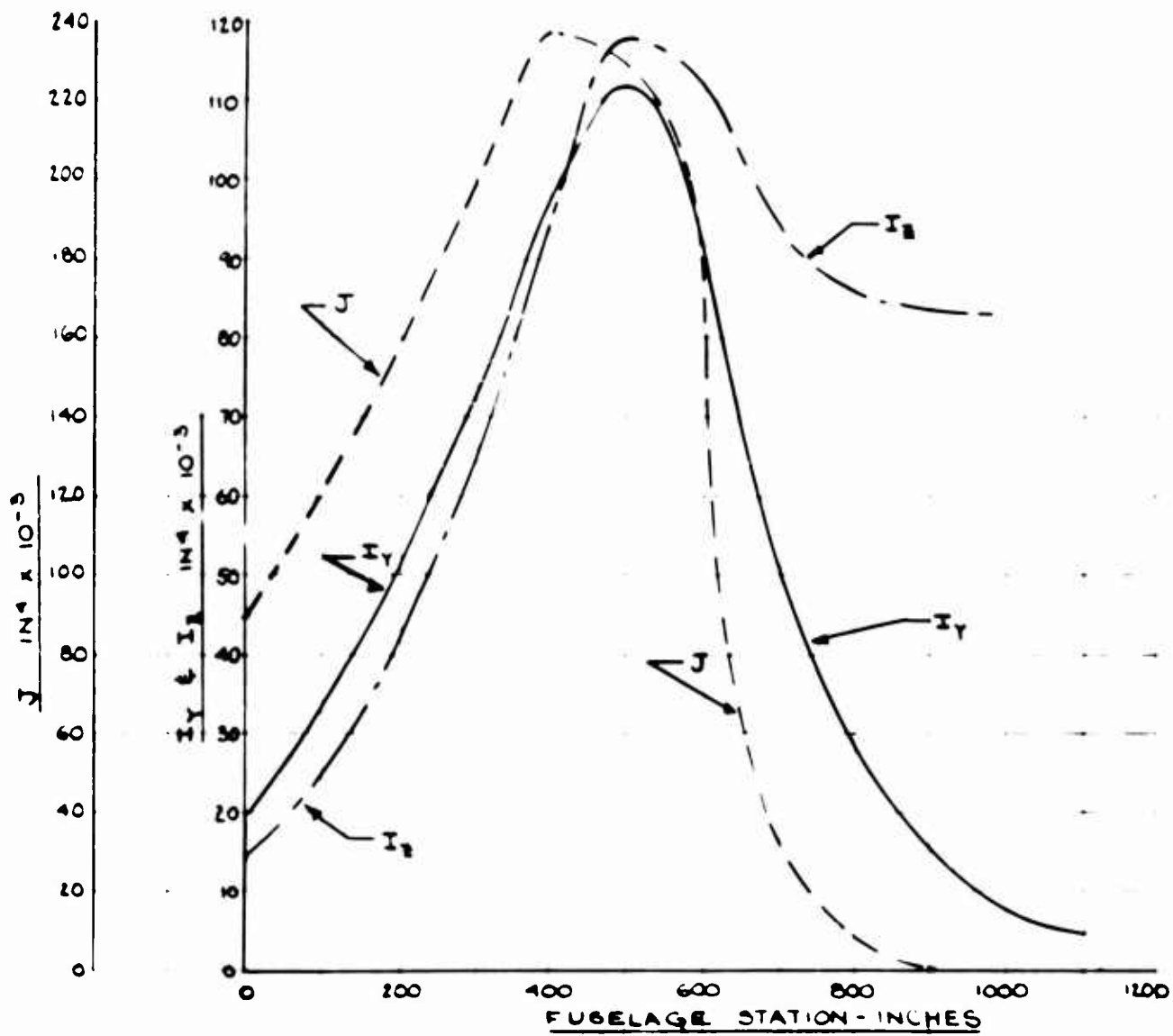


Figure 11 - Fuselage Section Properties: Fixed Jet

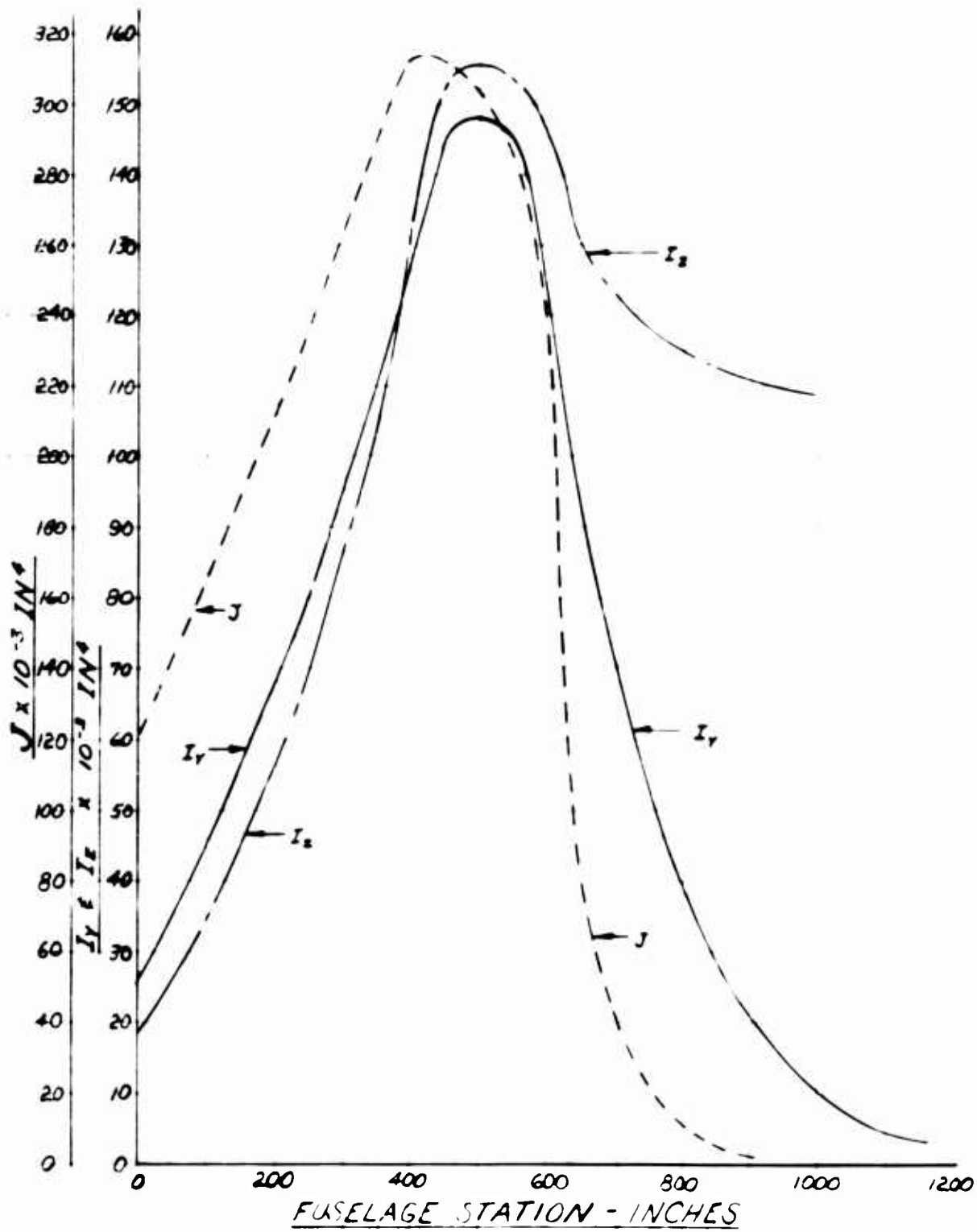


Figure 1 - Fuselage Inertia Properties vs. Station

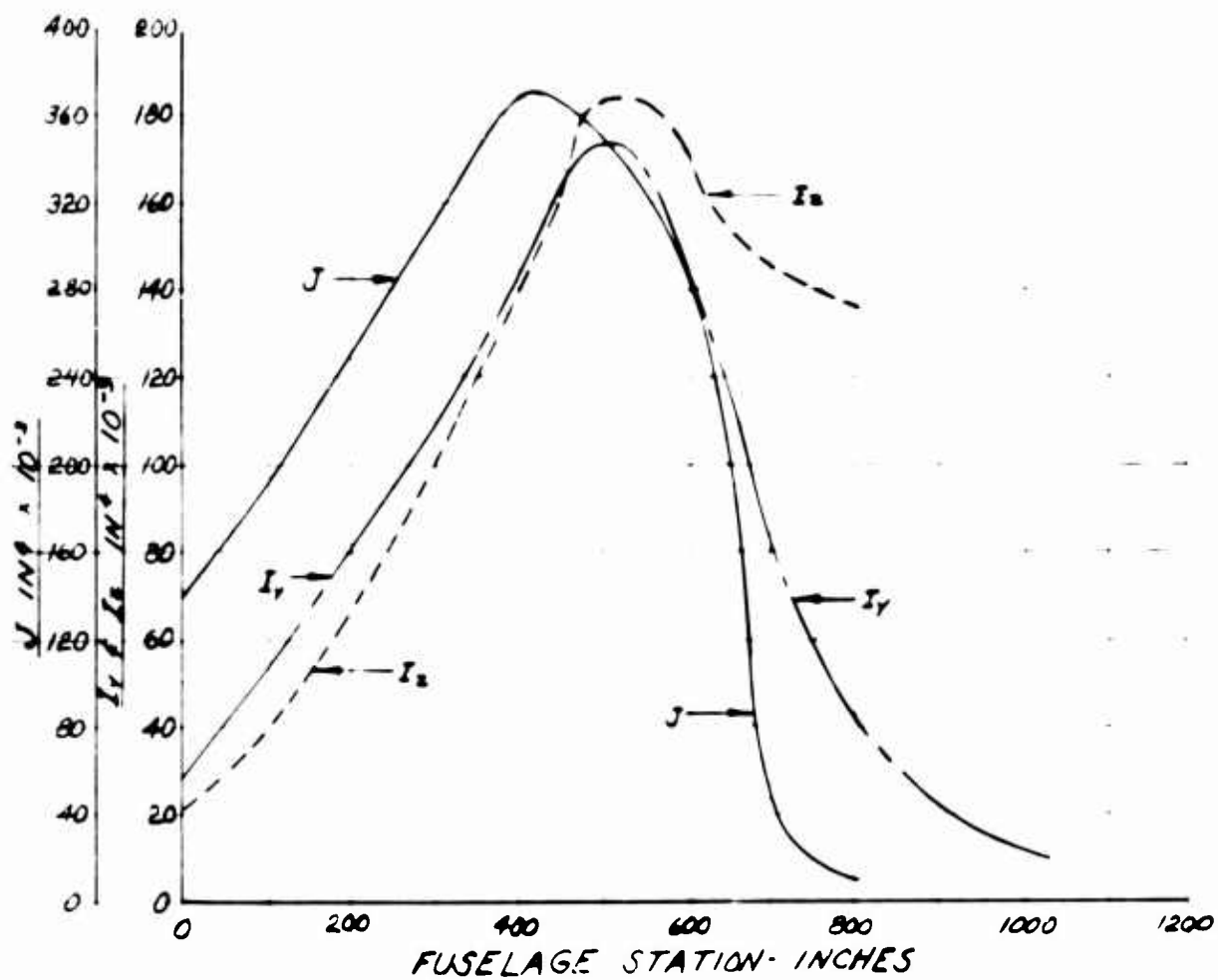


Figure 13 - Fuselage Section Properties: Extended Flap

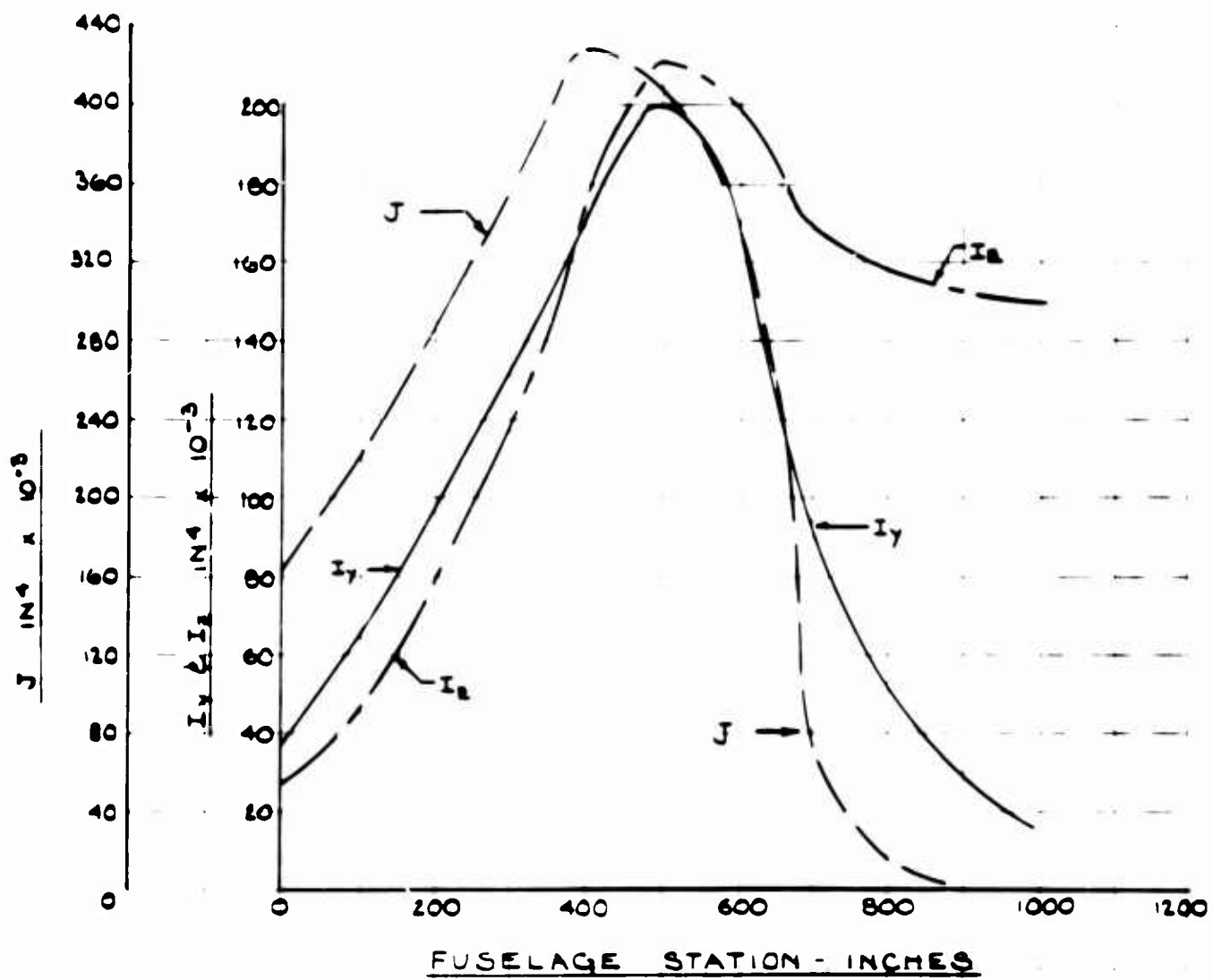


Figure 14 - Fuselage Section Properties: Tilt Prop

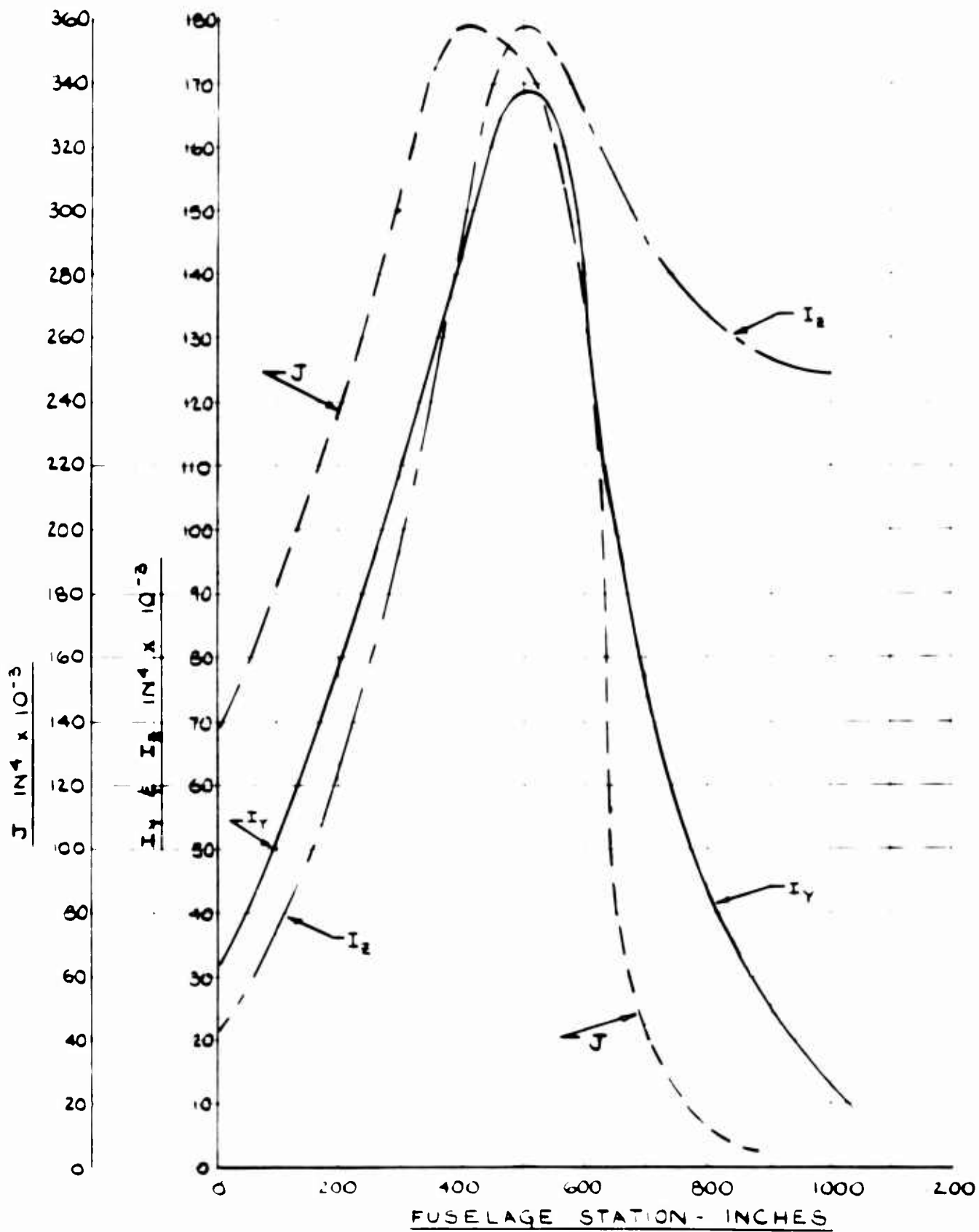


Figure 15 - Fuselage Section Properties

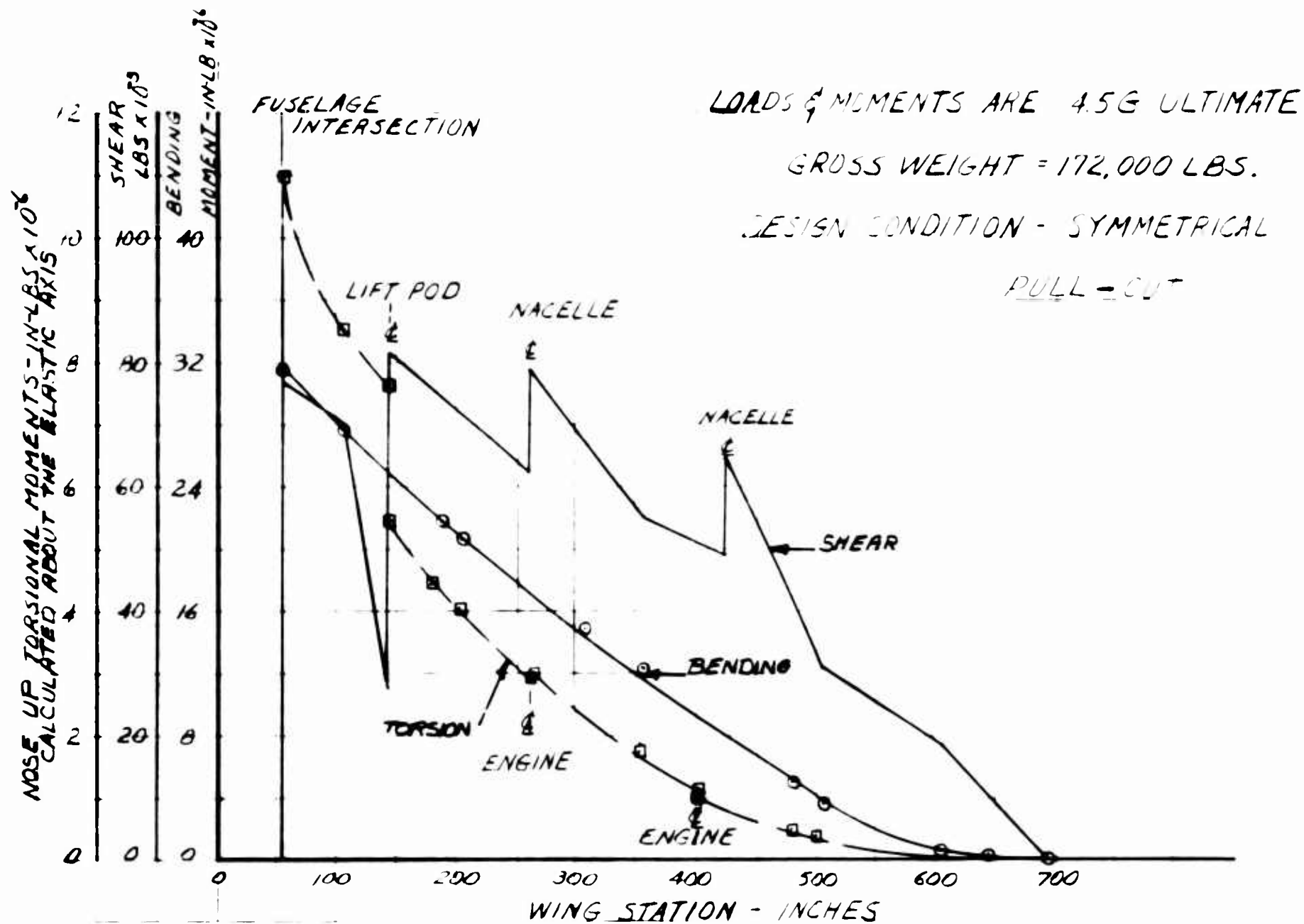


Figure 16 - Wing Ultimate Shears, Moments and Torsions: Fixed Jet

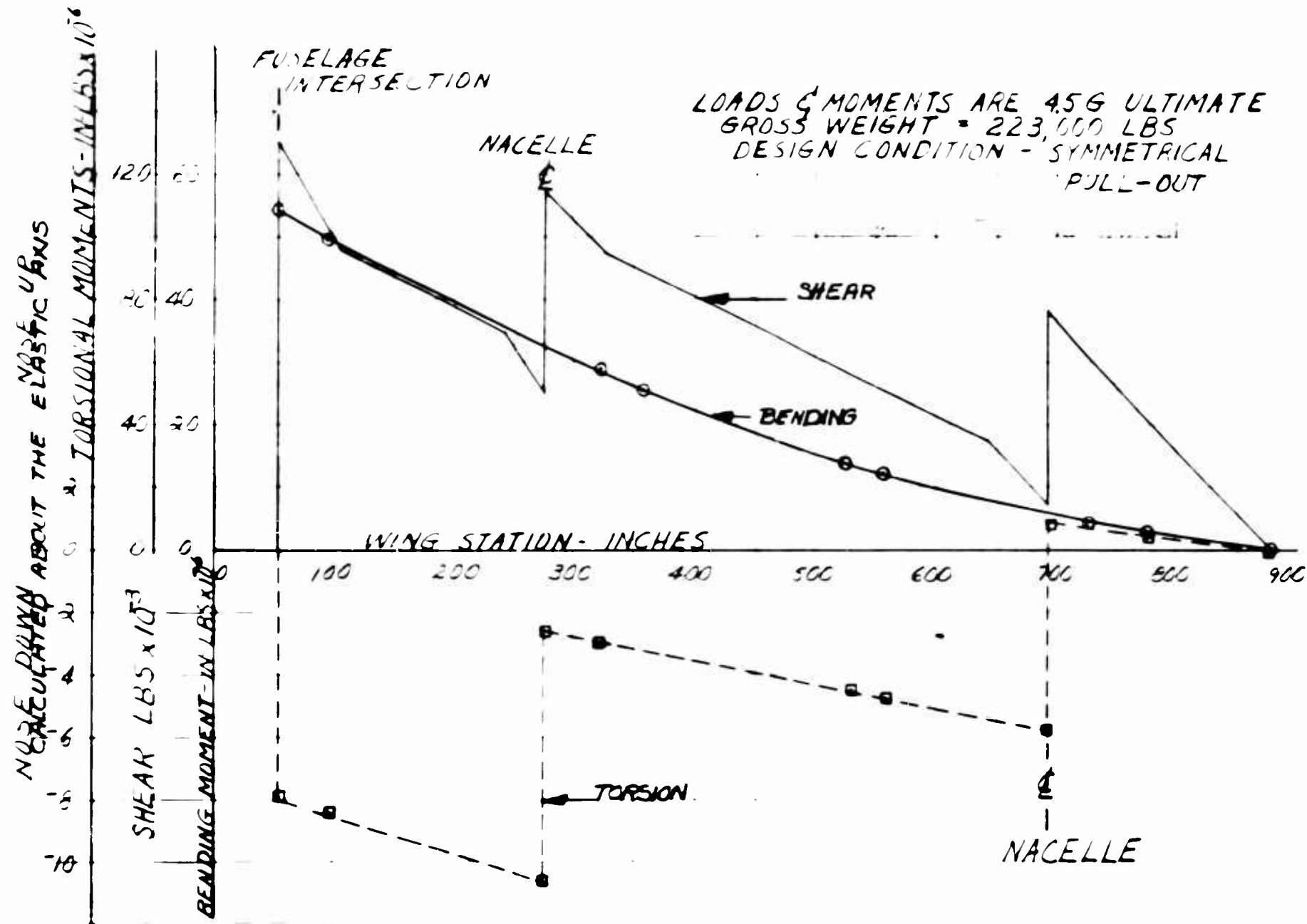


Figure 17 - Wing Ultimate Shears, Moments and Torsions: Tilt Wing

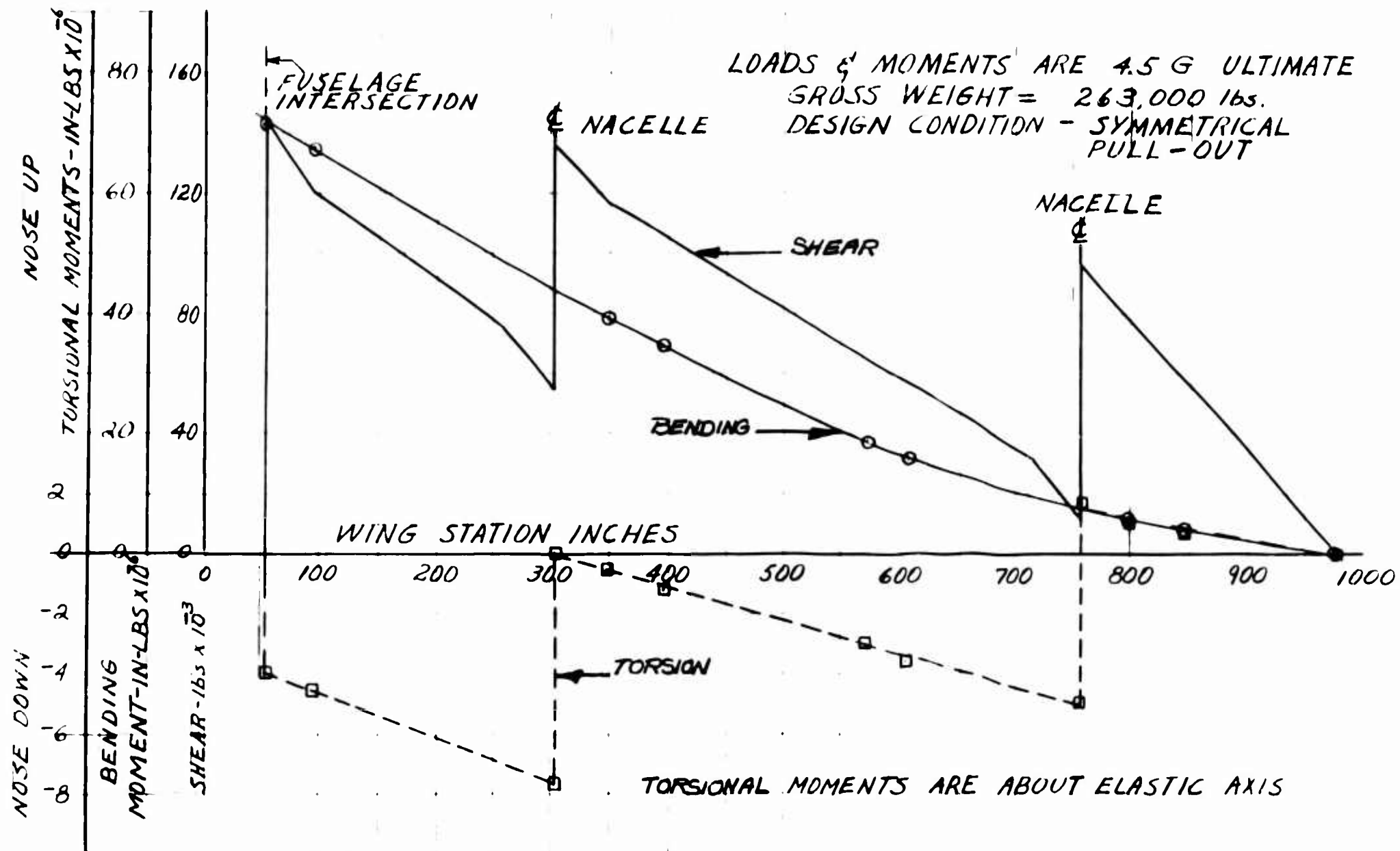


Figure 18 - Wing Ultimate Shears, Moments and Torsions: Extended Flap

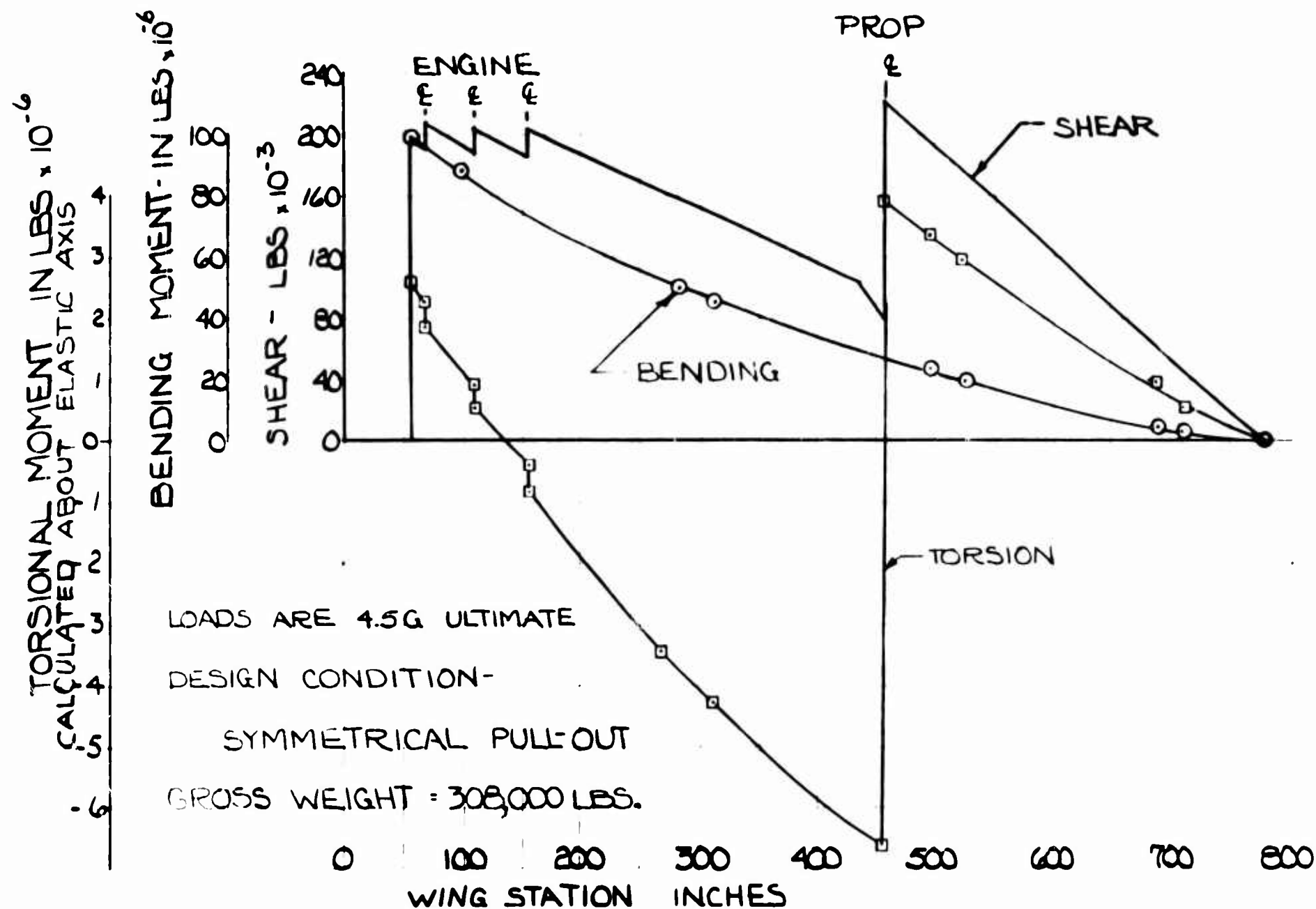


Figure 10 - Wing Ultimate Shears, Moments and Torsions: Tilt Prop

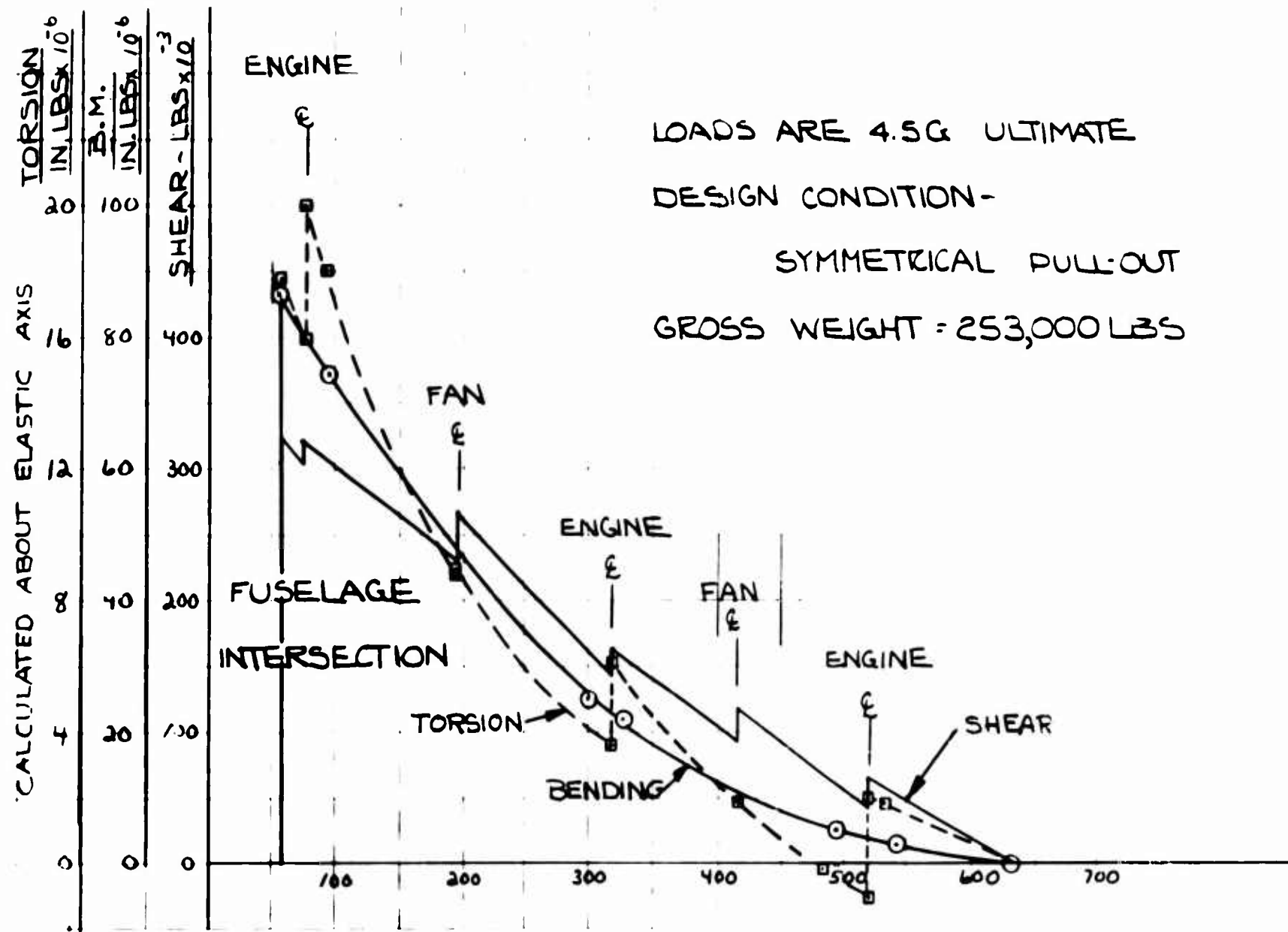


Figure 20 - Wing Ultimate Shears, Moments and Torsions: Buried Fan

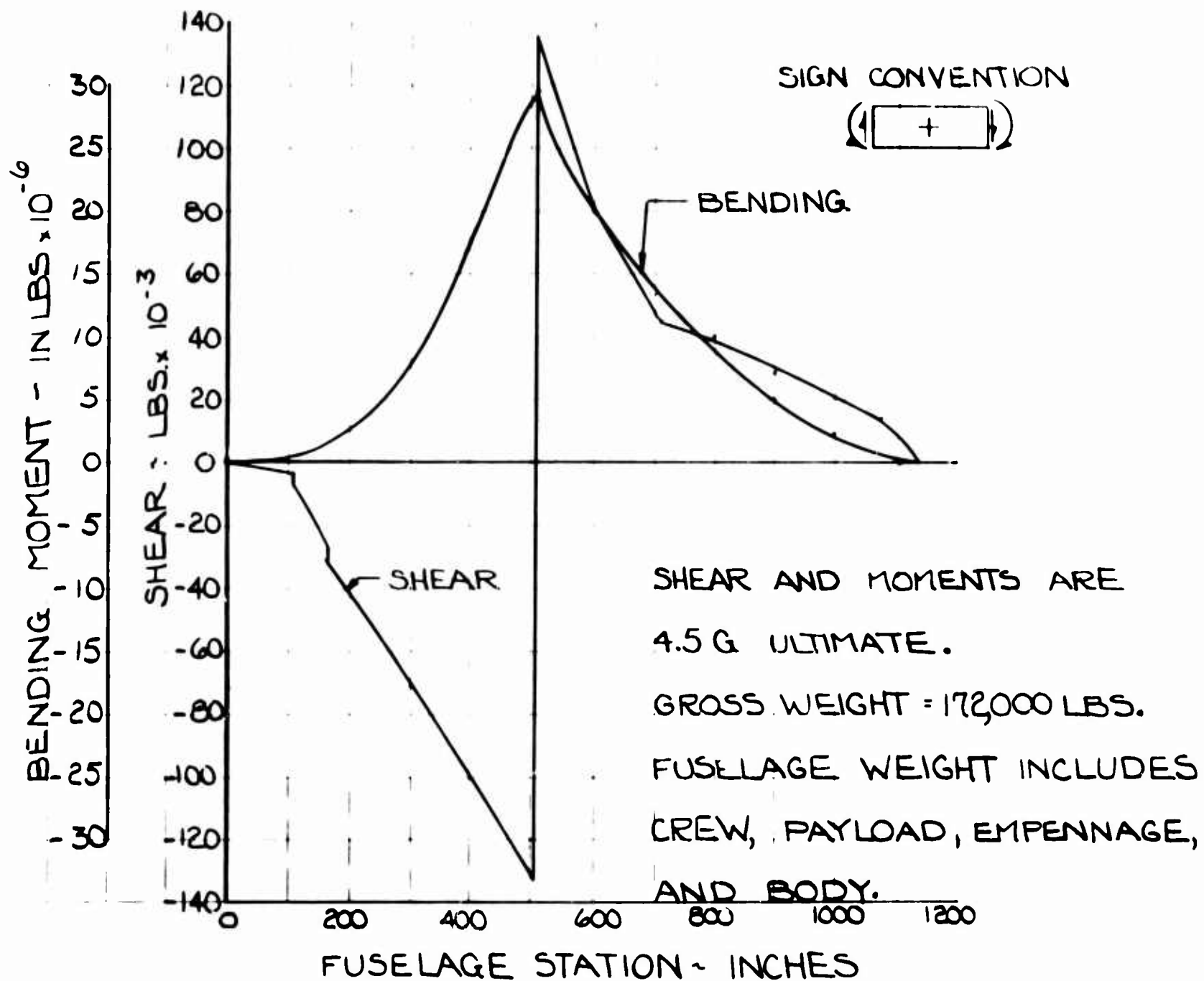


Figure 21 - Fuselage Ultimate Vertical Shear and Bending Moment Diagram: Fixed Jet

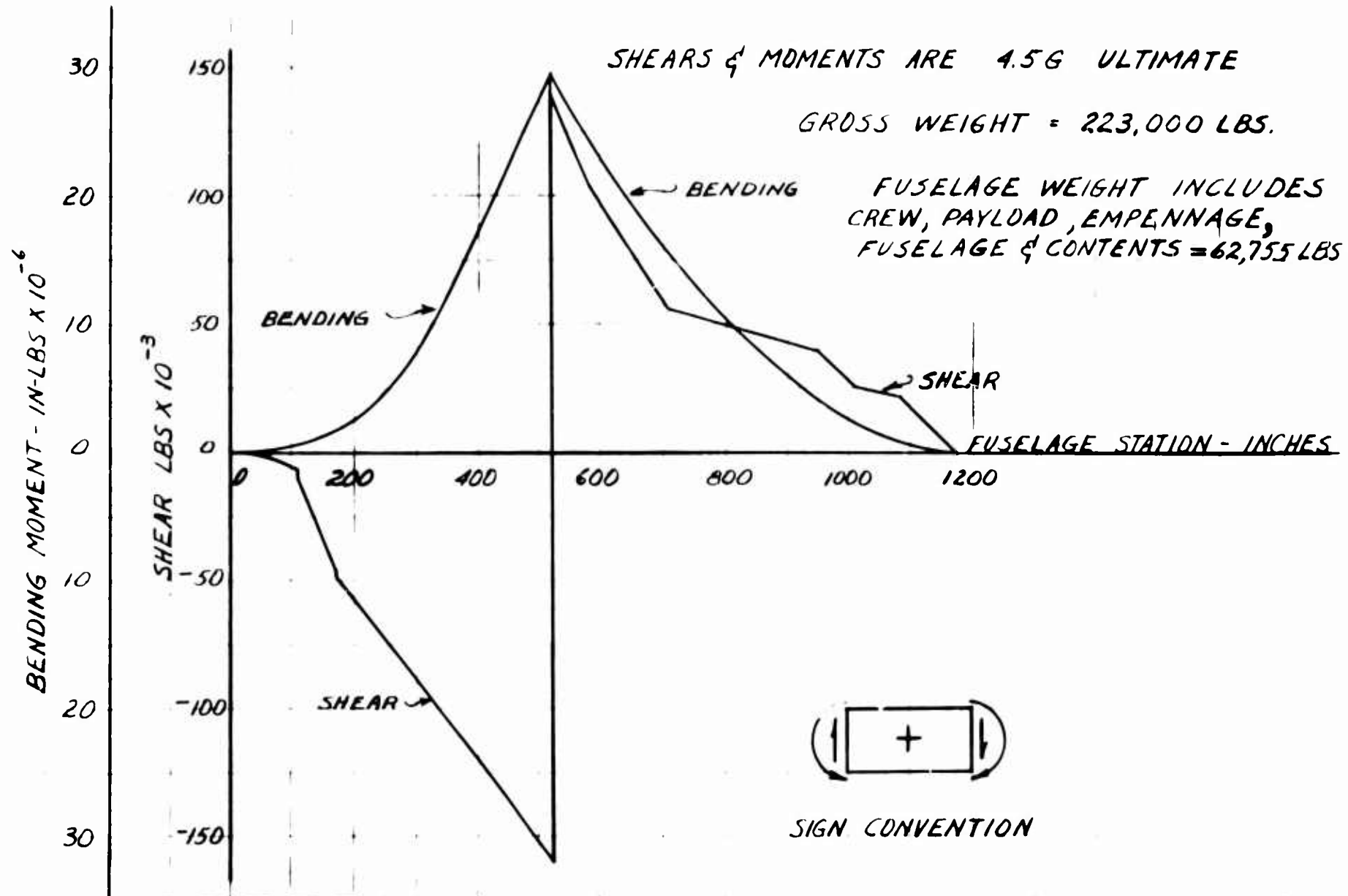


Figure 22 - Fuselage Ultimate Vertical Shear and Bending Moment Diagram: Tilt Wing

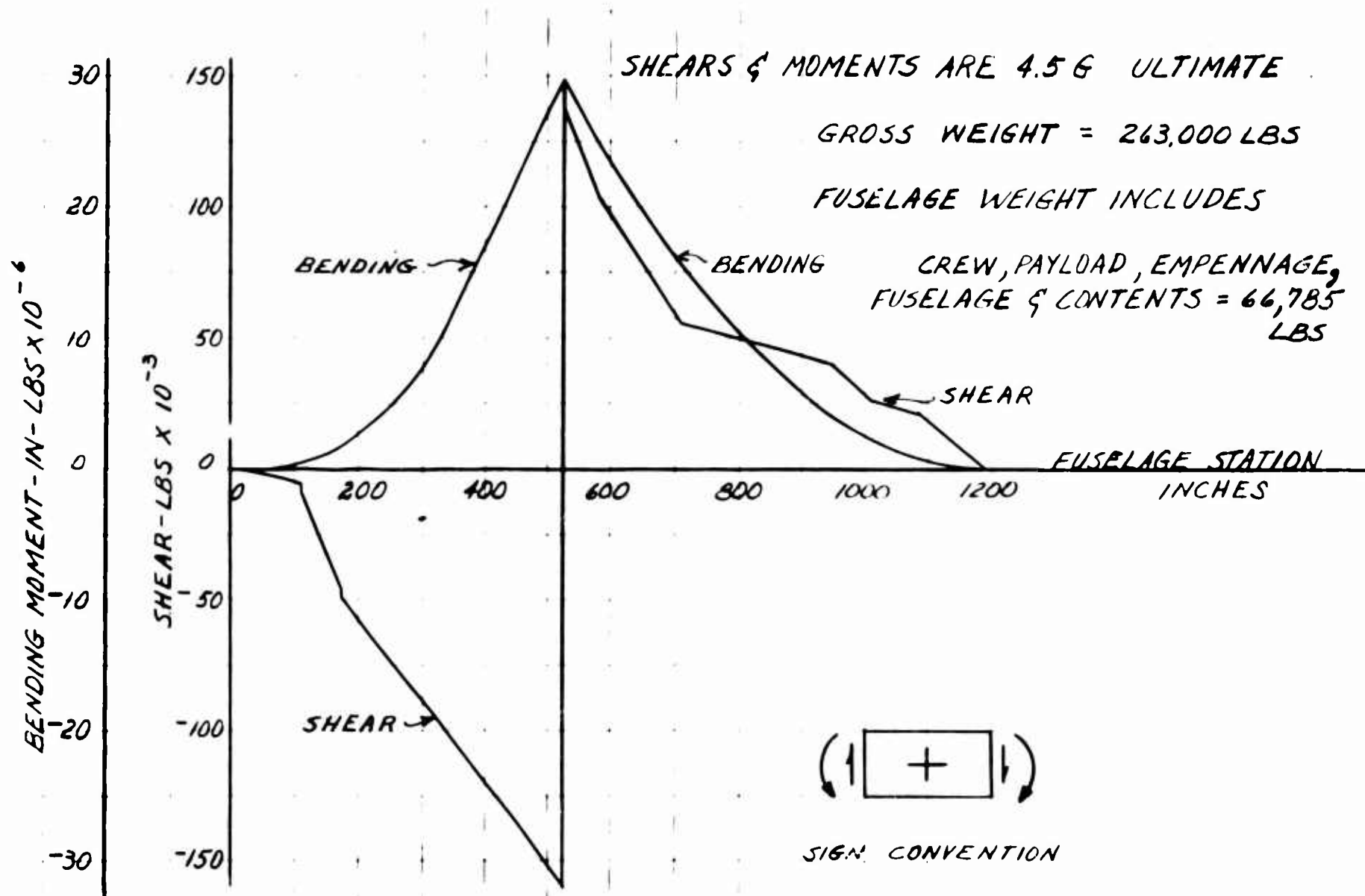


Figure 23 - Fuselage Ultimate Vertical Shear and Bending Moment Diagram: Extended Flap

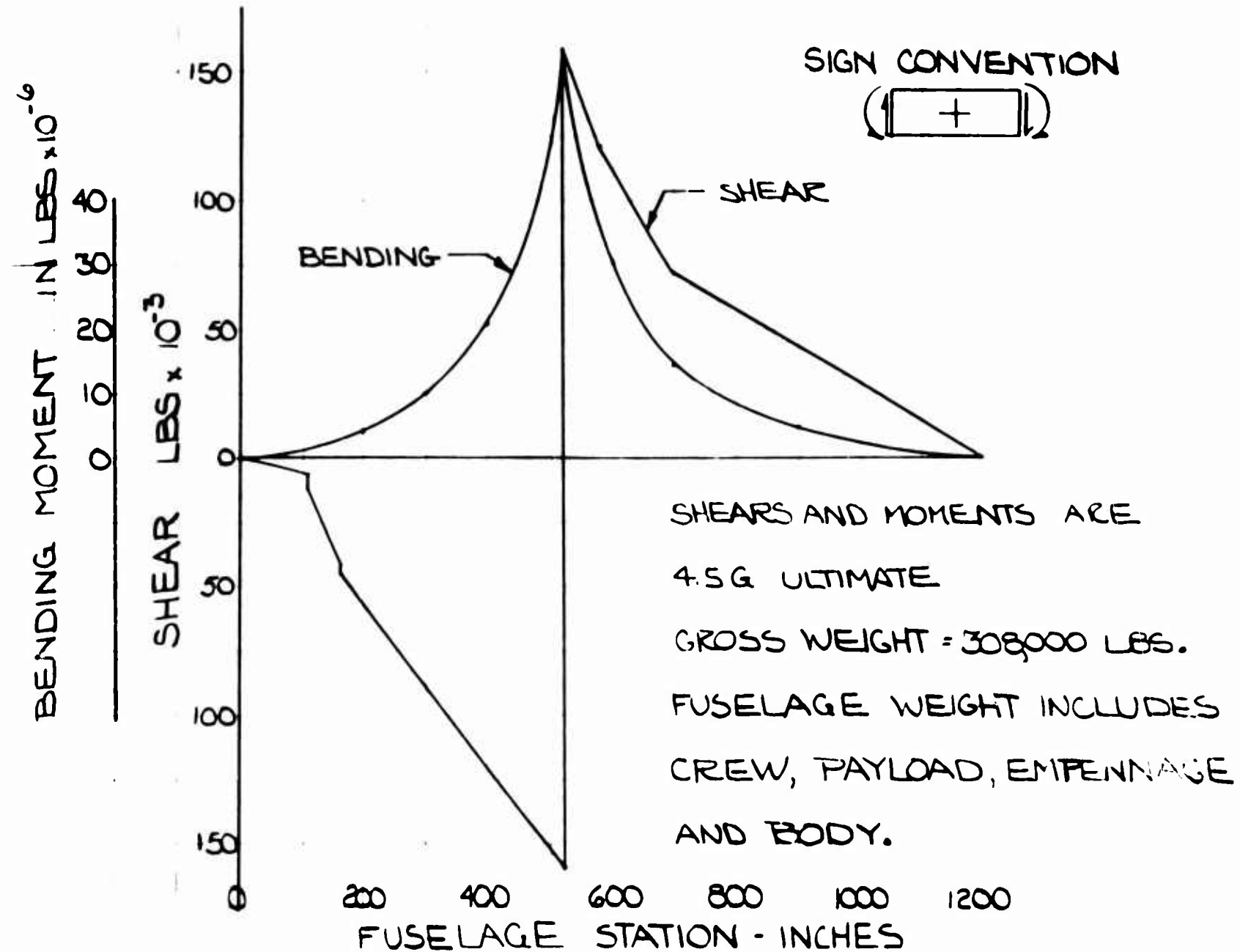


Figure 24 - Fuselage Ultimate Vertical Shear and Bending Moment Diagram: Tilt Prop

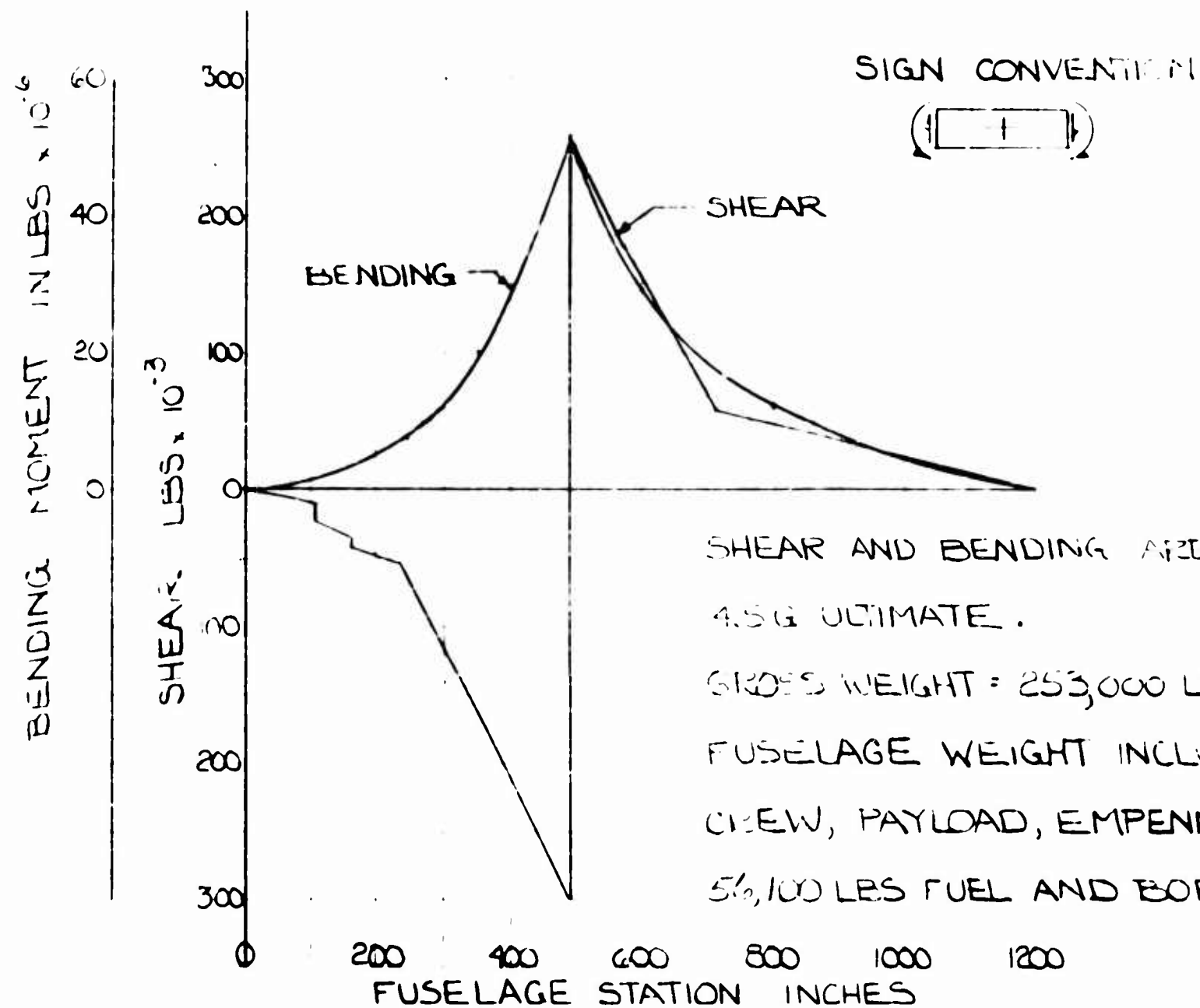


Figure 10 - Fuselage Ultimate Vertical Shear and Bending Moment Diagram: Buried Fan

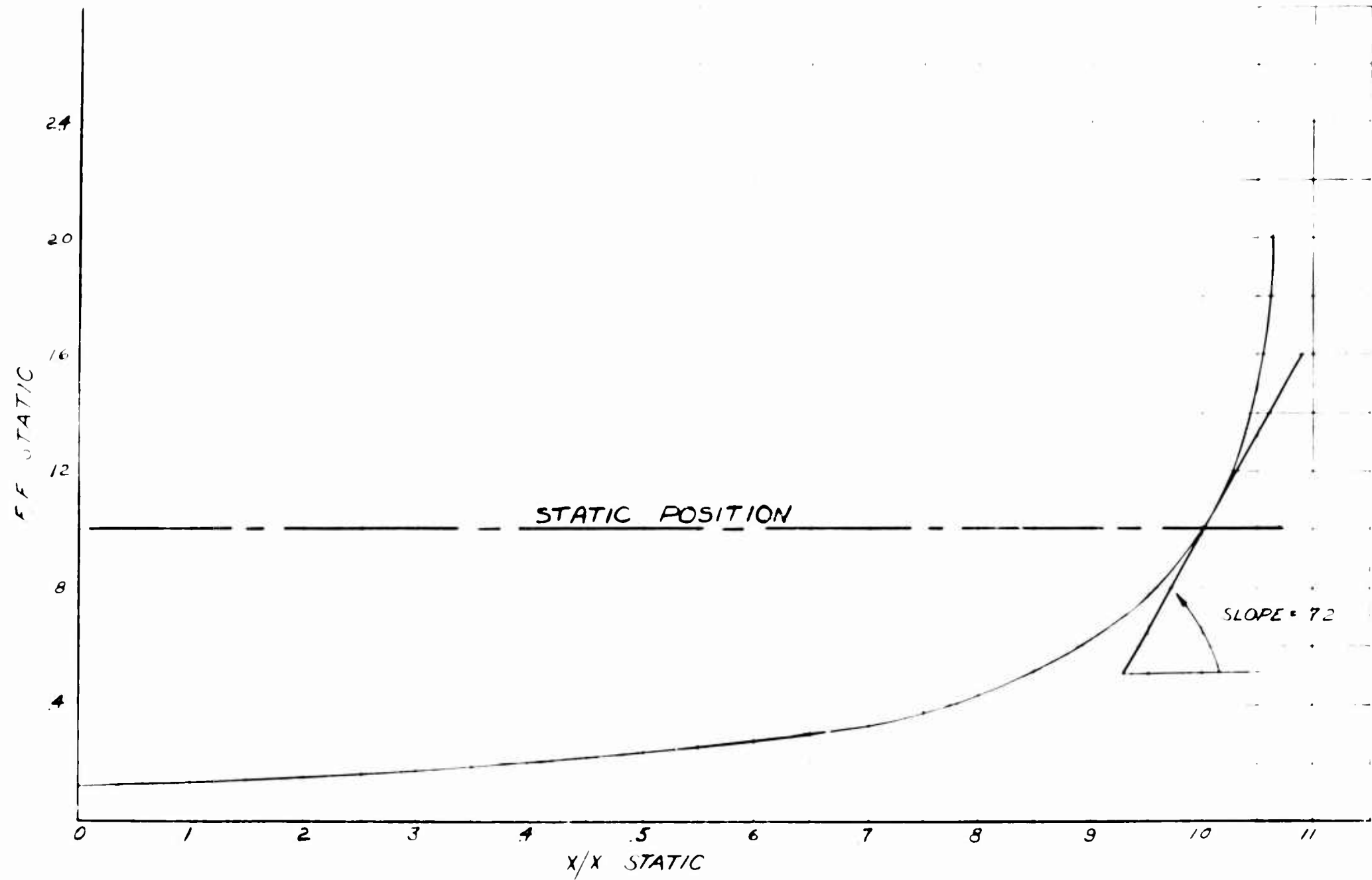


Figure 26 - Non-Dimensional Spring Rate for V/STOL Main and Nose Gear Oleo

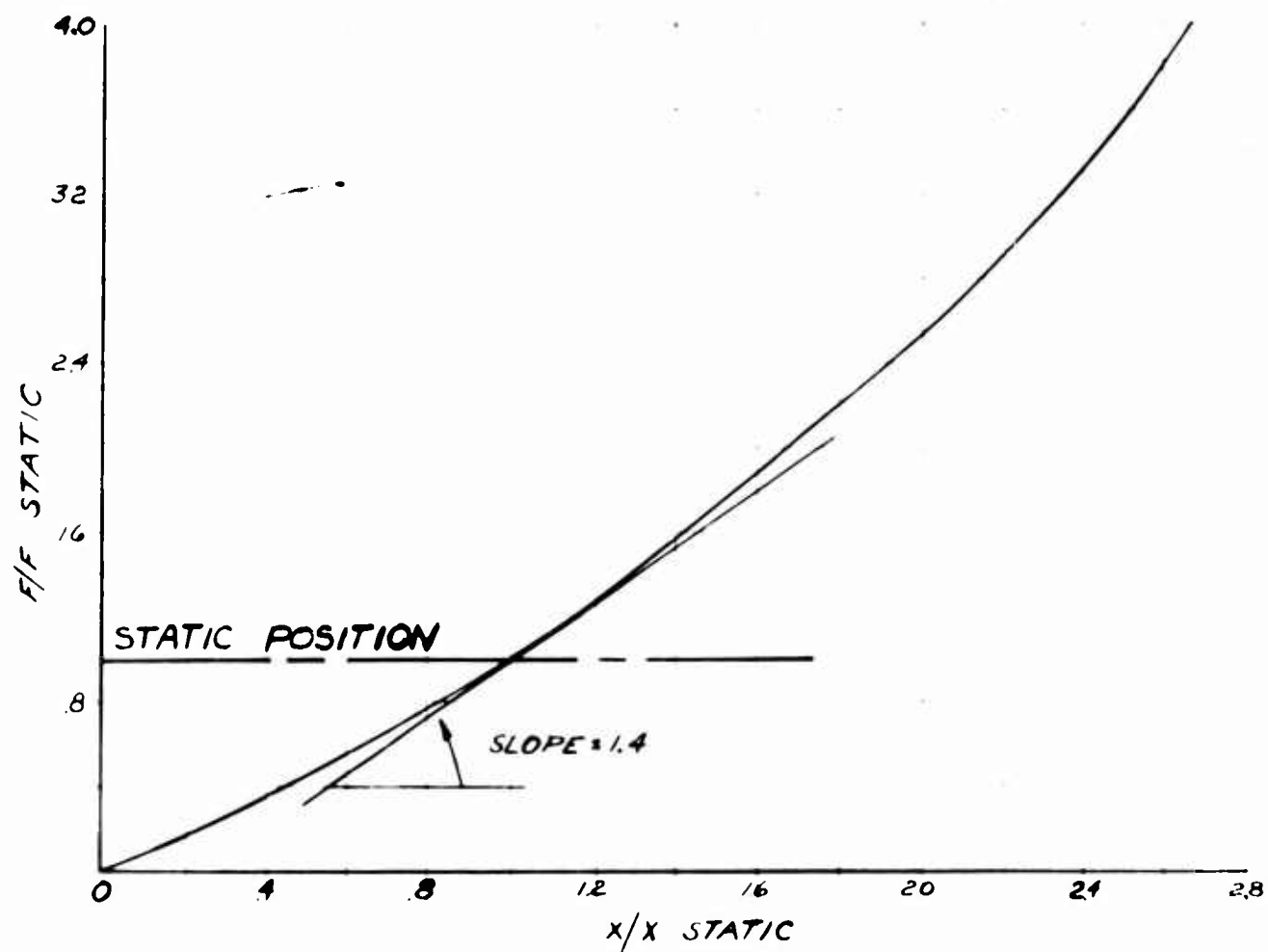


Figure 27 - Non-Dimensional Spring Rate for V/STOL Main and Nose Gear Oleo

Table 1

V/STOL Configuration General Data

Config. Data	Fixed Jet	Tilt Wing	Extended Flap	Tilt Prop	Buried Fan
a, Ft.	30.6	28.6	29.7	32.0	30.6
a ₁ , Ft.	1.47	3.43	2.34	2.51	1.43
a ₂ , Ft.	0.12	2.04	0.94	0.89	0.20
c ₁ , Lb-Sec/In	162	196	240	282	238
c ₂ , Lb-Sec/In	614	746	913	1070	905
e', Ft.	0.64	0.66	0.64	0.77	0.76
F _M , Lbs	-164,000	-200,000	-244,000	-286,000	-242,000
F _N , Lbs	- 8,000	-23,000	-19,000	-22,000	-11,000
h, Ft.	5.3	5.4	5.2	5.5	6.2
K ₁ , Lbs/In	4900	14,900	12,000	14,000	7,000
K ₂ , Lbs/In	118,000	143,000	175,000	205,000	174,000
K ₃ , Lbs/In	17,700	26,900	32,900	38,500	32,400
K ₄ , Lbs/In	44,300	52,700	65,800	77,100	65,200
K ₅ , Lbs/In	5,700	17,100	13,800	16,100	8,100
K ₆ , Lbs/In	60,900	73,900	90,400	77,100	89,700
l, Ft.	32.0	32.0	32.0	34.5	32.0
l ₁ , Ft.	10.3	10.2	10.4	10.5	9.2
l ₂ , Ft.	9.8	9.8	9.7	9.8	8.2
l ₃ , Ft.	11.0	11.3	11.4	11.5	10.0
M _M , Slugs	66.3	80.5	98.5	115.0	97.8
M _N , Slugs	7.97	24.1	19.5	22.6	11.4
r ² , Ft. ²	204	180	171	159	208
S, Ft. ²	1650	2365	2600	2560	2800
V _{LO} , Knots	108.5	53.5	59.0	65.1	114.0*
V _Z , Ft/Sec	9.0	9.0	9.0	9.0	9.0
W, Lbs	172,000	223,000	263,000	308,000	253,000
W ₀ , Lbs	232,000	334,000	394,000	462,000	380,000*
X _{MO} , In	10	10	10	10	10
X _{NO} , In	11.7	11.1	11.4	11.4	11.3
X _{MT} , In	5.1	5.2	5.1	5.2	5.2
X _{NT} , In	0.63	0.63	0.62	0.61	0.61
β, Radians	4.62	4.58	4.75	4.22	3.75
h _m = η _n	0.8	0.8	0.8	0.8	0.8
φ, Degrees	7.0	7.0	7.0	8.0	7.0

Notes: 1. K₂, K₄, K₆, C₂, M₁, and F_M are values for both main gears.

2. *Legislated for analyses where necessary.

III. PRELIMINARY STRUCTURAL DYNAMIC RESPONSE INVESTIGATION AND ANALYSIS

The purpose of these investigations and analyses is to provide a matrix of conditions and the resulting structural dynamic response. This data will eventually be reduced to a numerical chart that will provide the designer with a guide to the structural or operational problems involved for each of the V/STOL configurations. In addition, the matrix of analyses will point out the most severe operating condition in regard to structural response.

The parameters chosen are discussed in detail in each of the particular analyses as to the initial conditions for structural investigation.

In order to provide the matrix of analyses for five V/STOL configurations and eight separate parameter conditions it has been necessary to utilize preliminary design analysis methods. Within the scope of this contract investigation the preliminary analysis uses only linear methods in all parameter studies and the results form only a guide as to the structural responses. However, in such a large matrix of analyses the overall picture will provide a basis for determining the subsequent degree and relative criticalness of the configurations and the parameters.

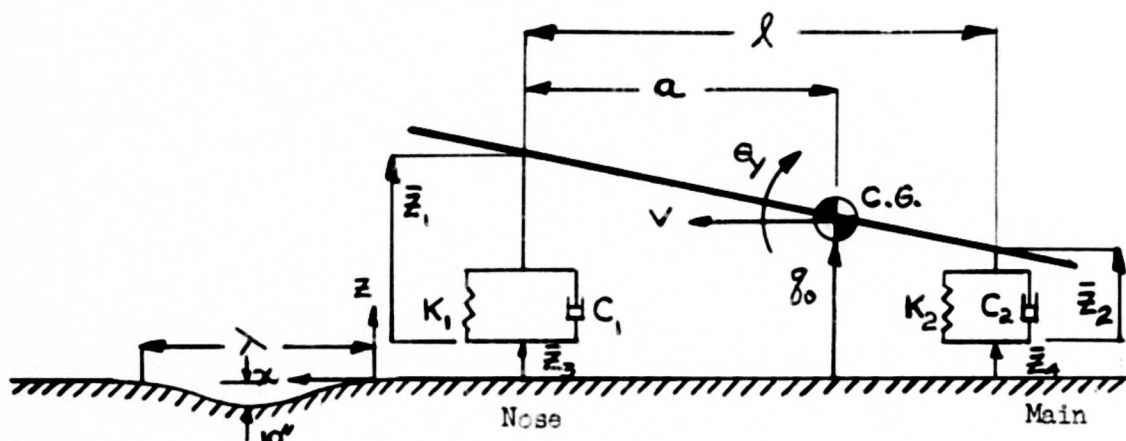
The structural data used in this section was defined and listed in the preceding section II. However the landing condition, Section IIIE, contains the analysis of gear impact loads and gear stroke which are used in the dynamic response analysis. The stroke used for condition IIIE is the result of considering the usual MIL Spec requirement (Ref. 2) which was required to furnish a basis for the subsequent impact analysis.

A. Ground Handling

1. Taxiing and Take-Off Run

The object of the analysis for this condition was to determine the degree of criticalness of landing gear loads upon entry into a runway dip. To simulate the maximum unprepared runway condition a 10 in. 1 - cosine dip was assumed and considered to be a once in a spectrum type load. The dynamic response analysis was made by numerically integrating the equations of motion in an IBM digital computer for a system with two degrees of freedom where the nose and main landing gear oleos are assumed to act as linear springs and dampers in the vertical direction.

The initial condition is with the aircraft in forward motion at a speed not exceeding the lift-off speed (Ref. Table 1). With the aircraft constrained to ground a rigid body analysis was performed as a preliminary investigation. The system is represented schematically in Fig. 28 where the positive sign convention and coordinates are defined.



Ref. Table 1 & 2 for values of K_1 , K_2 , C_1 , C_2 , a , l and λ

Figure 28 - Schematic of Aircraft and Runway Dip Geometry

The equation of the dip is:

$$z = -5(1 - \cos \frac{2\pi x}{\lambda})$$

where the total dip amplitude is equal to 10 inches.

The STOL gross weight (Ref. Table 1) was used for the structural response investigation. The take-off speed and STOL weight for the Buried Fan were legislated since no STOL capability for this aircraft exists within the requirement that the aircraft have the ability to take-off over a 50 ft. obstacle using a 1000 ft. runway. An approximate method for calculating STOL performance is contained in Appendix II. The objective of the STOL performance analysis is to determine at what overload gross weight each aircraft is capable of meeting STOL requirements.

The following is a derivation of the equations of motion of the nose and main gear. The absolute vertical motion at the center of gravity is:

$$\ddot{z}_0 = \ddot{z}_3 + \ddot{z}_1 + (\ddot{z}_4 + \ddot{z}_2 - \ddot{z}_3 - \ddot{z}_1) a/l \quad (6)$$

where \ddot{z}_3 is the nose gear forcing function and $x = Vt$.

$$\ddot{z}_3 = 0$$

$$\ddot{z}_3 = -5(1 - \cos \frac{2\pi Vt}{\lambda})$$

$$\ddot{z}_3 = 0$$

$$\text{for } t \leq 0$$

$$\text{for } \lambda/V \geq t \geq 0$$

$$\text{for } t \geq \lambda/V$$

and \ddot{z}_4 is the main gear forcing function.

$$\ddot{z}_4 = 0$$

$$\ddot{z}_4 = -5[1 - \cos \frac{2\pi V}{\lambda}(t - l/V)]$$

$$\ddot{z}_4 = 0$$

$$\text{for } t \leq l/V$$

$$\text{for } (l+\lambda)/V \geq t \geq l/V$$

$$\text{for } t \geq (l+\lambda)/V$$

Also the pitching motion at the center of gravity is:

$$\theta_y = -(\bar{z}_4 + \bar{z}_2 - \bar{z}_3 - \bar{z}_1)/l \quad (7)$$

The kinetic energy of the system is:

$$2KE = M \left[\dot{\bar{z}}_3 + \dot{\bar{z}}_1 + (\dot{\bar{z}}_4 + \dot{\bar{z}}_2 - \dot{\bar{z}}_3 - \dot{\bar{z}}_1) a/l \right]^2 + I_0 \left[(\dot{\bar{z}}_4 + \dot{\bar{z}}_2 - \dot{\bar{z}}_3 - \dot{\bar{z}}_1)/l \right]^2 \quad (8)$$

where M = aircraft mass, slugs, calculated from maximum gross weight.

I = pitching mass moment of inertia about the center of gravity, slug-ft.²

a = horizontal distance between nose gear and center of gravity, ft.

l = horizontal distance between nose and main gear, ft.

The potential energy of the system is:

$$2PE = K_1 \bar{z}_1^2 + K_2 \bar{z}_2^2 \quad (9)$$

where K₁ = nose gear spring constant, lbs/ft.

K₂ = main gear spring constant, lbs/ft.

And the energy dissipated per unit time is:

$$2DE = C_1 \dot{\bar{z}}_1^2 + C_2 \dot{\bar{z}}_2^2 \quad (10)$$

where C₁ = nose gear damping coefficient, lb. sec./ft.

C₂ = main gear damping coefficient, lb. sec./ft.

Expanding equation 8 and rearranging terms:

$$\begin{aligned} 2KE = & \dot{\bar{z}}_3^2 (M - 2Ma/l + Ma^2/l^2 + I_0/l^2) + \dot{\bar{z}}_4^2 (Ma^2/l^2 + I_0/l^2) \\ & + \dot{\bar{z}}_2^2 (M - 2Ma/l + Ma^2/l^2 + I_0/l^2) + \dot{\bar{z}}_1^2 (Ma^2/l^2 + I_0/l^2) \\ & + \dot{\bar{z}}_3 \dot{\bar{z}}_1 (2M - 4Ma/l + 2Ma^2/l^2 + 2I_0/l^2) + \dot{\bar{z}}_3 \dot{\bar{z}}_4 (2Ma/l - \\ & 2Ma^2/l^2 - 2I_0/l^2) + \dot{\bar{z}}_3 \dot{\bar{z}}_2 (2Ma/l - 2Ma^2/l^2 - 2I_0/l^2) + \\ & \dot{\bar{z}}_4 \dot{\bar{z}}_1 (2Ma/l - 2Ma^2/l^2 - 2I_0/l^2) + \dot{\bar{z}}_4 \dot{\bar{z}}_2 (2Ma^2/l^2 + \\ & 2I_0/l^2) + \dot{\bar{z}}_1 \dot{\bar{z}}_2 (2Ma/l - 2Ma^2/l^2 - 2I_0/l^2) \end{aligned} \quad (11)$$

Taking the partial derivative of the kinetic energy in equation 11 with respect to $\dot{\bar{z}}_1$:

$$\begin{aligned} \partial KE / \partial \dot{\bar{z}}_1 = & \dot{\bar{z}}_1 (M - 2Ma/l + Ma^2/l^2 + I_0/l^2) + \dot{\bar{z}}_3 (M - \\ & 2Ma/l + Ma^2/l^2 + I_0/l^2) + \dot{\bar{z}}_4 (Ma/l - Ma^2/l^2 - \\ & I_0/l^2) + \dot{\bar{z}}_2 (Ma/l - Ma^2/l^2 - I_0/l^2) \end{aligned} \quad (12)$$

If we let $A_{11} = (M - 2Ma/l + Ma^2/l^2 + I_0/l^2)$ and $A_{12} = (Ma/l - Ma^2/l^2 - I_0/l^2)$ then we can substitute A_{11} and A_{12} into equation 12 and find the time derivative.

$$\frac{d}{dt} \left(\frac{\partial KE}{\partial \dot{\bar{z}}_1} \right) = A_{11} \ddot{\bar{z}}_1 + A_{12} \ddot{\bar{z}}_2 + A_{12} \ddot{\bar{z}}_3 + A_{12} \ddot{\bar{z}}_4 \quad (13)$$

Now we determine the partial derivative of equation 9 with respect to \bar{z}_1 and equation 10 with respect to \bar{z}_1 .

$$\frac{\partial PE}{\partial \bar{z}_1} = K_1 \bar{z}_1 \quad (14)$$

$$\frac{\partial DE}{\partial \dot{\bar{z}}_1} = C_1 \dot{\bar{z}}_1 \quad (15)$$

Adding terms from the three energy equations we arrive at the Lagrange Equation with dissipative force.

$$\frac{d}{dt} \left(\frac{\partial KE}{\partial \dot{\bar{z}}_1} \right) + \frac{\partial PE}{\partial \bar{z}_1} + \frac{\partial DE}{\partial \dot{\bar{z}}_1} = 0 \quad (16)$$

Substituting from equations 13, 14, and 15 we determine the equation of motion for the nose gear.

$$A_{11} \ddot{\bar{z}}_1 + A_{12} \ddot{\bar{z}}_2 + C_1 \dot{\bar{z}}_1 + K_1 \bar{z}_1 = -A_{11} \ddot{\bar{z}}_3 - A_{12} \ddot{\bar{z}}_4 \quad (17)$$

In a similar manner, taking the partial derivative of equation 11 with respect to \bar{z}_2 :

$$\frac{\partial KE}{\partial \dot{\bar{z}}_2} = \dot{\bar{z}}_2 (Ma^2/l^2 + I_0/l^2) + \dot{\bar{z}}_3 (Ma/l - Ma^2/l^2 - I_0/l^2) + \dot{\bar{z}}_4 (Ma^2/l^2 + I_0/l^2) + \dot{\bar{z}}_1 (Ma/l - Ma^2/l^2 - I_0/l^2) \quad (18)$$

If we let $A_{13} = (Ma^2/l^2 + I_0/l^2)$ then we can substitute A_{12} and A_{13} into equation 18 and find the time derivative.

$$\frac{d}{dt} \left(\frac{\partial KE}{\partial \dot{\bar{z}}_2} \right) = A_{12} \ddot{\bar{z}}_1 + A_{13} \ddot{\bar{z}}_2 + A_{12} \ddot{\bar{z}}_3 + A_{13} \ddot{\bar{z}}_4 \quad (19)$$

Determining the partial derivative of equation 9 with respect to \bar{z}_2 and equation 10 with respect to \bar{z}_2 :

$$\frac{\partial PE}{\partial \bar{z}_2} = K_2 \bar{z}_2 \quad (20)$$

$$\frac{\partial DE}{\partial \dot{\bar{z}}_2} = C_2 \dot{\bar{z}}_2 \quad (21)$$

Using the same procedure that was used for the nose gear we determine the Lagrange Equation for the main gear.

$$\frac{d}{dt} \left(\frac{\partial KE}{\partial \dot{\bar{z}}_2} \right) + \frac{\partial PE}{\partial \bar{z}_2} + \frac{\partial DE}{\partial \dot{\bar{z}}_2} = 0 \quad (22)$$

Substituting from equations 19, 20 and 21 we determine the equation of motion for the main gear.

$$A_{12} \ddot{\bar{z}}_1 + A_{13} \ddot{\bar{z}}_2 + C_2 \dot{\bar{z}}_2 + K_2 \bar{z}_2 = -A_{12} \ddot{\bar{z}}_3 - A_{13} \ddot{\bar{z}}_4 \quad (23)$$

The natural frequency ω_N of the aircraft can now be determined by setting the right hand side of equations 17 and 23 equal to zero, omitting damping forces and substituting for $\ddot{\bar{z}}_1$ and $\ddot{\bar{z}}_2$.

Since the resulting equations now describe the free vibration condition it is therefore assumed that the relative motions are also harmonic, i.e.

$$\bar{z}_1 = \bar{z}_{1\max} \sin \omega t$$

$$\bar{z}_2 = \bar{z}_{2\max} \sin \omega t$$

therefore $\ddot{\bar{z}}_1 = -\bar{z}_{1\max} \omega_N^2 \sin \omega t$

and $\ddot{\bar{z}}_2 = -\bar{z}_{2\max} \omega_N^2 \sin \omega t$

$$-A_{11} \bar{z}_{1\max} \omega_N^2 - A_{12} \bar{z}_{2\max} \omega_N^2 + K_1 \bar{z}_{1\max} = 0 \quad (24)$$

$$-A_{12} \bar{z}_{1\max} \omega_N^2 - A_{13} \bar{z}_{2\max} \omega_N^2 + K_2 \bar{z}_{2\max} = 0 \quad (25)$$

Solving for ω_N^2 we arrive at:

$$\omega_N^2 = \frac{K_1 A_{12} + K_2 A_{11} \pm \sqrt{(K_1 A_{12} + K_2 A_{11})^2 - 4(A_{11} A_{13} - A_{12}^2)(K_1 K_2)}}{2(A_{11} A_{13} - A_{12}^2)} \quad (26)$$

Solving this equation yields the natural frequencies in translation and pitch. The critical dip wavelength λ for the pitch condition is equal to twice the distance between the nose and main gears or $\lambda = 2l$. To find the critical forward velocity we use the relation $\omega = 2\pi V/\lambda$ where ω_N is substituted for ω . If the velocity calculated from this equation exceeds the lift-off speed then the lift-off speed is substituted for V and λ is calculated. For the translation condition the critical speed is assumed to be equal to the lift-off speed. Using the rigid body natural frequencies the system is tuned to the corresponding λ from the equation $\omega = 2\pi V/\lambda$. Since ω_N and V are known λ can be calculated.

This analysis was conducted using the maximum gross weights and subsequently the static gear loads were computed on the same basis. Since these aircraft are traveling at high forward speeds (Ref. Table 2) the effect of wing lift may be a factor in computing the gear loads. This is accomplished by reducing the static gear loads according to the following equation.

$$F_{NS}, F_{MS} = F_N, F_M \left[1 - \left(\frac{V}{V_{LO}} \right)^2 \right] \quad (27)$$

where F_{NS}, F_{MS} = actual static gear load while traveling at V , lbs.

F_N, F_M = dead weight load, lbs.

V = forward velocity, ft./sec.

V_{LO} = lift-off velocity, ft./sec.

The total gear load is the sum of the static and dynamic loads (the dynamic load being over and above the static load). The dead weight gear loads were determined from static equilibrium conditions and the dynamic loads were computed by solving the equations of motion in the I.B.M. program.

The ultimate design landing gear loads are calculated from the usual design requirements for a three wheel level landing, braked roll, and tail down landing. The procedure for calculating loads is shown in Section IIIE and a summary of these loads is contained in Table 9.

The method of analysis specified in this portion was run on an IBM computer using the data specified in Table 2. The data of Table 9 lists the maximum loads on the main and nose landing gears. The loads were divided by the gross weight to show gear load factors for reference purposes. The maximum dynamic loads were superimposed onto the static loads and include the effects of possible wing lift. The analysis shows tension loads, which represent a condition where the aircraft would bounce off the ground. The limits of this analysis does not permit a discontinuous solution therefore it is obvious that it is only valid to the value of the compressive loading on the gear during the first initial impact.

In Figures 29 and 30 the time histories of the Tilt Wing nose and main landing gear loads are shown. The scale on the left hand side shows the loading without wing lift while the right hand scale is a superimposed wing lift effect. These figures illustrates that wing lift could cause a greater tendency for the gears to bounce off the ground. The compressive loads on the main and nose gears are more critical for the dip condition when tuned for translation.

BLANK PAGE

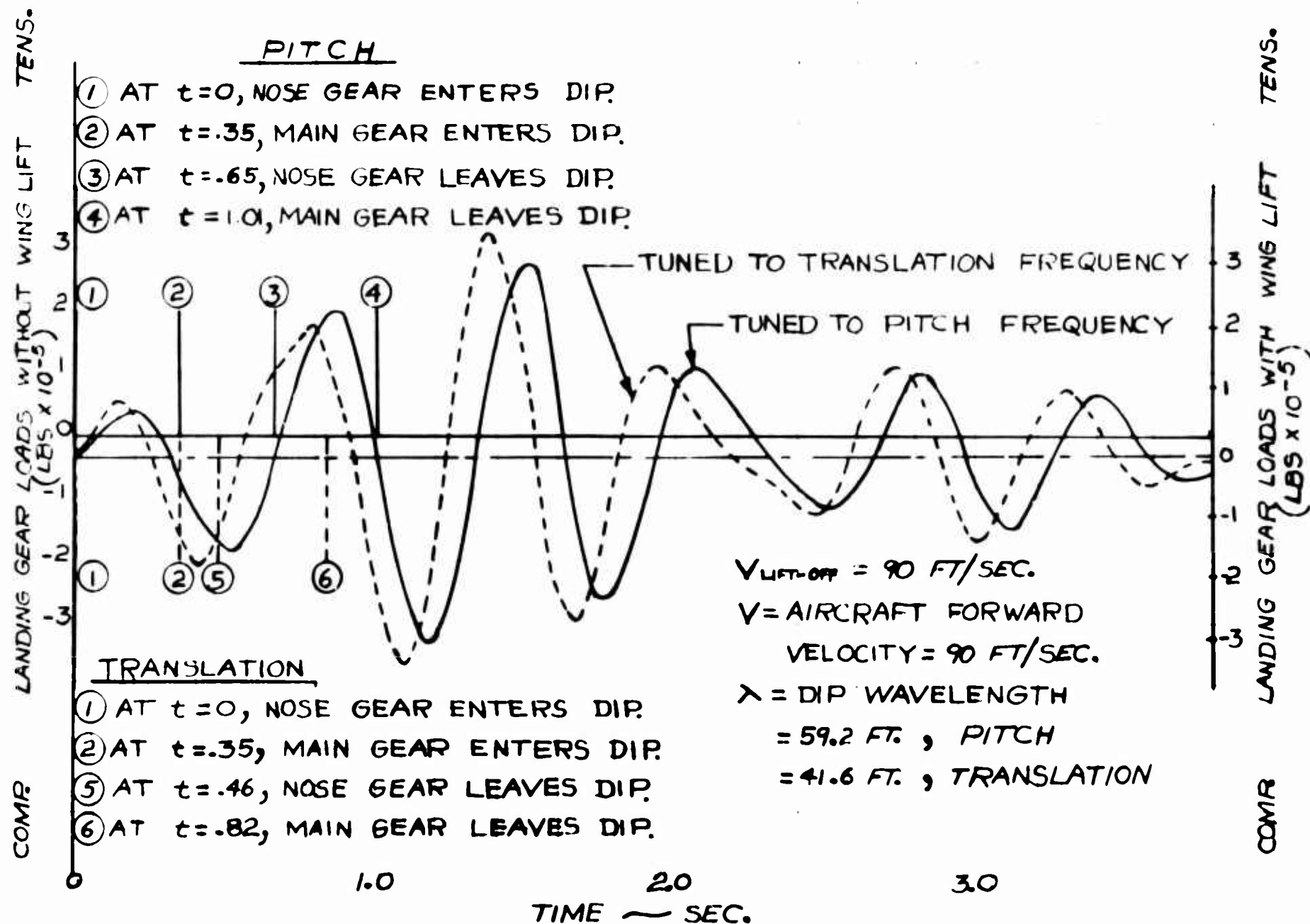


Figure 29 - Time History of Nose Landing Gear Loads for Preliminary Runway Dip Analysis

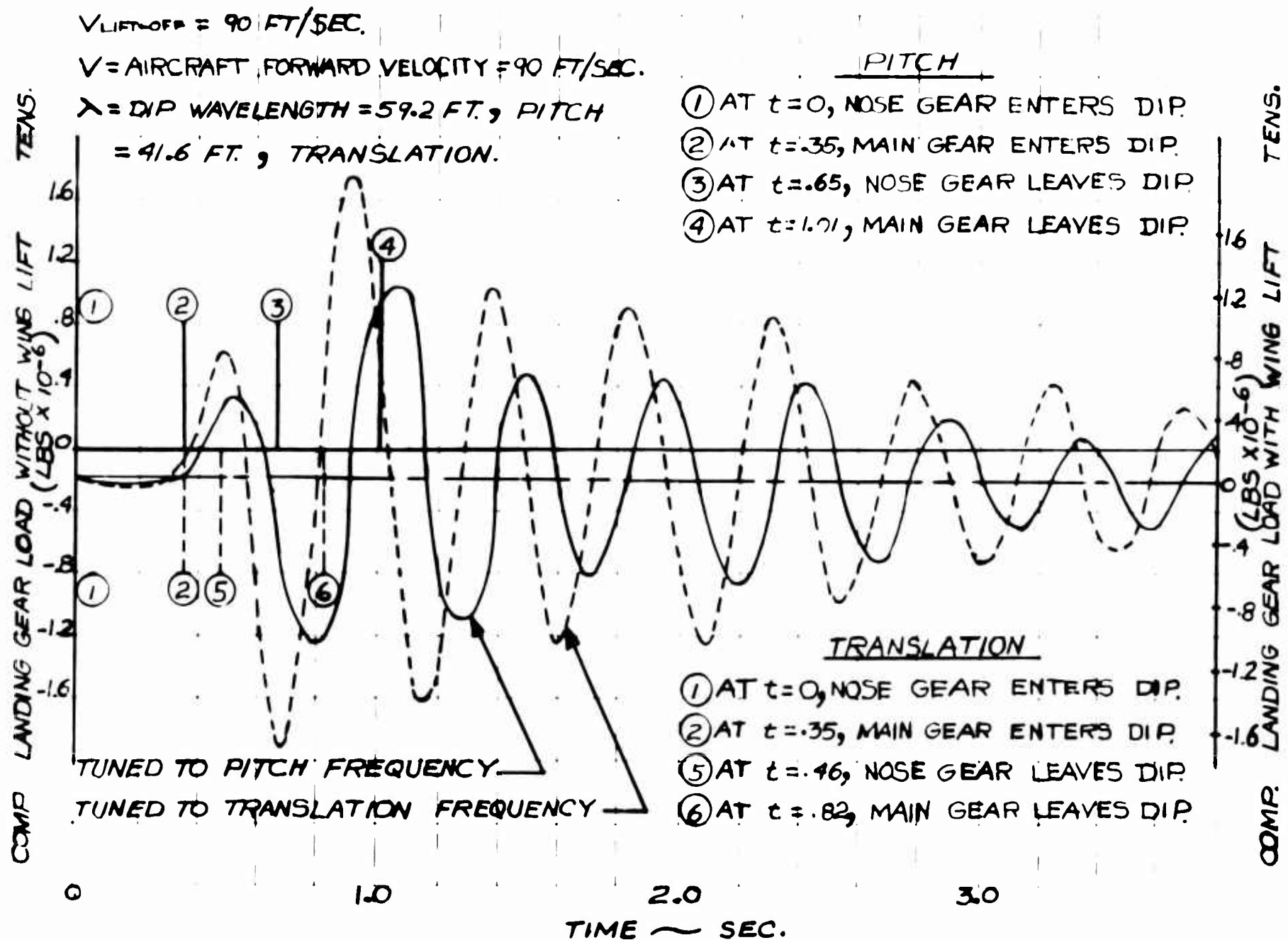


Figure 30 - Time History of Main Landing Gear Loads for Preliminary Runway Dip Analysis

BLANK PAGE

Table 2 - Ground Run Dip Analysis: Maximum Gear Loads

	Config. Data	Fixed Jet	Tilt Wing	Extended Flap	Tilt Prop	Buried Fan
	V _{Lift-Off} , Knots	108.5	53.5	59.0	65.1	114.0*
	FN, Nose Gear Dead Wt. at Max. G.W., Lbs	-10,700	-35,700	-28,800	-33,000	-17,000*
	FM, Total Main Gear Dead Wt. at Max.G.W.Lbs	-222,000	-299,000	-366,000	-429,000	-362,000*
PITCH	λ , Dip Wavelength, Ft	64	59.2	64	69	64
	V, Aircraft Fwd.Vel.,Kts.	37.6	53.5	49.4	58.6	36.5
	FNS,Nose Static Load $\pm V$	-9400	0	-8700	-6300	-15,300
	FMS Main Static Load $\pm V$	-195,000	0	-110,000	-81,500	-325,000
	FNS/W	-0.05	0	-0.03	-0.02	-0.06
	FMS/W	-1.13	0	-0.42	-0.26	-1.28
	FN DYN. (Max.) Lbs	+91,000 -86,000	+297,000 -297,000	+231,000 -253,000	+251,000 -291,000	+134,000 -126,000
	FN DYN. (Max.), Lbs	+219,000 -227,000	+1,253,000 -1,096,000	+757,000 -928,000	+1,402,000 -1,317,000	+324,000 -354,000
	FN DYN./W	+0.53 -0.50	+1.33 -1.33	+0.88 -0.96	+0.82 -0.95	+0.53 -0.50
	FM DYN/W	+1.28 -1.32	+5.62 -4.91	+2.88 -3.53	+4.55 -4.27	+1.28 -1.40
	(FNS + FN DYN)/W	+0.47 -0.56	+1.33 -1.33	+0.85 -1.00	+0.80 -0.97	+0.47 -0.56
	(FMS + FM DYN)/W	+0.14 -2.45	+5.62 -4.91	+2.46 -3.95	+4.29 -4.53	+0 -2.68
TRANSLATION	λ , Dip Wavelength, Ft	64	41.6	46.3	53.2	64
	V, Aircraft Forward Velocity, Kts.	86.0	53.5	59.0	65.1	81.7
	FNS,Nose Static Load $\pm V$	-4,000	0	0	0	-8,300
	FMS,Main Static Load $\pm V$	-82,800	0	0	0	-177,000
	FNS/W	-0.02	0	0	0	-0.03
	FMS/W	-0.48	0	0	0	-0.07
	FN DYN (Max), Lbs	+117,000 -87,000	+346,000 -342,000	+285,000 -318,000	+287,000 -353,000	+166,000 -125,000
	FM DYN (Max), Lbs	+1,327,000 -1,211,000	+1,918,000 -1,748,000	+2,119,000 -1,974,000	+2,527,000 -2,242,000	+2,020,000 -1,803,000

* Legislated for this analysis

Table 2 - Ground Run Dip Analysis: Maximum Gear Loads (Con't)

TRANSLATION ↓	Config. Data	Fixed Jet	Tilt Wing	Extended Flap	Tilt Prop	Burned Fan
↑	$F_N \text{ DYN}/W$	+0.68 -0.51	+1.55 -1.53	+1.08 -1.21	+0.94 -1.14	+0.66 -0.50
	$F_M \text{ DYN}/W$	+7.72 -7.03	+8.59 -7.83	+8.07 -7.50	+8.20 -7.27	+7.97 -7.13
	$(F_{NS} + F_N \text{ DYN})/W$	+0.65 -0.53	+1.55 -1.53	+1.08 -1.21	+0.94 -1.14	+0.62 -0.53
	$(F_{MS} + F_M \text{ DYN})/W$	+7.24 -7.51	+8.59 -7.83	+8.07 -7.50	+8.20 -7.27	+7.27 -7.83

Notes: (1) $F_{NS} = F_N \left[1 - \left(\frac{V}{V_{Lo}} \right)^2 \right]$

$$F_{MS} = F_M \left[1 - \left(\frac{V}{V_{Lo}} \right)^2 \right]$$

(2) Sign Convention:

+ Tension load in oleo

(3) F_M , F_{MS} , $F_M \text{ DYN}$, is the total load on both main gears.

(4) Loads are normalized by dividing by the design gross weight.

2. Starting and Stopping While Towing

The dynamic response analysis for this condition was made by numerically integrating the equations of motion in an I.B.M. digital computer. The computer program supplied information on the time variation of nose and main gear vertical loads as well as nose gear longitudinal loads for a system with 5 degrees of freedom. The nose and main landing gear oleo and tire are assumed to act as a linear spring and damper in the vertical direction in addition to a nose gear spring acting in the longitudinal direction. The input acceleration to the aircraft by the towing vehicle can be described by the following equation.

$$\begin{aligned}\ddot{x}_1 &= X \sin \omega t & \text{For } \omega t \leq \pi \\ \ddot{x}_1 &= 0 & \text{For } \omega t \geq \pi\end{aligned}\quad (28)$$

where \ddot{x}_1 = longitudinal acceleration at the nose gear, ft/sec²

X = maximum longitudinal input acceleration = $-1/3 g = -10.8 \text{ ft/sec}^2$

If $\ddot{x}_1 = X \sin \omega t$

then $\dot{x}_1 = -X/\omega \cos \omega t + C_1$

Since $\dot{x}_1 = 0$ at $t = 0$ it follows that $C_1 = \frac{X}{\omega}$

Therefore at $\omega t = \pi$, where $\omega = 6.35 \text{ rad/sec}$.

$$\dot{x}_1 = -X/\omega \cos \pi + X/\omega$$

or $X = \omega \dot{x}_1 / 2 \quad (29)$

Since the final velocity equals 2 knots, $X = -10.8 \text{ ft/sec}^2$. The forward velocity of the aircraft resulting from this input increases from 0 to 2 knots in approximately 0.5 sec. This can be represented graphically as follows:

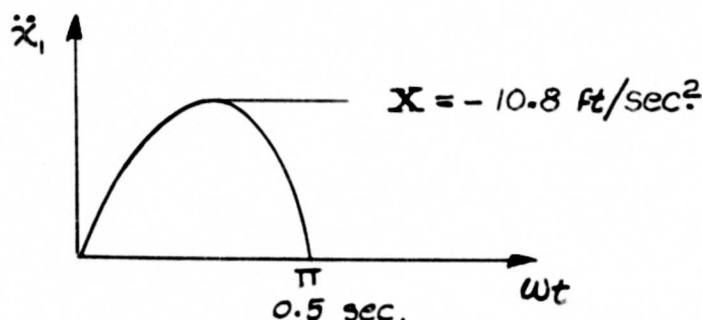


Figure 31 - Sinusoidal Towing Input Acceleration

This input yields maximum longitudinal nose gear loads which corresponds to a value resulting from the procedure specified in Mil-A-8862 (ASG), (Ref. 2).

A rigid body analysis was performed as a preliminary investigation with the aircraft constrained to ground. The system is represented schematically in Fig. 32 where the positive sign convention and coordinates are defined.

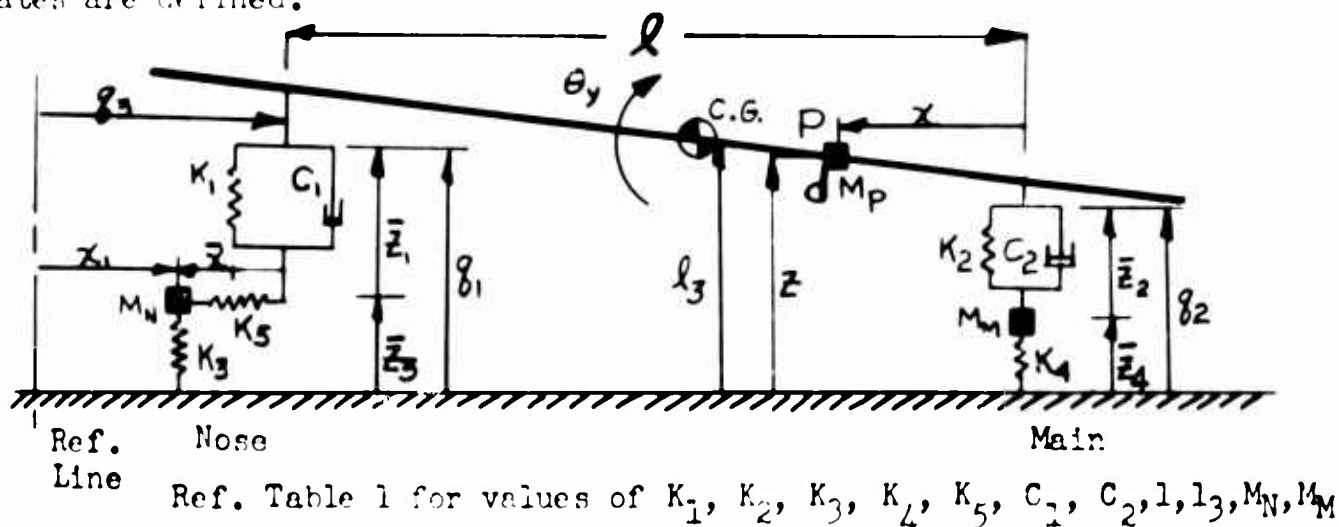


Figure 32 - Schematic of Aircraft Geometry for Towing Condition

The following is a derivation of the equations of motion of the system.

The absolute vertical motion of the main gear oleo is:

$$g_2 = \bar{z}_4 + \bar{z}_2 \quad (30)$$

The absolute vertical motion of the nose gear oleo is:

$$g_1 = \bar{z}_3 + \bar{z}_1 \quad (31)$$

The absolute vertical motion of an arbitrary point P is:

$$z_p = g_2(1-x/l) + (x/l)g_1 = (\bar{z}_4 + \bar{z}_2)(1-x/l) + x/l(\bar{z}_3 + \bar{z}_1) + z \quad (32)$$

where x = the horizontal distance between the main gear and the arbitrary point P.

The absolute longitudinal motion of the same point P is:

$$x_p = x_1 - \bar{z}_1 + l_3/l(g_1 - g_2) = x_1 - \bar{z}_1 + l_3/l(\bar{z}_3 + \bar{z}_1 - \bar{z}_4 - \bar{z}_2) - x$$

The absolute longitudinal motion of the nose gear is: (33)

$$g_3 = x_1 - \bar{z}_1 \quad (34)$$

We differentiate equations 30 thru 34 with respect to time and arrange them in matrix form where the left column is in absolute coordinates, the right column is in relative coordinates and $[\mu]$ is the transformation matrix.

$$\begin{Bmatrix} \dot{g}_2 \\ \dot{g}_1 \\ \dot{g}_3 \\ \dot{z}_p \\ \dot{x}_p \\ \dot{\bar{z}}_4 \\ \dot{\bar{z}}_3 \end{Bmatrix} = \begin{bmatrix} 1 & 1 & & & & \\ & & 1 & 1 & & \\ & & & & -1 & 1 \\ 1-\chi/l & 1-\chi/l & \chi/l & \chi/l & & \\ -l_3/l & -l_3/l & l_3/l & l_3/l & -1 & 1 \\ 1 & & & & & \\ & & 1 & & & \end{bmatrix} \begin{Bmatrix} \dot{\bar{z}}_4 \\ \dot{\bar{z}}_2 \\ \dot{\bar{z}}_3 \\ \dot{\bar{z}}_1 \\ \dot{\chi}_1 \\ \dot{\chi}_1 \end{Bmatrix}$$

This can be also written as $\{\dot{g}\} = [\mu]\{\dot{\bar{g}}\}$

The expression for the kinetic energy can be written as follows:

$$2KE = \int_{m_p} \{\dot{\bar{g}}\}' [\mu]' [M] [\mu] \{\dot{\bar{g}}\} \quad (35)$$

Evaluating $[\mu]' [M] [\mu]$ in equation 35:

$$[\mu]'[M][\mu] =$$

1			$1-x/l$	$-l_3/l$	1	
1			$1-x/l$	$-l_3/l$		
	1		x/l	l_3/l		1
	1		x/l	l_3/l		
		-1		-1		
		1		1		

					$-M_N$	M_N
$M_p(1-x/l)$	$M_p(1-x/l)$	$M_p(x/l)$	$M_p(x/l)$			
$-M_p(l_3/l)$	$-M_p(l_3/l)$	$M_p(l_3/l)$	$M_p(l_3/l)$	$-M_p$	M_p	
M_M						
		M_N				

$$=$$

A'	B'	C'	C'	D'	$-D'$
B'	B'	C'	C'	D'	$-D'$
C'	C'	E'	F'	$-D'$	D'
C'	C'	F'	F'	$-D'$	D'
D'	D'	$-D'$	$-D'$	G'	$-G'$
$-D'$	$-D'$	D'	D'	$-G'$	H'

where

$$A' = M_p(1-x/l)^2 + M_p(l_3/l)^2 + M_M$$

$$B' = M_p(1-x/l)^2 + M_p(l_3/l)^2$$

$$C' = M_p(1-x/l)(x/l) - M_p(l_3/l)^2$$

$$D' = M_p(l_3/l)$$

$$E' = M_p(x/l)^2 + M_p(l_3/l)^2 + M_N$$

$$F' = M_p(x/l)^2 + M_p(l_3/l)^2$$

$$G' = M_p + M_N + M_M$$

$$H' = M_p + M_N + M_M = G'$$

(36)

where dM_p = incremental mass at point P, slugs
 M_N = unsprung mass at nose gear, slugs
 M_M = unsprung mass at main gears, slugs

Integrating the preceding equations:

$$\left. \begin{aligned} A &= \int A' = M(1 + l_3^2/l^2) - 2S_0/l + I/l^2 + M_N \\ B &= \int B' = M(1 + l_3^2/l^2) - 2S_0/l + I/l^2 \\ C &= \int C' = -M(l_3/l)^2 + S_0/l - I/l^2 \\ D &= \int D' = M(l_3/l) \\ E &= \int E' = I/l^2 + M(l_3/l)^2 + M_N \\ F &= \int F' = I/l^2 + M(l_3/l)^2 \\ G &= \int G' = M + M_N + M_M \end{aligned} \right\} \quad (37)$$

where M = total sprung mass of the fuselage, slugs, calculated from the maximum gross weight $= \int_{m_p} dM_p$

S_0 = moment unbalance about the nose gear, slug ft. $= \int_{m_p} x dM_p$

I = mass moment of inertia about the nose gear, slug ft.² $= \int_{m_p} x^2 dM_p$

Writing the equations for the potential and dissipative energies of the system:

$$2PE = K_1 \bar{x}_1^2 + K_2 \bar{x}_2^2 + K_3 \bar{x}_3^2 + K_4 \bar{x}_4^2 + K_5 \bar{x}_1^2 \quad (38)$$

and

$$2DE = C_1 \dot{\bar{x}}_1^2 + C_2 \dot{\bar{x}}_2^2 \quad (39)$$

By following a procedure similar to that used with the kinetic energy equation we arrange equations 38 and 39 in matrix form and determine the final expression for the equations of motion of the system.

(40)

$$\begin{bmatrix} A & B & C & C & D \\ B & B & C & C & D \\ C & C & E & F & -D \\ C & C & F & F & -D \\ D & D & -D & -D & G \end{bmatrix} \begin{Bmatrix} \ddot{\bar{x}}_1 \\ \ddot{\bar{x}}_2 \\ \ddot{\bar{x}}_3 \\ \ddot{\bar{x}}_4 \\ \ddot{\bar{x}}_1 \end{Bmatrix} + \begin{bmatrix} & & & & \\ & C_2 & & & \\ & & & & \\ & & & C_1 & \\ & & & & \end{bmatrix} \begin{Bmatrix} \dot{\bar{x}}_1 \\ \dot{\bar{x}}_2 \\ \dot{\bar{x}}_3 \\ \dot{\bar{x}}_4 \\ \dot{\bar{x}}_1 \end{Bmatrix} + \begin{bmatrix} K_4 & & & & \\ & K_2 & & & \\ & & K_3 & & \\ & & & K_1 & \\ & & & & K_5 \end{bmatrix} \begin{Bmatrix} \ddot{\bar{x}}_4 \\ \ddot{\bar{x}}_2 \\ \ddot{\bar{x}}_3 \\ \ddot{\bar{x}}_1 \\ \ddot{\bar{x}}_1 \end{Bmatrix} = \ddot{\bar{x}} \begin{Bmatrix} D \\ D \\ -D \\ -D \\ G \end{Bmatrix}$$

Since the dynamic gear loads computed from the preceding equation are over and above static loads the total gear loads are the sum of the dynamic and static loads. Static gear loads were calculated using the maximum gross weights since the dynamic analysis was performed on this basis. The dead weight gear loads were computed from static equilibrium conditions.

The calculations of the resulting loads are shown in Table 3. The dead weight forces are superimposed onto the vibratory forces resulting in the maximum gear loadings. The data calculated shows the maximum loads on the main gear will always be a compressive loading which is almost obvious from the fact that the main gear is aft of the aircraft c.g. The nose gear peak loads indicate a tension load could exist, therefore the analysis can only be used as a guide since it could be expected that the nose gear will bounce off the ground during some portion of the towing impulse.

Table 3 shows only the loads that pertain to towing start. If the aircraft were stopped abruptly the signs of the dynamic loads would change for all cases. The drag loads are the most critical and bending of the gear in the drag direction is the major problem. The absolute value for the drag loads apply for either starting or stopping while towing. Therefore the analysis is complete for this condition for the most critical load in absolute value.

Table 3 - Towing Start Analysis: Maximum Landing Gear Loads

Config. Data	Fixed Jet	Tilt Wing	Extended Flap	Tilt Prop	Buried Fan
F_N , Nose Gear Dead Wt. at Max. G.W. - Lbs	-10,700	-35,700	-28,800	-33,000	-17,000
F_M , Total Main Gear Dead Wt. at Max. G.W. - lbs	-222,000	-299,000	-366,000	-429,000	-362,000
F_N/W	-0.06	-0.16	-0.11	-0.11	-0.07
F_M/W	-1.29	-1.34	-1.39	-1.39	-1.43
F_N DYN. - Lbs (Max. Vertical)	+27,300 -27,700	+63,600 -63,600	+59,000 -60,000	+70,700 -72,000	+40,000 -40,700
F_M DYN. - Lbs (Max. Vertical)	+30,700 -71,000	+78,700 -95,700	+65,300 -113,000	+52,400 -124,000	+52,700 -104,000
F_{ND} DYN. - Lbs (Max. Longitudinal)	+74,000 -76,000	+129,000 -130,000	+137,000 -144,000	+160,000 -167,000	+111,000 -115,000
F_N DYN/W	+0.16 -0.16	+0.29 -0.29	+0.22 -0.23	+0.23 -0.23	+0.16 -0.16
F_M DYN./W	+0.18 -0.41	+0.35 -0.43	+0.25 -0.43	+0.17 -0.40	+0.31 -0.41
F_{ND} DYN/W	+0.43 -0.44	+0.58 -0.58	+0.52 -0.55	+0.52 -0.54	+0.44 -0.45
$(F_N + F_N \text{ DYN})/W$	+0.10 -0.22	+0.13 -0.45	+0.11 -0.34	+0.12 -0.34	+0.09 -0.23
$(F_M + F_M \text{ DYN})/W$	-1.11 -1.70	-0.99 -1.77	-1.14 -1.82	-1.22 -1.79	-1.12 -1.84

Notes: (1) F_M , F_M DYN. = Dead weight and dynamic vertical load on both main gears.

(2) F_N , F_N DYN. = Dead weight and dynamic vertical load on nose gear.

(3) F_{ND} DYN. = Longitudinal dynamic load on nose gear

(4) W = Normal design gross weight.

(5) Sign Convention: + Tension load in Oleo

+ Aft acting load

3. Tiedown

Tiedown conditions are usually checked for local structures and fitting attachments. Because the V/STOL configurations represent some departure in wing structural characteristics a brief analytical check was made on the criticality of the ground gust condition.

The initial condition is with the aircraft tied down rigidly to the ground through landing gear and/or fuselage attachment points. For the purposes of this analysis the aircraft was considered rigid to ground with only the elasticity of the wing responding to the transient air loading.

For a preliminary type of analytical investigation, it is assumed that the gust is rapidly applied and from a vector direction so as to obtain the maximum effect. The gust is then assumed to die out rapidly so that the effect is equivalent to a full cycle versed-sine pulse. The peak gust velocity is 60 knots.

The lift loading on the wing is then:

$$L = \beta \alpha_w \frac{1}{2} \rho U^2 S / 2 \quad (41)$$

where L = the gust lift per wing, lbs.

β = airfoil lift slope, radians

α_w = geometric angle of attack = .175 radians (10°),
a representative value for this analysis

U = gust velocity, 84.6 ft./sec. as peak value

$\frac{1}{2} S$ = $\frac{1}{2}$ actual wing area, ft.²

The forcing function on the wing is the lift loading assumed as an exponential ramp input. Each of the modes will respond to this type of dynamic loading and the response will depend on the ratio of the pulse period to the natural period of the structure.

The resulting bending moment is conservatively taken as the result of the full fundamental response of 1.7. The value of 1.7 is the maximum response factor that can be obtained from a versed-sine impulse (Fig. 4-13 of Ref. 5). Undoubtedly some relief will be due to the fact that the higher modes will have their own reduced modal response factor. However, the vibration analysis (Appendix IV) has shown the fundamental mode to be a dominant contributor for bending with induced torsion coupling.

The half exponential input was selected as being most representative for the gust from the study of the gust penetration analysis subsequently shown in this report. The initial build up of lift will be similar to the type found for the aircraft free to translate in a vertical direction. However, the reduction usually considered (gust alleviation factor) due to the vertical aircraft velocity (which would reduce the effective angle of attack) is omitted for the aircraft fixed to ground. The pulse time is used as twice the time usually taken to build up to peak lift, this being dependent on the chord and velocity of the gust, i.e.

$$t = sC/2U = \text{time for peak build-up} \quad (42)$$

where s is the number of semi-chords

C is the chord of the wing in ft.

U is the gust velocity, ft./sec.

Other equations for this forcing function are the same as subsequently shown in detail for the gust penetration in Section III D. The response factor is dependent on the ratio of the lift build up time to the natural period of the structure. The response factor is then the ratio of the dynamic to static amplitudes of wing motion. In this case the resulting bending moment will be the combination of the lg wing loadings with the peak wing lift (in positive direction) plus the vibratory response on the wing inertial loadings from a first modal contribution. Since the body is fixed to ground the inertial loadings are about the lg dead weight condition.

The steady state loads and the resultant moments, torsions and stresses are contained in Table 4. Maximum bending and shear stresses at the wing root are calculated from the following equations.

$$S_b = \frac{BM}{Z_b} \quad (43)$$

$$S_s = \frac{TM}{Z_t} \quad (44)$$

where S_b, S_s = bending and shear stresses, lbs/in²

BM, TM = bending and torsional moments, in - lbs

Z_b, Z_t = bending and torsional section moduli, in³

Table 4 - Tiedown Condition: 60 Knot Wing Root Moments, Torsions
and Stresses

Config. Data	Fixed Jet	Tilt Wing	Extended Flap	Tilt Prop	Buried Fan
β , Lift Slope, Radians	4.62	4.58	4.75	4.22	3.75
$1/2S$, Wing Area, Ft ²	825	1183	1300	1280	1400
$L = \beta \alpha_w (1/2) \rho V^2 (S/2)$ Wing Lift, Lbs.	8080	11,500	13,100	11,450	11,120
$N_z = L/(W/2)$, Load Factor	0.094	0.103	0.100	0.074	0.088
Inertial Response Factor	2.0	2.0	2.0	2.0	1.9
1G Steady Weight Loads					
Bending Moment	11,200,000	26,800,000	36,700,000	25,200,000	9,300,000
Torsional Moment	300,000	3,400,000	3,400,000	2,100,000	1,600,000
Peak Gust Loading					
Bending Moment	1,700,000	3,900,000	5,200,000	3,500,000	2,500,000
Torsional Moment	153,000	151,000	196,000	196,000	566,000
Peak Loading with Response					
Bending Moment	-	-	-	-	-47,000
Torsional Moment	-700,000	2,800,000	3,500,000	3,400,000	-870,000
	+244,000	-111,000	-144,000	-2,400,000	-2,900
Maximum Loading					
Bending Moment	10,200,000	25,700,000	34,900,000	25,100,000	7,800,000
Torsional Moment	697,000	3,300,000	3,300,000	4,300,000	1,100,000
Maximum Bending Stress, PSI	15,900	22,800	25,200	11,200	3,700
Maximum Shear Stress, PSI	1,360	7,100	7,500	8,100	790

Notes: (1) $\alpha_w = 10/57.3$ Rad.

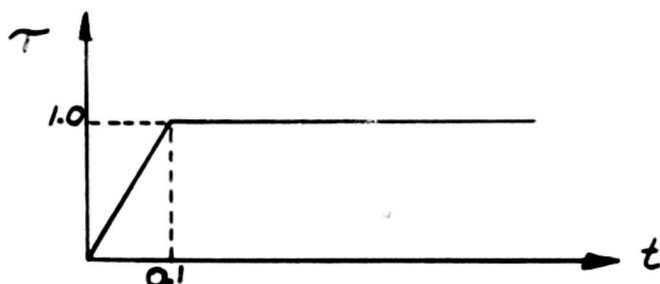
(2) Sign Convention

Bending + Compression on upper surface of wing

Torsion + Nose up twist

4. Braking

This condition was analyzed for an initial forward velocity of 30 knots assuming a linear force-time gradient (rise time = 0.1 sec.) until the maximum drag load is reached. This can be represented graphically as follows:



where \mathcal{T} = instantaneous braking force/steady state braking force

Figure 33 - Drag Load Force - Time Gradient

The main and nose gear braking or drag forces are:

$$F_{MD} = -C_F(-K_4 Z_2 + F_M) \mathcal{T} |\dot{x}_2| / \dot{x}_2 \quad (45)$$

where F_{MD} = main gear drag force , lbs.

C_F = coefficient of friction

F_M = main gear static vertical dead weight load , lbs.

$|\dot{x}_2| / \dot{x}_2$ = sign of x_2 where x_2 = absolute motion

$$F_{ND} = -C_F(-K_3 Z_1 + F_N) \mathcal{T} |\dot{x}_1| / \dot{x}_1 \quad (46)$$

where F_{ND} = nose gear drag force , lbs.

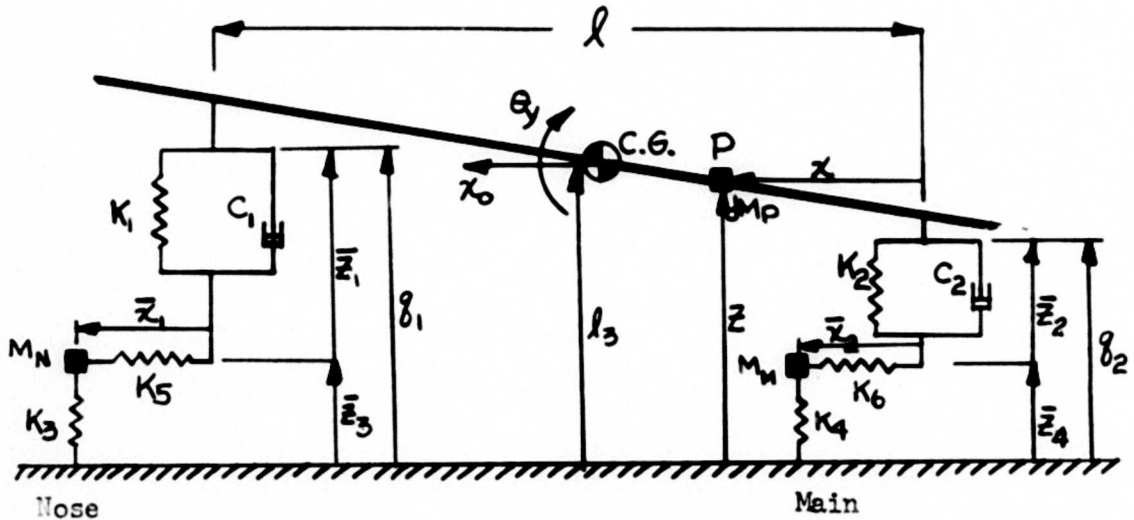
F_N = nose gear static vertical dead weight load , lbs.

$|\dot{x}_1| / \dot{x}_1$ = sign of x_1 where x_1 = absolute motion

When the brakes are applied there is a possibility that under the action of the braking force a condition can exist where the landing gears will have a velocity in the aft direction (with respect to the fuselage) greater than the forward velocity of the aircraft. If this occurs the direction of the drag force is reversed. The terms $|\dot{x}_1| / \dot{x}_1$ and $|\dot{x}_2| / \dot{x}_2$ are used in the computer analysis to change the sign of the absolute longitudinal motions of the nose and main gears and hence change the sign of the drag load.

The equations of motion were solved by numerical integration in an I.B.M. digital computer for a system with 6 degrees of freedom. The output from the computer program supplied information on the time variation

of nose and main gear vertical and longitudinal loads. A rigid body analysis was performed as a preliminary investigation. The system is represented schematically in Fig. 34 where the positive sign convention and coordinates are defined. The nose and main landing gear oleos and tires are assumed to act as a linear spring and damper in both the vertical and longitudinal directions.



Ref. Table 1 for values of $K_1, K_2, K_3, K_4, K_5, K_6, C_1, C_2, l, l_3, M_N$ and M_M

Figure 34 - Schematic of Aircraft Geometry for Braking Condition

The following is a derivation of the equations of motion of the system.

The absolute vertical motion of the main gear oleo is:

$$g_2 = \bar{z}_4 + \bar{z}_2 \quad (47)$$

The absolute vertical motion of the nose gear oleo is:

$$g_1 = \bar{z}_3 + \bar{z}_1 \quad (48)$$

The absolute longitudinal motion of the nose gear is:

$$x_1 = -l_3/l(\bar{z}_4 + \bar{z}_2) + l_3/l(\bar{z}_3 + \bar{z}_1) + \bar{x}_1 + x_0 \quad (49)$$

The absolute longitudinal motion of the main gear is:

$$x_2 = -l_3/l(\bar{z}_4 + \bar{z}_2) + l_3/l(\bar{z}_3 + \bar{z}_1) + \bar{x}_2 + x_0 \quad (50)$$

The absolute vertical motion of an arbitrary point P is:

$$z_p = (1 - x/l)(\bar{z}_4 + \bar{z}_2) + x/l(\bar{z}_3 + \bar{z}_1) + z \quad (51)$$

where x = the horizontal distance between the main gear and the arbitrary point P.

We differentiate equations 47 thru 51 with respect to time and arrange them in matrix form where the left column is in absolute coordinates, the right column is in relative coordinates and $[\mu]$ is the transformation matrix.

$$\left\{ \begin{array}{c} \dot{\bar{z}}_4 \\ \dot{g}_2 \\ \dot{\bar{z}}_3 \\ \dot{g}_1 \\ \dot{\chi}_1 \\ \dot{\chi}_2 \\ \dot{\bar{z}}_p \\ \dot{\chi}_0 \end{array} \right\} = \begin{bmatrix} 1 & & & & & & \\ 1 & 1 & & & & & \\ & & 1 & & & & \\ & & 1 & 1 & & & \\ -l_3/l & -l_3/l & l_3/l & l_3/l & 1 & & 1 \\ -l_3/l & -l_3/l & l_3/l & l_3/l & & 1 & 1 \\ 1-\chi/l & 1-\chi/l & \chi/l & \chi/l & & & \\ & & & & & & 1 \end{bmatrix} \left\{ \begin{array}{c} \dot{\bar{z}}_4 \\ \dot{\bar{z}}_2 \\ \dot{\bar{z}}_3 \\ \dot{\bar{z}}_1 \\ \dot{\chi}_1 \\ \dot{\chi}_2 \\ \dot{\chi}_0 \end{array} \right\}$$

This can be written as $\{\dot{g}\} = [\mu]\{\dot{\bar{g}}\}$

The expression for the kinetic energy is:

$$2KE = \int \{\dot{\bar{g}}\}' [\mu]' [M] [\mu] \{\dot{\bar{g}}\} \quad (52)$$

Evaluating $[\mu] [M] [\mu]$ in equation 52:

$$[\mu][M][\mu] =$$

1	1			$-\frac{l_3}{l}$	$-\frac{l_3}{l}$	$1-\frac{\chi}{l}$	
	1			$-\frac{l_3}{l}$	$-\frac{l_3}{l}$	$1-\frac{\chi}{l}$	
		1	1	$\frac{l_3}{l}$	$\frac{l_3}{l}$	$\frac{\chi}{l}$	
			1	$\frac{l_3}{l}$	$\frac{l_3}{l}$	$\frac{\chi}{l}$	
				1			
					1		
				1	1		1

M_M						
		M_N				
$-M_N(\frac{l_3}{l})$	$-M_N(\frac{l_3}{l})$	$M_N(\frac{l_3}{l})$	$M_N(\frac{l_3}{l})$	M_N		M_N
$-M_M(\frac{l_3}{l})$	$-M_M(\frac{l_3}{l})$	$M_M(\frac{l_3}{l})$	$M_M(\frac{l_3}{l})$		M_M	M_M
$M_P(1-\frac{\chi}{l})$	$M_P(1-\frac{\chi}{l})$	$M_P(\frac{\chi}{l})$	$M_P(\frac{\chi}{l})$			
						M_P

$$=$$

A'	B'	C'	C'	-D'	-E'	-F'
B'	B'	C'	C'	-D'	-E'	-F'
C'	C'	G'	H'	D'	E'	F'
C'	C'	H'	H'	D'	E'	F'
-D'	-D'	D'	D'	M_N		M_N
-E'	-E'	E'	E'		M_M	M_M
-F'	-F'	F'	F'	M_N	M_M	I'

$$\begin{aligned}
 \text{where } \left. \begin{aligned}
 A' &= M_M + (l_3/l)^2(M_N + M_M) + (1 - x/l)^2 M_P \\
 B' &= (l_3/l)^2(M_N + M_M) + (1 - x/l)^2 M_P \\
 C' &= -(l_3/l)^2(M_N + M_M) + (1 - x/l)(x/l) M_P \\
 D' &= (l_3/l) M_N \\
 E' &= (l_3/l) M_M \\
 F' &= (l_3/l)(M_N + M_M) \\
 G' &= M_N + (l_3/l)^2(M_N + M_M) + (x/l)^2 M_P \\
 H' &= (l_3/l)^2(M_N + M_M) + (x/l)^2 M_P \\
 I' &= M_N + M_M + M_P
 \end{aligned} \right\} \quad (53)
 \end{aligned}$$

where dM_P = incremental mass at point P, slugs.

M_N = unsprung mass at nose gear, slugs.

M_M = unsprung mass at main gear, slugs.

Integrating equation 53.

$$\begin{aligned}
 A &= \int A' = M_M + (l_3/l)^2(M_N + M_M) + (M - 2S_U/l + I/l^2) \\
 B &= \int B' = (l_3/l)^2(M_N + M_M) + (M - 2S_U/l + I/l^2) \\
 C &= \int C' = -(l_3/l)^2(M_N + M_M) + S_U/l - I/l^2 \\
 D &= \int D' = (l_3/l) M_N \\
 E &= \int E' = (l_3/l) M_M \\
 F &= \int F' = (l_3/l)(M_N + M_M) \\
 G &= \int G' = M_N + (l_3/l)^2(M_N + M_M) + I/l^2 \\
 H &= \int H' = (l_3/l)^2(M_N + M_M) + I/l^2 \\
 J &= \int I' = M + M_N + M_M
 \end{aligned} \quad (54)$$

where M = total sprung mass of the fuselage, slugs, calculated from
maximum gross weight = $\int_{M_P} dM_P$

S_U = moment unbalance about the nose gear, slug - ft. = $\int_{M_P} x dM_P$

I = mass moment of inertia about the nose gear, slug - ft.² = $\int_{M_P} x^2 dM_P$

Writing the equations for the potential and dissipative energies:

$$2PE = K_1 \bar{z}_1^2 + K_2 \bar{z}_2^2 + K_3 \bar{z}_3^2 + K_4 \bar{z}_4^2 + K_5 \bar{x}_1^2 + K_6 \bar{x}_2^2 \quad (55)$$

and

$$2DE = C_1 \dot{\bar{z}}_1^2 \quad (56)$$

The formation of the matrices for the potential and dissipative energies is similar to the procedure used in forming the kinetic energy matrix. We can now write the matrix which contains the equations of motion of the system.

A	B	C	C	-D	-E	-F
B	B	C	C	-D	-E	-F
C	C	G	H	D	E	F
C	C	H	H	D	E	F
-D	-D	D	D	M_N		M_N
-E	-E	E	E		M_M	M_M
-F	-F	F	F	M_N	M_M	J

$\left\{ \begin{array}{c} \ddot{z}_4 \\ \ddot{z}_2 \\ \ddot{z}_3 \\ \ddot{z}_1 \\ \ddot{\chi}_1 \\ \ddot{\chi}_2 \\ \ddot{\chi}_0 \end{array} \right\} +$

	C_2					
			C_1			

$\left\{ \begin{array}{c} \dot{z}_4 \\ \dot{z}_2 \\ \dot{z}_3 \\ \dot{z}_1 \\ \dot{\chi}_1 \\ \dot{\chi}_2 \\ \dot{\chi}_0 \end{array} \right\} +$

$K_4(1+C_{FT}P_2l_3/l)$		$C_{FT}K_3P_1l_3/l$				
$C_{FT}K_4P_2l_3/l$	K_2	$C_{FT}K_3P_1l_3/l$				
$-C_{FT}K_4P_2l_3/l$		$K_3(1-C_{FT}P_1l_3/l)$				
$-C_{FT}K_4P_2l_3/l$		$-C_{FT}K_3P_1l_3/l$	K_1			
		$-C_{FT}K_3P_1$		K_5		
$-C_{FT}K_4P_2$					K_6	
$-C_{FT}K_4P_2$		$-C_{FT}K_3P_1$				

$\left. \begin{matrix} \bar{z}_4 \\ \bar{z}_2 \\ \bar{z}_3 \\ \bar{z}_1 \\ \bar{x}_1 \\ \bar{x}_2 \\ z_0 \end{matrix} \right\} =$

$$-C_{FT} \left\{ \begin{matrix} -l_3/l(P_1 F_N + P_2 F_M) \\ -l_3/l(P_1 F_N + P_2 F_M) \\ l_3/l(P_1 F_N + P_2 F_M) \\ l_3/l(P_1 F_N + P_2 F_M) \\ P_1 F_N \\ P_2 F_M \\ P_1 F_N + P_2 F_M \end{matrix} \right\} \quad (57)$$

where

$$P_1 = |\dot{x}_1|/\dot{x}_1$$

$$P_2 = |\dot{x}_2|/\dot{x}_2$$

The static gear loads, based on maximum gross weight, were superimposed on the dynamic loads in order to determine the total gear load. Here, as in the taxi condition, the effect of wing lift due to forward speed has been accounted for by using equation 27 in computing static gear loads (Ref. Table 5). Because the aircraft begins slowing down at the instant the brakes are applied the static gear loads gradually increase since wing lift decreases. The most critical gear loads are determined at a point where the sum of the static and dynamic loads are a maximum.

Table 5 - Braking Condition: Maximum Landing Gear Loads

Config. Data	Fixed Jet	Tilt Wing	Extended Flap	Tilt Prop	Buried Fan
V. Initial Fwd. Vel., Kts.	30	30	30	30	30
FMS + FM DYN., Lbs. (Max. Vertical)	-253,000	-299,000	-412,000	-429,000	-362,000
FNS + FN DYN., Lbs. (Max. Vertical)	+38,800 -80,800	-	-	-	-
FMD DYN., Lbs. (Max. Longitudinal)	+145,000 -113,000	+176,000 -	+215,000 -176,000	+182,000 -	+214,000 -
FND DYN., Lbs. (Max. Longitudinal)	+6,400 -3,800	+19,000 -7,900	+16,000 -6,100	+19,000 -6,000	+9,300 -2,800
(FMS + FM DYN.)/W	-1.47	-1.34	-1.57	-1.39	-1.43
(FNS + FN DYN.)/W	+0.23 -0.47	-	-	-	-
FMD DYN./W	+0.84 -0.66	+0.79 -	+0.82 -0.67	+0.59 -	+0.85 -
FND DYN./W	+0.04 -0.02	+0.09 -0.04	+0.06 -0.02	+0.06 -0.02	+0.04 -0.01

- Notes: (1) FMS, FM DYN. = Static and dynamic vertical loads on both main gears.
- (2) FNS, FN DYN. = Static and dynamic vertical load on nose gear.
- (3) FND DYN., FMD DYN. = Longitudinal dynamic nose gear load and longitudinal dynamic load on both main gears.
- (4) W = Normal design gross weight.
- (5) (FMS + FM DYN.) and (FNS + FN DYN.) are determined at a point such that the combination of the two is a maximum.
- (6) FMS and FNS are calculated taking into account the effect of lift due to forward velocity of the aircraft.
- (7) $F_{MS} = F_M \left[1 - \left(\frac{V}{V_{Lo}} \right)^2 \right]$
 $F_{NS} = F_N \left[1 - \left(\frac{V}{V_{Lo}} \right)^2 \right]$
- (8) Sign Convention: + Tension load in Oleo
+ Aft acting load

B. Take-Off Abort (VTOL)

For the take-off abort condition the analysis consists of predicting a safe operational envelope of height and forward speed that considers a partial power failure. The initial condition is a partial power failure occurring while in a normal VTOL mode of operation during take-off. If there was no problem of partial power failure, these aircraft configurations could simply make a vertical take-off and proceed to clear all obstacles before entering transition. However, there always exists the potential hazard of a partial power failure with the attendant problems of not having the ability to recover, thus enabling the aircraft to alight within the aircrafts landing gear structural limits. Since all these configurations have four or more engines, consideration was made of having at least one engine out and shutting down, if necessary, other power plants for symmetry in order to maintain sufficient lateral stability. The configurations are assumed to have a single engine failure with a resulting 25% loss of power with the exception of the Buried Fan configuration. The latter will require two engines out of it's six engine installation due to the lateral stability problem which appears to be inherent with the engine arrangement of this design. The Buried Fan configuration was considered to have two large and two small fans in the wing structure with no cross ducting to the individual fans.

The method of analysis was based on considering the percent of hover power required with forward speed. A survey of technical literature (Ref. 9&15) has provided a comparative power with forward speed relationship of the configurations and is shown in Fig. 35. The percent power with forward speed is then related to variations of the lift to weight ratio with forward speed by considering the remaining power and the required power for a particular forward speed. The estimated lift to weight ratio is then based on the ratio of the available to the required power. A plot of this lift to weight ratio versus forward speed is shown in Fig. 36.

The data as presented shows that the Extended Flap, Fixed Jet, Tilt Wing, and Tilt Propeller configurations have roughly the same lift to weight ratios in the low speed range. The Buried Fan configuration definitely has a poor lift to weight ratio due to the greater power required with forward speed and the greater power loss due to the fan arrangement. It is not inferred that the data provided in Fig. 36 are absolute value capabilities, but rather a relative picture of the configurations that have been studied. The analysis was then divided into two parts for the lift to weight ratio concerned; that of the Buried Fan and the approximation for all the other configurations.

Within the scope of this study a simplified method for predicting the height velocity envelope is as follows:

Equations of Motion

The vertical acceleration of the aircraft following a power failure will be equal to the net difference between the weight and the remaining vertical capability.

$$M\ddot{z} = W - L$$

(53)

where M = mass of the aircraft , slugs

Z = height lost subsequent to time of power failure , ft.

$$\ddot{z} = (1 - L/W)g , \text{ ft./sec.}^2$$

W = VTOL design gross weight , lbs.

L = vertical lift , lbs.

The result of this force balance is a relation between the required height to limit the ground contact velocity to a specified value and the L/W ratio (assuming that the lift to weight ratio remains constant) as follows:

$$\ddot{z} = \frac{d^2z}{dt^2} = (1 - L/W)g \quad (59)$$

$$z = \frac{\dot{z}^2}{2g(1 - L/W)} + \text{Arbitrary constants} \quad (60)$$

The conditions are that $\dot{z} = 0$ at $Z = 0$; and $Z = H$, total height lost, when $\dot{z} = V_z$, the vertical ground contact velocity.

Thus the total height lost for a given resultant contact velocity for a constant L/W ratio is:

$$H = \frac{V_z^2}{2g(1 - L/W)} \quad (61)$$

Solution for H-V Envelope

The H-V envelope was found by using the specific allowable vertical contact velocity and the lift to weight ratios for each velocity considered at which a partial power failure is assumed to occur. The resulting H-V envelope diagram is shown in Fig. 37 for the Buried Fan and other configurations. The interpretation of this diagram is that there is a maximum height to permit staying within the safe envelope for these designs. It should be noted that this portion of the H-V envelope only defines the lower boundaries of the areas of safe operation. There is an upper height that is not shown which would permit a dive-out procedure to limit the contact velocity with the ground and/or permit continued flight by entering into lower power required speed ranges. The latter portion of the H-V envelope would be associated with continued operation rather than a take-off abort condition.

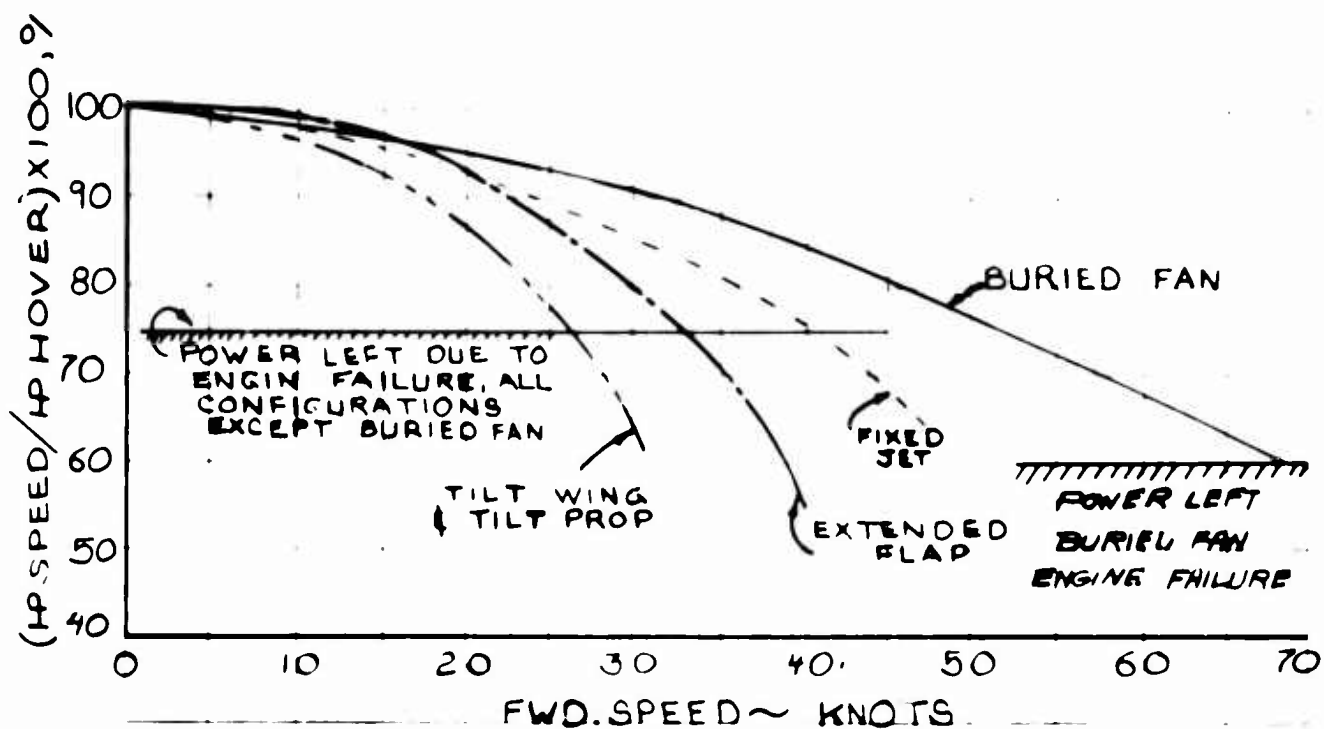


Figure 35 - Percent Hovering Power with Forward Speed

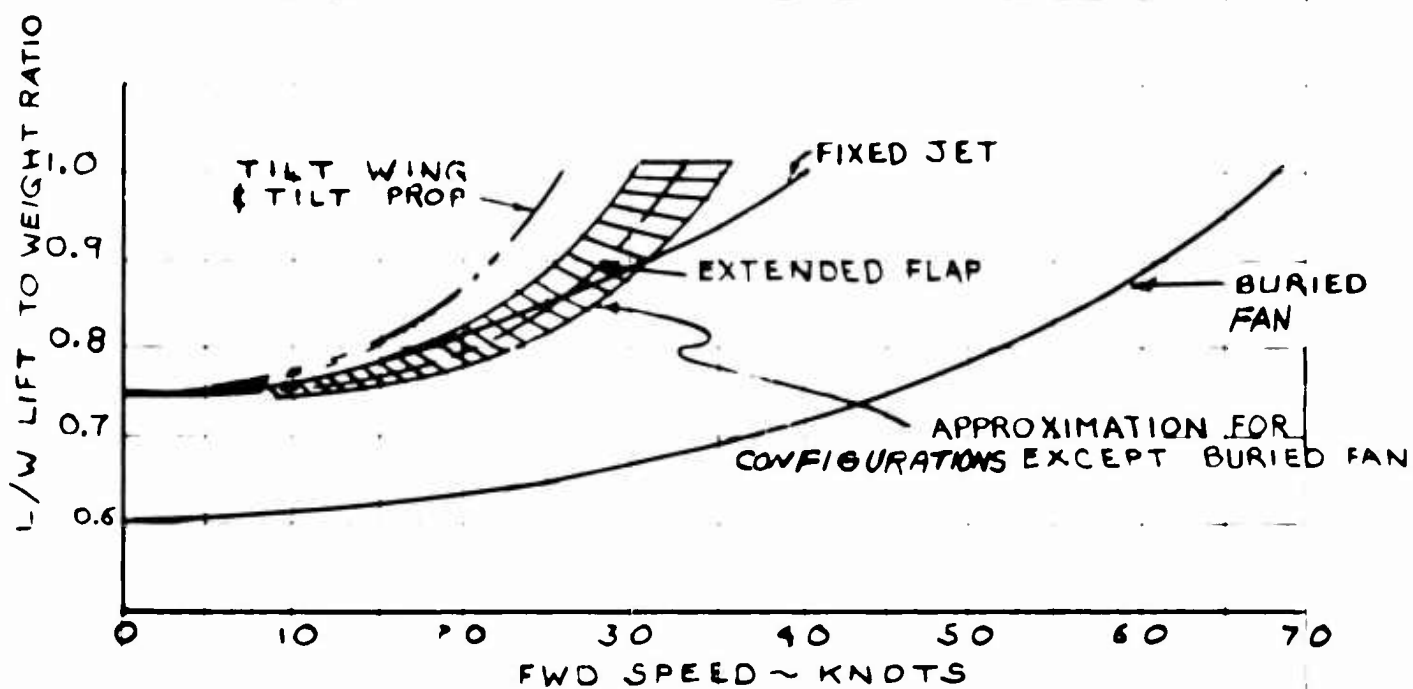


Figure 36 - L/W Ratio with Forward Speed After Power Failure

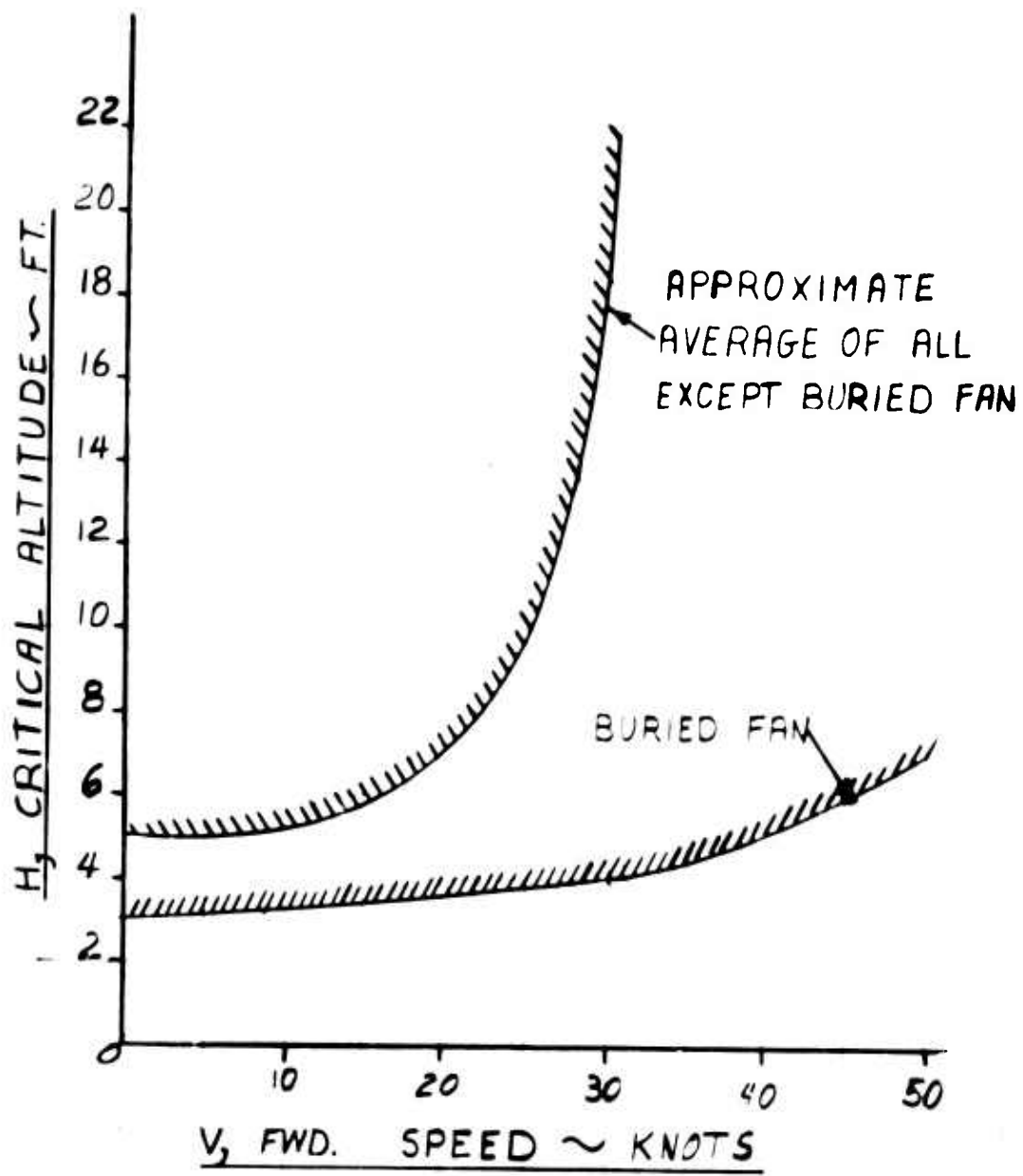


Figure 37 - H-V Envelope

C. Maneuvers

The five V/STOL configurations were designed for a limit maneuver loading resulting from a 3g normal load factor. For the wing structural design the design loads are divided into three types, these being:

- (a) Aerodynamic loads on wing
- (b) External forces due to propeller, etc.
- (c) Inertial loading

The breakdown of the above loadings are shown in Table 6 for the wing bending moments and torsions. In general, the inertial forces relieve wing bending in normal design practice and therefore the designer usually tries to include the heavy equipment or loadings to counterbalance the wing lift forces. A compromise is, of course, required when consideration is given to the landing loads conditions wherein the wing lift has usually one or less g's with the predominant loading being from the landing gear.

A simple type of maneuver condition has been used for this portion of the load investigation and consists of prescribing the build-up of maneuver normal load factor. The build-up was assumed to be from the normal level flight condition (1g) to a limit normal load factor (3g's) in .10 seconds and held constant thereafter at the 3g level. This rapid acceleration build-up is an extreme condition and is to be used only for a relative comparison of the structural response problems of the V/STOL configurations.

The method of analysis for the maneuver condition was to apply the prescribed acceleration on the body. For the purposes of this analysis only the wing dynamic response was considered in order to study the effects of the structural rigidity and mass distribution of designs peculiar to the V/STOL configurations.

The method of analysis considered only the lowest modal frequency response of the wing structures. In the general solution of the dynamic system the equation of dynamic equilibrium (in tensor form) for a homogeneous or free vibration case is:

$$M_{ab} \ddot{q}^a + K_{ab} q^a = 0 \quad (62)$$

where M_{ab} is the mass tensor

q^a is the coordinate tensor of the system and includes both translatory and rotary displacements.

The coordinate tensor q^a is assumed to be a linear combination of the modes and a time dependent function, that is, a separation of variables.

$$q^a(x, y, z, t) = \sum_{r=1}^{r=n} g_r^a(x, y, z) \phi^r(t) \quad (63)$$

where $q^a_{(r)}$ is the rth mode, $r = 1 - - - n$

The kinetic energy of the system is then

$$KE = 1/2 M_{ab} \dot{q}^a \dot{q}^b = 1/2 M_{ab} \dot{\phi}^a \dot{\phi}^b g_r^a g_r^b \quad (64)$$

By normalizing the modal shapes and using the concept that the modes are orthogonal to the mass tensor,

$$(55) KE = 1/2 \dot{\xi}^a \tilde{M}_{ab} \dot{\xi}^b \quad (65)$$

and $\tilde{M}_{ab} = g_{(r)}^a g_{(r)}^b = \text{kronecker delta tensor}$

A similar approach is used with the potential energy of the system.

$$(56) PE = 1/2 K_{ab} g^a g^b = 1/2 \tilde{K}_{ab} \xi^a \xi^b \quad (66)$$

where, K_{ab} is the spring tensor

$$(57) \tilde{K}_{ab} = K_{ab} g_{(r)}^a g_{(r)}^b \quad (67)$$

The system now becomes diagonalized, that is, the spring tensor in the new coordinate system is diagonalized and the terms are the square of the frequencies. In matrix form:

$$[K_{ab}] = \begin{bmatrix} \omega_1^2 & & \\ & \ddots & \\ & & \omega_n^2 \end{bmatrix} \quad (68)$$

When assuming only a lowest modal contribution the result is an equation in normal coordinates:

$$(59) \ddot{\xi} + \omega_1^2 \xi = 0 \quad (69)$$

This is the equivalence of a single degree of freedom system. Thus, by assuming the body and wing mass as separate systems with a single spring between, the classical solutions for response factor of single degree of freedom systems can be used.

The response of a rapidly applied load when maintained indefinitely depends on the ratio of the rise time to the natural period of the elastic structure. The response curve is shown in non-dimensional form in Fig. 38 for reference.

The natural periods of the wing fixed at its root have been analyzed and are shown in Table 19 in Appendix IV of which the first bending data has been used for this analysis. For this analysis the response ratio is defined as follows:

$$R_f = \frac{\text{Maximum Wing Acceleration}}{\text{Maximum incremental body g's}}$$

The maximum incremental body g's equal 2 g's going from a 1g flight condition to the limit of 3 g's. The response factor is a factor on the lowest modal shape and the bending and torsional moments are found by the following (Ref. Fig. 39).

$$\text{B.M.} \left(\begin{smallmatrix} \text{Bending} \\ \text{Wing Root} \end{smallmatrix} \right) = \sum w_i g_{(i)}^i 2 R_f (y_i - y_{\text{root}}) \quad (70)$$

where w_i = weight at i th coordinate.

q_1^i = modal shape of i th coordinate (normalized to unity at wing tip) for first mode.

R_f = response factor.

$(y_i - y_{\text{root}})$ = distance from i th section to root section.

2 = the number of incremental g 's.

$$\text{T.M.} \left(\begin{smallmatrix} \text{Torsion} \\ \text{Wing Root} \end{smallmatrix} \right) = \sum w_i g_{(i)}^i 2 R_f (x_i - x_{\text{root}}) \quad (71)$$

where $(x_i - x_{\text{root}})$ = distance from wing elastic axis at root.

The final resulting peak bending moments and torsions consider the direction of the vibrating wing.

Case (1) Wing Vibration Up (See Fig. 40)

In this case the maximum vibration g 's are reinforced by the $1g$ loading and all the inertial forces oppose the air loads and external forces. This is not a critical condition for bending but must be investigated because the predominate forces in torsion are inertial.

Case (2) Wing Vibration Down (See Fig. 40)

In this case the maximum vibration g 's add to the external forces with some relief from the $1g$ steady loads. The bending will be greatest in this case.

The maximum bending and torsional stresses at the wing root are found by using the section modulus of the wing (Ref. equations 43, 44, part A 3). The resulting calculations are shown in Table 6 and tabulate the maximum wing response factors, bending moments and torsions. The resulting maximum bending and torsion stresses are shown for all five V/STOL configurations.

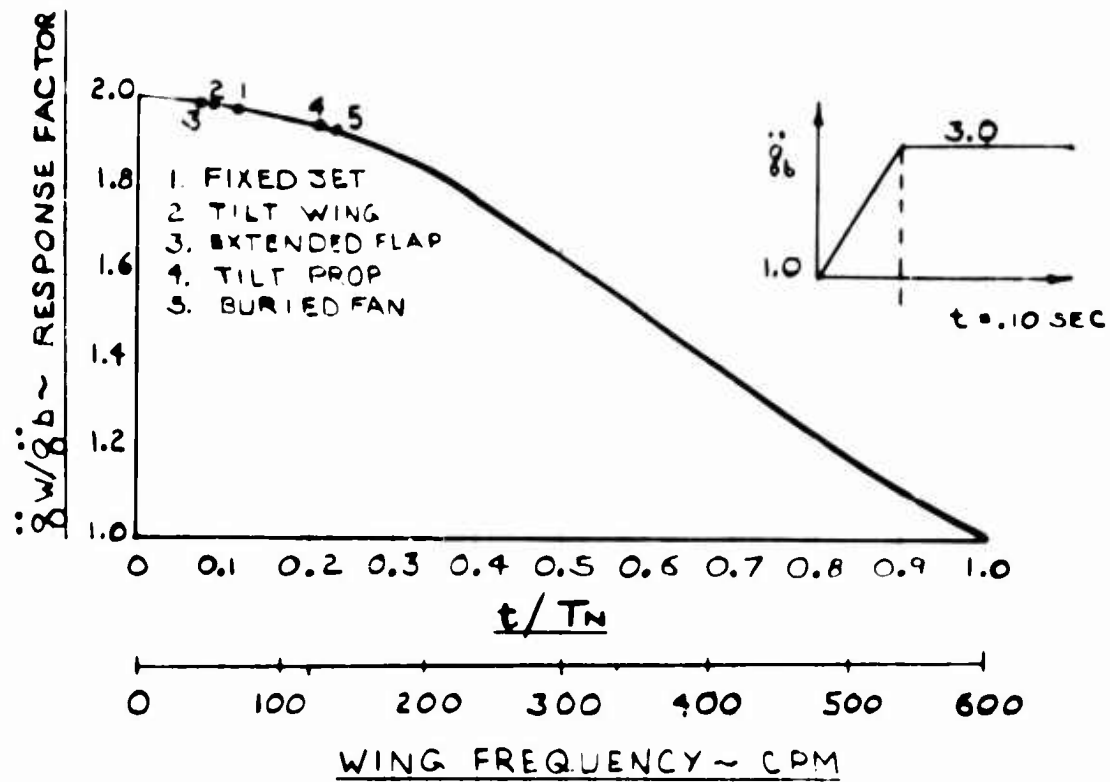


Figure 38 - Maneuver Acceleration Response

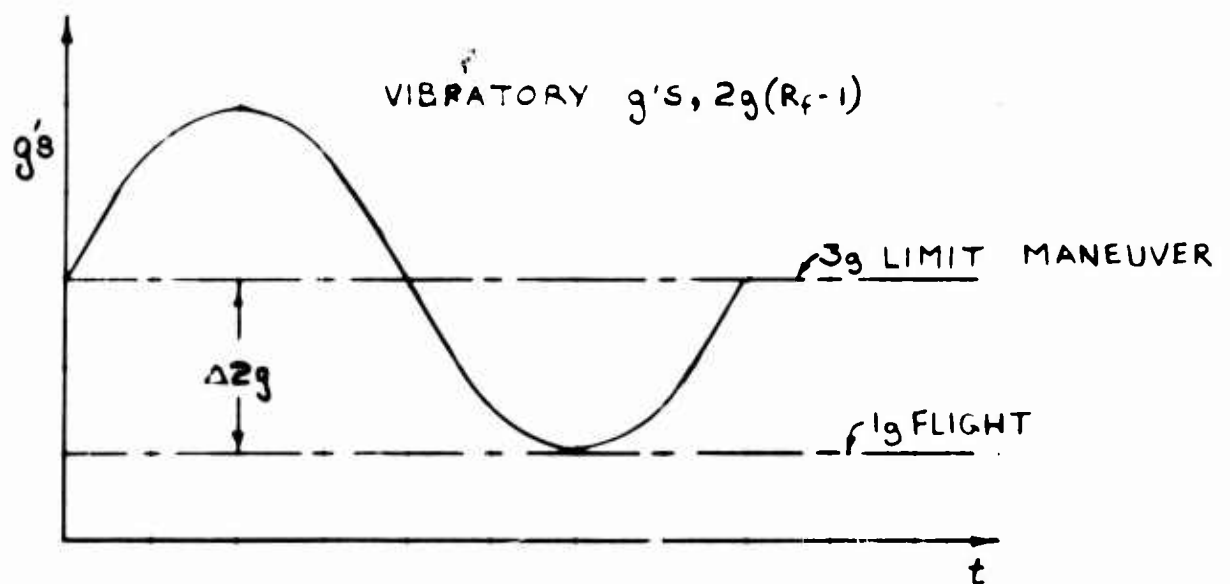


Figure 39 - Schematic of Maneuver $g's$

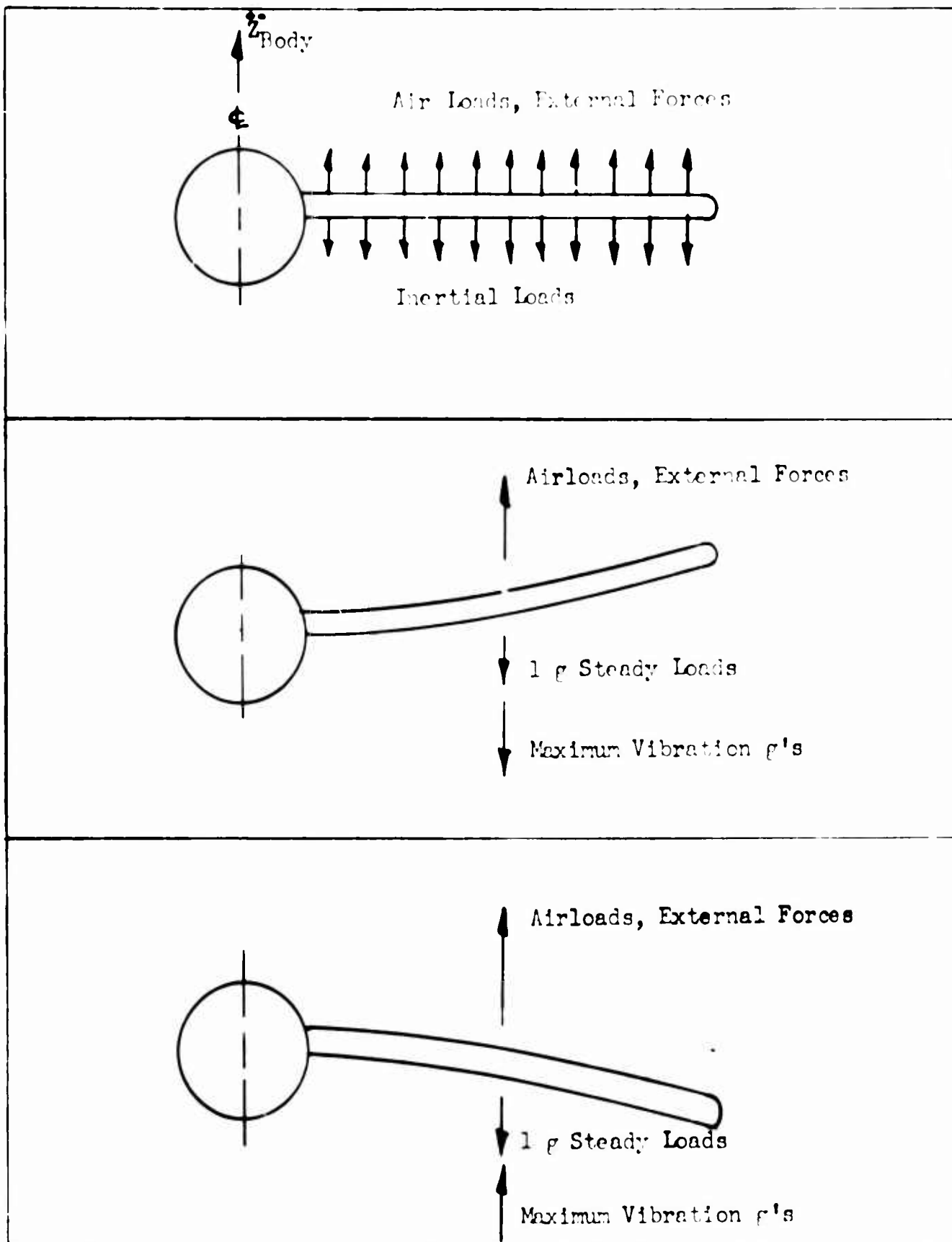


Figure 4.2 Schematic of Vibrating Wing

**Table 6 - Maneuver Condition: Wing Root Moments, Torsions
and Stresses**

Config. Data	Fixed Jet	Tilt Wing	Extended Flap	Tilt Prop	Buried Fan
Airloads and External Loads					
Bending Moment	54,700,000	114,900,000	157,000,000	110,600,000	86,300,000
Torsional Moment	6,100,000	4,700,000	7,700,000	7,900,000	16,500,000
1G Steady State Flight Inertia Loads					
Bending Moment	-11,200,000	-26,800,000	-36,700,000	-25,200,000	-9,300,000
Torsional Moment	300,000	3,300,000	-3,400,000	-2,100,000	-1,600,000
1st Modal Inertial Response Loads					
Response Factor	2.0	2.0	2.0	1.9	1.9
Bending Moment	-	-	-	-4,600,000	-1,000,000
Torsional Moment	-15,000,000	-55,200,000	-69,200,000	-87,000,000	-19,800,000
	5,200,000	2,200,000	2,900,000	61,200,000	-1,200,000
Maximum Loading					
Bending Moment	13,500,000	88,100,000	120,300,000	110,800,000	76,000,000
Torsional Moment	11,600,000	1,400,000	4,300,000	5,100,000	14,800,000
Maximum Bending Stress, PSI	68,000	78,200	87,000	49,500	37,000
Maximum Shear Stress, PSI	22,700	3,040	9,650	104,000	10,800

Notes: (1) Sign Convention:

Bending + Compression on upper surface of wing
Torsion + Pitch up twist

D. Gust Penetration

As a preliminary investigation of the criticality of gust penetration, a simplified analysis was used to determine the maximum wing bending and torsion loads.

The flight condition is taken at 125 percent of the cruise speed condition for all the V/STOL configurations. The gust velocity is 50 fps using standard sea level density as a most severe condition.

The calculation of the gust loads on the aircraft is based on a single discrete gust to determine the effects on the wing root bending moment. This involves the character of the gust and the dynamic response of the rigid and elastic structure.

For the purposes of this portion of the investigation of dynamic response on the V/STOL configurations, a reasonable design evaluation is made in the following steps:

- (a) Steady state gust response of the rigid aircraft, neglecting the degree of freedom in translation and aerodynamic lag.
- (b) Gust alleviation factor based on the aerodynamic parameters including only the translatory degree of freedom and considering the aerodynamic lag.
- (c) Non-dimensional acceleration-time history for the configurations for the rigid body gust loading.
- (d) First modal structural dynamic response of the wing structure based on the resulting acceleration-time history of the rigid body gust loading in the translatory degree of freedom.
- (e) Combining the wing aerodynamic loading with the dynamic inertial loadings of the fundamental modal response.

While this is a simplified type of gust response, previous work as described in section 10-6 of Ref. 4, shows that this is a rational approach with reasonable results.

Steady State Gust Response

The incremental lift load on the wings is:

$$\Delta L = \beta \Delta \alpha_w \frac{1}{2} \rho V^2 S \quad (72)$$

where β = the lift slope $\frac{dC_L}{d\alpha_w}$ in radians.

$\Delta \alpha_w$ = the incremental change in aerodynamic wing angle of attack (radians) from a vertical gust.

V = 125% of normal cruise speed, ft./sec.

S = wing area, ft.²

For small changes in angle of attack, the vertical acceleration for a steady state condition is:

$$\Delta \ddot{z}_{ss} = \frac{A U V \sqrt{2} \rho q}{W/S} \quad (73)$$

where U is the gust velocity in ft./sec.

Gust Alleviation Factor

The aircraft was assumed to enter a region of a sharp edged vertical gust. The solution to this type of entry into a sharp edged gust has been presented in Reference 4 and consists of the solution in terms of the ratio of the rigid body acceleration to the steady state rigid body acceleration with respect to the number of semi-chord lengths of wing travel. An independent variable, that is part of this solution, is the non-dimensional mass parameter λ_M .

$$\lambda_M = M / \pi \rho S c^2 \quad (74)$$

where M = aircraft mass, slugs

C = wing chord, ft.

A plot of the peak ratio of accelerations versus the mass parameter is shown in Fig. 41. The gust alleviation factor K_g is defined as the ratio of the peak accelerations and is plotted in Fig. 41 and tabulated for the five V/STOL configurations in Table 7.

Non-Dimensional Acceleration-Time History

The gust loading acceleration is non-dimensionalized by dividing the gust acceleration by the peak value. The time history is non-dimensionalized by dividing by the time to reach the peak acceleration.

In order to provide the time history, a solution of the acceleration ratio versus semi-chords of Fig. 10-22 of Reference 4 was used. Therefore the actual time was found from:

$$t = s c / V = \frac{s c}{2 V} \quad (75)$$

where s is the number of semi-chords traveled.

Since the mass ratios of the V/STOLs are sufficiently close to the range of $\lambda_M = 30$ to 70, there is no appreciable difference in their acceleration-time history, and the resulting non-dimensional acceleration time history shown in Fig. 42 applies for all the dynamic response calculations.

First Modal Structural Dynamic Response

The characteristic acceleration-time history is shown in Fig. 43. This history can be approximated by a step function having an exponential front such as shown in Fig. 4-20 of Reference 8.

$$\frac{\ddot{z}}{\ddot{z}_{\max}} = \frac{1 - e^{\pi/t_3}}{1 - e^{\pi}} \quad 0 \leq t \leq t_3 \quad (76)$$

$$\frac{\ddot{z}}{\ddot{z}_{\max}} = 1 \quad t \geq t_3$$

In this case $n = -2\pi$ best represents the non-dimensional data and the resulting response factor is:

$$R_f = 1 + \frac{-2\pi}{1 - e^{-2\pi}} \sqrt{\frac{1 - 2e^{-2\pi} \cos(2\pi t_3/T_N) + e^{-4\pi}}{4\pi^2 + 4\pi^2(t_3/T_N)^2}} \quad (77)$$

where t_3 is the time to reach peak acceleration and T_N is the natural period.

The acceleration response factor R_f is shown in Fig. 43 with the ratio of the time to peak pulse to fundamental wing period. Since the fall-off in acceleration is gradual, and the peak response will occur at less than the unit ratio of t_3/T_N , the use of the functional input is considered sufficiently accurate for the purposes of this analysis.

In Fig. 43, the acceleration response factor is shown with points referenced to the V/STOL configurations. While the ratios of t_3/T_N vary from .10 to .56 for the gusts, all the V/STOL wings have a response close to the maximum of 2.0.

Wing Loads and Stresses

The total wing bending moment is a combination of the following:

1. The 1g steady state flight loads consist of wing lift equal to the weight of the aircraft. The root bending moment is the result of the 1g air loading less the 1g weight forces on the wing.
2. The Δg air loading from the rigid body wing gust loading.
3. The dynamic inertial loading on the wing, which will be the full Δg condition times the response factor for the wing vibrating up, increases the usual inertial relief. A second condition will be for the wing vibrating down when the inertial relief is reduced as shown in Fig. 40.

The wing bending moments, torsional moments, and stresses are shown in Table 8. The most critical of the moment combinations is resolved into bending and torsional stresses. The maximum bending and shear stresses at the wing root are calculated from equations 43 and 44 of part A² of this section.

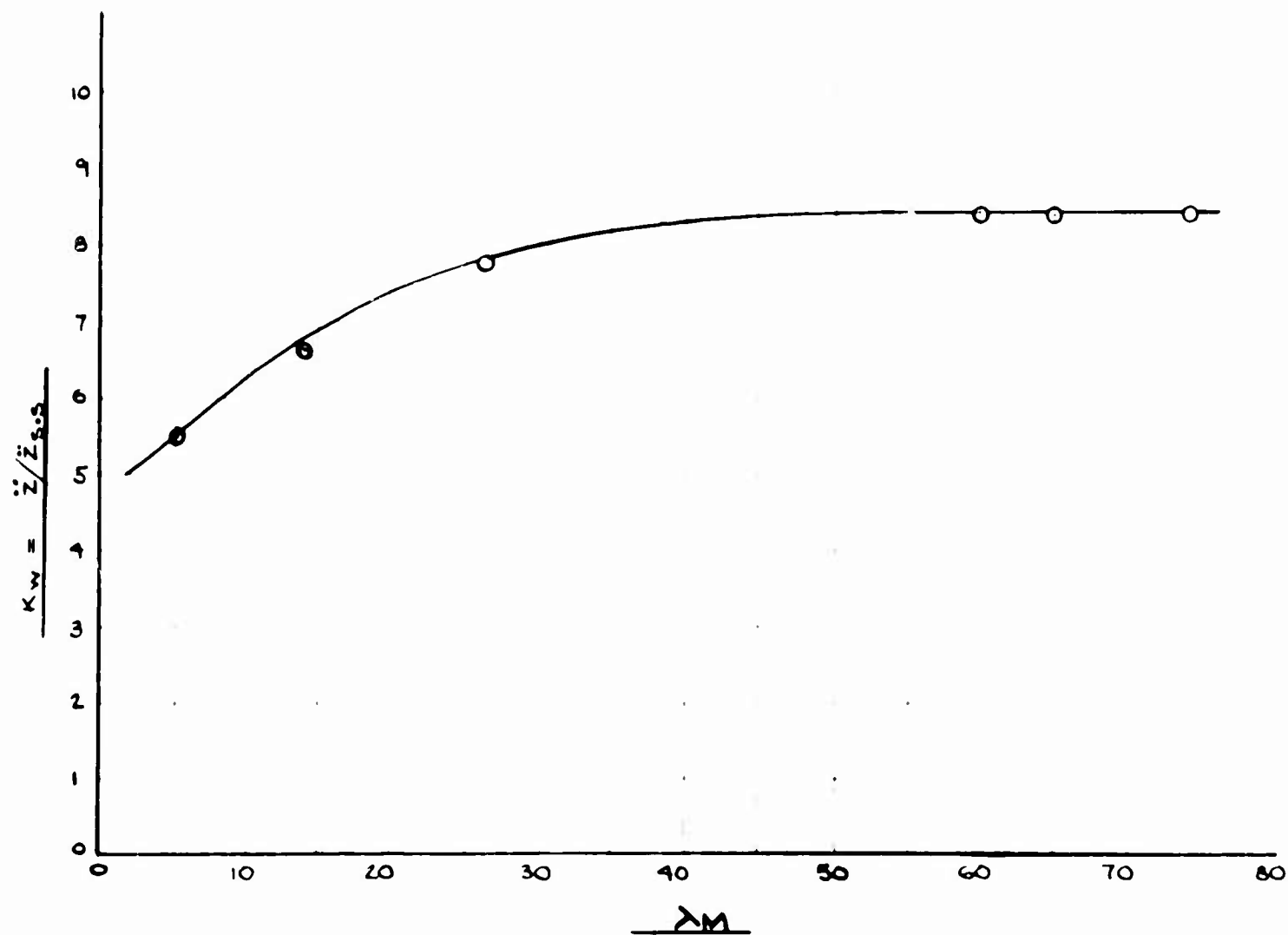


Figure 4.1 - Gust Alleviation Factor vs Mass Ratio

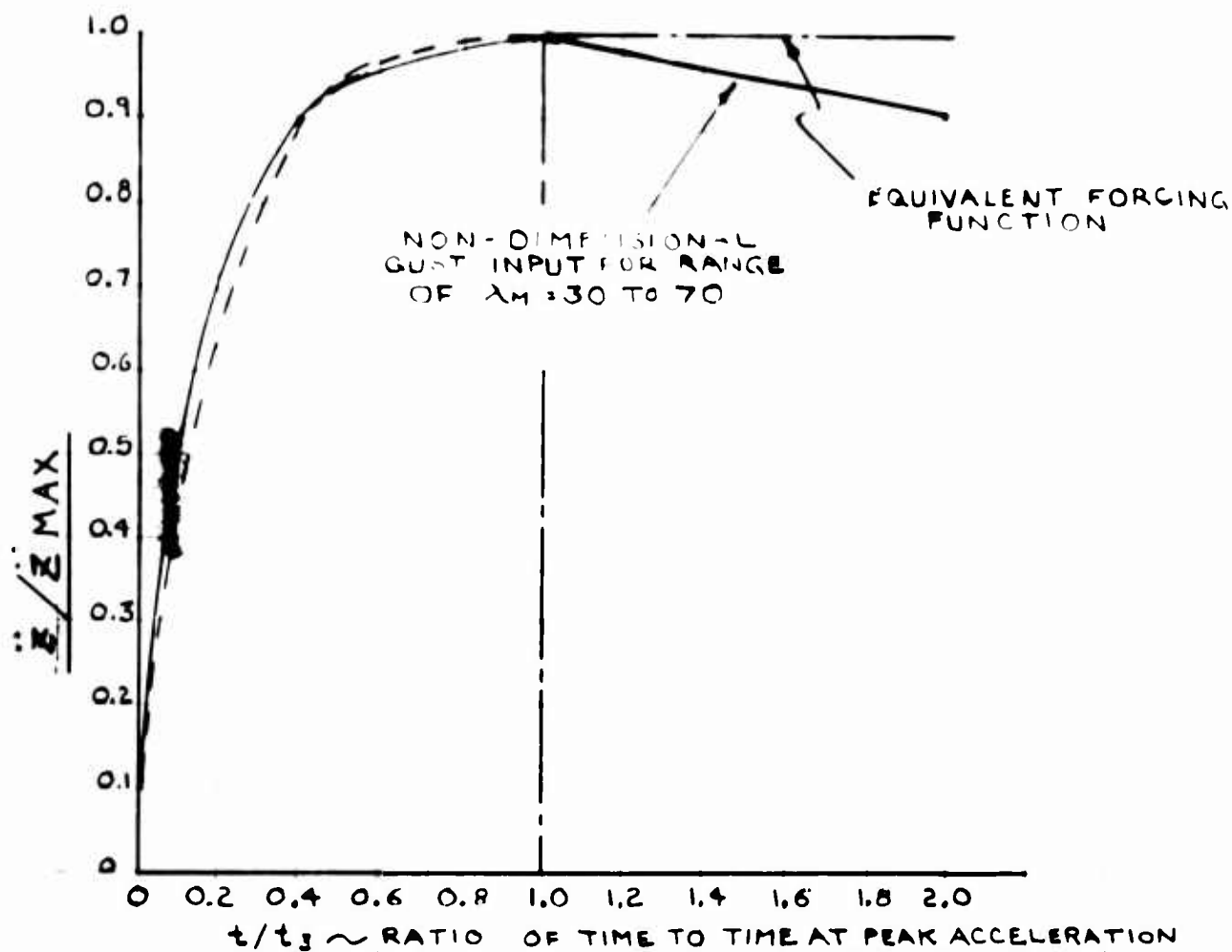


Figure 42 - Gust Non-Dimensional Rigid Body Load - Time History

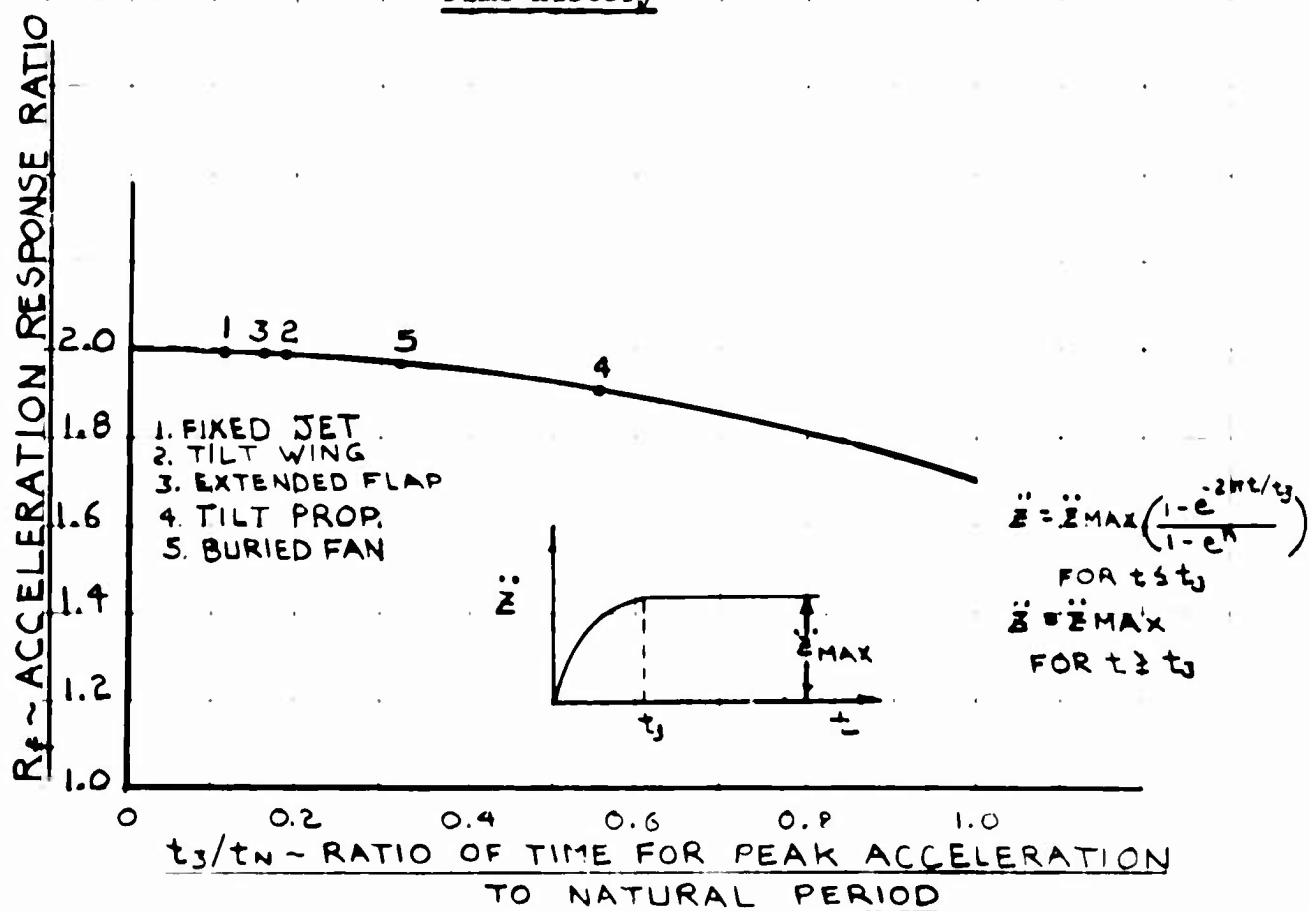


Figure 43 - Gust Acceleration Response

Table 7 - Gust Penetration : Rigid Body Data

Config. Data	Fixed Jet	Tilt Wing	Extended Flap	Tilt Prop	Buried Fan
β , Lift Slope, Rad.	4.62	4.58	4.75	4.22	3.45
V, 125% Cruise, Ft/Sec	850	580	580	630	850
$\Delta \alpha_w$, U/V, Rad.	0.056	0.087	0.087	0.079	0.056
W/S, Lbs/Ft ²	86.7	93.0	100	120	74.3
$\Delta \ddot{E}_{ss}$, Ft/Sec ²	91	55	53	43	86
W/SC	8.67	7.60	7.00	6.80	3.20
λ_M , Mass Ratio	73	64	59	57	27
K _w , Alleviation Factor	0.84	0.84	0.84	0.84	0.78
$\Delta \ddot{Z}$, Ft/Sec ²	77	46	45	36	74
ΔN_z , Δg 's	2.38	1.42	1.40	1.11	2.30
C/2V	5.6×10^{-3}	12.6×10^{-3}	12.3×10^{-3}	13.9×10^{-3}	12.6×10^{-3}
t ₃ , Time to Peak Acceleration, Sec.	0.112	0.252	0.246	0.278	0.151
t ₃ /T _N , Time Ratio	0.105	0.186	0.152	0.556	0.320

**Table 8 - Gust Penetration: 50 fps Gust Wing Root Moments, Torsions
and Stresses**

Config. Data	Fixed Jet	Tilt Wing	Extended Flap	Tilt Prop	Buried Fan
1 g Steady State Flight Loads					
Bending Moment	7,000,000	11,500,000	15,600,000	21,600,000	19,500,000
Torsional Moment	3,200,000	-1,600,000	360,000	530,000	2,000,000
Δ g Gust Aerodynamic Wing Lift Loads					
Bending Moment	43,400,000	54,400,000	73,300,000	52,000,000	66,100,000
Torsional Moment	3,900,000	2,100,000	2,800,000	2,900,000	14,800,000
1st Modal Inertial Gust Response Loads					
Response Factor	2.0	2.0	2.0	2.0	1.9
Bending Moment	-	-	-	-	-1,200,000
Torsional Moment	-17,800,000	-39,200,000	-46,500,000	-50,800,000	-22,800,000
	6,200,000	1,500,000	2,000,000	35,700,000	-1,100,000
Maximum Loading					
Bending Moment	50,400,000	65,900,000	88,900,000	73,600,000	84,400,000
Torsional Moment	13,200,000	-1,000,000	3,100,000	32,300,000	16,800,000
Maximum Bending Stress, PSI	78,700	58,500	64,200	32,900	41,000
Maximum Shear Stress, PSI	25,700	2,170	7,000	60,500	12,200

Notes: (1) Sign Convention

Bending + Compression on upper surface of wing

Torsion + Pitch up twist

E. Landing Condition

The initial conditions for landing impact are high forward speed, a vertical sinking speed of 9 fps., and lift equal to $2/3$ gross weight. The following three landing conditions are used to provide the basis of landing gear stroke and loads subsequently used in the dynamic response analysis.

(1) Three Point Level Landing

In Fig. 44 a schematic representation of the forces on the gears is shown for a three point level landing which produces the maximum vertical nose gear loads. The equations of motion are related to the aircraft center of gravity as follows:

$$\Sigma F_z = M \ddot{z}_0 \quad (78)$$

$$\bar{F}_N + \bar{F}_M + L - N_z W = 0$$

where \bar{F}_N = average vertical nose gear oleo load, lbs.

\bar{F}_M = average vertical main gear oleo load for both gears, lbs.

L = lift at the center of gravity, lbs.

W = aircraft design gross weight, lbs.

N_z = vertical load factor at the center of gravity equal to $(2 + L/W)$, g's

$$\Sigma F_y = 0$$

$$\bar{F}_N a - \bar{F}_M a_1 - .25 \bar{F}_N l_1 - .25 \bar{F}_M l_2 = 0 \quad (79)$$

where a = horizontal distance between nose gear and center of gravity.

a_1 = horizontal distance between main gear and center of gravity.

l_1 = vertical distance between nose gear axle and center of gravity.

l_2 = vertical distance between main gear axle and center of gravity.

Considering the total drop energy of the aircraft:

$$E = \left[\frac{V_z^2}{2g} + \delta_{LG} \right] W$$

where V_z = vertical sinking speed, ft./sec.

δ_{LG} = average landing gear deflection which is assumed equal to the main gear stroke, ft.

The drop energy is absorbed by the landing gear as follows:

$$E = \bar{F}_N \delta_N + \bar{F}_M \delta_M + L \delta_{LG}$$

where δ_N and δ_M are the nose and main gear strokes, ft.

Equating the two energies:

$$\left[\frac{V^2}{2g} + \delta L_6 \right] W = \bar{F}_N \delta_N + \bar{F}_M \delta_M + L \delta L_6 \quad (80)$$

Solving equations 79 and 80 simultaneously and recognizing the gear efficiencies $F_N = F_N \eta_N$ and $F_M = F_M \eta_M$, where η_N and η_M are assumed equal, we arrive at expressions for the nose and main gear loads F_N and F_M .

$$F_N = \frac{1}{\eta_N} \left[\frac{(a_1 + .25l_2) \left[\frac{V^2 W}{2g} + \delta_M (W - L) \right]}{\delta_M (a_1 - .25l_1) + \delta_N (a_1 + .25l_2)} \right] \quad (81)$$

$$F_M = \frac{1}{\eta_M} \left[\frac{(a_1 - .25l_1) \left[\frac{V^2 W}{2g} + \delta_M (W - L) \right]}{\delta_M (a_1 - .25l_1) + \delta_N (a_1 + .25l_2)} \right] \quad (82)$$

Substituting the expressions for F_N and F_M in equation 78 and solving for δ_N :

$$\delta_N = \frac{1}{\eta_M} \frac{\left[\frac{V^2 W}{2g} + \delta_M (W - L) \right] \left[(a_1 + .25l_2) + (a_1 - .25l_1) \right] - \delta_M (N_2 W - L)(a_1 - .25l_1)}{(N_2 W - L)(a_1 + .25l_2)} \quad (83)$$

By plotting δ_M vs. δ_N for each configuration it was determined that δ_M equals δ_N when the stroke is approximately 1 ft. This value can now be used in equations 81 and 82 to determine the gear loads assuming an overall gear efficiency of 80 percent. The drag loads are equal to 25 percent of the oleo load. (Ref. Table 9).

(2) Tail Down Landing

In Fig. 44 a schematic representation of the forces on the gears is shown for a tail down landing condition which produces the maximum vertical main gear loads. The equations of motion are related to the aircraft center of gravity as follows:

$$\begin{aligned} \sum F_z &= M \ddot{z}_0 \\ \bar{F}_M + L - W &= (W/g) \ddot{z}_0 \end{aligned}$$

where \ddot{z}_0 = vertical acceleration at the center of gravity

$$\ddot{z}_0 = g/W (\bar{F}_M + L - W) \quad (84)$$

$$\sum M_y = I_y \ddot{\theta}_y$$

$$-\bar{F}_M a_2 - L e' = I_y \ddot{\theta}_y = (r^2 W/g) \ddot{\theta}_y$$

$$\ddot{\theta}_y = (-\bar{F}_M a_2 - L e') (g/r^2 W) \quad (85)$$

where $\ddot{\theta}_y$ = aircraft angular pitching acceleration, rad/sec.²
 $r^2 = I_y/M$ = pitching radius of gyration, ft.²
 e = horizontal distance between the center of pressure and the center of gravity = 0.
 h = vertical distance between the center of pressure along the wing chord and the center of gravity.
 l_3 = vertical distance between static ground line and center of gravity.
 ϕ = angle of inclination between aircraft and ground.
 $e' = h \sin \phi$
 $a_2 = a_1 \cos \phi - l_3 \sin \phi$

The total linear acceleration at the main gear is:

$$\ddot{z}_{MG} = \ddot{z}_0 - \ddot{\theta}_y a_2$$

Substituting from equations 84 and 85

$$\ddot{z}_{MG} = g/r^2 W [r^2(\bar{F}_M + L - W) + a_2(\bar{F}_M a_2 + L e')] \quad (86)$$

From the equation of uniformly accelerated motion (no rotation):

$$V_F^2 = V_1^2 + 2\ddot{z}\delta$$

where V_F = final velocity, ft./sec. = 0

V_1 = initial velocity, ft./sec. = V_2

$$\ddot{z} = -\ddot{z}_{MG}$$

$$\delta = \delta_M$$

Substituting and solving for \ddot{z}_{MG}

$$\ddot{z}_{MG} = \frac{V_2^2}{2\delta_M} \quad (87)$$

Equating the two expressions for \ddot{z}_{MG} from equations 86 and 87

$$\frac{V_2^2}{2\delta_M} = g/2\delta_M [r^2(\bar{F}_M + L - W) + a_2(\bar{F}_M a_2 + L e')]$$

Since $L = 2/3 W$ and considering the overall efficiency η_M we solve for the peak load $F_M = \frac{\bar{F}_M}{\eta_M}$ (88)

$$F_M = \frac{W}{\eta_M} \left[\frac{V_2^2}{2g\delta_M} + \frac{1}{3} - \frac{2}{3} e' \frac{a_2}{r^2} \right] \left[\frac{r^2}{r^2 + a_2^2} \right]$$

F_M is a vertical load with respect to the ground but since the aircraft is inclined at an angle ϕ , the axial load in the strut F_M and the drag load normal to the strut F_{MD} are determined as follows.

$$F_M' = F_M \cos \phi + .25 F_M \sin \phi \quad (89)$$

$$F_{MD}' = .25 F_M \cos \phi - F_M \sin \phi \quad (90)$$

(3) Two Point Braked - Roll

The maximum main gear drag loads are produced by a 2 point braked-roll condition at the maximum gross weight. In Fig. 44 the forces on the gears are illustrated schematically for this condition.

The loads are calculated as follows:

$$F_M = W$$

$$F_{MD} = C_f F_M \quad (91)$$

where F_{MD} = main gear drag load on both gears, lbs.

C_f = coefficient of friction = 0.8

For the calculations of the gear loads the ground friction factor (with some braking) is taken as .25. The overall gear efficiency is estimated as being 80 percent. The summary of the gear data loads and c.g. accelerations is contained in Table 9.

Dynamic Impact Analysis

The acceleration-time history for the aircraft c.g. is best represented by the general characteristics of known landing gear data. The pulse period and general character have been reviewed in the jig drop test data of Reference 17 and a non-dimensional relationship is shown in Fig. 45. An assumed equivalent function and drop test data (Ref. 17) are illustrated in Fig. 45.

The equivalent forcing function is approximated as a symmetrical pulse with a rise of one quarter of the pulse period, a dwell having constant amplitude for one half the pulse period and, a decay symmetrical with the rise. The response factor for such a forcing function is solved in Figure 4-21 (a) of Ref. 18 and is calculated with reference to the ratio of times with the V/STOL configurations' fundamental period. The calculated values are shown in Table (10).

The landing pulse time for gears investigated indicate a total period of .4 seconds is representative. The time to peak acceleration is in the order of .1 to .15 seconds. For this analysis the approximation used should be sufficiently representative.

The limit loads arrived at in the preceding landing loads analysis are multiplied by a factor of 1.5 to arrive at ultimate loadings. Using these ultimate loads as applied to the aircraft and considering the wing structural response factor the wing bending, torsion, and stresses are found. These data are compiled in Table 10. The combination of 1g steady state wing loads is added to the dynamic response inertial loadings of the landing impact.

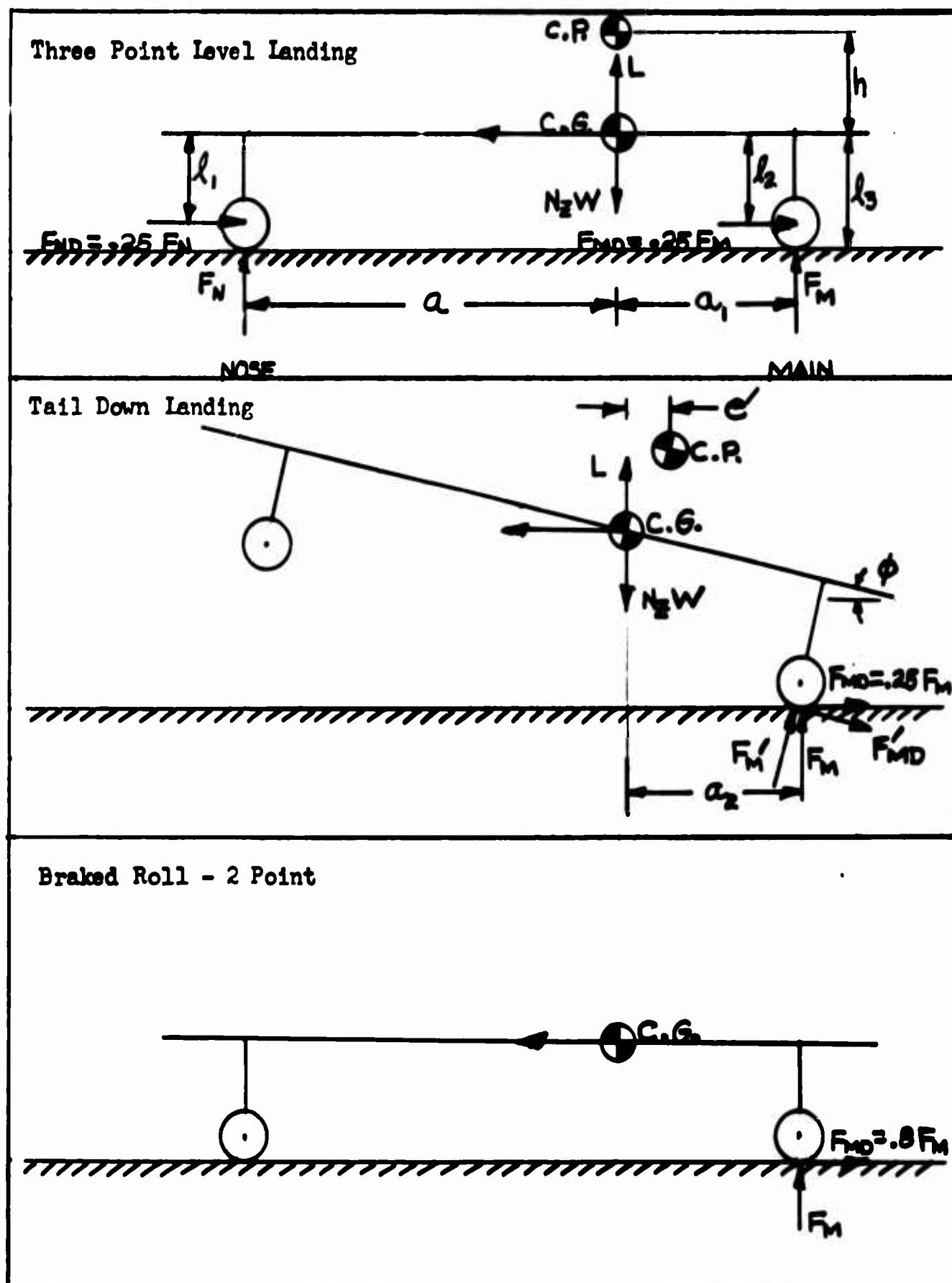


Figure 44 - Schematic of Landing Gear Loads

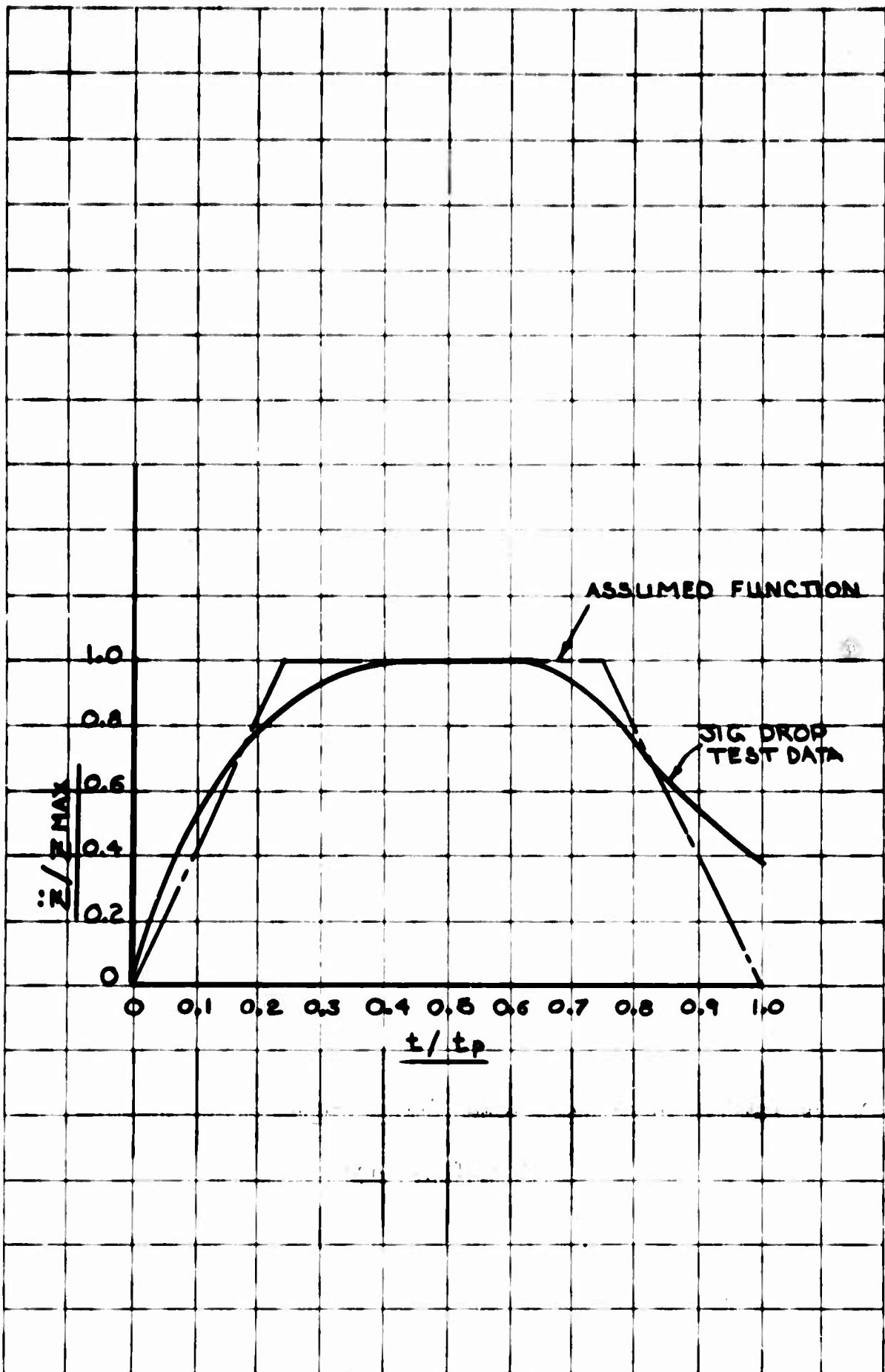


Figure 45 - Non-Dimensional Acceleration - Time History
For Landing Impact

Table 9 - Ultimate Design Landing Gear Loads

Data \ Config.		Fixed Jet	Tilt Wing	Extended Flap	Tilt Prop	Buried Fan
3 Point Level Landing	δ_N , Stroke-Ft.	1.0	1.0	1.0	1.0	1.0
	δ_M , Stroke-Ft.	1.0	1.0	1.0	1.0	1.0
	F_N , Lbs.	-62,000	-123,000	-116,000	-132,000	-84,000
	F_M , Lbs.	-450,000	-544,000	-670,000	-791,000	-676,000
	F_{ND} , Lbs.	15,000	31,000	29,000	34,000	21,000
	F_{MD} , Lbs.	114,000	136,000	168,000	197,000	169,000
	F_N/W	-0.36	-0.55	-0.44	-0.43	-0.33
	F_M/W	-2.62	-2.44	-2.55	-2.57	-2.67
	F_{ND}/W	0.09	0.14	0.11	0.11	0.08
	F_{MD}/W	0.66	0.61	0.64	0.64	0.67
	N_z At C.G.	2.66	2.66	2.66	2.66	2.66
	N_z At Gear	2.0	2.0	2.0	2.0	2.0
Braked Roll, 2P	F_{MD} , Lbs.	279,000	401,000	474,000	555,000	455,000
	F_{MD}/W	1.62	1.80	1.80	1.80	1.80
Tail Down Landing	δ_M , Stroke-Ft.	1.0	1.0	1.0	1.0	1.0
	F_M' , Lbs.	-525,000	-665,000	-797,000	-940,000	-772,000
	F_{MD} , Lbs.	64,000	83,000	100,000	99,000	96,000
	F_M'/W	-3.05	-2.98	-3.03	-3.05	-3.05
	F_{MD}/W	0.37	0.37	0.38	0.32	0.38

- Notes: (1) $F_{ND}, F_{MD} = \frac{1}{4}$ of F_N & F_M
- (2) F_M = the total load on both main gears
- (3) All loads are normalized by dividing by the design gross weight.
- (4) For the braked roll condition gear loads are calculated from the STOL weight.
- (5) For the tail down landing condition F_M' & F_{MD} are the vertical and drag loads with respect to the aircraft coordinate axis rotated through the angle ϕ .

Table 10 - Landing Impact Wing Root Moments, Torsions, and Stresses

Config. Data	Fixed Jet	Tilt Wing	Extended Flap	Tilt Prop	Buried Fan
tp/T_y	0.34	0.30	0.25	0.80	0.85
1 g Steady State Flight Loads					
Bending Moment	7,000,000	11,500,000	15,600,000	21,600,000	19,500,000
Torsional Moment	3,200,000	-1,600,000	360,000	530,000	2,000,000
1st Modal Inertial Response Loads					
Response Factor	1.54	1.42	1.20	1.63	1.56
Bending Moment	-3,400,000 -11,500,000	16,000,000 -39,200,000	27,700,000 -41,500,000	16,800,000 -74,600,000	-4,600,000 -16,300,000
Torsional Moment	1,200,000 4,000,000	-626,000 -1,540,000	-1,200,000 -1,730,000	11,900,000 -52,500,000	-286,000 -1,000,000
Maximum Loading					
Bending Moment	-4,500,000	27,700,000	25,900,000	53,000,000	14,900,000
Torsional Moment	7,200,000	-3,100,000	-1,400,000	52,000,000	1,800,000
Maximum Bending Stress, PSI	7,050	24,600	18,700	23,700	7,250
Maximum Shear Stress, PSI	14,000	6,700	3,070	97,500	1,280

Notes: (1) Sign Convention

Bending / Compression on upper surface of wing
Torsion / Pitching moment

IV. DETERMINATION OF DEGREE AND RELATIVE CRITICALNESS OF STRUCTURAL RESPONSE

Based on the analyses of Section III, the structural response calculations were presented in tabular form for all 5 V/STOL configurations and for each parameter investigated.

The determination of the degree of relative criticalness is based on the ratio of the value of the peak dynamic response load or stress including all steady state conditions with a corresponding normal design ultimate load or stress. These normal design ultimate loads and stresses were determined in the landing gear loads analysis and the wing structural analysis respectively for each V/STOL configuration. Landing gear loads were determined for three conditions; (1) 3-Point Level Landing, (2) Braked Roll-2 Point, and (3) Tail Down Landing (Ref. Section III E). The maximum nose and main gear vertical and drag loads were chosen from these three conditions for comparison with a corresponding dynamic load in determining the degree of criticalness. The maximum wing bending and torsional moments were calculated at the wing root of each configuration from a 4.5 g ultimate maneuver condition and are subsequently used with a corresponding dynamic wing bending or torsional moment to determine the degree of criticalness.

The degree of criticalness (Ref. Table 11) was determined for two types of conditions.

(1) Wing Structural Conditions

- a. Tiedown
- b. Maneuver
- c. Gust Penetration
- d. Landing Impact

(2) Landing Gear Conditions

- a. Taxiing and Take-Off Run
- b. Starting and Stopping While Towing
- c. Braking

In the first group, Wing Structural Conditions, the degree of criticalness is defined as the ratio of the dynamic and steady state stress to the ultimate design stress at the wing root. This can also be stated as:

Wing Structural Degree of Criticalness = $\frac{\text{Dynamic} + \text{Steady State Stress}}{\text{Ultimate Stress}}$

$$= \frac{S_{\text{DYN}} + S_{\text{SS}}}{S_{\text{UIT}}}$$

If $\frac{S_{DYN} + S_{SS}}{S_{ULT}}$ is ≥ 1.0 ————— Failure of structure
 ≥ 0.897 ————— Yielding for 7075-T6

For the second group, Landing Gear Conditions, the degree of criticalness is defined as the ratio of the maximum total main or nose gear load (static and dynamic) to the maximum ultimate design load calculated for the gear (Ref. Table 9). In equation form:

$$\text{Landing Gear Degree of Criticalness} = \frac{(F_{DYN} + F_{Static})/W}{F_{ULT}/W}$$

All gear loads have been normalized for convenience by dividing by the design gross weight of the aircraft in question.

A ratio of 1.0 indicates that a failure condition is eminent and above 1.0 failure occurs. A value of less than 1.0 may not be critical if the material used is such that the yielding is close to the ultimate stress. However, normal practice usually requires that a factor of safety of 50 percent be used with the limit load or stress.

There is a condition in which no ratio can be established such as take-off abort. In this case only relative numbers indicate the criticalness of the configurations and the condition.

With all the conditions of Section III analyzed for all 5 configurations, a matrix is formed and shown in Table 11.

Upon examination of the matrix, the most critical condition appears to be starting and stopping while towing. However, this condition is believed to be conservative and can be eliminated by providing an energy absorption device such as that discussed in Section VI, item A.

The next most critical condition is taxiing and take-off run. It is recognized that the method of linear analysis utilized for this condition may be conservative. However, the trend is such as to indicate that further detail investigation is warranted for the runway dip condition on the Tilt Wing V/STOL configuration.

Other conditions also indicate a relative degree of criticalness that warrants further investigation. But within the scope of the contract, only the runway dip condition is to be analyzed in detail. Recommendations for further studies are contained in Section VIII.

Table 11- Degree of Criticalness

Condition \ Config.		Fixed Jet	Tilt Wing	Extended Flap	Tilt Prop	Buried Fan
Taxiing & Take-Off Run	Nose Gear Translation	1.80	2.82	2.73	2.65	1.90
	Main Gear Translation	2.46	2.88	2.66	2.69	2.57
Starting & Stopping While Towing	Nose Gear Vertical	0.60	0.82	0.77	0.79	0.70
	Nose Gear Horizontal	4.83	4.23	4.95	5.00	5.48
	Main Gear Vertical	0.56	0.59	0.60	0.59	0.60
Tiedown	Wing Bending Stress	0.20	0.29	0.32	0.14	0.05
	Wing Shear Stress	0.03	0.15	0.16	0.18	0.02
Braking	Nose Gear Vertical	1.29	0.93	1.08	1.07	1.34
	Nose Gear Longitudinal	0.44	0.66	0.54	0.56	0.49
	Main Gear Vertical	Not Critical	Not Critical	Not Critical	Not Critical	Not Critical
	Main Gear Longitudinal	0.52	0.44	0.46	0.33	0.47
Take-Off Abort		Not Critical VTOL	Not Critical VTOL	Not Critical VTOL	Not Critical VTOL	Not Critical VTOL
Maneuver	Wing Bending Stress	0.87	1.00	1.12	0.64	0.47
	Wing Shear Stress	0.49	0.07	0.21	2.26	0.24
Gust Penetration	Wing Bending Stress	1.01	0.75	0.82	0.42	0.53
	Wing Shear Stress	0.56	0.05	0.15	1.32	0.27
Landing Impact	Wing Bending Stress	0.09	0.32	0.24	0.30	0.09
	Wing Shear Stress	0.30	0.15	0.07	2.12	0.03

Notes: (1) Structural Degree of Criticalness = $\frac{\text{Dyn. / S.S. Stress}}{\text{Ult. Stress}} = \frac{S_{\text{dyn}} / S_{\text{ss}}}{S_{\text{ult}}}$

If $\frac{S_{\text{dyn}}}{S_{\text{ult}}}$ is ≥ 1.0 Failure of structure
 $\geq .897$ Yielding for 7075-T6

(2) Landing Gear Degree of Criticalness = $\frac{(F_{\text{dyn}} - F_{\text{static}})/W}{F_{\text{ult}}/W}$

V. DETAIL STRUCTURAL RESPONSE ANALYSIS

A. Discussion of Problem

The purpose of the detailed dip analysis is to investigate the effects of wing-fuselage flexibility, runway speed, and runway roughness on the degree of relative criticalness. Consider the fully coupled aircraft response as it moves over a single (1 - cosine) dip of fixed depth for various values of dip length. The mathematical model for the aircraft includes flexibility of wing and fuselage, main and nose gear tire spring rates, as well as oleo spring and damping rates. Only symmetrical responses of the aircraft are assumed for this analysis, that is, anti-symmetric response including roll is not considered. This requires that the dip be wide enough in the direction perpendicular to the direction of aircraft motion to encompass all the gears.

The aircraft chosen for detail study is the Tilt Wing configuration which was found to be most critical in the preliminary investigation (Ref. Section IV). Parameters used in the analysis are explained and summarized in part C. Aerodynamic effects have not been included.

B. Mathematical Model

Formulation of the mathematical model of the aircraft was based on representation by normal modes. This allowed the use of a large number of panel points in the wing and fuselage, but at the same time did not require large dynamic matrices. A standard transformation technique was employed using Lagrange equations. Due to the character of the dip forcing function, a simple closed form was not readily attainable. Finite difference integration proved to be most easily adaptable to solve the transformed dynamic equations.

The aircraft model is shown below.

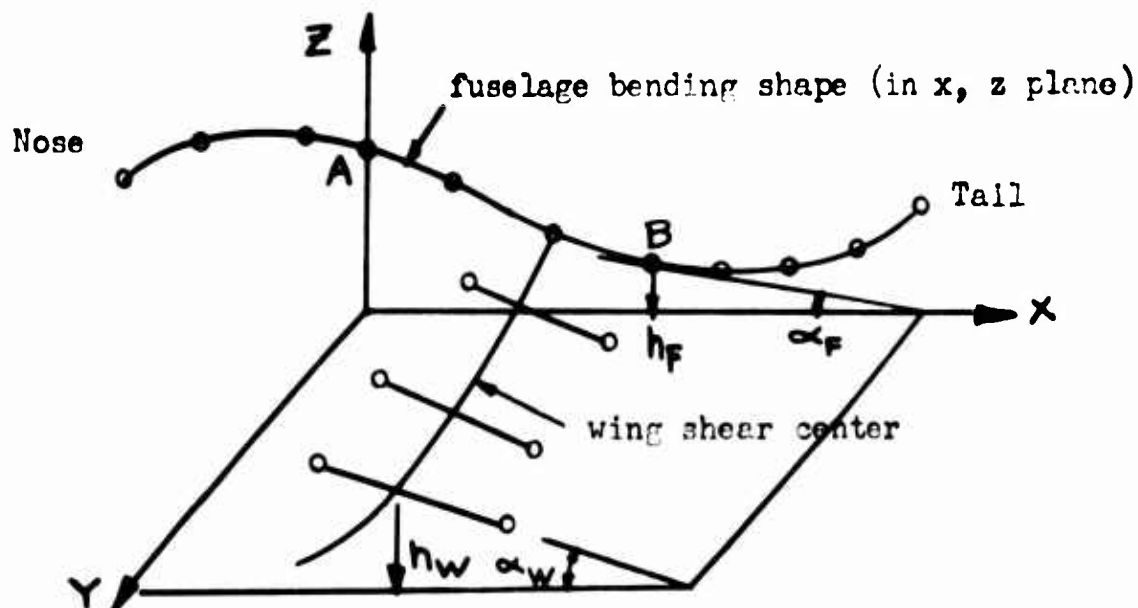


Figure 46 Aircraft Model for Detailed Runway Dip Analysis

Note that the wing coordinates are given on the wing shear center. Point A, the axis origin, represents the location of the nose gear and Point B represents the main gear. The distance between the main and nose gear is l .

The analysis is simplified by considering one wing and half the fuselage since only symmetric motions are being taken into account.

To properly consider half the fuselage and one wing the analysis was carried out as follows:

1. One-half the fuselage kinetic and potential energy is determined. This is done by halving the masses and doubling the influence coefficients.
2. One-half the nose gear potential and kinetic energy is used. This is accomplished by halving the mass and halving the spring rates. These factors are not shown in the following analysis.

The aircraft fixed coordinate matrix is:

$$\{X_F\} = \begin{Bmatrix} h_W \\ h_F \\ \alpha_W \\ \alpha_F \\ \bar{z}_3 \\ \delta_1 \\ \bar{z}_1 \\ \delta_2 \end{Bmatrix}$$

where \bar{z}_3 , q_1 , \bar{z}_4 , and q_2 are the coordinates assigned to the nose and main landing gear and x is measured positive aft from the nose gear. The gear systems are shown in the following schematic drawing.

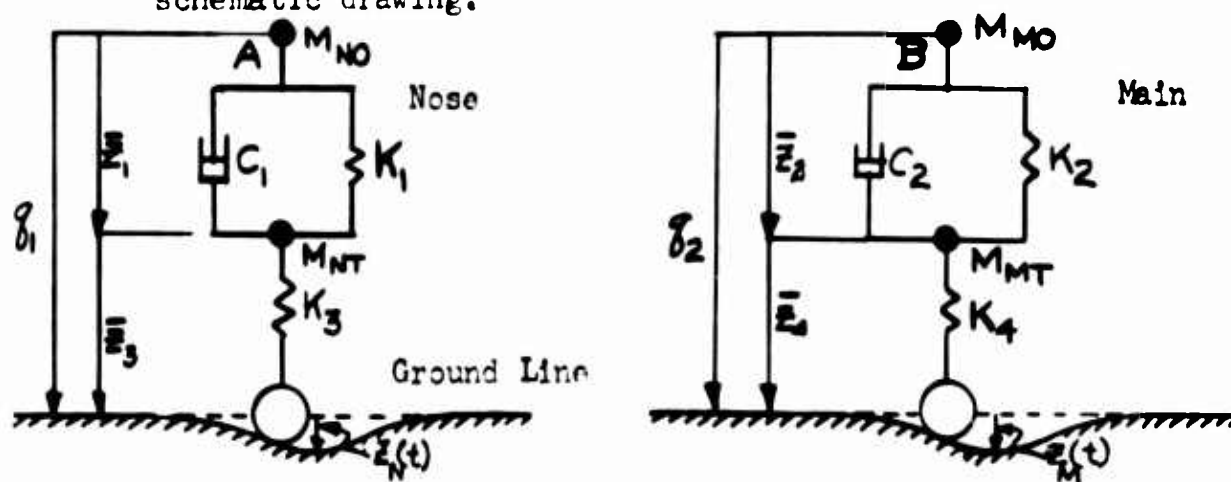


Figure 1-1 Schematic Drawing of Nose and Main Landing Gear

The absolute mass matrix is:

$$[M] = \begin{bmatrix} M_w & 0 & 0 & 0 & 0 & 0 & 0 \\ 0 & M_p & 0 & 0 & 0 & 0 & 0 \\ 0 & 0 & I_w & 0 & 0 & 0 & 0 \\ 0 & 0 & 0 & I_p & 0 & 0 & 0 \\ 0 & 0 & 0 & 0 & M_{\pi} & 0 & 0 \\ 0 & 0 & 0 & 0 & 0 & M_{\delta} & 0 \\ 0 & 0 & 0 & 0 & 0 & 0 & M_{\theta} \end{bmatrix}$$

The total kinetic energy of the system will be:

$$2KE = \{\dot{x}_p\}' [M] \{\dot{x}_p\} \quad (92)$$

The systems' potential energy is best given by using relative coordinates. We have chosen to work with the free-free modes of the structure to obtain the potential energy.

The required transformation matrix is arrived at as follows. Consider the aircraft on its gear as shown below.

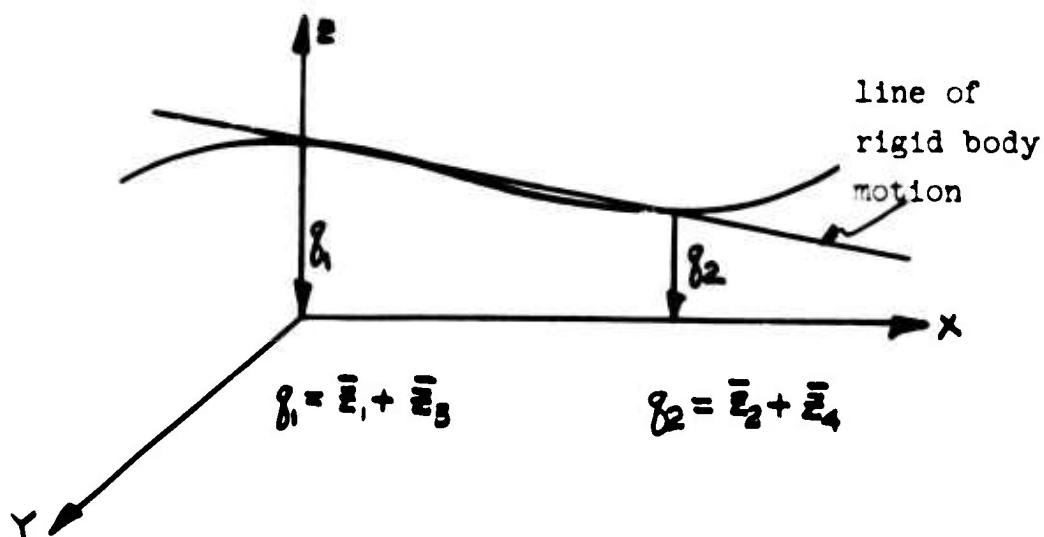


Figure 48 - Schematic of Aircraft Deformation

A line of rigid body motion is defined by the location of the gear. The motion of **every** point in the aircraft can be given as the sum of the rigid body motion and bending with respect to the rigid body.

$$h_F = (1-x/l)(\bar{z}_1 + \bar{z}_3) + x/l(\bar{z}_2 + \bar{z}_4) + \sum_{i=1}^n f_i \phi_{Fi} \quad (93)$$

and

$$h_W = (1-x/l)(\bar{z}_1 + \bar{z}_3) + x/l(\bar{z}_2 + \bar{z}_4) + \sum_{i=1}^n f_i \phi_{Wi} \quad (94)$$

ϕ_{Fi} is a normalized fuselage bending shape and ξ_i is a modal coordinate for that shape. Similarly ϕ_{wi} is a normalized wing bending shape and since we are obtaining coupled wing-fuselage modes, both wing and fuselage have the same ξ_i . Notice that there is a boundary condition placed on ϕ_{Fi} , i.e. ϕ_{Fi} must be zero at the gear points. In order to satisfy this condition we have several alternatives, two of which are, (1) generate pinned-pinned modes of the wing fuselage, and (2) generate free-free modes and reference the shapes to the line of rigid body motion. The latter alternative was chosen. The rereferencing of the free modes is shown graphically in the following schematic.

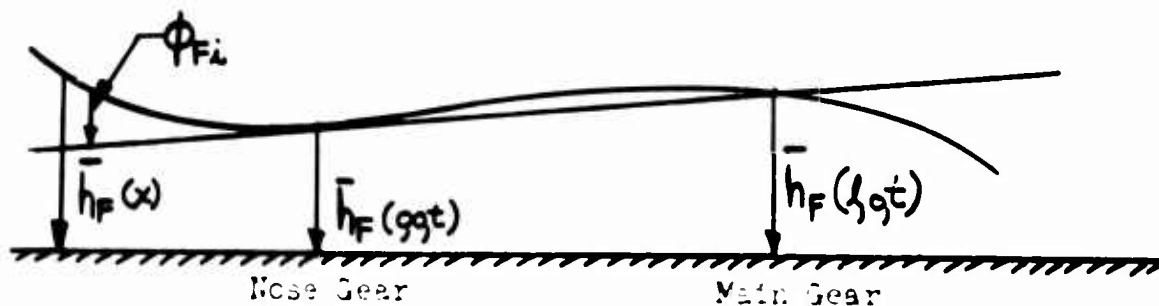


Figure 49- Schematic of Transformation of Free-Free Modes to Pinned - Pinned Shapes

$$\phi_{Fi} = \bar{h}_{Fi}(x, 0, t) - x/l \bar{h}_{Fi}(l, 0, t) - (1 - x/l) \bar{h}_{Fi}(0, 0, t) \quad (95)$$

Similarly

$$\phi_{wi} = \bar{h}_{wi}(x, y, t) - x/l \bar{h}_{wi}(l, 0, t) - (1 - x/l) \bar{h}_{wi}(0, 0, t) \quad (96)$$

In order to obtain α_F , the relative fuselage free-free pitching, $\bar{\alpha}_F$ is added to the derivative of the deflection shape.

$$\alpha_F = \sum_{i=1}^n \bar{\alpha}_{Fi} + \frac{\partial h_F}{\partial x} \quad (97)$$

α_w is the sum of the relative wing pitching $\bar{\alpha}_w$ and α_F of the fuselage at the wing root intersection.

$$\alpha_w = \sum_{i=1}^n \bar{\alpha}_{wi} + \frac{\partial h_F}{\partial x} \quad (\text{wing root}) \quad (98)$$

Performing the required differentiation leads to:

$$\alpha_F = 1/l(\bar{z}_4 + \bar{z}_2 - \bar{z}_3 - \bar{z}_1) + \sum_{i=1}^n (g_i \frac{\partial \phi_{Fi}}{\partial x} + \bar{\alpha}_{Fi}) \quad (99)$$

and

$$\alpha_W = 1/l(\bar{z}_4 + \bar{z}_2 - \bar{z}_3 - \bar{z}_1) + \sum_{i=1}^n (g_i \frac{\partial \phi_{Fi}}{\partial x} + \bar{\alpha}_{Fi}) \Big|_{\text{WING ROOT}} + \sum_{i=1}^n \alpha_{Wi} \quad (100)$$

But

$$\frac{\partial \phi_{Fi}}{\partial x} = 1/l(\bar{h}_{Fi}(0,0,t) - \bar{h}_{Fi}(l,0,t) + \frac{\partial \bar{h}_{Fi}}{\partial x}(x,0,t)) \quad (101)$$

Identifying

$$\psi_{Fi} \equiv \frac{\partial \bar{h}_{Fi}}{\partial x}(x,0,t) + \bar{\alpha}_{Fi} + 1/l(\bar{h}_{Fi}(0,0,t) - \bar{h}_{Fi}(l,0,t)) \quad (102)$$

and

$$\psi_{Wi} \equiv \frac{\partial \bar{h}_{Fi}}{\partial x} \Big|_{\text{WING ROOT}} + \bar{\alpha}_{Wi} + 1/l(\bar{h}_{Fi}(0,0,t) - \bar{h}_{Fi}(l,0,t)) \quad (103)$$

Combining all these expressions we arrive at the following transformation.

$\left\{ \begin{array}{l} h_F \\ h_W \\ \alpha_F \\ \alpha_W \\ \bar{z}_3 \\ \bar{z}_2 \\ g_1 \\ \bar{z}_4 \\ g_2 \end{array} \right\} =$	$\phi_{Fi} \rightarrow \phi_{Fn}$	$1-x/l$	$1-x/l$	x/l	x/l
	$\phi_{Wi} \rightarrow \phi_{Wn}$	$1-x/l$	$1-x/l$	x/l	x/l
	$\psi_{Fi} \rightarrow \psi_{Fn}$	$-1/l$	$-1/l$	$1/l$	$1/l$
	$\psi_{Wi} \rightarrow \psi_{Wn}$	$-1/l$	$-1/l$	$1/l$	$1/l$
	0	0	1	0	0
	0	0	1	1	0
	0	0	0	0	1
	0	0	0	0	1
	0	0	0	0	1
	0	0	0	0	1

 $\left\{ \begin{array}{l} g_1 \\ g_2 \\ g_3 \\ g_4 \\ g_5 \\ g_6 \\ g_7 \\ g_8 \\ g_9 \\ g_{10} \end{array} \right\}$

where

$$\phi_{Fi} \equiv \bar{h}_{Fi}(x, 0, t) - x/l \bar{h}_{Fi}(l, 0, t) - (1 - x/l) \bar{h}_{Fi}(0, 0, t)$$

$$\phi_{Wi} \equiv \bar{h}_{Wi}(x, y, t) - x/l \bar{h}_{Fi}(l, 0, t) - (1 - x/l) \bar{h}_{Fi}(0, 0, t)$$

$$\psi_{Fi} \equiv \frac{\partial \bar{h}_{Fi}}{\partial x}(x, 0, t) + \bar{\alpha}_{Fi} + 1/l \left(\bar{h}_{Fi}(0, 0, t) - \bar{h}_{Fi}(l, 0, t) \right)$$

$$\psi_{Wi} \equiv \frac{\partial \bar{h}_{Fi}}{\partial x} \Big|_{\text{WING ROOT}} + \bar{\alpha}_{Wi} + 1/l \left(\bar{h}_{Fi}(0, 0, t) - \bar{h}_{Fi}(l, 0, t) \right)$$

Consider in detail the $\bar{h}(x, y, t)$ free-free displacements.

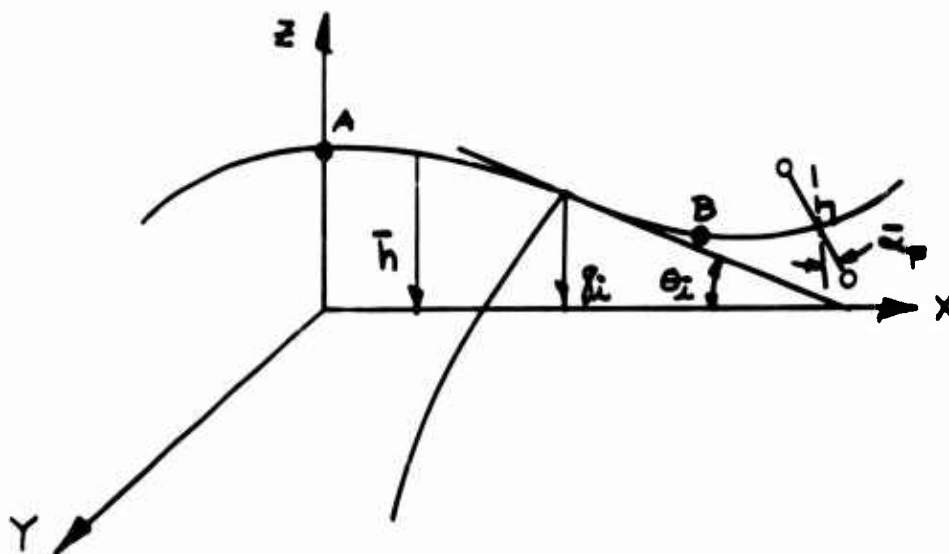


Figure 50 - Schematic of Aircraft Coordinates for Normal Mode Analysis

We define 2 ignorable coordinates θ_1 and q_1 at the wing root. The potential energy of the system can be calculated using influence coefficients for a cantilever boundary conditions at the wing root.

Let

$$\bar{h}_W = g_i + \theta_i(x - x_{\text{WING}}) + f h_W$$

$$\bar{h}_F = g_i + \theta_i(x - x_{\text{WING}}) + f h_F$$

$$\left. \begin{aligned} \bar{\alpha}_F &= f \alpha_F \\ \bar{\alpha}_W &= f \alpha_W \end{aligned} \right\} \text{defined relative torsion of wing or fuselage}$$

where

Fh_w = wing displacement relative to cantilever point.

Fh_F = fuselage displacement relative to cantilever point.

$F\alpha_w$ = wing rotation relative to cantilever point.

$F\alpha_F$ = fuselage rotation relative to cantilever point.

Therefore

$$\begin{Bmatrix} \bar{h}_w \\ \bar{h}_F \\ \bar{\alpha}_w \\ \bar{\alpha}_F \end{Bmatrix} = \begin{bmatrix} 1 & 0 & 0 & 0 & 1 & x-x_{wing} \\ 0 & 1 & 0 & 0 & 1 & x-x_{wing} \\ 0 & 0 & 1 & 0 & 0 & 0 \\ 0 & 0 & 0 & 1 & 0 & 0 \end{bmatrix} \begin{Bmatrix} Fh_w \\ Fh_F \\ F\alpha_w \\ F\alpha_F \\ g_i \\ \theta_i \end{Bmatrix}$$

$$\equiv [\bar{\mu}] \begin{Bmatrix} Fh_w \\ Fh_F \\ F\alpha_w \\ F\alpha_F \\ g_i \\ \theta_i \end{Bmatrix}$$

The mass matrix for this system is:

$$[M] = \begin{bmatrix} M_w & 0 & \delta_w & 0 \\ 0 & M_F & 0 & 0 \\ \delta_w & 0 & I_w & 0 \\ 0 & 0 & 0 & I_F \end{bmatrix}$$

The systems' equations of motion are:

(104)

$$-\omega_i^2 [\bar{\mu}]' [M] [\bar{\mu}] \begin{Bmatrix} Fh_w \\ Fh_F \\ F\alpha_w \\ F\alpha_F \\ g_i \\ \theta_i \end{Bmatrix} + \begin{bmatrix} K_{11} & K_{12} & K_{13} & K_{14} & & \\ K_{21} & K_{22} & K_{23} & K_{24} & & \\ K_{31} & K_{32} & K_{33} & K_{34} & & \\ K_{41} & K_{42} & K_{43} & K_{44} & & \\ & & & & & \\ & & & & & \\ & & & & & \end{bmatrix} \begin{Bmatrix} Fh_w \\ Fh_F \\ F\alpha_w \\ F\alpha_F \\ g_i \\ \theta_i \end{Bmatrix} = 0$$

where K_{ij} is the flexibility tensor, lbs/in.

Solutions may be obtained for this eigenvalue problem by simple matrix techniques and result in a set of normal modes and frequencies. These are subsequently designated by ω_i and

$$\left\{ \begin{array}{c} F_{hwi} \\ F_{hFi} \\ F_{\alpha wi} \\ F_{\alpha Fi} \\ \delta_i \\ \theta_i \end{array} \right\} \quad \text{and} \quad \left\{ \begin{array}{c} \bar{h}_{wi} \\ \bar{h}_{Fi} \\ \bar{\alpha}_{wi} \\ \bar{\alpha}_{Fi} \end{array} \right\}$$

The equations of motion will come from the Lagrange equation.

$$\frac{d}{dt} \left(\frac{\partial KE}{\partial \dot{x}_R} \right) - \frac{\partial KE}{\partial x_R} = - \frac{\partial PE}{\partial x_R} + F_R \quad (105)$$

where F_R forces are not derivable from a potential function.

The kinetic energy is;

$$2KE = \{\dot{x}_F\}' [M] \{\dot{x}_F\}$$

and $\{x_F\} = [\mu] \{x_R\}$

$$2KE = [\dot{x}_R]' [\mu]' [M] [\mu] \{\dot{x}_R\} \quad (106)$$

Therefore $\frac{\partial KE}{\partial x_R} = 0$

and

$$\frac{d}{dt} \left(\frac{\partial KE}{\partial \dot{x}_R} \right) = [\mu]' [M] [\mu] \{\ddot{x}_R\} \quad (107)$$

Since we have written the bending-torsion motions as the sum of a series of motions of the free-free structure the total strain energy can be arrived at by summing the strain energies of the participating normal mode.

The potential for a normal mode is equal to:

(108)

$$PE_i = \begin{Bmatrix} F_{h_{wi}} \\ F_{h_{Fi}} \\ F_{\alpha_{wi}} \\ F_{\alpha_{Fi}} \end{Bmatrix}' \quad \begin{bmatrix} K_{11} & K_{12} & K_{13} & K_{14} \\ K_{21} & K_{22} & K_{23} & K_{24} \\ K_{31} & K_{32} & K_{33} & K_{34} \\ K_{41} & K_{42} & K_{43} & K_{44} \end{bmatrix} \quad \begin{Bmatrix} F_{h_{wi}} \\ F_{h_{Fi}} \\ F_{\alpha_{wi}} \\ F_{\alpha_{Fi}} \end{Bmatrix}$$

Since the normal modes are solutions to the equations of motion:

$$-\omega_i^2 [\mu]' [M] [\bar{u}] \begin{Bmatrix} F_{h_{wi}} \\ F_{h_{Fi}} \\ F_{\alpha_{wi}} \\ F_{\alpha_{Fi}} \\ g_i \\ \theta_i \end{Bmatrix} + \begin{bmatrix} K_{11} & K_{12} & K_{13} & K_{14} & & \\ K_{21} & K_{22} & K_{23} & K_{24} & & \\ K_{31} & K_{32} & K_{33} & K_{34} & & \\ K_{41} & K_{42} & K_{43} & K_{44} & & \\ & & & & & \\ & & & & & \end{bmatrix} \begin{Bmatrix} F_{h_{wi}} \\ F_{h_{Fi}} \\ F_{\alpha_{wi}} \\ F_{\alpha_{Fi}} \\ g_i \\ \theta_i \end{Bmatrix} = 0$$

$$[\bar{u}]' [M] [\bar{u}] \text{ can be shown to be} \quad (109)$$

M_w		S_w			
	M_F				
S_w		I_w			
			I_F		
				M_{55}	
					I_{66}

where M_{55} = mass of aircraft.

I_{xx} = total aircraft inertia about gimbal coordinate.

Substituting the equations for PF_i gives:

$$2PE_i = \begin{Bmatrix} f_{h_{wi}} \\ f_{h_{Fi}} \\ f_{\alpha_{wi}} \\ f_{\alpha_{Fi}} \end{Bmatrix} \begin{bmatrix} K_{11} & K_{12} & K_{13} & K_{14} \\ K_{21} & K_{22} & K_{23} & K_{24} \\ K_{31} & K_{32} & K_{33} & K_{34} \\ K_{41} & K_{42} & K_{43} & K_{44} \end{bmatrix} \begin{Bmatrix} f_{h_{wi}} \\ f_{h_{Fi}} \\ f_{\alpha_{wi}} \\ f_{\alpha_{Fi}} \end{Bmatrix} \xi_i^2$$

$$= \omega_i^2 \begin{Bmatrix} f_{h_{wi}} \\ f_{h_{Fi}} \\ f_{\alpha_{wi}} \\ f_{\alpha_{Fi}} \end{Bmatrix} \begin{bmatrix} M_w & & S_w & \\ & M_F & & \\ S_w & & I_w & \\ & & & I_F \end{bmatrix} \begin{Bmatrix} f_{h_{wi}} \\ f_{h_{Fi}} \\ f_{\alpha_{wi}} \\ f_{\alpha_{Fi}} \end{Bmatrix} \xi_i^2 = -\omega_i^2 M_i \xi_i^2$$

Therefore $2PE_i = \xi_i^2 \omega_i^2 M_i \quad (110)$

and summing over all modes

$$PE = \sum_{i=1}^n PE_i = \sum_{i=1}^n 1/2 \omega_i^2 M_i \xi_i^2 \quad (111)$$

Equation 111 gives all the structural potential energy.

The spring energies are simply:

(112)

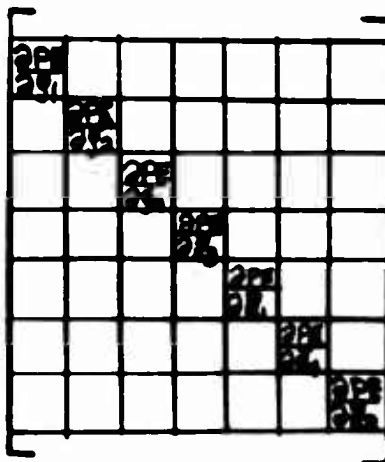
$$PE = 1/2 K_1 \bar{x}_1^2 + 1/2 K_2 \bar{x}_2^2 + 1/2 K_3 (\bar{x}_3 - \bar{x}_N)^2 + 1/2 K_4 (\bar{x}_4 - \bar{x}_M)^2$$

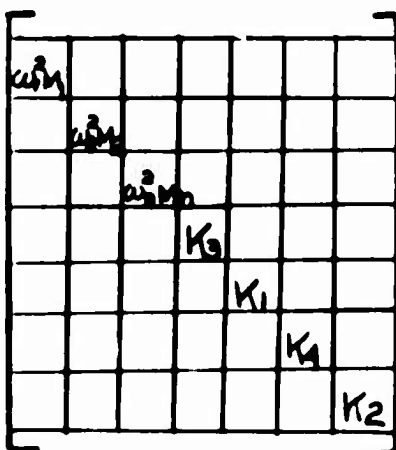
so that finally

(113)

$$PE = \sum_{i=1}^n 1/2 \xi_i^2 \omega_i^2 M_i + 1/2 K_1 \bar{x}_1^2 + 1/2 K_2 \bar{x}_2^2 + 1/2 K_3 (\bar{x}_3 - \bar{x}_N)^2 + 1/2 K_4 (\bar{x}_4 - \bar{x}_M)^2$$

We can now form $\frac{\partial PE}{\partial x_R}$

$$\frac{\partial PE}{\partial x_R} =$$


$$=$$


$$\begin{Bmatrix} \xi_1 \\ \xi_2 \\ \xi_3 \\ \xi_4 \\ \xi_N \\ \xi_M \\ \xi_2 \end{Bmatrix} - \begin{Bmatrix} 0 \\ 0 \\ 0 \\ 0 \\ K_3 \bar{x}_N \\ 0 \\ K_4 \bar{x}_M \end{Bmatrix}$$

A similar dissipation potential can be assigned to the damper, which is differentiated and added to the equations of motion.

If this is done, after combining all equations, we can finally write the equations of motion.

$$[\mu][M][\mu]\{\ddot{x}_R\} + [K_R]\{x_R\} + [C_R]\{\dot{x}_R\} = \{F_R\} + \{F_{DIP}\} \quad (114)$$

where

$$\{x_R\} = \begin{Bmatrix} \xi_1 \\ \xi_n \\ \bar{z}_3 \\ \bar{z}_1 \\ \bar{z}_4 \\ \bar{z}_2 \end{Bmatrix} \quad [K_R] = \begin{bmatrix} K_1 & & & & & \\ & K_2 & & & & \\ & & K_3 & & & \\ & & & K_4 & & \\ & & & & K_5 & \\ & & & & & K_6 \end{bmatrix}$$

and

$$[C_R] = \begin{bmatrix} 0 & & & & & \\ & 0 & & & & \\ & & 0 & & & \\ & & & C_1 & & \\ & & & & 0 & \\ & & & & & C_2 \end{bmatrix} \quad [M] = \begin{bmatrix} M_{ww} & S_w & & & & \\ & M_{\theta\theta} & & & & \\ S_w & & I_{ww} & & & \\ & & & I_{\theta\theta} & & \\ & & & & M_{tt} & \\ & & & & & M_{nn} \\ & & & & & & M_{tt} \\ & & & & & & & M_{nn} \end{bmatrix}$$

$$\{F_{DIP}\} = \begin{Bmatrix} 0 \\ 0 \\ 0 \\ K_3 \bar{z}_N(t) \\ 0 \\ K_4 \bar{z}_M(t) \\ 0 \end{Bmatrix}$$

and $\{F_R\}$ is any other applied external loading.

Dip Description

$$\bar{z}_N(t) = A/2 \left[1 - \cos 2\pi vt/\lambda \right] \quad 0 \leq t \leq \lambda/v \quad (115)$$

$$\bar{z}_M(t) = A/2 \left[1 - \cos(2\pi v/\lambda)(t - \lambda/v) \right] \quad \lambda/v \leq t \leq (\lambda + \lambda)/v \quad (116)$$

and $\bar{x}_N(t) = \bar{x}_M(t) = 0$ for all other time.

These equations describe the aircraft rolling over a single dip of maximum depth A and of length λ .

Static Deflection

The initial deflection of the aircraft is due entirely to the force of gravity.

The gravity potential is given by

$$PE_g = -M_w g h_w - \delta_w g \alpha_w - M_F g h_F - M_{NT} \bar{z}_3 g \quad (117)$$

$$- M_{NO} g_1 g - M_{MT} \bar{z}_4 g - M_{MO} g_2 g$$

Therefore

$$F_{\text{GRAVITY}} = - \frac{\partial PE}{\partial q} = \begin{Bmatrix} M_w g \\ M_F g \\ \delta_w g \\ 0 \\ M_{NT} g \\ M_{NO} g \\ M_{MT} g \\ M_{MO} g \end{Bmatrix} = [M] \begin{Bmatrix} g \\ g \\ g \\ 0 \\ g \\ g \\ g \\ g \end{Bmatrix} = [M]\{g\}$$

$$[K_R]\{x\}_{\text{STATIC}} = [\mu]'[M]\{g\} \quad (118)$$

$$\{x\}_{\text{STATIC}} = [K_R]^{-1}[\mu]'[M]\{g\}$$

and

$$\{x\}_{\text{STATIC}} = [\mu][K_R]^{-1}[\mu]'[M]\{g\} \quad (119)$$

Problem Simplification

1. Using the aircraft structural characteristics given in Section II the free-free structural modes were calculated. These are tabulated in Table 19. For the detailed analysis, only the first and second wing fuselage modes were used.

2. The non-linear oleo and tire spring rates were linearized in the neighborhood of the static deflection.

3. No aerodynamics either steady or unsteady were included.

C. Choice of Parameters

Critical Pitch Condition

The largest rigid body total pitching motion was assumed to occur when $\lambda/l = 2$ (Ref. Section III, Part A1). Using $\lambda/l = 2$ it is possible to calculate the speed at which the time required to traverse the dip is the same as the period of one of the normal modes of aircraft vibration. These are given in the following table.

Table 12 - Summary of Critical Pitch Condition

ω_n rad/sec	Condition Investigated	τ	V ft/sec.
5.869	1st flexible wing fuselage	1.07	60.
10.046	2nd flexible wing fuselage	.625	102.5
8.53	rigid body pitch	.736	87.
9.88	rigid body trans.	.635	101.

Cases were run at forward velocities of 57 and 90 ft/sec for $\lambda/l = 2.0$. Speeds in excess of $V_{\text{Lift-Off}}$ (90 ft/sec) were not considered.

Translation Criteria

The most critical case was considered to be the highest speed case which is $V_{\text{Lift-Off}}$. Using $V_{\text{Lift-Off}}$, λ/l values were calculated to match the periods of normal vibration.

Table 13 - Summary of Critical Translation Condition

ω_n	Cond. Investigated	λ/l
5.869	1st flexible	3.0
10.046	2nd flexible	1.75
8.53	rigid pitch	2.06
9.88	rigid trans.	1.78

In addition, cases were run at $\lambda/l = 1.85, 3.13, 2.0, 2.5, 3.8,$ and 1.0.

Discussion of Results

Shown in Fig. 52 is a summary of information taken at $V_{\text{Lift-Off}}$ and various values of λ/l .

The assumption that \ddot{x}_{max} is greatest at values of $\lambda/l = 2.0$ is not borne out in this case. However, the condition for translation appears reasonable since the c.g. translation acceleration continues to increase as the period of the dip pulse decreases. Hence, maximum translational response is obtained with the shortest dip length at fixed speed with the greatest speed at fixed dip length.

The maximum wing root bending moment, c.g. pitch acceleration, compressive load in nose gear and wing root torsional moment all peak in the same region, $\lambda/l = 1.5$.

This is probably due to the excitation of the second wing mode which has large wing torsion components. The fact that the peak response is at a higher frequency than the wing mode is due to the increase of the wing-fuselage frequencies because of modal coupling with the gear.

Fig. 51 is a detailed time history study of conditions at $\lambda/l = 3$. Here the mode principally involved is the first wing bending mode. Notice first that the c.g. vertical acceleration is reduced due to the coupling of flexible aircraft modes while the pitch acceleration is only slightly changed. The wing torsional moment indicates a large excitation of the bending-torsion mode. The wing root bending moment shows the sum of the increased wing bending moment due to this response and the decrease due to the reduced fuselage motion. The character of the wing root bending moment is different from the character of the c.g. vertical acceleration. Since at the wing root the acceleration is essentially that of the c.g. the indication is that the wing outboard sections are responding with the low harmonic character seen in the bending moment. Here the multiple frequency acceleration input to the wing root is being filtered by the wing and amplification is occurring only at the wings natural frequency.

The nose and main gear loads do not appear to change appreciably in magnitude although there is again a frequency shift due to mode coupling. This result has been previously noted by F. Allen and L. Mosby of Douglas Aircraft (Ref. 3).

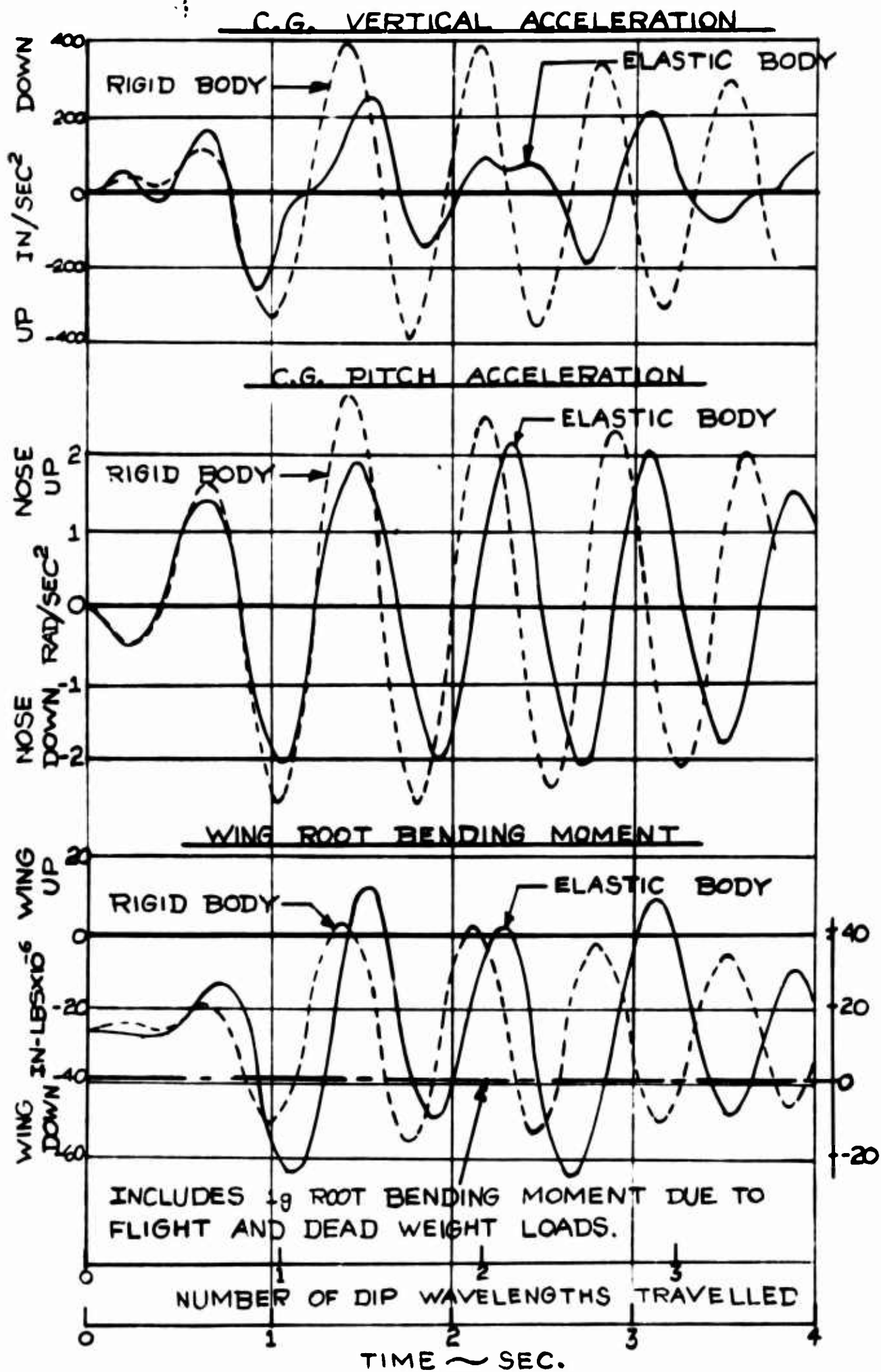
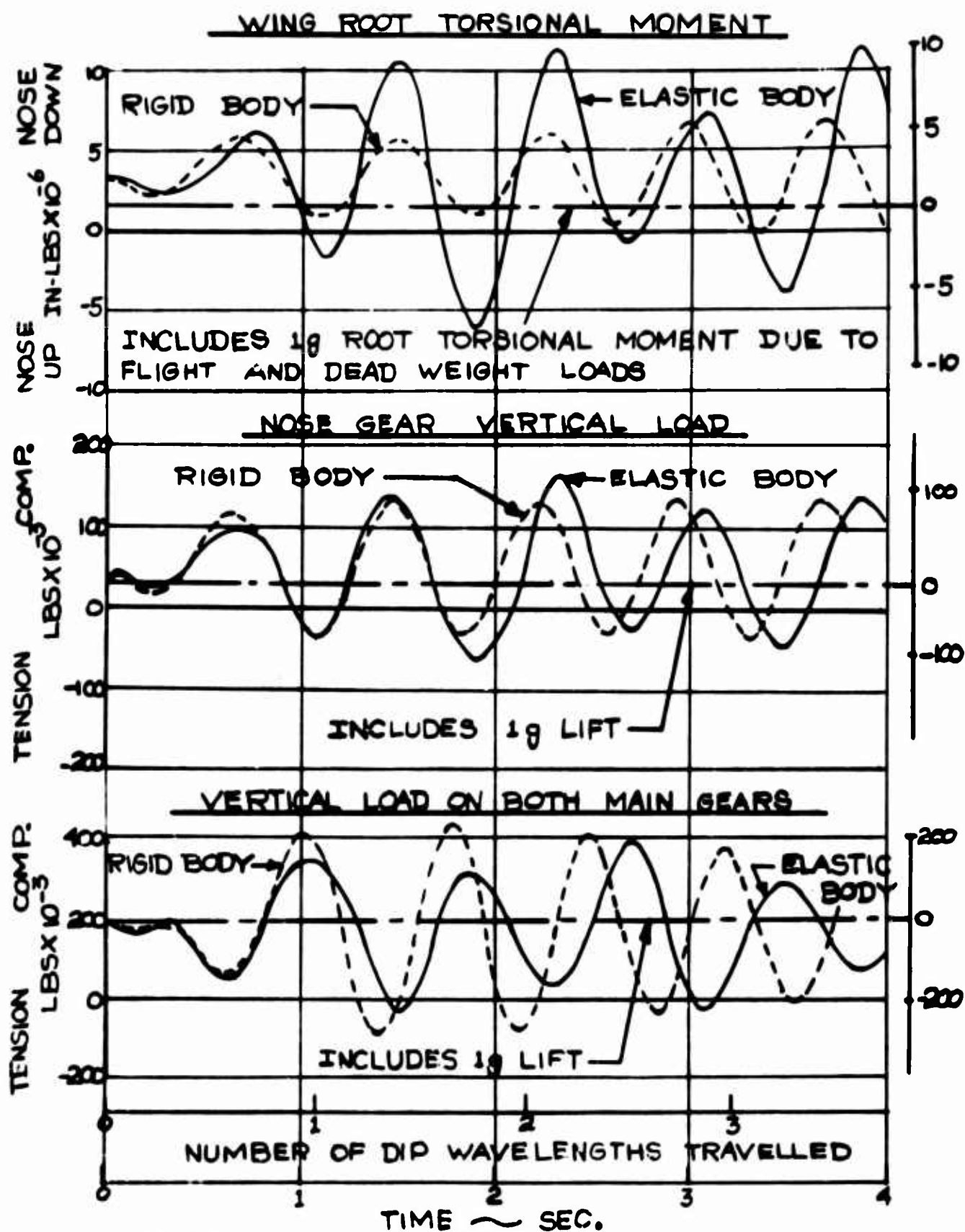


Figure 51 - Tilt Wing Detailed Runway Dip Analysis, Time History of Aircraft Acceleration, Pitch and Gear Loads.



NOTES:

- (1) λ = DIP WAVELENGTH = 96 FT.
- (2) $V = V_{\text{LIFT-OFF}} = 90 \text{ FT/SEC.}$
- (3) $\lambda/l = 3.0$

(continued)

Figure 51 - Tilt Wing Detailed Runway Dip Analysis, Time History of Aircraft Accelerations, Moments and Gear Loads.

BLANK PAGE

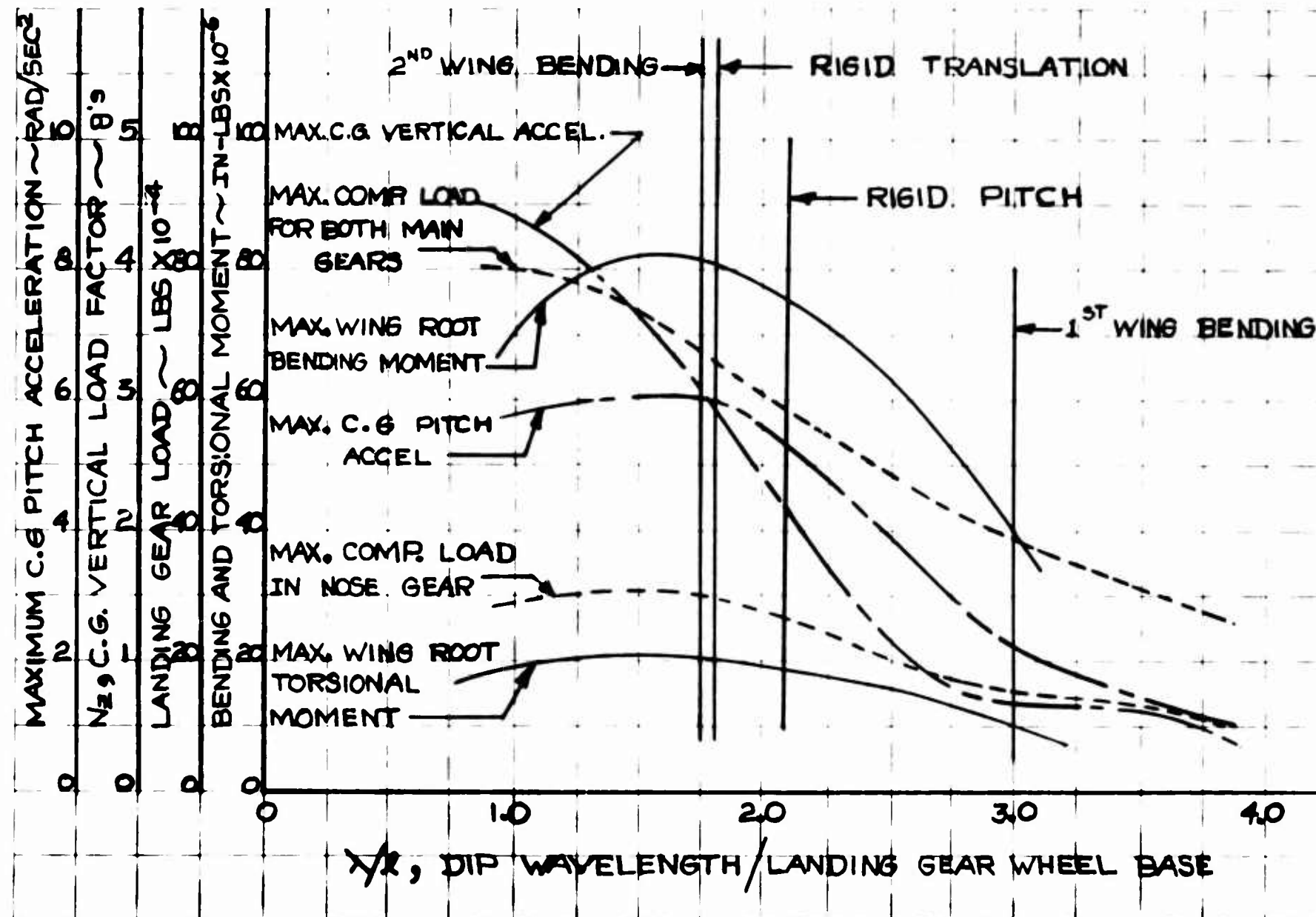


Figure 52 - Tilt Wing Detailed Runway Dip Analysis. Variation of Accelerations, Moments and Gear Loads vs. Dip Wavelength for Elastic Body Analysis.

VI. SPECIAL DESIGN CONSIDERATIONS

A. Towbar Shock Strut

The preliminary analysis of the starting and stopping condition showed that high prescribed accelerations at the towbar could result in serious structural response problems in the landing gear structures. While the analysis of this condition is conservative, it did become evident that for very large V/SIOL aircraft, structural design could be predicated by a ground handling condition.

Therefore, the following analysis presents a schematic of a towbar design to eliminate the shock loadings that could be imposed through "rough handling".

To simplify the analysis, a suddenly applied acceleration of constant magnitude is used as a basis for a simple mathematical model.

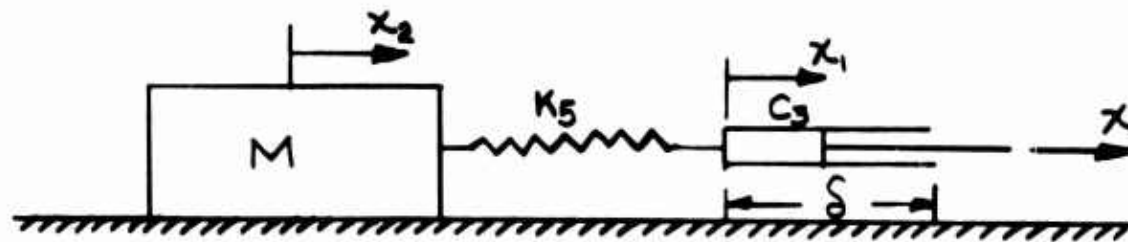


Figure 23 - Schematic of Aircraft and Towbar

The spring K_5 and the mass M represents the aircraft up to the towbar and includes the effect of the elasticity of the gear in the forward direction. The damper C_3 is part of the towbar with a useful stroke of δ which is the relative motion of the towing vehicle and the end of the towbar attached to the aircraft (see Figure 53).

(a) Without damper

The equation of dynamic equilibrium without damping with the prescribed towbar motion is:

$$M \ddot{x}_2 + K x_2 = K x \quad \text{and} \quad x_1 = x \quad (120)$$

or
$$\ddot{x}_2 + \omega_N^2 x_2 = \omega_N^2 x$$

differentiating twice and letting $\eta = \ddot{x}_2$

$$\ddot{\eta} + \omega_N^2 \eta = \omega_N^2 x = \text{constant} \quad (121)$$

The general solution is:

$$\eta = \ddot{\chi}_2 = C_1 \sin \omega_N t + C_2 \cos \omega_N t + \ddot{\chi} \quad (122)$$

with initial conditions of $\eta = \dot{\eta} = 0$

$$\ddot{\chi}_2 = \ddot{\chi} (1 - \cos \omega_N t) \quad (123)$$

The maximum value is reached if the prescribed acceleration is held for $t \geq \pi/\omega_N$ seconds

$$\text{and } \ddot{\chi}_{2 \text{ MAX}} = 2 \ddot{\chi}$$

Similarly, the spring force is:

$$F_S = K_5(\chi - \chi_2) = K_5(\ddot{\chi} - \ddot{\chi}_2) \quad (124)$$

and has a maximum value of $F_{S \text{ MAX}} = 2K_5\ddot{\chi}$

The inertial and spring forces therefore are amplified by a factor of 2 over the prescribed input. Thus, if the input is severe the problem is amplified due to the dynamic characteristics.

(b) With damper

A constant force damper which is illustrated in Fig. 54 is used to reduce the dynamic forces on the aircraft.

The damper consists of a honeycomb core enclosed in the towbar. Shear pins are used to prevent activation of the device and are set at some force value specified here as F_D . A similar device has been used on Sikorsky Aircraft to prevent high loads in extremely hard landings. Detail discussion of the device is contained in Ref. 18. By precrushing the honeycomb, little or no overshoot in load occurs and has been confirmed in dynamic landing gear tests of such structures. The design is modified to act in two directions i.e. compression and tension in the towbar.

The time of activation for a high input acceleration (relative to the activation force F_D) is small so that the analysis can proceed neglecting the time the spring is picking up the load.

The force in the spring is

$$F_S = K_5(\chi_2 - \chi_1) = F_D = \text{constant} \quad (125)$$

$$\text{and } \chi_1 = \chi - \delta$$

therefore

$$F_D = K_5(\chi_2 - \chi + \delta) = \text{constant} \quad (126)$$

Since K is the spring constant

$$x_2 - x + \delta = \text{constant}$$

then

$$\dot{\delta} = \dot{x} - \dot{x}_2$$

$$x = \ddot{x}t \quad \text{and} \quad x_2 = F_D t / M$$

Therefore the velocity of the towbar damper is:

$$\dot{\delta} = t [\ddot{x} - F_D / M] \quad (127)$$

With the critical condition of $\delta = \dot{\delta} = 0$, then

$$\delta = (t^2/2) [\ddot{x} - F_D / M] \quad (128)$$

The stroke required to eliminate the shock and hold the loading in the towbar to F_D depends on the prescribed acceleration, the activation loads of the damper, and the time of the prescribed acceleration. All these are, of course, dependent on the aircraft mass.

For example, the core that was previously analyzed without the damper showed that the critical time of pulse was $t_p = \pi / \omega_N$. Considering that the pulse time is sufficiently realistic for the natural period, the following would be the stroke required.

$$\delta = (T_N^2/2) [N_0 g - N_x g] \quad N_0 > N_x \quad (129)$$

where N_0 = the input factor of accelerations.

N_x = the desired limitation on input to aircraft.

Let $N_0 = 1/3$ (see Section III part A2).

$$N_x = \frac{1}{4}$$

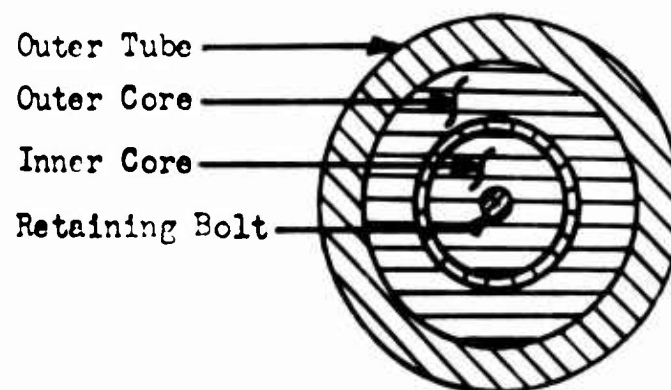
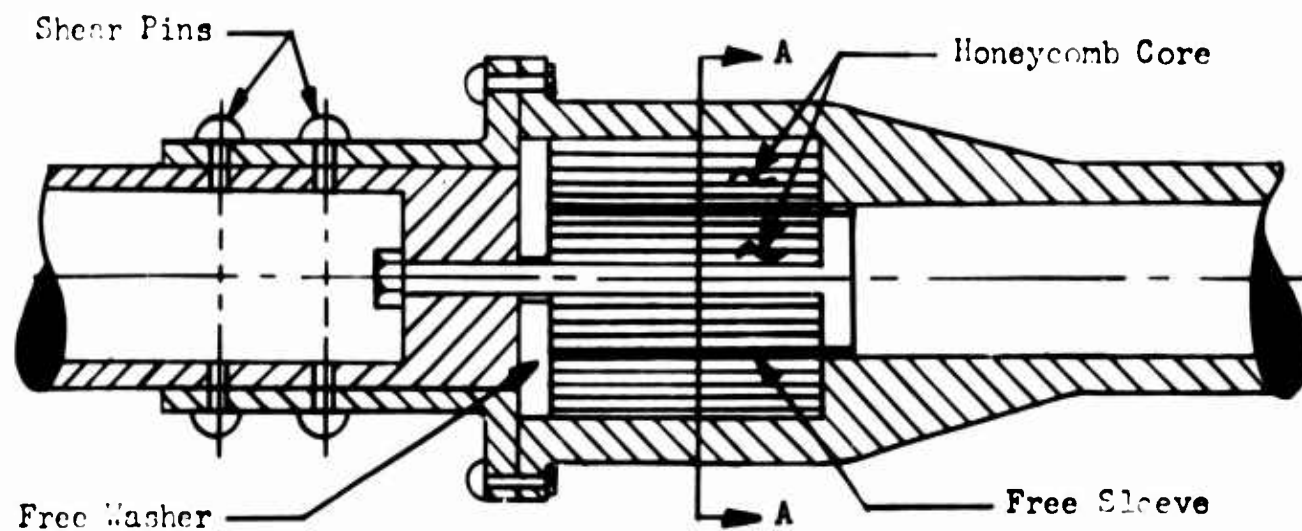
$$T_N = 1 \text{ (conservative).}$$

then

$$\delta = (1/2)g(1/12) \approx 1\frac{1}{2} \text{ ft. or 15" of stroke.} \quad (130)$$

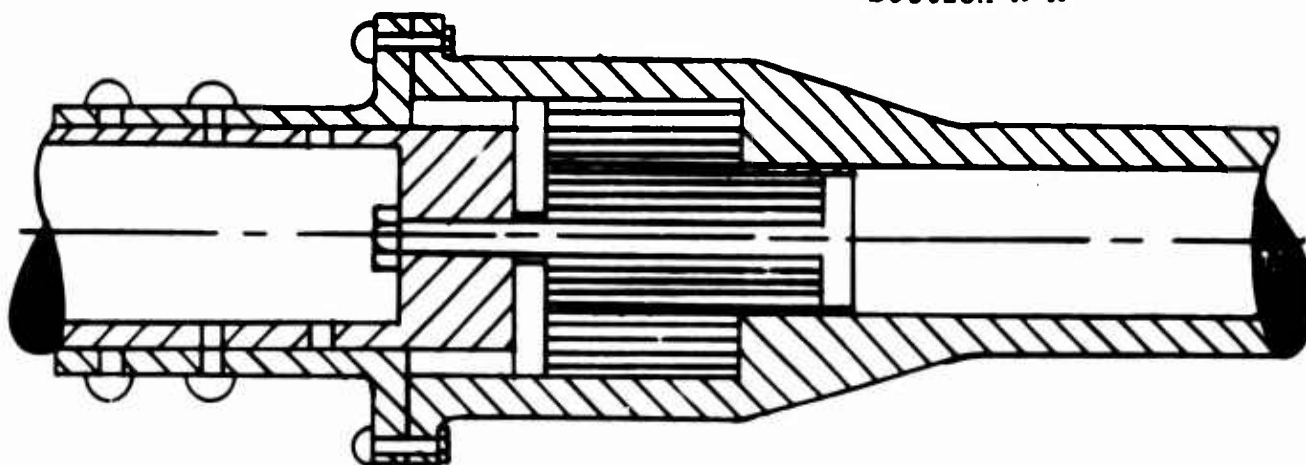
Thus, a reasonable device would eliminate the impact and render this condition not critical.

The towbar shown in Fig. 54 is a safety device designed to protect the aircrafts' nose gear structure from being damaged by abnormally high towing loads. In the event of a sudden start or stop by the towing vehicle, where longitudinal nose gear design loads are exceeded in either the fore or aft direction, the energy absorption unit in the towbar will prevent catastrophic failure. The absorption of energy is accomplished by the use of a precrushed honeycomb core which will function from the time the design load on the shear pins is exceeded until the core is bottomed out. The cut-away view shows the operation of the safety unit, after failure of the shear pins, for both a tensile and compressive load.



Section A-A

Operation For
Compressive Impact



Operation For
Tensile Impact

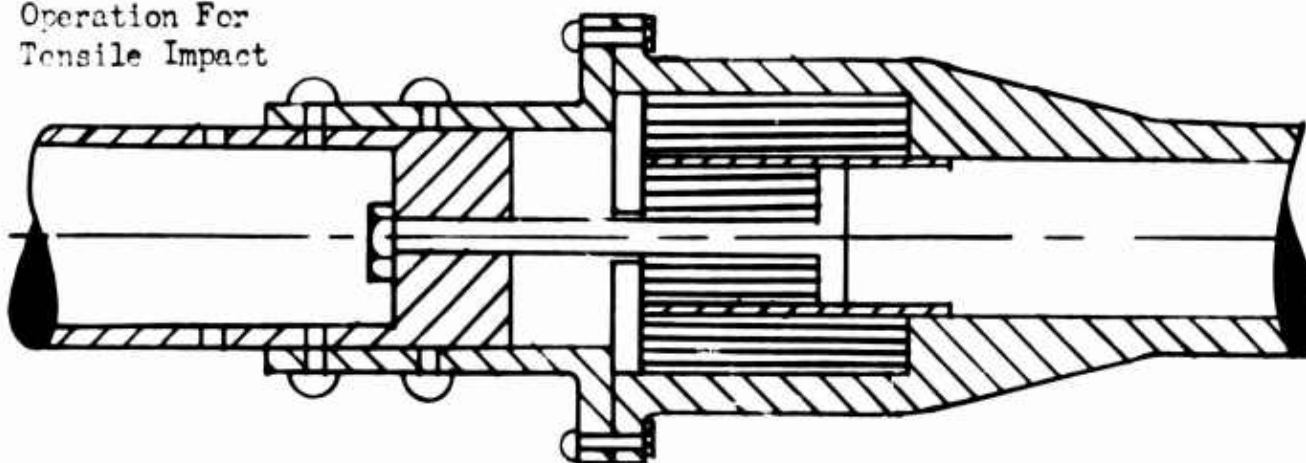


Figure 54 - Schematic of Towbar
Incorporating Honeycomb Core Safety Device

B. Shock Absorption For Landing Gear

The detail analysis of the take-off run and the resultant gear load time history (Ref. Fig. 51) indicates that under extreme ground dip conditions very large loadings can be imposed on the landing gear. These high loadings are of further importance since in large size aircraft the wing structural response is very large due to the coupling of the rigid and elastic body frequencies.

The principle problem with the gear, as a shock absorption device, is that as the velocity of the oleo increases the gear resistance is greater than desired, in fact with sufficient velocity build-up the gear locks up and all shock absorption is lost.

The normal landing gear can be represented by a spring and a damper. A more sophisticated analysis could make both the spring and damper non-linear. However, the basic problem can be illustrated by the linear case and for this portion of the report a linear analysis is sufficient to illustrate the problem.

The gear forces could be controlled by at least two means, these being (1) a built in pressure relief valve and (2) a shock absorber whose resistance is constant and is in series with the oleo. Both systems are load limiters and suppress the high peak loadings on the gear from dynamic conditions. Both are desirable from an operational viewpoint in that the device is a sacrificial element to safeguard the primary structure of the aircraft. Both, however, are "extra weight" items from the viewpoint of present structural design specifications but might be justified by the weight saved if the gear had to be designed for extreme conditions that are not yet specified explicitly in structural specifications, such as rough field landings.

As an example of the effectiveness of a load limiter and the requirements in stroke to be effective, an analysis is made of a gear entering a 1 - Cos dip. Since this is a transient load problem the damper is neglected for simplicity of analysis.

Case (1) 1 - Cos Dip, Simple Sprung Mass System

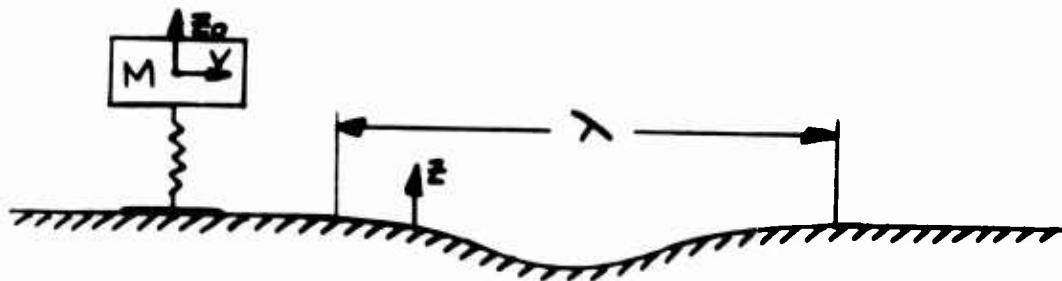


Figure 55 - Simple Sprung Mass System

The equation of the dip is:

$$\begin{aligned} z &= -A/2(1 - \cos \omega t) & \text{for } t_1 \geq t \geq 0 & \quad (131) \\ z &= 0 & \text{for } t \geq t_1 \end{aligned}$$

where A = dip amplitude, in.

$$\omega = 2\pi v/\lambda \quad , \text{ Rad.}$$

$$t_4 = \lambda/v \quad , \text{ Sec.}$$

The solution to this case is specified in 4-3 (a) and 4-3 (b) of Ref. (8) for an amplitude response on a fixed spring condition. The same solution applies, but in this case, to the acceleration. (132)

$$\frac{\ddot{z}_a}{z} = \frac{1/2}{1-(t_4/T_N)^2} \left[1 - \cos \omega_N t - (t_4/T_N)^2 (1 - \cos 2\pi t/t_4) \right]$$

Equation 132 applies during wheel penetration into the dip. When the wheel is out of the dip, that is $t \geq t_4$, then the residual amplitude is:

$$\frac{\ddot{z}_a}{z} = \frac{\sin \pi t_4/T_N}{1-(t_4/T_N)^2} \sin \omega_N (t - t_4/2) \quad (133)$$

For a t_4/T_N ratio of 1 a plot of the acceleration response is shown in Figure 57 and the maximum acceleration occurs while the wheel is in the dip region.

For $t_4/T_N = 1$ the system is in "resonance" i.e. $\omega_N = \omega$ and equation 132 must be solved by L'Hospital's method. Since an indeterminacy exists at the exact value of $t_4 = T_N$.

The peak response is 1.7 at $t = .75$.

The dip acceleration is $\ddot{z} = -\frac{A}{2} \omega^2 \sin \omega t$ and the peak dip acceleration is:

$$\ddot{z} = -A 4 \pi^2 (v/\lambda)^2 \quad (134)$$

Thus, the peak force on the gear is:

$$F_{MAX} = 1.7 M A 4 \pi^2 (v/\lambda)^2 \quad (135)$$

Case (2) Inclusion of a Load Limiting Device

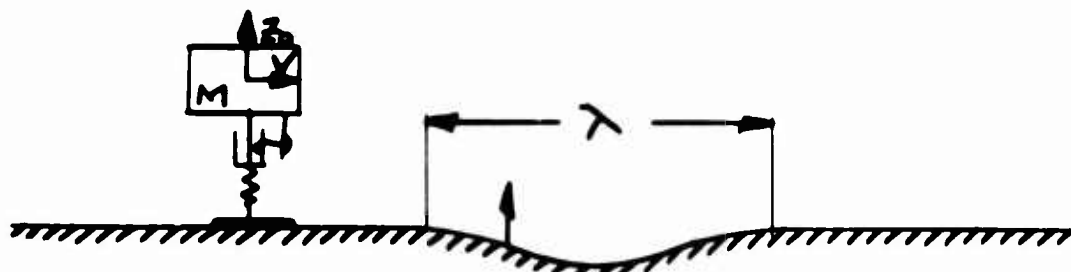


Figure 56- Spring-Mass System with Load Limiting Device

The load limiting device would be either a pressure relief valve or a plastic energy absorber (constant force resistance). The activation would occur only when the gear loads start to exceed a desired value. Since the critical range is within $t \leq t_1$, i.e. while the gear is in the dip, then the solution is evolved as follows:

Prior to load limiter activation, the equations of dynamic equilibrium are:

$$M\ddot{z}_0 - K(z - z_0) = 0 \quad (136)$$

The solution of \ddot{z}_0/\ddot{z} is the same as shown in equation 132. At $\ddot{z}_0/\ddot{z} = 1$ the value of t is $\frac{1}{2}$ as shown in Fig. 4 - 12 of Ref. (8), then:

$$\ddot{z} = -A/2 [1 - \cos \omega t] \quad (137)$$

and the velocity at t/t_1 of $1/2$ is:

$$\dot{z}_0 = -A/2 \omega \sin \omega t_1/2 \quad (138)$$

Since $\omega = 2\pi V/\lambda$, then $\omega t_1/2 = \pi$ radians and $\dot{z}_0 = A\omega/2$ (fps)

² The excess kinetic energy to be dissipated has a value of $1/8 M A^2 \omega^2$. It is then necessary to provide sufficient stroke for the load limiter to permit absorption of energy to hold the gear load down to its response of unity. The gear load for a response of unity is $M A 4 \pi^2 (V/\lambda)^2$ or $M A \omega^2/2$.

Therefore the energy equivalence is:

$$M A/2 (\omega^2 \delta) = 1/8 (M A^2 \omega^2)$$

$$\delta = A/4 \quad (139)$$

The required absorption stroke is related to the dip amplitude for the most critical case of $t_d/T_N = 1$ (resonance) and is one fourth of the total dip amplitude. The inference should not be drawn that only a fourth of the dip amplitude is required for the dissipator device stroke but rather to hold the response to unity a certain value is required. Due to the fact the acceleration load increase is proportional to the dip amplitude and the square of the speed (for a given dip wavelength) it may be necessary to consider even lower response factors than unity.

For the purposes of this report the previous analysis illustrates the effectiveness of a load limiting device in series with the normal oleo and how little stroke is required to reduce the response factor. The following is a numerical example to illustrate the order of magnitude of the physical values of the problem:

For an aircraft with a natural period of one second the dip wavelength for a resonant condition is:

$$T_N = t_d = 1 = \lambda/V \quad \text{or } \lambda = V \text{ ft.} \quad (140)$$

For a 90 fps aircraft ground run speed

$$\lambda = 90 \text{ ft.}$$

$$\omega = 2\pi V/\lambda = 2\pi \text{ Rad/Sec}$$

$$|\ddot{z}| = A 4\pi^2 V/\lambda$$

and for a 10" dip amplitude

$$|\ddot{z}| = 10/12 (4\pi^2)(1) = 32.8 \text{ Ft/Sec}^2 \quad (141)$$

= 1g vertical ground accel.

$$\delta = A/4 = 10/4 = 2\frac{1}{2}'' \text{ auxillary stroke required.} \quad (142)$$

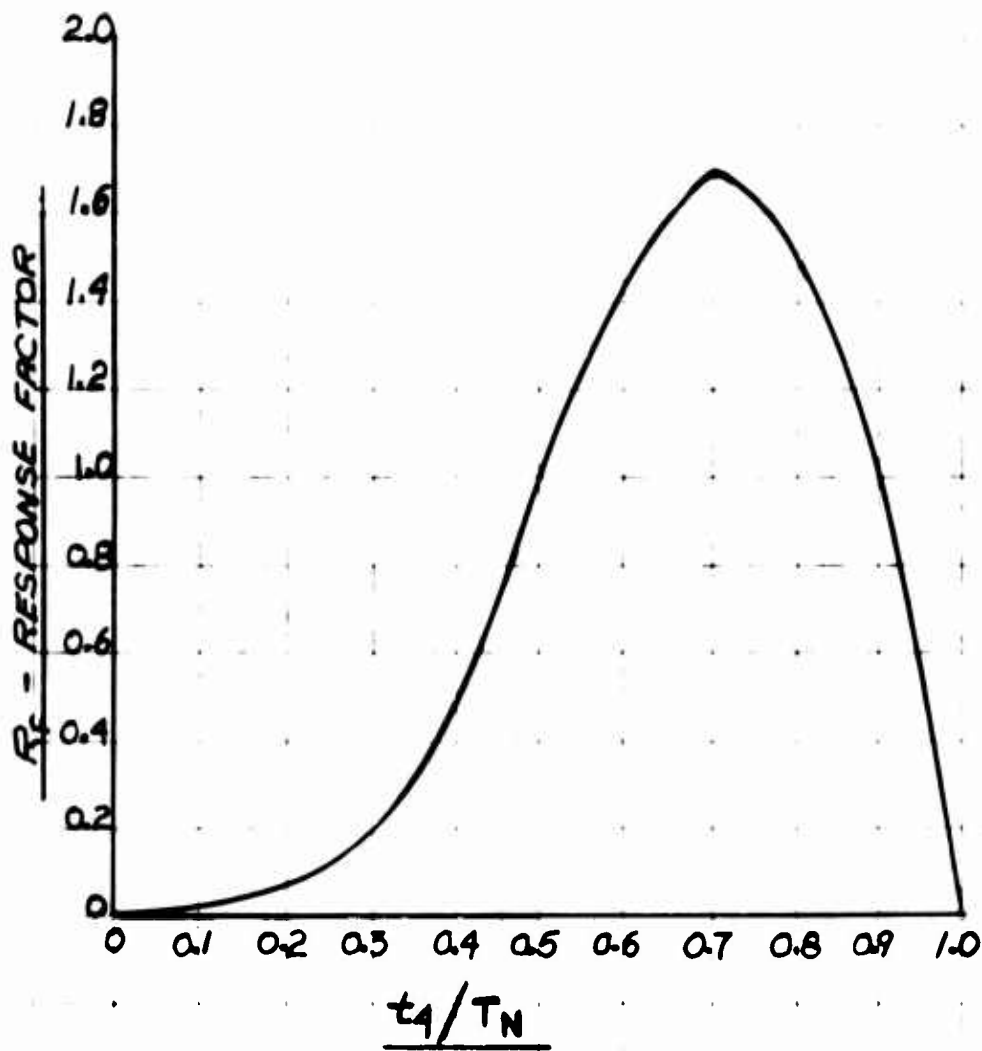


Figure 57 - Response Factor vs. Time Ratio

VII CONCLUSIONS

The conclusions of this report are based in some respects on the design solutions of the V/STOL configurations. Since these designs represent a large extrapolation to what has been built, there exists a basic problem that changes in the state of the art or different design solutions, will appreciably modify the details of the structure and/or the dynamic problems involved. However, the trends found from this report may well influence the designer to recognize basic problems and allow some insight into the structural problems involved. Therefore, recognizing the preceding remarks, the conclusions of this report are as follows:

The large logistic V/STOL designs studied in this report will produce some basic wing structural problems in that:

(a) The wing structures are sufficiently reduced in stiffness to have natural frequencies low enough to strongly couple with the rigid body frequencies of the aircraft on its landing gear.

(b) The strong coupling of the wing elastic structure with the landing gear precludes using the rigid body landing gear forces as a separate forcing function into the wings. The effect of coupling reduces the rigid body acceleration but appreciably increases the dynamic bending moments on the wing. The data of Fig. 51 of the detail dip analysis shows the difference in calculating loads by the rigid body method and the effects of coupling.

(c) Due to the coupling effects of the elastic structure with the rigid body on the landing gear, the most critical λ/l ratio for runway dips cannot be ascertained by inspecting the free-free elastic body frequencies or the aircraft rigid body frequencies on its' landing gear. In addition, the critical λ/l ratio is not a single value since different parts of the structure are critical for different values of the λ/l ratio. The main gear compressive load is critical for low values of λ/l (in the order of 1) and follows the value of the vertical c.g. acceleration. The nose gear was found to be critical for a higher value of λ/l (in the order of $1\frac{1}{2}$) and appears to follow pitching acceleration at the c.g. Wing torsion is critical at the same λ/l ratios as the nose gear and is also due to pitching accelerations of the c.g. Wing root bending moments are critical for a slightly higher λ/l (approximately 1.6) and appear to be the result of the induced bending from torsional response.

(d) The most critical V/STOL configuration was found to be the Tilt Wing design. The criticality was predominately due to the low natural frequencies and strong bending-torsion coupling.

(e) Critical conditions can be controlled by introducing operating equipment designed to absorb shock such as the tower design specified in the section including Special Design Considerations. Special devices such as a landing gear load-limiting device, also included in the section for Special Design Considerations, may well be the answer to the problem associated with high dynamic loads by attacking the basic problem

at its source. While "tuning" the landing gear to reduce response is a possible solution, there always exist the problem that basic design considerations of the geometry of the landing gear and required stroke for specified sink speeds will govern the designs.

(f) The problem of an aborted take-off appears to be an operational condition of specifying the height-velocity range for safety in hover. The Buried Fan design appears to be the configuration which is most restricted since it has a relatively poor height-velocity envelope due to the inefficiency of the fan with forward speed. The only solution that appears reasonable for the latter design is having sufficient power in the basic design that a partial power failure will not allow less than that required for operation during take-off. This is a penalty requiring excess power over and above that required for normal operation, but is a problem that appears to be associated with the Buried Fan design.

VIII RECOMMENDATIONS FOR FURTHER STUDY

1. The design solutions of this report should be used as the basis for further studies in structural response. The structural data arrived at for the V/STOL designs is based on configuration studies that have a reasonable amount of engineering work, sufficient to arrive at relatively valid conclusions.
2. The concept of a load limiter on the gears offers a possible inexpensive means of minimizing structural response for extremely rough field landings. Therefore, the analysis should be extended to include, in the equations of motion, a load limiter and to assess how much stroke is required for the gears.
3. The landing gear analysis should be extended to a matrix of speeds, wave length ratios, and dip depths to assess the full range of response. A spectrum of loadings can then be established to further assess the fatigue problems associated with anticipated rough-field runway operations.

APPENDIX I

CONFIGURATION DESIGN METHODS AND ANALYSIS

Presented herein is a method for estimating design solutions of V/STOL aircraft to meet a specific mission and payload requirement. There are five different V/STOL configurations considered as required by Reference 13 .

1. Fixed Jet
2. Buried Fan
3. Tilt Wing
4. Tilt Propeller
5. Extended Flap

The assumptions and conditions employed in the analysis, along with the basis for the assumptions are presented. The development of the parametric equations is presented in detail.

The results of the analysis show that wing loading increases rapidly while the weight empty to take-off weight ratio decreased slightly (propeller configurations) with decreasing take-off gross weight. However, due to limiting factors such as aspect ratio, number of propellers (in some cases) and STOL performance (in some cases), which are a function of wing loading, the minimum take-off gross weight must be limited. The choice of the design solution was not always selected at these limiting values if the take-off gross weight reduction is only slightly beneficial. Thus, the useful load (propeller type), STOL capability and wing structural efficiency of the aircraft are improved while reducing wing propeller dynamic response problems.

The design solutions for each of the aircraft are presented in Table 14.

Method of Analysis

The objective of this analysis is to estimate a design solution for the five different V/STOL aircraft which are capable of carrying a 10 ton payload 1800 nautical miles, initially taking off vertically. Since the configurations are different in many respects a completely general analysis is not possible. However, some generality may be obtained if the propeller aircraft (Tilt Wing, Tilt Propeller, and Extended Flap) are grouped together. The jet types, being similar in the cruise mode only, are considered separately.

V/STOL Conditions and Assumptions

A. General Conditions and Assumptions

1. The required range and payload are 1800 nautical miles and 20,000 lbs. respectively, including a 10% fuel reserve.
2. The cruise speed shall not be less than 250 knots.
3. Standard day conditions.
4. Hover out of ground effect.
5. The net lift to gross weight ratio is 1.3.

6. An average airfoil section is used for lift and drag estimates.
7. Cruise altitudes range from 30,000 ft. to 38,000 ft.
8. The weight of the crew plus trapped fluids is approximately 2000 lbs.
9. The sum of the propeller diameters plus the fuselage width equals the wing span (propeller configurations only).
10. State of the art thrust to propulsion weight ratio. (engines, transmission, and propeller - turboprop system) is approximately 5.3 lbs/lb. (see Reference 12) (propeller configurations only).
11. Installed thrust to brake horsepower ratio is 2.9 lbs/HP.
12. $W_{fu} = 14$ ft. (see B51).

B. Individual Configuration Properties and Assumptions

1. Tilt Wing

- a. $n = 4$, the number of props.
- b. $\eta_o = .7$, static propulsive efficiency including transmission losses.
- c. $\eta = .75$, propulsive efficiency including transmission losses (cruise).
- d. $sfc = .52$ lbs/BHP/hr (cruise), specific fuel consumption.
- e. Cruise altitude = 30,000 ft.
- f. NACA-23021 airfoil section.
- g. $\lambda_1 = 0.6$, wing taper ratio
- h. $k_3 = 1.0$, factor accounting for wing-propeller interference losses.

2. Tilt Propeller

- a. $n = 2$
- b. $\eta_o = .7$
- c. $\eta = .75$
- d. $sfc = .52$ lbs/BHP/hr (cruise).
- e. Cruise altitude = 30,000 ft.
- f. NACA 23021 airfoil section.

c. $\lambda_1 = 0.6$

h. Wing section outboard of propeller nacelle tilts with the propeller.

i. Vertical drag = $0.1 W$; $k_3 = .9$

3. Extended Flap

a. $n = 4$

b. $\eta_o = .7$

c. $\eta = .75$

d. sfc = $.52 \text{ lbs/BHP/hr. (cruise)}$.

e. Cruise altitude = $30,000 \text{ ft.}$

f. NACA 23021 airfoil section.

g. $\lambda_1 = 0.6$

h. The flow turning losses are 10% of the propeller thrust; $k_3 = .9$

4. Fixed Jet

a. NACA 23012 airfoil section.

b. Tsfc = $.75 \text{ lbs/lb/hr}$, thrust specific fuel consumption (turbo-fan engines).

c. $k_3 = 1.0$

d. Cruise altitude = $38,000 \text{ ft.}$

e. Engine nacelle equivalent parasite drag increment equals 7.3 ft^2 (total for two nacelles).

5. Buried Fan

a. $\epsilon = .06d$, ratio of fan turbine blade length to fan diameter disc loading

b. DL = 558 psf , disc loading, (the corresponding augmentation ratio = 2.2 lbs./lb.).

c. $n = 4$, number of fans.

d. Tsfc = $.82 \text{ lbs/lb/hr}$ (turbojet).

e. Cruise altitude = $55,000 \text{ ft.}$

f. NACA 23015 airfoil section.

- g. $\lambda_1 = .4$
- h. $\lambda_a = .2$, ratio of flap width to chord.
- i. For this configuration $w_{fu} = 14 + 6 = 22$ ft. - fuselage width plus fan clearance distance.
- j. $k_3 = 1.0$

Discussion of Assumptions

Considering part A, Items 1 through 4 are stipulated by Reference 13. Item 5 is required to insure hovering and control capability at altitude and temperature conditions other than sea level. Items 6 and 8 are used for simplicity. The chosen cruise altitudes, Item 7, are typical of present day transports. Item 9 arises from the requirement that the wing be emerged in the propeller slipstream during transition to limit severe wing stall. Reference 12 points out representative values for thrust to propulsion system weights for various lift systems (Item 10). This study incorporates a conservative value, 5.3 lbs/lb (compared to 5.9 lbs/lb), to reflect the large extrapolation of the required turboprop systems used by these configurations as compared to the largest system available today. Thrust to installed horsepower (Item 11) was initially optimized and the resulting value was found to be consistent with Item 10. (see equations 6 and 7). Item 12 is consistent with present day transports.

The assumptions of part B reflect the characteristic differences of the configurations. For instance, the Tilt Propeller and the Extended Flap configurations have large wing-propeller interference in hover as compared to the Tilt Wing aircraft (B1h). Reference 10 indicates about a 10% turning loss when converting the propeller induced flow into lift (B3h, Extended Flap), while the net lift loss due to wing drag (wing planform normal to the propeller slipstream) is estimated to be about 10% of the propeller thrust (B2i, Tilt Propeller). (B2h) was incorporated to minimize this drag and to improve transition flight.

Assumptions B1b, B1c, B1d, B2d, B3b, B3c, B3d, B4b, and B5d are based on present day propeller, transmission, and engine characteristics. The 21% (average) thick airfoil section (B1f, B2f, B3f) for the propeller configurations were chosen because of the requirement for large chord double slotted flaps and the desirable C_L max. characteristics of a thick airfoil. The 15% (average) thick airfoil section (B5f) chosen for the Buried Fan is a compromise between a thin airfoil requirement for a high speed vehicle and a lift fan efficiency requirement which calls for a deep shroud, i.e., large airfoil thickness. Obviously, with no abnormal requirements for large wing thickness (other than structural), the Fixed Jet has the thinnest average section, 12% (B4a).

For the Buried Fan, λ_1 , (B5g) is chosen based on optimum span efficiency (see Reference 9) and proper wing geometry. The number of fans (B5c) is dictated by wing geometry and fan diameter while DL (B5b) which also influences fan diameter, is a compromise between diameter and fan augmentation ratio, i.e., size and number of turbojet engines which should be minimized in order to match cruise thrust requirements for the

internal space of the wing. λ_a (B5h) was held to a normal value for a fixed wing aircraft. Lift Fan turbine buckets normally have a length of about 6% of the fan diameter, (B5a).

Range of Possible Solutions

Figures 62b, 63b, 64b and 65b show the range of possible solutions for the various configurations. In each case the required take-off weight decreases as wing loading is increased. However, since AR varies directly as W_s and since these aircraft are required to have STOL capability, a restriction must be placed on W_s . AR must be limited since structural efficiency decreases and dynamic response problems increase with increasing AR. The limits for these two parameters, chosen consistent with existing transport aircraft, is as follows: (see part a and c of Figures 62, 63, 64 and 65).

$$W_s = 120 \text{ psf}$$

$$AR = 11.0$$

Selection of Final Configuration

It must be noted that the solutions were not always chosen at these extreme values. For instance, if it appeared that there was not significant gain in reducing W by increasing W_s (Figures 62a, 63a and 65a) the solution is set at a lower W_s .

For a given number of propellers or lift fans, the results point out that diameter increases with W . But, since the diameters did not grow to extreme values (except in the case of the Tilt Propeller) it was not considered a limiting factor.

It now remains only to select the number of propellers for the propeller configurations. Four is chosen for the Tilt Wing (B1a) in order to allow a relatively small diameter and to achieve a smooth slipstream velocity over the wing than would result with a 2 propeller version. A 6 propeller version would result in undue complexity, higher aspect ratios, and higher concentrated loads of more extreme spanwise positions along the wing. This solution is unfavorable in view of wing-propeller flutter characteristics. For this same reason, four propellers (B3a) were chosen for the Extended Flap configuration, even though a smooth slipstream velocity is most important for this aircraft when in transition flight. Concerning the Tilt Propeller configuration, tilting a minimum number of propellers is considered the governing factor (B2a). Unfortunately, the propeller diameter becomes quite large as is shown in Figure 64d.

Table 14 gives a complete listing of the pertinent parameters for each configuration.

Derivations of Equations for Configuration Design

A. Propeller Configurations: (Tilt Wing, Extended Flap and Tilt Prop)

The major weight categories of the aircraft can be separated and summed in the following manner.

$$W = W_E + PL + FL + W_{Cr} + \text{Trapped Fluids}$$

Dividing through by W and assuming that the crew weight and trapped fluids equal about 2000 lbs. (A 8) and $PL = 20,000$ lbs. (A1), the non-dimensionalized equation becomes:

$$1 = W_E/W + FL/W + 22,000/W \quad (143)$$

Expressions for the various ratios must now be derived in terms of the aircraft parameters and the mission requirements.

Consider the hovering condition first. The propeller size requirements are dictated by this condition. The installed thrust to horsepower ratio according to momentum theory is: (144)

$$\left(\frac{T}{BHP}\right)_{ins.} = 550 \eta_o \sqrt{\frac{\rho n \pi d^2}{2 T_{ins}}} = \frac{550 \eta_o}{k_4^{1/2}} \sqrt{\frac{\rho n \pi d^2}{2 W}} \quad (\text{Ref. Par. A3, A4})$$

The wing span is expressed in terms of the propeller diameter, the number of propellers and the fuselage width as:

$$b = nd + w_{fu} \quad (\text{Ref. Par. A9})$$

Rearranging:

$$\frac{nd}{b} = \frac{b - w_{fu}}{b} = \frac{1}{b_1} \quad (\text{Ref. Par. A12}) \quad (145)$$

where $b_1 = \frac{b}{b - w_{fu}}$

Substituting equation 145 into equation 144 and solving for W/b^2

$$\frac{W}{b^2} = \left(\frac{\rho \pi}{2}\right) \left[\frac{550 \eta_o}{b_1 (T/BHP)_{ins.}}\right]^2 \left(\frac{1}{k_4 n}\right) = C_1$$

For a given installed thrust to horsepower ratio, a given installed thrust to W ratio, and a given number of propellers, $(1/b_1)$ remains essentially constant for $b \geq 120$ W/b^2 is essentially a constant $= C_1$. A similar expression can be derived from the relationship of wing loading and aspect ratio.

$$w_3 = W/S \quad (146)$$

$$AR = b^2/S \quad (147)$$

Combining:

$$W/w_s = b^2/AR$$

$$W/b^2 = w_s/AR = C_1 \quad (147 a)$$

Therefore, for the same conditions as mentioned above, the ratio of w_s to AR is also a constant.

To determine a value for $(T/BHP)_{ins.}$:

$$(T/BHP)_{ins} = (T/W_p)(W_p/BHP)_{ins} \quad (148)$$

From the weights section:

$$\left. \begin{array}{l} \frac{W_{engine}}{BHP} = 0.5 \\ \frac{W_{propeller}}{BHP} = 0.21 \\ \frac{W_{drive\ system}}{BHP} = 0.1875 \end{array} \right\} \frac{W_p}{BHP_{ins}} = 0.5475$$

Recall that $W_p/T = .189$ (Ref. Par. A10)

Therefore, equation 148 becomes:

$$(T/BHP)_{ins} = .5475/.189 = 2.9 \text{ lb}_s/\text{HP} \quad \begin{array}{l} \text{(Ref. Par.} \\ \text{A11)} \end{array} \quad (149)$$

For sea level, standard day conditions, $k_4 = 1.3 k_3$ (A5, B1h, B21, B3h), and (B2b, B2b, B3b)

$$C_1 = 54.8/k_4 n \quad (150)$$

and from equations 145, 147a, and 150,

$$d = \frac{1.35}{b_1} \left(\frac{b_2 W}{n} \right)^{1/2} \quad (151)$$

Now that a relationship between w_s and AR, and W and b has been found, the expressions for the ratios of equation 142 are simpler to establish. Consider first FL/W.

The cruise fuel, assuming an average gross weight, \bar{W} , for the mission, is:

$$W_{fc} = \frac{(W)(1.69)TV(sf_c)R}{550\eta V} \quad \begin{array}{l} \text{(Ref. Par.} \\ \text{A1, B1c, B1d, B2c, B2d, B3c, B3d)} \end{array} \quad (152)$$

Assuming that the fuel required for a one minute hover and climb to cruise altitude is about 8% of the total fuel load, then

$$\frac{FL}{W} = .00365 \frac{(sf_c)R}{\eta} \left(\frac{T}{W} \right) \quad (153)$$

The cruise thrust is that required to overcome aircraft drag.

$$\frac{T}{W} = \frac{D_o + D_w}{W} = g \left[\frac{F}{W} + \frac{(C_{D_o} + C_L^2 / \pi A R \eta_w) S}{W} \right] \quad (154)$$

(Ref. Par. A6)

Figure 59 shows that f can be expressed as a function of W . The figure also reflects the difference in aerodynamic cleanliness between propeller driven aircraft and jet driven aircraft. This function for f has the form:

$$F = C_{Df}(W)^{\pi_1} \quad (154a)$$

Using this expression for f along with equations 146, 147, and 154 equation 143 becomes

$$\frac{F_L}{W} = \left[.00365 \frac{(sfc) R}{\eta} \right] \left[\frac{C_{D_o}}{W_s} + C_{Df} W^{\pi_1-1} + \frac{C_L^2}{\pi \eta_w A R W_s} \right] g \quad (155)$$

Recall that the cruise thrust is assumed based on the average cruise weight \bar{W} .

$$\bar{W} = W - \left(\frac{1}{1.08} \right) \left(\frac{F_L}{W} \right) \frac{W}{2} = W \left[1 - .463 \frac{F_L}{W} \right]$$

$$\bar{W}_s = \bar{W} / g$$

$$\frac{\bar{W}_s}{W_s} = \left[1 - .463 \frac{F_L}{W} \right] \quad (155a)$$

now

$$C_L = \bar{W}_s / g \quad (155b)$$

and

$$\begin{aligned} \frac{C_L^2}{\pi \eta_w A R W_s} &= \left(\frac{1}{\pi \eta_w} \right) \left(\frac{\bar{W}_s^2}{g^2} \right) \left(\frac{1}{A R W_s} \right) = \left(\frac{1}{\pi \eta_w} \right) \left(\frac{\bar{W}_s}{W_s} \right)^2 \left(\frac{W_s}{A R} \right) \left(\frac{1}{g^2} \right) \\ &= \frac{C_L}{\pi \eta_w} \left[1 - .463 \frac{F_L}{W} \right]^2 \frac{1}{g^2} \\ &= \frac{C_L}{\pi \eta_w} \left[1 - \frac{F_L}{W} \right] \frac{1}{g^2} \quad (\text{expanded by series neglecting higher order terms}) \end{aligned}$$

Substituting this expression into equation 155,

$$\frac{FL}{W} = \left[.00365 \frac{(sf)R}{\eta} \right] \left[\frac{C_{D0}}{W_s} + C_{Df} W^{(\tau_i-1)} + \frac{C_L}{\pi \eta W} \left(1 - \frac{FL}{W} \right) \right] \frac{1}{g^2} g \quad (156)$$

let

$$A_3 = \frac{C_{D0}}{W_s} + C_{Df} \left(W^{(\tau_i-1)} \right)$$

For a long range vehicle fuel economy is important. Minimum fuel will be used if the aircraft cruises at a velocity corresponding to $(L/D)_{max}$.

Reference 11 provides an expression for this speed which in terms of q has the form:

$$g(L/D)_{max} = \frac{\bar{u}_h}{\left[\pi \eta W AR (C_{D0} + C_{Df} \frac{W^{(\tau_i-1)}}{g}) \right]^{1/2}} \quad \begin{matrix} \text{(Ref. Par. A2,} \\ \text{A3, A7, B1d, B1f,} \\ \text{B2e, B2f, B3d, B3f)} \end{matrix} \quad (156a)$$

The airfoil data used is obtained from Reference 1. Equation (156a) can be rearranged into the form:

$$g(L/D)_{max} = \frac{1}{\left[\pi \eta W \left(\frac{AR}{W_s} \right) \left(\frac{W_s}{W} \right) \left(\frac{C_{D0}}{W_s} + C_{Df} W^{(\tau_i-1)} \right) \right]^{1/2}}$$

But using equations 147a and 155a

$$\pi \eta W \left(\frac{AR}{W_s} \right) \left(\frac{W_s}{W} \right) = \pi \eta W \left(\frac{AR}{W_s} \right) \left(\frac{W_s}{W} \right)^2 = \left(\frac{\pi \eta W}{C_l} \right) \left[1 - \frac{FL}{W} \right]$$

Combining and simplifying the symbolism:

$$g(L/D)_{max} = \frac{1}{\left[\left(\frac{\pi \eta W}{C_l} \right) \left(\frac{\frac{C_{D0}}{W_s} + C_{Df} W^{(\tau_i-1)}}{1 - FL/W} \right) \right]^{1/2}} = \frac{1}{\left[\frac{A_3}{B_3 (1 - FL/W)} \right]^{1/2}} \quad (157)$$

Solving for A_3

$$\frac{B_3}{g^2} (1 - FL/W) = A_3 \quad \text{where} \quad B_3 = C_l / \pi \eta W$$

Now substituting this expression and equation 157 into equation 156 and rearranging:

$$\frac{FL}{W} = C_2 \left[A_3 B_3 (1 - \frac{FL}{W}) \right]^{1/2} \quad (158)$$

where $C_2 = .073 \frac{(sf)R}{\eta}$

Since $FL/W < 1$, a series expansion can be used to expand the square root term in equation 158. Dropping the terms of second order and higher:

$$\left(1 - \frac{FL}{W} \right)^{1/2} \approx 1 - 1/2 \left(\frac{FL}{W} \right)$$

Substituting this into equation 158 and rearranging, an approximate expression for the fuel load to take-off gross weight is obtained.

$$\frac{F_L}{W} = \frac{C_2(A_3 B_3)^{1/2}}{1 + \frac{C_2}{2}(A_3 B_3)^{1/2}} \quad (159)$$

Using equations 143 and 159 an expression for the weight empty to take-off gross weight in terms of aerodynamic requirements is derived.

$$\frac{W_E}{W} = 1 - \frac{22,000}{W} - \frac{C_2(A_3 B_3)^{1/2}}{1 + \frac{C_2}{2}(A_3 B_3)^{1/2}} \quad (160)$$

The W_E/W curves for the Tilt Wing, Extended Flap and Tilt Prop are shown in Figures 62b, 63b and 64b based on equation 160 and the weights equations solved in Appendix III. Intersections of the aerodynamic and weights curves were used to obtain the optimum solutions within design considerations. Curves showing the relations between wing loading and take-off weight, aspect ratio and wing loading, and propeller diameter and take-off weight are also shown for the three aircraft mentioned above.

B. Buried Fan

For this configuration it is possible to relate the wing planform to the size of the lifting fans. Except for the geometrical formulation, the approach to deriving expressions for the ratios of equation 142 is exactly the same as used for the propeller configurations. Consider Figure 58, an assumed planform and airfoil section.

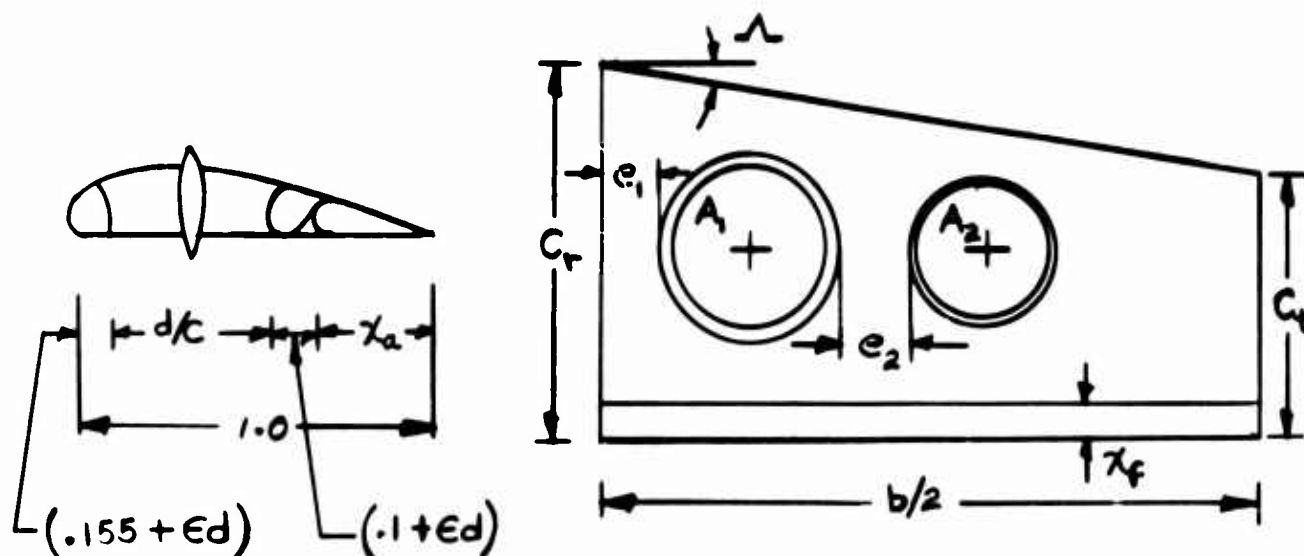


Figure 58 - Buried Fan Airfoil Section and Wing Planform

Assuming that there are two fans in each wing (not necessarily the same size) (B5c), that their disc loading is the same, and the geometry of Figure 58, the following relationships are derived.

$$T/2 = b_4 W/2 = DL(A_1 + A_2) = DL A_1 (1 + A_2/A_1) = DL A_1 (1 + \delta_1)$$

$$A_1/S = 1/2 \left(\frac{b_4}{DL} \right) \left(\frac{1}{1 + \delta_1} \right) \omega_3 \quad (161)$$

and

$$A_2/S = 1/2 \left(\frac{b_4}{DL} \right) \left(\frac{\delta_1}{1 + \delta_1} \right) \omega_3 \quad (162)$$

Sweep angle Λ

$$\tan \Lambda = \frac{C_r - C_s}{b/2} = \frac{2C_r}{b} (1 - \lambda_1)$$

but

$$S = \frac{b}{2} C_r (1 + \lambda_1)$$

and

$$\frac{2C_r}{b} = \left(\frac{4S}{b^2} \right) \frac{1}{(1 + \lambda_1)} = \left(\frac{4}{AR} \right) \frac{1}{(1 + \lambda_1)} \quad (162a)$$

$$\tan \Lambda = \left(\frac{4}{AR} \right) \left(\frac{1 - \lambda_1}{1 + \lambda_1} \right) \quad (163)$$

or

$$\lambda_1 = \frac{1 - (AR/4) \tan \Lambda}{1 + (AR/4) \tan \Lambda} \quad (164)$$

Consider the airfoil section

$$1.0 = .155 + .1 + d/c + \chi_a + 2\epsilon d/c \quad (Ref. Par. B5A)$$

where

$$\chi_a = \chi_c/c$$

Therefore

$$d/c = \frac{.745 - \chi_a}{(1 + 2\epsilon)} = B_2 \quad (165)$$

The chord lengths at the centerlines of the fans are

$$C_{A_1} = C_r - (e_1 + d_1/2) \tan \Lambda$$

$$C_{A_2} = C_r - (e_1 + e_2 + d_1 + d_2/2) \tan \Lambda$$

$$C_{A_2} = C_r - C_{A_1} - (e_2 + \frac{d_1 + d_2}{2}) \tan \Lambda$$

where

$$e_1 = w_{fu}/2 + \epsilon d_1$$

$$e_2 = \epsilon (d_1 + d_2) \text{ the minimum distance between fans (B5i)}$$

Therefore

$$C_{A_1} = C_r - \left[w_{fu}/2 + (\epsilon + 1/2) d_1 \right] \tan \Lambda$$

Substituting equation 165 into the above, the fan inner diameter becomes:

$$d_i = \frac{B_2(C_r - \frac{w_{fu}}{4} \tan \Lambda)}{1 + (\epsilon + 1/2) \tan \Lambda} \quad (166)$$

Solving equation 162a for C_r and introducing equation 164 into the result,

$$C_r = \frac{b}{AR} \left(1 + \frac{AR}{4} \tan \Lambda \right)$$

Substituting into equation 166,

$$d_i = \frac{(B_2 b) \left[1 + (1/4 - b_2/2) AR \tan \Lambda \right]}{AR \left[1 + (1 + 2\epsilon)(B_2/2) \tan \Lambda \right]} \quad b_2 = w_{fu}/b \quad (167)$$

Now

$$\frac{A_i}{S} = \pi \left(\frac{d_i}{2} \right)^2 \frac{1}{S}$$

$$\frac{A_i}{S} = \frac{\pi}{4} \frac{(B_2)^2}{AR} \frac{\left[1 + (1/4 - b_2/2) AR \tan \Lambda \right]^2}{\left[1 + (1 + 2\epsilon)(B_2/2) \tan \Lambda \right]^2} \quad (168)$$

Consider the denominator, note that:

$$\tan \Lambda < 1 \text{ since } \Lambda < 45^\circ$$

$$B_2 < 1, \epsilon < 1$$

$$\begin{aligned} \left[1 + (1 + 2\epsilon)(B_2/2) \tan \Lambda \right]^2 &= \left[1 + (B_2/2) \tan \Lambda + \epsilon B_2 \tan \Lambda \right]^2 \\ &\doteq 1 + (1 + 2\epsilon) B_2 \tan \Lambda + \dots \quad (\text{neglecting higher order terms}) \end{aligned}$$

Consider the second part of the numerator

$$\left[1 + (AR/4) \tan \Lambda - (b_2/2) AR \tan \Lambda \right]^2 \doteq 1 + (1/2 - b_2) AR \tan \Lambda$$

if

$$\begin{cases} b_2/2 AR \tan \Lambda < 1 \\ (AR/4) \tan \Lambda < 1 \end{cases}$$

But since $1/4 > b_2/2$ for any reasonable span ($b > 44.0$ ft.) the necessary and sufficient condition for the expansion to hold is:

$$AR \tan \Lambda < 4 \quad (169)$$

Substituting these expansions into equation 168,

$$\frac{A_i}{S} \doteq \left(\frac{\pi B_2^2}{4AR} \right) \left[\frac{1 + (1/2 - b_2) AR \tan \Lambda}{1 + (1 + 2\epsilon) B_2 \tan \Lambda} \right]$$

Substituting into 162 and solving for w_s

$$w_s \doteq \left[\frac{\pi D L B_2^2 (1 + \gamma_1)}{2 k_f AR} \right] \left[\frac{1 + (1/2 - b_2) AR \tan \Lambda}{1 + (1 + 2\epsilon) B_2 \tan \Lambda} \right]$$

Incorporating equation 163, (170)

$$\omega_3 = \left[\frac{\pi D L B_2^2 (1 + \gamma_1)}{2 R_4 A R} \right] \left[\frac{1 + 4(1/2 - b_2)(1 - \lambda_1)}{1 + 4(1 + 2\epsilon)(\frac{B_2}{A R})(\frac{1 - \lambda_1}{1 + \gamma_1})} \right]$$

It can also be shown that

$$\gamma_1 = \frac{1 - 4(1/2 + \epsilon)(\frac{B_2}{A R})(\frac{1 - \lambda_1}{1 + \gamma_1})}{1 + 4(1/2 + \epsilon)(\frac{B_2}{A R})(\frac{1 - \lambda_1}{1 + \gamma_1})} \quad (171)$$

For the established k_4 , a given DL , λ , and λ_a (A5), (B5j), (B5b), (B5g), (B5h) w is directly related to AR . This is similar to the relationship (equation 5a) developed for the propeller configurations. With this relationship determined, the FL/W relationship can be developed.

The fuel load required, again assuming an average gross weight W , but increasing the allotment of fuel for hover and climb to cruise altitude to 10% of the total fuel to reflect the higher cruise altitudes and higher hover fuel consumption, the total fuel load is:

$$FL = (1.1)(1.1)(T)(T_{3fc})(R/V) \quad (\text{Ref. Par. A1, B5d}) \quad (172)$$

Using equations 172 and 154a, a similar expression to equation 155 can be derived except that FL/W is a function of V and not V^2 .

$$\frac{FL}{W} = \left[2.045(T_{3fc})R \right] \left[\frac{C_{D0}}{\omega_3} + C_{DF} W^{(\tau-1)} + \frac{C_L^2}{\pi \eta_w \omega_3 AR} \right] V \quad (\text{Ref. Par. B5f})$$

The airfoil data used is obtained from Reference 1. Note that C_{D0} must be corrected for compressibility as shown in Figure 61 (obtained from Reference 5). Substituting equation 156a, reduced to $V(L/D)_{max}$.

(A2, A3, A7, B5c). FL/W has the form:

$$\frac{FL}{W} = \left[2.045(T_{3fc})R \right] \left[\frac{C_{D0}}{\omega_3} + C_{DF} W^{(\tau-1)} + \frac{C_L^2}{\pi \eta_w \omega_3 AR} \right] \left[\frac{\bar{\omega}_a^{2/p}}{[\pi \eta_w AR (C_{D0} + C_{DF} W^{(\tau-1)})]^{1/2}} \right]$$

Again, letting $A3 = \frac{C_{D0}}{\omega_3} + C_{DF} W^{(\tau-1)}$ and using equations 155b and 156a, the above expression reduces to

$$\frac{FL}{W} = \left[4.09(T_{3fc})R A3 \right] \frac{\bar{\omega}_a^{1/2} (2/p)^{1/2}}{[\pi \eta_w AR \omega_3 A3]^{1/4}}$$

$$\frac{FL}{W} = M_a \left(\frac{\bar{\omega}_a}{\omega_3} \right)^{1/2} \left(\frac{\omega_3}{AR} \right)^{1/4} \quad (173)$$

We arrive at an expression similar to equation 155a.

$$\left(\frac{\bar{\omega}_a}{\omega_3} \right)^{1/2} = \left[1 - 1/2(FL/W) \right]^{1/2}$$

Substituting this approximation into equation 173

$$\frac{FL}{W} = M_A \left[1 - \frac{1}{2} \left(\frac{FL}{W} \right) \right]^{\frac{1}{2}} \left(\frac{W_E}{AR} \right)^{\frac{1}{4}} \quad (174)$$

Squaring and solving for FL/W

$$\frac{FL}{W} = - \frac{M_A^2}{4} \left(\frac{W_E}{AR} \right)^{\frac{1}{2}} + \left[\frac{M_A^4}{16} \left(\frac{W_E}{AR} \right) + M_A^2 \left(\frac{W_E}{AR} \right)^{\frac{1}{2}} \right]^{\frac{1}{2}}$$

where

$$M_A = \left[\frac{5.9(T_{SFC})R}{\rho^{\frac{1}{2}}(\pi\eta_w)^{\frac{1}{4}}} \right] (A_3)^{\frac{3}{4}}$$

The ratio W_E/AR is governed by equations 170 and 171.

Since the equations used in these analyses are approximate, the final solution must be checked using the exact equations to get the exact values for the W_E and FL. The W_E/W curve for the Buried Fan is shown in Fig. 65b based on weight equations listed in Appendix III and from substituting the proper expressions into equation 143. The intersection of the two curves resulting from these equations was used in determining the optimum design solution. Curves showing the relations between take-off weight and wing loading, aspect ratio and wing loading, and take-off weight and fan diameter are given in Fig. 65a, c and d.

C. Fixed Jet

In this case, there is no fixed relationship between the thrust producer and the wing planform. A trial and error method was used, solving FL/W and W_E/W ratios for various combinations of AR and W_E for a fixed λ_1 (B3) and sweep back angle (B4c). The cruise speed was increased by about 25% over that which would be dictated by equation 156a because productivity is increased while the fuel load, and consequently W_E , increases only slightly. It is also noted that an increment in equivalent parasite drag over that predicted by Figure 59, to account for the engine nacelle drag, is incorporated and estimated to be 7.3 ft.² (total for two nacelles). The airfoil data used for this configuration is obtained from Reference 1. The assumptions of part B4 apply here.

Because this was the first aircraft analyzed, equations are not given since the solution was obtained by a trial and error process. The design solution was arrived at using graphical methods by plotting the aerodynamic and weights relationships. It became evident that since four more aircraft would be analyzed a derivation of design equations was desirable and necessary. Subsequently, equations were derived for the remaining four V/STOL aircraft as already presented.

BLANK PAGE

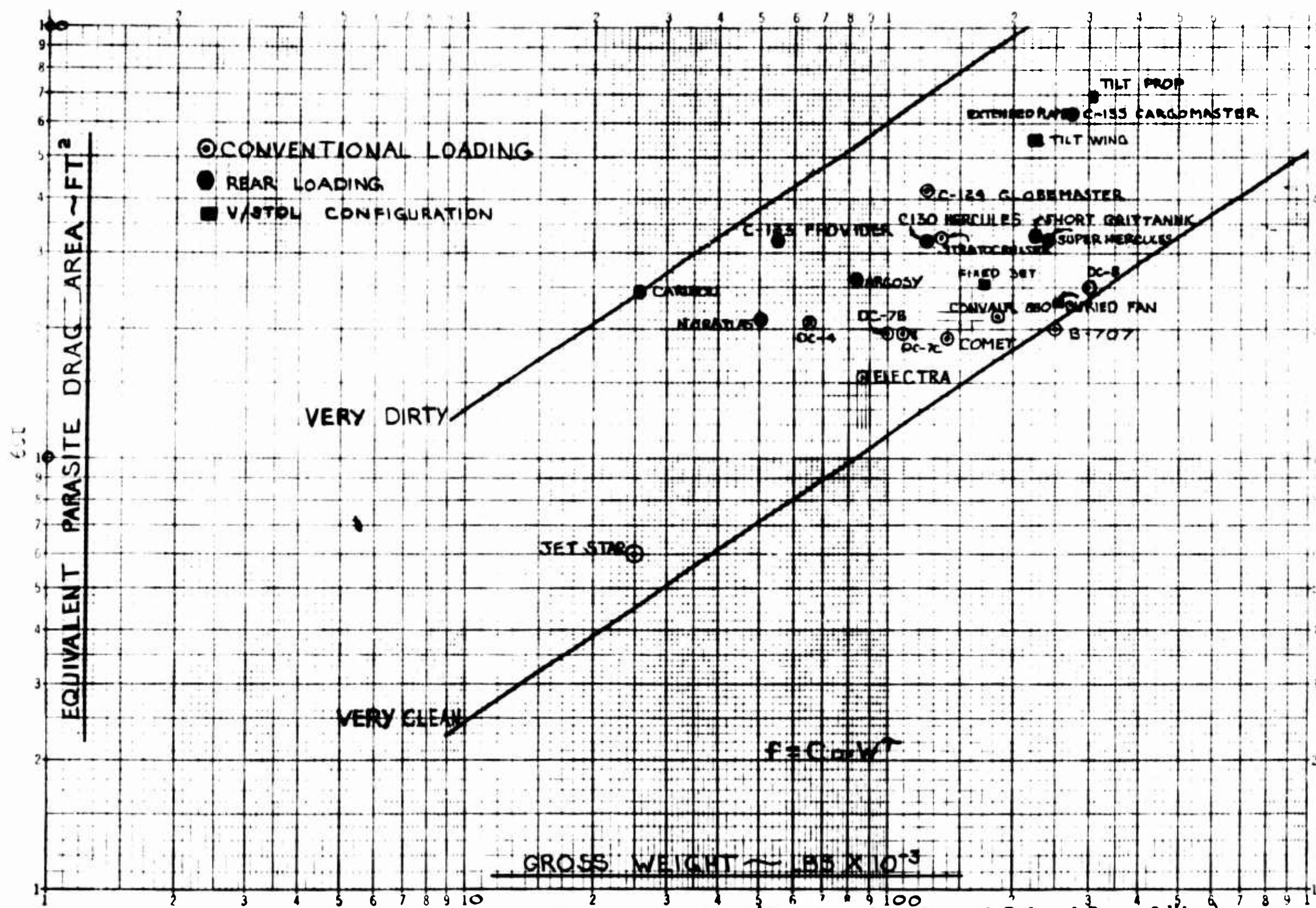
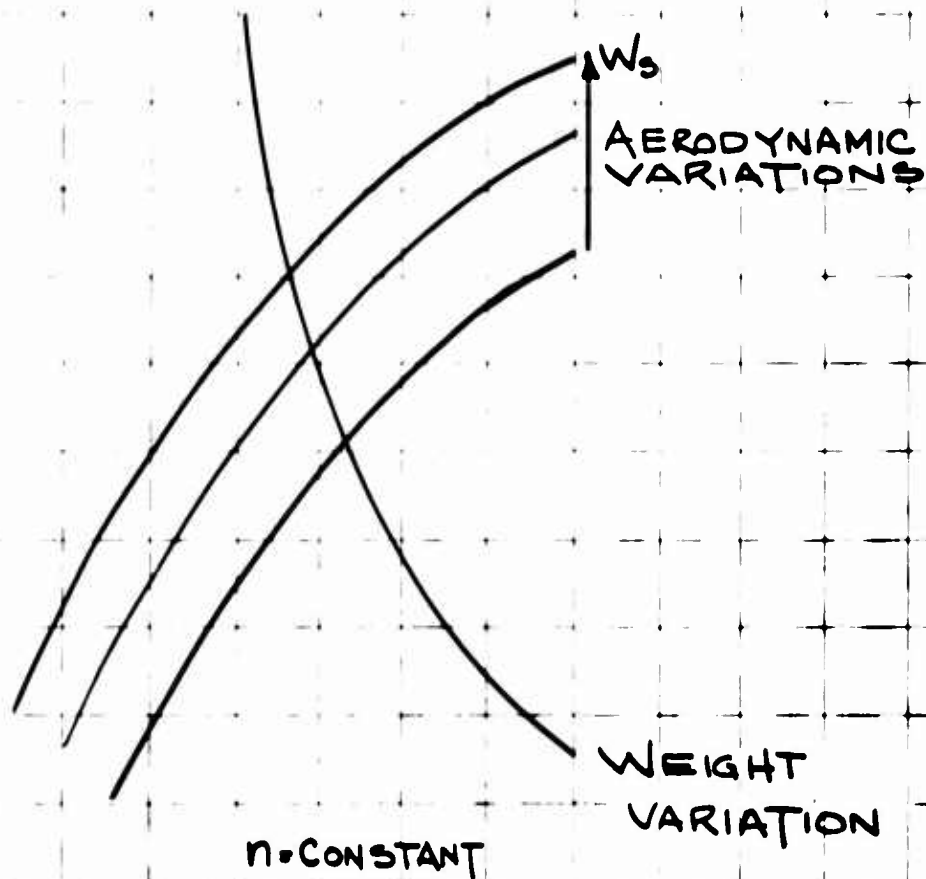


Figure 59 - Fixed Wing Transport Aircraft Parasite Drag Area (Excluding Parasite and Induced Drag of Wing)

WGT. EMPTY / TAKE-OFF WGT.



TAKE-OFF WGT.

Figure 60 - Typical Aerodynamic and Weight Variation of Configuration Solution

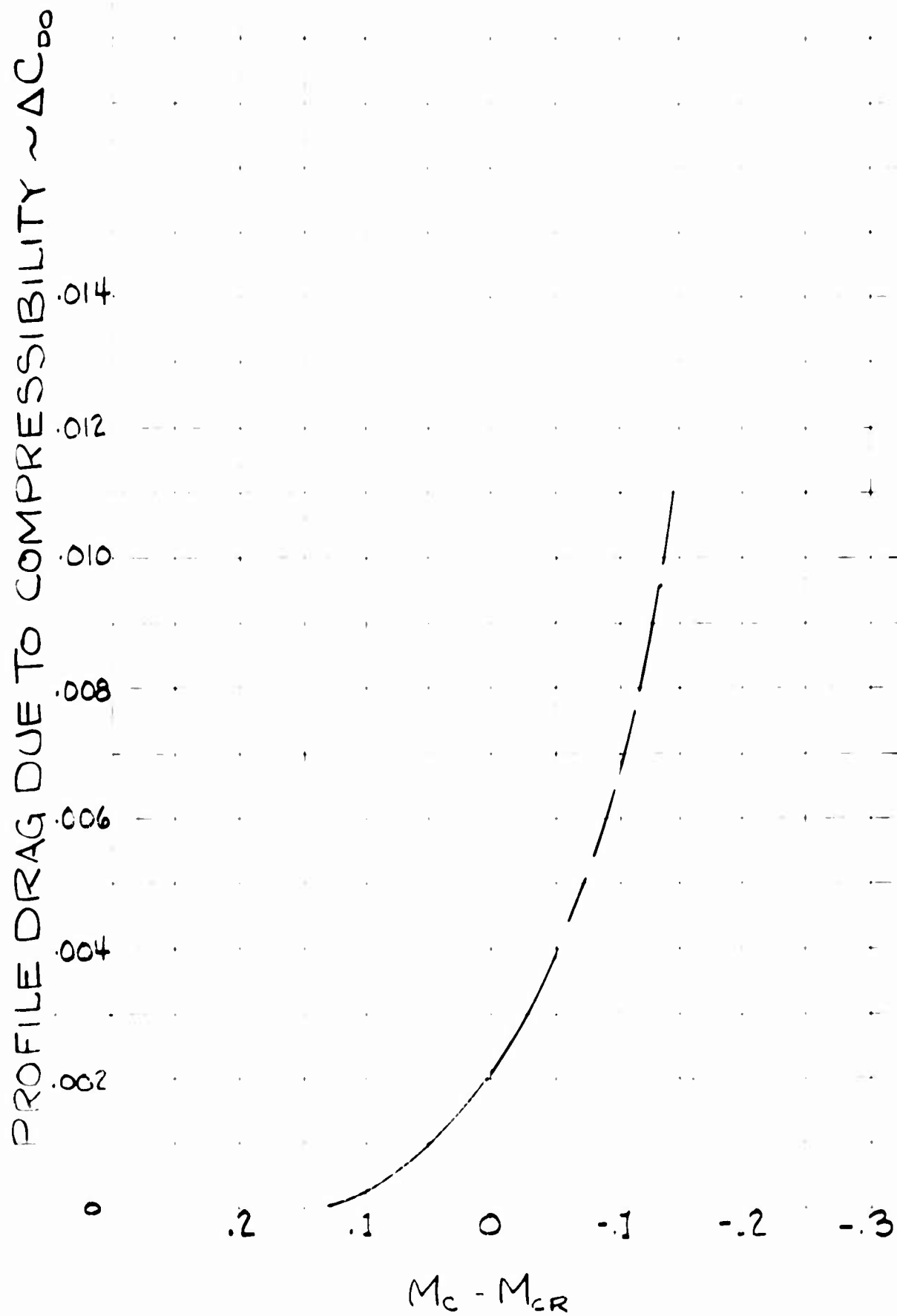


Figure 61 - Variation of Profile Drag With Mach Number

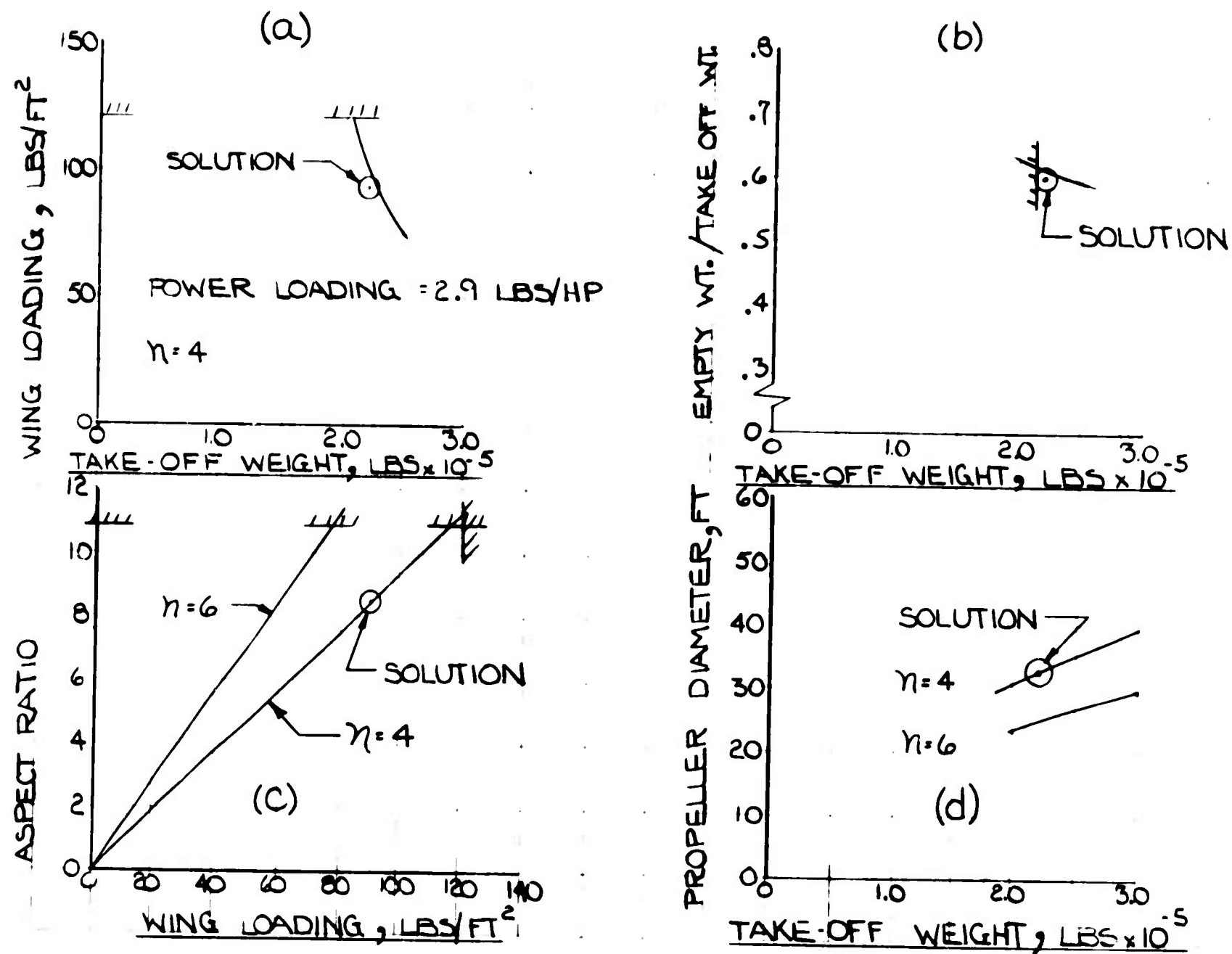


Figure 62 - Configuration Design Solution for Tilt Wing

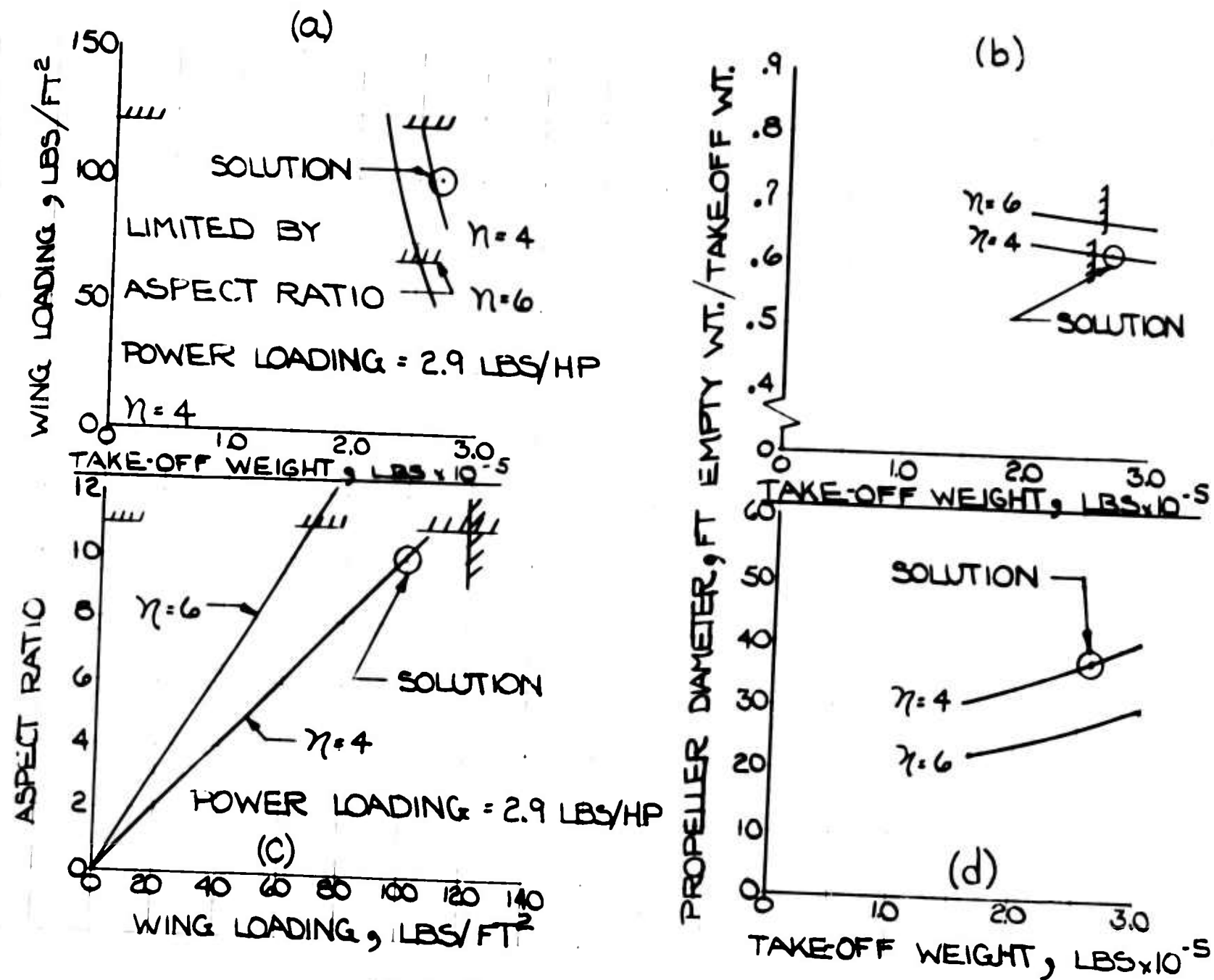


Figure 63 - Configuration Design Solution for Extended Flap

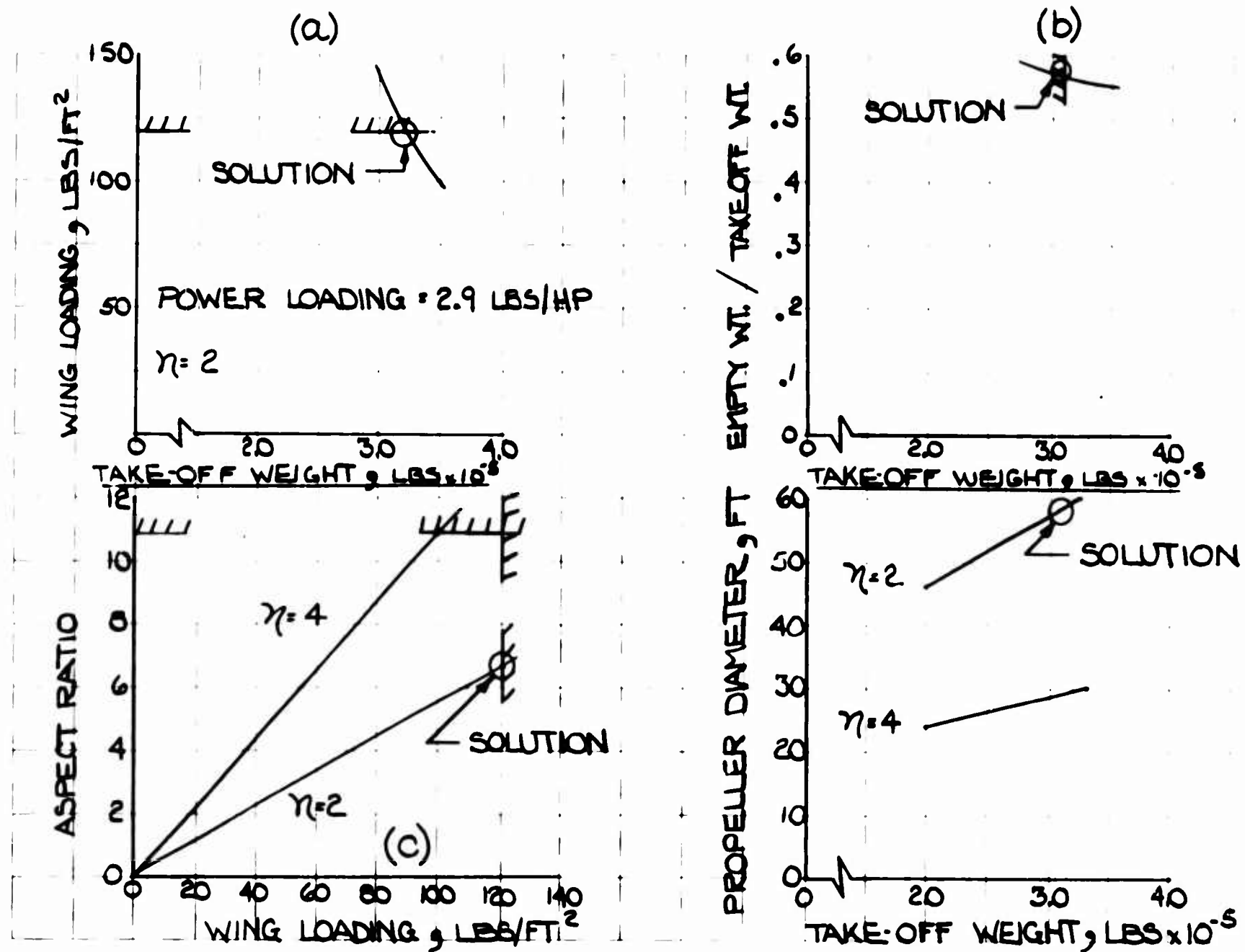


Figure 64 - Configuration Design Solution for Tilt Propeller

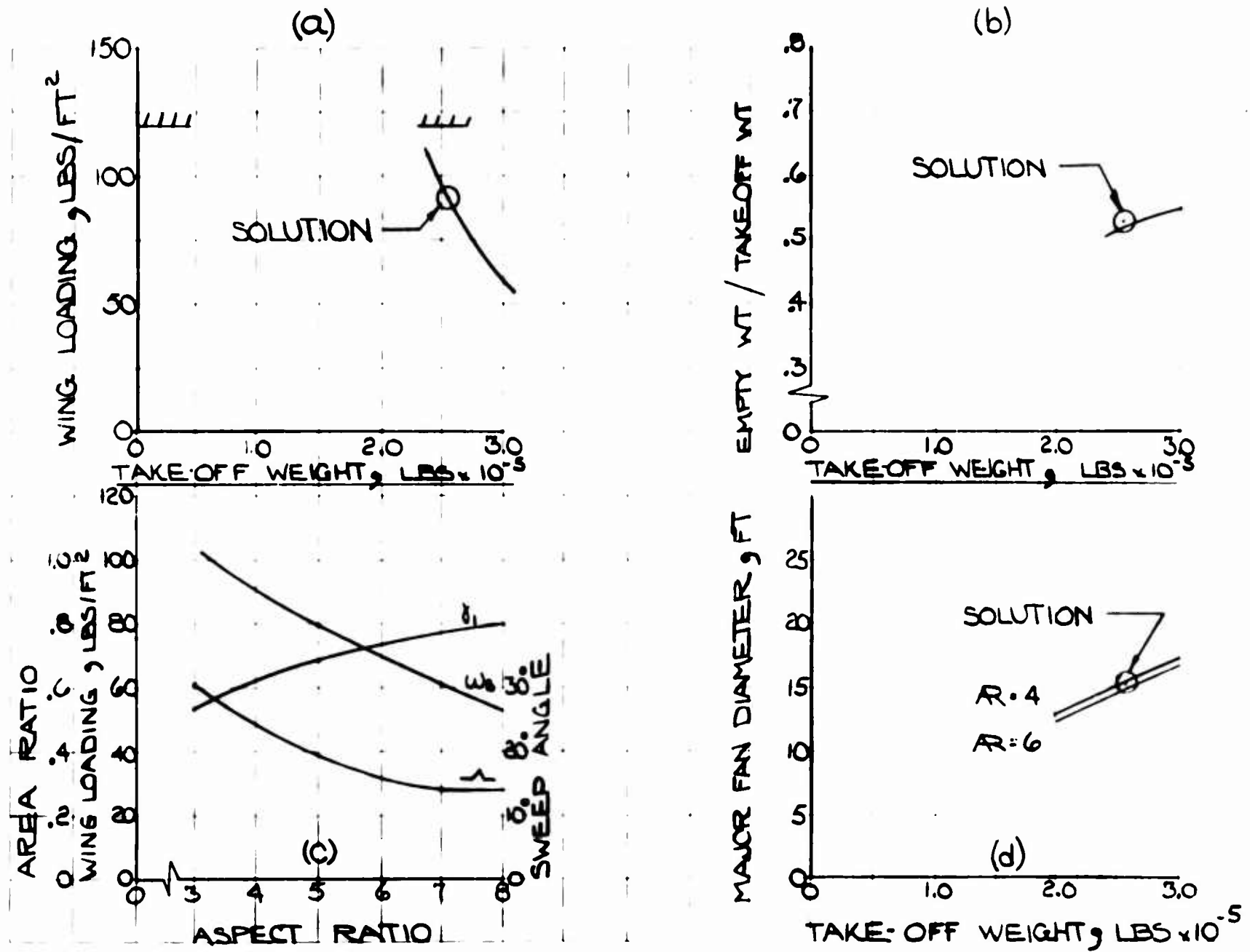


Figure 65 - Configuration Design Solution for Buried Fan

Table 14 - V/STOL Configuration Data

Aircraft Data \ Config.	Fixed Jet	Tilt Wing	Extended Flap	Tilt Prop	Buried Fan
Take-off Design Gross Weight (VTOL), W, Lbs.	172,000 (172,200)	223,000 (222,768)	263,000 (262,563)	308,000 (307,921)	253,000 (253,044)
Weight Empty, W _E , Lbs.	94,272	132,418	162,708	177,304	136,043
Payload, P, Lbs.	20,000	20,000	20,000	20,000	20,000
Crew & Trapped Fluids, Lbs.	2,168	2,275	2,355	2,617	2,501
Total Fuel, F _L , Lbs.	52,520	68,075	77,500	108,000	94,500
Useful Load/W	0.452	0.405	0.379	0.425	0.463
Wing Area, S, Ft. ²	1,650	2,365	2,600	2,560	2,800
Aspect Ratio, AR.	8.0	9.0	10.3	6.6	4.0
Sweepback at 1/4 Chord, Degrees	32.0	-	-	-	13.0
Span, Ft.	115	146	164	130	105.8
Airfoil	23,012	23,021	23,021	23,021	23,015
Thickness/Chord	.18 to .10	.21	.21	.21	.15 to .10
High Lift Devices	Slats and Flaps	Full Span Slats and Double Slotted Flaps	Full Span Slats and Double Slotted Flaps	Full Span Slats and Double Slotted Flaps	Full Span Slats and Flaps
Tip Chord/Root Chord	0.282	0.6	0.6	0.6	0.441
Prop Diameter, Ft.	-	33.0	37.5	57.5	Fan Dia. 15.1, 11.95
Number of Props, n	-	4	4	2	No. of Fans 7
Installed Thrust/W	1.3	1.3	1.445	1.43	1.3
DL Hover = $1.3W$ (Losses)/ πnR^2 Lbs/ Ft. ²	-	84.8	84.8	84.8	558

(Continued)

Table 14 - V/STOL Configuration Data

Aircraft Data \ Config.	Fixed Jet	Tilt Wing	Extended Flap	Tilt Prop	Buried Fan
Figure of Merit	-	0.7	0.7	0.7	-
Prop Cruise Efficiency	-	0.75	0.75	0.75	-
Inst. Static HP or Thrust, Lbs.	Thrust 221,000	98,600 HP	130,000 HP	152,000 HP	147,500 Jets
Power Loading, Lbs/HP	-	2.9	2.9	2.9	-
Thrust Distribution	77% Vertical 23% Variable	-	-	-	147,500 Horiz 328,000 Vert.
Equivalent Parasite Drag Area, Ft. ²	25.3	55.0	61.0	69.0	22.7
Cruise Altitude, Ft.	38,000	30,000	30,000	30,000	35,000
Cruise Speed, Knots	400	275	275	300	400
Average Weight, Lbs.	143,000	181,250	228,500	251,500	200,650
Cruise C _L	0.595	0.797	0.872	0.849	0.440
Cruise SFC or TSFC	0.75	0.52	0.52	0.52	0.82
Cruise Thrust, Lbs.	13,810	15,100	16,950	23,700	20,650
W/S, Lbs./Ft. ²	86.7	93.0	100.0	120.0	90.4
Chord/Diameter Ratio	-	0.491	0.424	0.339	-
Prop Area/Wing Area Ratio	-	1.45	1.70	2.01	0.21
Lift-off Speed (STOL) Knots	108.5	53.5	59.0	65.0	-
Overload Gross Weight (STOL)	232,000	334,000	394,000	462,000	No STOL Capabilities
STOL Overload Factor	1.35	1.5	1.5	1.5	-
α_{to} Degrees	10	5	5	-	1.3
α_{max} Degrees	10	10	10	10	6
δ Degrees	20	Full Down	Full Down	Full Down	-
No. of Ratio Units used for STOL	2(Parallel)*	-	-	1 *	1 Plus 2 Parallel*

* Thrust = 115,700 lbs/unit

APPENDIX II

STOL PERFORMANCE METHODS

Presented herein is an approximate method for calculating the STOL performance of VTOL type aircraft. There are five different VTOL configurations analyzed as required by Reference 13 namely:

1. Fixed Jet
2. Buried Fan
3. Tilt Wing
4. Tilt Propeller
5. Extended Flap

The assumptions and conditions employed in this analysis are presented along with a discussion of these assumptions. The detailed equations and procedures used to carry out the analysis are also presented. The design solution of each of these aircraft, which were previously determined, is given in Table 14.

Method of Analysis

The objective of this analysis is to determine at what overload gross weight each of the five configurations is capable of clearing a 50 ft. obstacle located at the end of a 1000 foot runway. Since the configurations are different in many respects, a completely general analysis is not possible. Some generality may be obtained if the aircraft are grouped into two classes - the propeller types (Tilt Wing, Tilt Propeller, and Extended Flap) and the jet types (Fixed Jet and Lift Fan). These groupings are used wherever possible

V/STOL Conditions and Assumptions

A. General Conditions and Assumptions

1. Runway length - 1000 ft. maximum.
2. Obstacle height - 50 ft.
3. Sea level, standard day conditions.
4. Ground friction coefficient = .2, equivalent to a plowed field or sand.
5. No ground effect.
6. The climb out phase of the STOL flight path is accomplished at constant forward speed.
7. An average airfoil section is used for lift and drag estimates.
8. Flap deflections are held constant and at a maximum unless otherwise specified.
9. The tail trim fan has a maximum thrust capability - 10% of the main propulsion thrust. 65% is used for trim and 35% is used for maneuver.
10. Each configuration has a total length of 100 ft.
11. Maximum forward acceleration during the ground run is limited to approximately 1.2 g's.
12. The forward speed for climb-out is the minimum speed, where there is about .4 g's vertical acceleration capability when the aircraft is trimmed in the horizontal direction.

13. RATO assist is used only during the ground run.
14. RATO units are turned on during the latter portion of the ground run to minimize the required runway length.
15. The net lift to gross weight ratio is 1.3.

B. Individual Configuration Properties and Assumptions

1. Tilt Wing

- a. $\eta = \eta_0 = .7$, propulsive and static propulsive efficiencies including transmission losses.
- b. $\dot{\Theta} = 15$ deg./sec., angle between thrust vector and horizontal.
- c. No RATO assistance is required.
- d. $\Theta_0 = 10^\circ$, thrust tilt angle during ground run.
- e. $k_3 = 1.0$, factor accounting for wing-propeller interference losses.

2. Tilt Propeller

- a. $\eta = \eta_0 = .7$
- b. Vertical drag = .1 W, lbs; $k_3 = .9$
- c. 1 RATO unit required.
- d. The fuselage is rotated during transition instead of the propeller masts. $\alpha_f = 20^\circ$, fuselage angle of attack with respect to horizontal.
- e. $\Theta_0 = 48^\circ$, propeller normal force is included because of high required Θ .
- f. $\dot{\Theta} = 0$
- g. The outboard section of the wing is assumed to rotate with the propeller for simplicity.

3. Extended Flap

- a. $\eta = \eta_0 = .7$
- b. The flow turning losses are assessed to be 10% of the propeller thrust; $k_3 = .9$
- c. No RATO assistance is required.
- d. A variable wing incidence range of 20° is required.
- e. $\dot{\Theta} = 10$ deg./sec.
- f. $\Theta_0 = 27^\circ$

4. Fixed Jet

- a. $\theta_o = 11.3^\circ$
- b. $\alpha_{f_o} = 0^\circ$, fuselage angle of attack during ground run.
- c. Two RATO units in parallel are required.
- d. $v_e = 1500$ ft./sec., exit downwash velocity.
- e. Induced lift loss in forward flight is assessed to be 5% of T_j , lbs., the vectored jet thrust.
- f. $k_j = 1.0$

5. Buried Fan

- a. The lift fans are assumed to be ineffective for the STOL take-off and therefore the take-off is accomplished using the installed jets in combination with 3 RATO units.
- b. One RATO unit is used for the first 4 seconds and 2 RATO units are used in parallel for the last 4 seconds of the ground run.
- c. $\alpha_{f_o} = 4^\circ$
- d. $k_j = 1.0$

C. Discussion of Assumptions

Considering part A, Items 1 through 3 are stipulated by Reference 13, while Items 5 through 10 are used for simplicity. Item 4 is considered a reasonable representation of the expected runway conditions. Item 11 is considered as being the upper limit of forward acceleration within the envelope of limit structural design loads for transport type aircraft. Item 12 is the criteria established to determine V_o and insure a fair climb acceleration so that the climb-out phase of the STOL take-off would require less horizontal distance than the ground run. Item 12 is assumed to effect safety into the STOL operation. If the RATO units were used for the transition and climb-out phases and failed during one of these phases, a crash would unavoidably occur. However, when the RATO assist is limited to the ground run phase only, Should it fail, the take-off can be aborted. Deceleration is accomplished on the ground using the full benefit of the ground resistance force. No horizontal distance must be expended to lose altitude before the ground resistance force can come into effect. Item 14 is obviously the most optimum way to employ RATO. Item 15 is required to insure hovering and control capability at altitude and temperature conditions other than sea level.

The assumptions of part B reflect the characteristic differences of the configurations. For instance, the time for transition should be as small as possible. Thus, the $\dot{\theta}$ or $\dot{\alpha}_f$ should be as large as possible. However, each configuration has a different $\theta_1 - \theta_0 = \Delta \theta$ requirement, some large, some small, and small $\Delta \theta$ requirements allow relaxation of the high $\dot{\theta}$ requirement in favor of mechanical simplicity. Consequently, the Tilt Wing has a large $\Delta \theta$ requirement, and thus, $\dot{\theta}$ is relatively large (B1b). The Tilt Propeller and Extended Flap have small $\Delta \theta$ requirements and $\dot{\theta}$ is small (B2d and B3e). In fact, for the Tilt propeller, $\Delta \theta$ is essentially zero; the fuselage is rotated instead of the propeller. A small wing tilt range is required for the Extended Flap configuration in order to rotate the wing into a favorable position without having to rotate the fuselage when it is in the proximity of the ground (B3d).

Three configurations have significant losses connected with the interaction of the thrust producer and the wing. The Extended Flap has about a 10% turning loss when converting the propeller induced flow into lift (B3b) (see Reference 10). The Tilt Propeller configuration has a large vertical drag loss in hover, estimated to be about 10% of hover thrust (B2b). The Fixed Jet configuration has an induced lift loss in forward flight assessed at 5% of the maximum vertical jet thrust. The interaction of high induced velocities perpendicular to and in the vicinity of the wing with the forward velocity are the cause of this phenomenon (B4e) (see Reference 9).

All the fuselage angles during the ground run (B1e, B2f, B3g, B4b, and B5c) are obviously small, but are generally inclined in the direction of trim attitude in the climb-out phase in order to reduce the time for transition.

Finally, it is generally well known that no theory has yet been developed to realistically describe the performance of a lift fan in forward flight. To date, experimenters have had to rely on model and full scale test data to understand this concept. This data has shown the rapid washout of horizontal force with forward speed. This makes it difficult to trim the aircraft horizontally at the speeds required for climb-out without using extremely large louver angles. These large louver angles throttle the fan and consequently the lift is greatly reduced. In view of these limitations, it was assumed for this analysis that a pure jet take-off with RATO assist would be the best procedure for a STOL take-off (see Reference 14).

Analytical Development of STOL Flight Path

I. Propeller Configurations

A. General Equations

Propeller plus transmission efficiency is defined as:

$$\eta = \frac{T_{HP}}{BHP}$$

$$\eta = \frac{T(\dot{x} \cos \theta + \dot{z} \sin \theta + v)}{550 BHP} = \eta_0 \quad (175)$$

(See Figure 66)

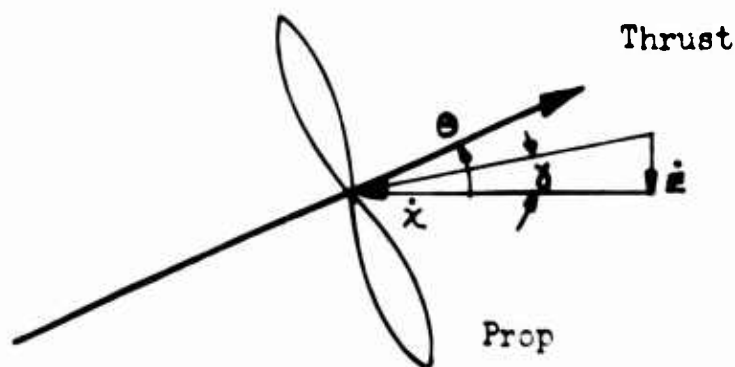


Figure 66 - Airflow Through Propeller Plane

For the static condition:

$$\eta_0 = \frac{T v_0}{550 BHP} \quad (\text{Ref. Par. B1a, B2a, B3a}) \quad (176)$$

The induced velocity through the rotor using momentum theory is: (177)

$$v = - \left(\frac{\dot{x} \cos \theta + \dot{z} \sin \theta}{2} \right) + \left[\left(\frac{\dot{x} \cos \theta + \dot{z} \sin \theta}{2} \right)^2 + \frac{T}{2 \rho A_P} \right]^{1/2}$$

(See Figure 67)

The local flow about the wing assuming a fully developed slipstream (v_t) is:

$$v = \left[(\dot{z} + v_t \sin \theta)^2 + (\dot{x} + v_t \cos \theta)^2 \right]^{1/2} \quad (178)$$

where

$$v_t = 2v$$

The angle of attack of the wing in this combination is:

$$\alpha_w = \theta - i_p - \alpha_g \quad (\text{See Figure 67}) \quad (179)$$

where

$$\alpha_g = \tan^{-1} \frac{\dot{z} + v_t \sin \theta}{\dot{z} + v_t \cos \theta} \quad (180)$$

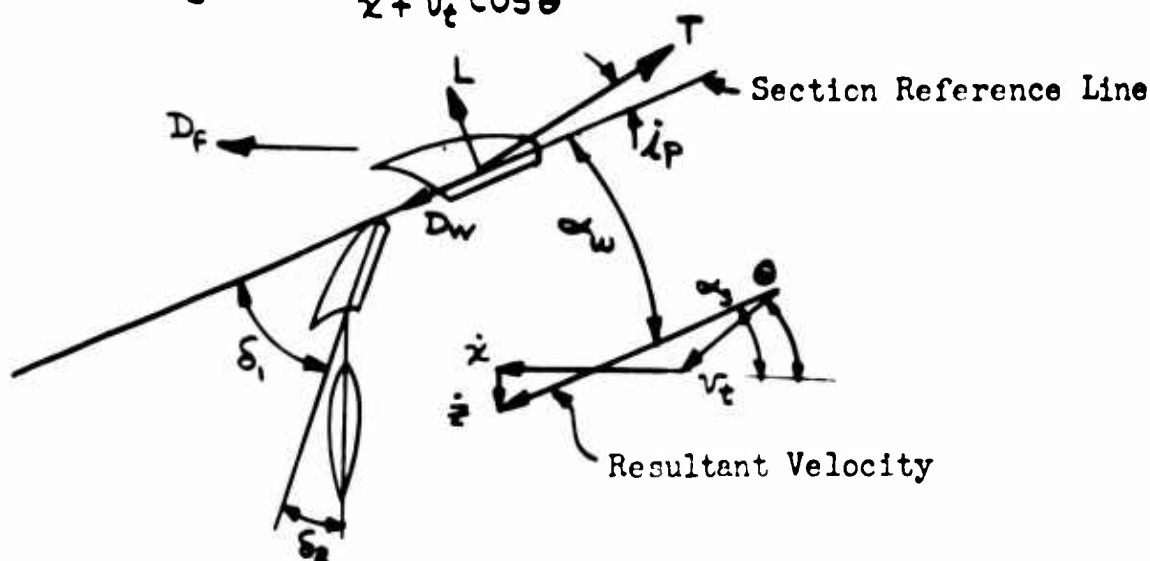


Figure 67 - Wing Local Airflow

The local flow about the wing as described by Figure 67 and equations 179 and 180 is not compatible with classical lift theory because the mass of air driven by the propeller is not the same as that assumed by classical theory. Consider Figure 68.

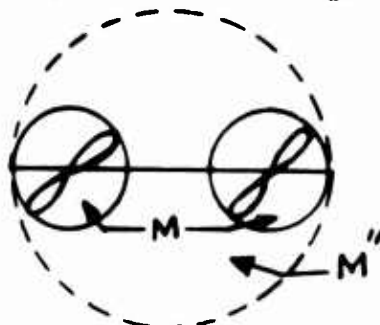


Figure 68 - Mass Flow of Air Affected by Propellers

The classical lift theory assumes that a mass of air equal to a circle, whose diameter is equal to the wing span, is accelerated downward to produce lift. However, it can be seen from Figure 68 that the mass of air affected by the propellers is considerably less than the assumed value. Therefore, a correction in the form of a ratio of masses must be applied to the lift and drag coefficients of the airfoil section when using equations 179 and 180 to determine lift and drag. These corrections take the form:

$$k_c = \text{ratio of masses}$$

$$\begin{cases} C_{L \text{ corrected}} = k_c C_L \\ C_{D \text{ corrected}} = k_c (C_{D0} + C_L^2 / \pi A R \eta_w) \end{cases} \quad (181)$$

For the assumed airfoil data see References 1, 7 and 16. In Reference 6, k is shown to be a function of the so-called slipstream thrust coefficient T_c'' and is shown in Figure 72.

$$T_c'' = [1 - 8\omega/8]^{1/2}$$

For a more rigorous treatment of this subject, see Reference 6.

B. The Ground Run:

The forces acting on the aircraft as it accelerates down the runway are: (See Figure 67). (182)

$$\begin{aligned} \Sigma F_H &= T \cos \theta - D_w \cos \alpha_3 - L \sin \alpha_3 - D_f - C_f (F_{N3} + F_{M3}) \\ &= W_0 \ddot{x}/g \end{aligned} \quad (183)$$

$$\Sigma F_V = T \sin \theta - D_w \sin \alpha_3 + L \cos \alpha_3 - W_0 = -(F_{N3} + F_{M3})$$

Since acceleration down a runway is usually accomplished at maximum power available, the maximum thrust available for acceleration is found from equations 175 and 177 assuming that the propeller and transmission efficiency remain essentially constant in the low speed flight region. When the available thrust verses \dot{x} for constant power is determined, it is found that this relationship is essentially linear with \dot{x} up to a speed of approximately 60 knots.

$$T = T_0 - k_1 \dot{x} \quad (184)$$

where T_0 is the static thrust and k_1 the slope of the linear function. Due to the dynamic pressure of the propeller downwash over the wing in low speed flight the propeller aircraft do not have to accelerate to high forward speeds to obtain lift-off capability and hence, wing and fuselage drag forces are small compared to the other forces. Also, since the thrust tilt angle is relatively low and always greater than α_3 the product of $L \sin \alpha_3$ is also small. Using the above, substituting equations 182 and 184 into equation 182 and rearranging:

$$W_0 \ddot{x}/g = -k_1 (\cos \theta + C_f \sin \theta) \dot{x} = C_f W_0 + C_f L \cos \alpha_3 + T_0 (\cos \theta + C_f \sin \theta)$$

Again, the product of $C_f L \cos \alpha_3$ is small compared to the other forces and can be neglected. Finally, dividing through by W_0/g and introducing:

$$k_0 = W_0/W \quad \text{the overload factor}$$

$$\lambda_0 = -(k_1 g/W) (\cos \theta + C_f \sin \theta)$$

$$\Xi = (T_0/W) (\cos \theta + C_f \sin \theta)$$

$$\Xi = C_f g$$

Note that T_0 is determined by the hover condition where:

$$T_0 = (1.3/b_3)W = k_4 W \quad (\text{Ref. Par. A15}) \quad (184a)$$

k_3 accounts for the wing-propeller interaction and the equation takes the form:

$$\ddot{x} + (\lambda_0/b_0)\dot{x} = \bar{x}/k_0 + \bar{x} = \eta \quad (\text{Ref. Par. B1c, B2b, B3b}) \quad (185)$$

The solution of this equation for the initial conditions of $\dot{x} = \dot{x}_0$ and $x = x_0$ determines the characteristics of the motion for the ground run. (186)

$$\begin{aligned} \dot{x} &= k_0 \eta / \lambda_0 \left[1 - e^{-\lambda_0 t / b_0} \right] + \dot{x}_0 e^{-\lambda_0 t / b_0} \\ x &= -k_0^2 \eta / \lambda_0^2 \left[(1 - e^{-\lambda_0 t / b_0}) - \lambda_0 t / b_0 \right] + \dot{x}_0 k_0 / \lambda_0 (1 - e^{-\lambda_0 t / b_0}) + x_0 \end{aligned} \quad (187)$$

The approximate optimum θ for the ground run can be obtained by taking the partial derivative of \dot{x} with respect to θ and minimizing. The resulting θ becomes:

$$\theta = \tan^{-1} C_f \quad (188)$$

It must be noted that the physical restriction of propeller ground clearance may limit the minimum θ . However, it is obvious that θ should be as low as possible but not lower than the angle given by equation 188. (B1d, B2e, B3f, B4a)

If RATO is used during acceleration, T_0 is increased by the amount of the RATO force, this force should act at an angle given by equation 182. Note that RATO units can be used in series and/or in parallel for 4.15 seconds duration. (B1c, B2c, B3c, B4c, B5b).

C. Vertical Acceleration At Maximum Horsepower:

As was explained earlier, accelerated climb is investigated to determine at what minimum speed V_C , there exists a good climb potential. To carry out this examination, equations 175 & 177 are used to determine the thrust available for various \dot{x} and \dot{h} . Equations 181 & 182 are then used in conjunction with the above results to find the horizontal trim ($\dot{x} = 0$) and θ_1 for various \dot{h} when $\dot{x} = V_C$. Using equation 183, modified to reflect acceleration:

$$\Sigma F_V = W_0 \ddot{z} / g \quad (189)$$

The vertical acceleration potential and the maximum rate of climb can be determined for maximum power. Obviously, this procedure is iterative. With this information it is now possible to calculate transition from ground acceleration to maximum \dot{h} .

D. Transition Phase

The transition phase of the STOL flight path is defined as that phase where the moveable thrust vector or the fuselage is rotated from its ground run attitude to its climb-out attitude. The time for transition depends on the values of θ required for ground acceleration and vertical acceleration, and the tilt rate capability of the aircraft. (B2d, B2g, B3d)

Explicitly, the time for transition is:

$$t_{01} = (\theta_1 - \theta_0) / \dot{\theta} \quad (190)$$

$\dot{\theta}$ is the tilt rate (B1b, D2f, B3e)

Unlike the ground acceleration condition, where an explicit solution for the resulting motion is possible, an approximate solution must be used here. The approach chosen assumes a linear variation of forces from the ground acceleration value to vertical acceleration value. In Figure 69 this linear variation is shown as the solid line.

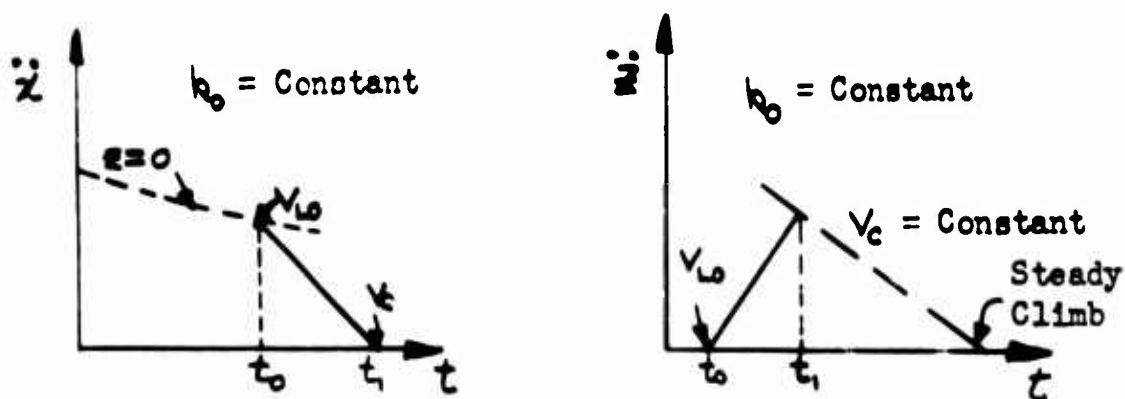


Figure 69 - Time Variation of Horizontal and Vertical Accelerations During Transition

At some time, t_0 , before V_c is reached at V_{L0} , the tilting begins. Knowing the time for transition from equation 190 and using the following equations, V_{L0} can be found. Also, the resulting distances, x_{t1} plus the climb velocity, z_{t1} can be found for this time period.

$$V_{L0} = V_c - 1/2(\ddot{x}_{t0})(t_{01}) \quad (191)$$

$$\Delta x_{t01} = V_{L0}(t_{01}) + 1/4(\ddot{x}_{t0})(t_{01})^2 \quad (192)$$

$$\dot{z}_{t1} = 1/2(\ddot{z}_{t1})(t_{01}) \quad (193)$$

$$z_{t1} = 1/4(\ddot{z}_{t1})(t_{01})^2 \quad (194)$$

Now that V_{LO} is known, the time for the ground run can be determined from equation 186 and the distance required to accelerate to V_{LO} from equation 187.

E. Climb-out

Just as in the case of the ground run, the summation of acceleration forces for climb at constant forward speed, V_C , are found to be essentially linear with \dot{z} , see Figure 70. Recall that the vertical acceleration capability has already been determined, lift as a function of \dot{z} for $\dot{x} = V_C$. To derive the equations for the explicit solution for climb-out it is necessary to modify equation 135 to account for the forces in the vertical direction as follows. Using equations 183 & 189 determine:

$$\Sigma F_V = L_0 + b_1 \dot{z} - W_0 \quad (195) \quad \Sigma F_V$$

Substituting equation 195 into equation 189

$$W_0 \ddot{z}/g - k_2 \dot{z} = L_0 - W_0 \quad (196)$$

and

$$\ddot{z} + \lambda_0 \dot{z}/k_0 = \Xi/k_0 + \Xi = \eta \quad (197)$$

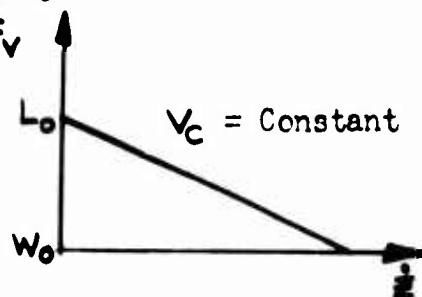


Figure 70 - Acceleration Forces vs. Constant Forward Speed

which is the exact form of equation 185. The solution of equation 197 has the exact form as equations 186 and 187.

The incremental time required to climb over the 50 ft. obstacle, t_{12} , can be obtained from equation 198

$$50 = -\frac{k_2 \eta}{\lambda_0} \left[(1 - e^{-\lambda_0 t_{12}/k_0}) - \lambda_0 t_{12}/k_0 \right] + \frac{\Xi t_{12} k_0}{\lambda_0} (1 - e^{-\lambda_0 t_{12}/k_0}) + z_{t1} \quad (198)$$

Knowing the time required for climb-out, the horizontal distance covered during this portion of the flight path is:

$$\Delta x_{t12} = V_C t_{12} \quad (199)$$

F. The Total Required Runway Length

The total required runway length is the sum of all the horizontal distances required for the various phases of the STOL flight path plus one aircraft length (100 ft.).

$$x_{TOTAL} = \underbrace{\Delta x_{t0}}_{\text{Eq. 187}} + \underbrace{\Delta x_{t01}}_{\text{Eq. 192}} + \underbrace{\Delta x_{t12}}_{\text{Eq. 199}} + 100 = 1000 \quad (200)$$

The desired overload gross weight is determined when equation 200 is numerically equal to 1000 ft. However, since this equation can only be evaluated for one k_0 at a time, this whole procedure must be iterated until the proper conditions for equation 200 have been satisfied.

II. Jet Configurations:

The jet configurations' STOL performance is calculated in approximately the same manner, (B5a). Note that the installed thrust for the VTOL mode is again governed by equation 184a, (B4f, B5d).

A. The Ground Run

The decrease in jet thrust with forward speed is approximately linear up to about 150 knots. Therefore, the ground run characteristics of the jet are similar to that of the propeller aircraft. Equations 181 through 188 apply along with the previously mentioned assumptions. It is noted that even though V_{LO} is twice that for the propeller configurations (approximately 200 fps), the forces due to lift and drag are still reasonably small.

There is an additional drag and lift term that must be added to equation 182 to account for the jet lift producer. The additional drag term, called momentum drag, evolves from the fact that the air flowing through the lift producer must be accelerated up to the forward speed of the aircraft. This drag has the form.

$$D_M = T\dot{x}/v_e \quad (\text{Ref. Par. B4d}) \quad (201)$$

Note that this term is a function of \dot{x} and is incorporated in the λ_0 coefficient of equation 185 when a jet lift producer is used. The lift term is a constant but must be reduced according to assumption B4e.

B. Vertical Acceleration:

Vertical Acceleration capability is determined for horizontal trim ($\ddot{x} = 0$) for different V_c . Three unknowns are found from this calculation. First, the V_c needed to give a reasonably \dot{z}_1 , second, the variation of z with \dot{z} and last, the α_f , required during climb-out. Equations 182 & 183, equation 183 being modified by equation 189, are used for this calculation. The local wing angle of attack to be used is:

$$\alpha_w = \alpha_f + i_w - \delta \quad (202)$$



Figure 71 - Local Wing Angle of Attack

C. Transition

The time for transition depends on the values of α_f for ground acceleration and vertical acceleration, and the rate that the fuselage can be rotated in pitch. The pitching rate depends upon the

moment of inertia and the thrust produced by the tail fan multiplied by the tail length (from the center of the fan to the center of gravity of the aircraft). Recall that only 35% of the fan thrust is used for maneuvering (A9). Therefore:

$$t_1 - t_0 = \left[\frac{3270(\alpha_{f1} - \alpha_{f0})I_0}{k_0 l_t W} \right]^{1/2} \quad \begin{matrix} \text{(Ref. Par.} \\ \text{B4db, B5c)} \end{matrix} \quad (203)$$

A step by step analysis using one second intervals from t_0 to t_1 , is used to calculate the flight path. The forces are evaluated at the average velocities during each interval using an iterative technique.

Transition begins at t_0 which is $t_1 - t_0$ seconds before V_c is reached. The velocity at this time, t_0 , is \dot{X}_0 and is calculated by equation 186. A change in \dot{X} and \dot{Z} is assumed and the forces and accelerations are determined by equations 182, 183 (modified by 189), and 202. Equations 191 & 193 are applied, dropping the subscripts to reflect the smaller time interval being used here. When the iteration on \dot{X} and \dot{Z} is completed the distances covered can be calculated by equations 192 and 194. This procedure is followed until transition is completed. The forward velocity should now be V_c , while \dot{Z}_{t1} and \dot{Z}_{t1} are still small.

D. Climb-Out

All equations (195 through 199) and assumption of part I E are applied to this case. The climb-out phase is determined in exactly the same manner as in part I E.

E. The Total Required Runway Length

The completion of the calculation is exactly the same as part I F. The same equation and conditions must be satisfied to determine the desired overload gross weight. As is the case of the propeller configurations, this entire procedure must be iterated to determine the final overload gross weight that can climb over a 50 ft. obstacle at the end of a 1000 ft. runway.

BLANK PAGE

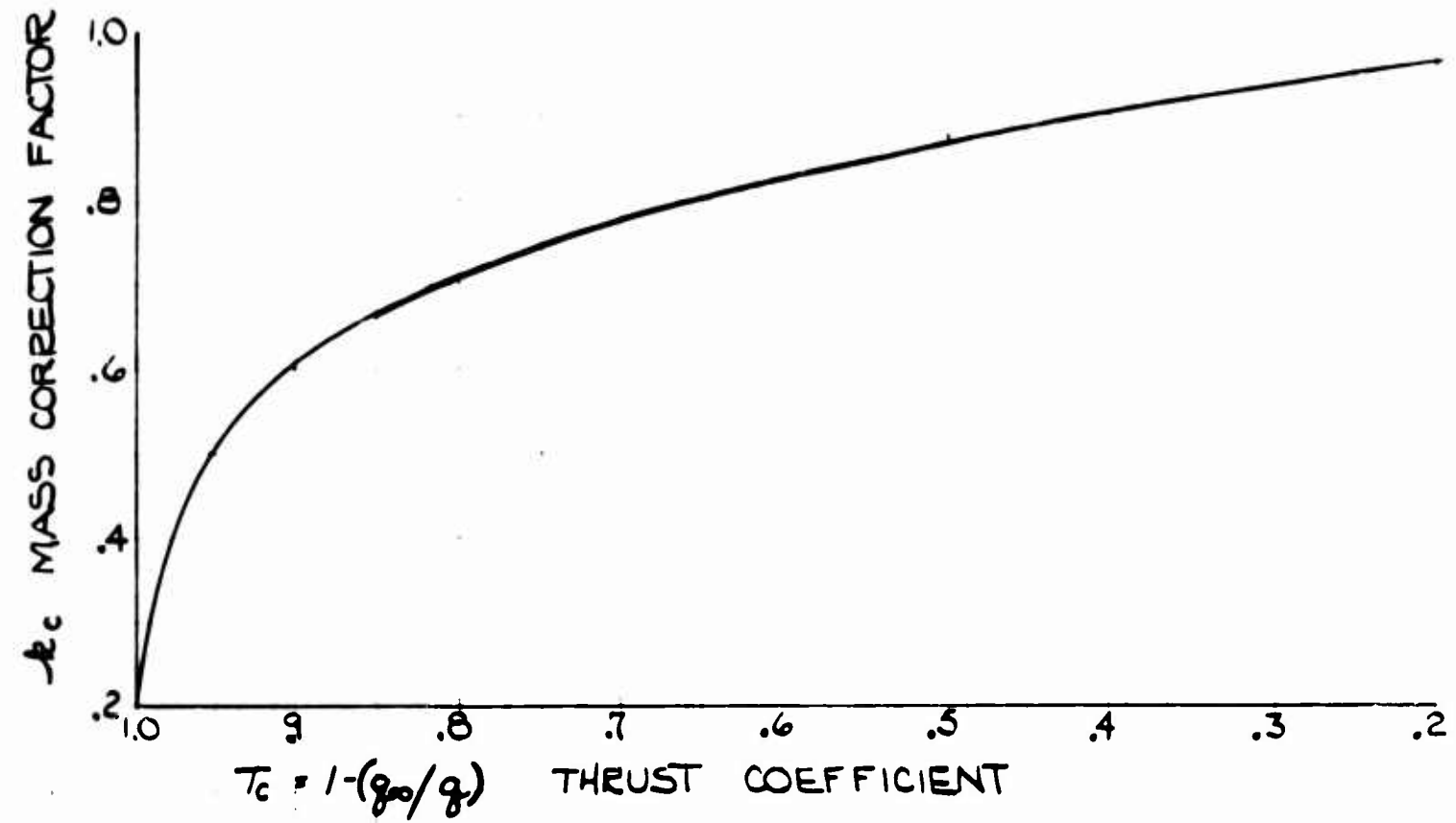


Figure 72 - Variation of Mass Correction Factor With Thrust Coefficient

APPENDIX III

WEIGHT SUMMARY, PANEL POINT DISTRIBUTION AND GROUP WEIGHT

STATEMENTS

BLANK PAGE

Table 15 - Panel Point Weights: Fuselage and Contents

Panel Point No.	Fixed Jet		Tilt Wing		Extended Flap		Tilt Prop		Buried Fan	
	Sta.	Weight	Sta.	Weight	Sta.	Weight	Sta.	Weight	Sta.	Weight
1	0	308.3	0	341.3	0	367.1	0	407.5	0	387.1
2	95	5012.0	95	5471.6	95	5833.5	95	6396.4	95	6110.5
3	215	9887.6	215	10,555.3	215	11,030.5	215	11,898.1	215	20,485.0
4	370	9210.2	370	9603.6	370	9913.2	370	10,395.0	370	25,947.8
5	487	9005.1	487	9539.4	487	9959.9	487	10,614.3	487	21,723.6
6	567	11,149.6	567	11,769.0	567	12,256.3	567	13,014.6	567	27,930.2
7	770	5814.3	770	6225.5	770	6549.4	770	7053.5	770	12,404.9
8	920	2357.4	920	2567.3	920	2732.5	920	2989.5	920	2853.9
9	1011	2984.5	1011	3411.6	1011	3981.9	1011	4430.8	1011	3736.2
10	1168	2645.3	1180	3270.4	1196	4110.7	1204	4716.3	1187	3637.8
Totals		58,374.3		62,755.0		66,785.0		71,916.0		125,222.0

Table X - Panel Point Weights: One-Half Wing and Contents

Panel Point No.	Fixed Jet		Tilt Wing		Extended Flap		Tilt Prop		Buried Fan	
	B.L.	Weight	B.L.	Weight	B.L.	Weight	B.L.	Weight	B.L.	Weight
1	0	409.3	0	470.8	0	519.2	0	369.8	0	10,383.8
2	55	3039.5	55	1193.6	55	973.5	22	7903.7	55	10,749.0
3	110	8080.1	104	8542.4	95	10,906.0	55	11,224.9	69	7221.4
4	146	7993.2	237	9494.2	261	11,797.0	110	13,834.4	135	4233.7
5	203	7070.7	280	15,869.4	306	20,595.4	154	17,149.6	197	7773.4
6	266	12,470.9	323	7048.9	351	8398.3	258	16,092.4	317	10,399.8
7	421	11,858.1	468	13,732.8	525	15,465.2	362	13,433.9	414	5462.4
8	512	3955.5	645	7033.5	715	7390.9	465	35,287.8	527	6896.2
9	604	1765.2	688	15,888.1	760	20,876.7	622	1935.9	578	557.0
10	690	270.5	876	732.8	984	966.8	780	770.1	635	234.3
Totals		56,913.0		80,006.5		97,889.0		118,002.5		63,911.0

BLANK PAGE

Table 17 - Group Weight Statements

Config. Data	Fixed Jet	Tilt Wing	Extended Flap	Tilt Prop	Buried Fan
Wing Group	15,605	23,890	30,344	25,327	22,716
Tail Group	5236	6276	7626	8586	6861
Body Group	16,436	18,132	18,810	20,300	18,800
Lighting Gear Group	7361	9526	11,280	13,350	10,825
Flight Controls Group	2510	5020	5755	6615	5465
Engine Section	5170	2650	3485	4080	3970
Engines	28,900	14,790	19,500	22,800	22,200
Air Induction System	610	320	423	495	481
Exhaust System	810	414	545	640	621
Lubricating System	1390	710	936	1198	1065
Fuel System	980	1278	1498	2059	1768
Engine Controls	445	227	300	431	342
Starting System	1340	685	905	1060	1030
Props or Lift Fans		20,706	27,300	31,900	26,550
Drive System	1445	18,500	24,360	28,420	3717
Aux. Power Plant	786	439	527	590	579
Instruments, Electronics & Electrical Group	4912	4912	4912	4912	4912
Hydraulic Group	453	491	522	559	514
Furnishings	1812	1812	1812	1812	1812
Air Conditioning	310	310	310	310	310
Anti-Icing	809	1044	1220	1460	1180
Aux. Gear Group	221	286	338	400	325
Weight Empty	97,541	132,418	162,708	177,304	136,043
Useful Load	74,659	90,350	99,855	130,617	117,001
Crew (5)	1200	1200	1200	1200	1200
Payload	20,000	20,000	20,000	20,000	20,000
Fuel - Unusable	451	587	667	929	813
Fuel - Usable	52,520	68,075	77,500	108,000	94,500
Oil - Unusable & Oil - Usable	472	472	472	472	472
Miscellaneous	16	16	16	16	16
Gross Weight	172,200	222,768	262,563	307,921	253,044

Table 18 - Weight Formulae and Assumptions

Item	Formula	Assumptions
Wing Group	$w = 0.005884 (WtBS/t_R)^{0.6047}$ W = Design Gross Weight (LB) N = Ultimate Load Factor (G) b = Wing Span (FT) S = Gross Wing Area (SQ FT) t_R = Root Thickness	Kelly's short formula from AAF TR 5161. Formula weights are increased by various percentages to allow for sweepback, wing tilt, complexity, etc.
Tail Group Vertical Surfaces Horizontal Surfaces Tail Fan	$w = 2.5 \times \text{Profile Area (SQ FT)}$ $w = 3.0 \times \text{Profile Area (SQ FT)}$ $w = 0.15 \times \text{Fan Thrust (LB)}$	Fan Thrust = 0.1 x Total Main Propulsion Thrust (LB)
Door Group	$w = 14,000 (W/108,000)^{0.355}$	Based on a Sikorsky formula modified by weight data from a large transport aircraft
Landing Gear Group	$w = 0.0433 \times \text{Design Gross Wt. (LB)}$	Ratio based on a large transport aircraft
Flight Controls Group	$w = 975 + 975 (W/108,000)$	Partial ratio based on a large transport aircraft. Formula weight is adjusted to allow for wing tilt, prop tilt, complexity, etc.
Engine Section	$w = 0.179 \times \text{Engine Weight (LB)}$	Sikorsky Ratio
Engines Turbojet Gas Turbines Lift Jet	$w = 0.15 \times \text{Engine Thrust (LB)}$ $w = 0.15 \times \text{Horsepower (HP)}$ $w = 0.125 \times \text{Engine Thrust (LB)}$	} Future high horsepower engines
Air Induction System	$w = 0.0217 \times \text{Engine Weight (LB)}$	

Table 18 - Weight Formulae and Assumptions (continued)

Item	Formula	Assumptions
Exhaust System	$w = 0.028 \times \text{Engine Weight (LB)}$	Sikorsky Ratio
Lubricating System	$w = 0.048 \times \text{Engine Weight (LB)}$	Sikorsky Ratio
Fuel System	$w = 0.0187 \times \text{Usable Fuel (LB)}$	Ratio based on a large transport aircraft
Engine Controls	$w = 0.0154 \times \text{Engine Weight (LB)}$	Sikorsky Ratio
Starting System	$w = 0.0464 \times \text{Engine Weight (LB)}$	Sikorsky Ratio
Propellers/Lift Fans Propellers Lift Fans	$w = 0.21 \times \text{Horsepower (HP)}$ $w = 0.15 \times \text{Fan Thrust (LB)}$	Constant Activity Factor & Power Loading
Drive System Fixed Jet Tilt Wing, Extended Flap & Tilt Propeller Buried Fan	$w = 0.05 \times \text{Engine Weight (LB)}$ $w = 1.25 \times \text{Engine Weight (LB)}$ $w = 0.14 \times \text{Lift Fan Weight (LB)}$	Sikorsky Ratio Sikorsky Ratio Sikorsky Ratio
Auxiliary Power Plant	$w = 160 + 80 (\text{Engine Wt.}/4200)$	Partial Sikorsky Ratio
Instruments, Electronics and Electrical Groups	Constant at 4912 LB	Based on a large transport aircraft
Hydraulic Group	$w = 323 + 82 (W/108,000)$	Partial ratio based on a large transport aircraft
Furnishings	Constant at 1812 LB	
Air Conditioning	Constant at 310 LB	

Table 18 - Weight Formulae and Assumptions (continued)

Item	Formula	Assumptions
Anti-Icing	$w = 0.0047 W + 10$	Partial ratio based on a large transport aircraft
Auxiliary Gear	$w = 0.0013 \times \text{Design Gross Wt. (LB)}$	Sikorsky Ratio
Crew	5 at 240 LB Each	In accordance with HIAD
Payload	Constant at 20,000 LB	
Fuel-Unusable	$w = 0.0086 \times \text{Usable Fuel (LB)}$	Sikorsky Ratio
Fuel-Usable	Determined Aerodynamically	
Oil-Usable & Unusable	Constant at 472 LB	Based on a large transport aircraft
Miscellaneous	Constant at 16 LB	Flares

APPENDIX IV

NORMAL MODE METHOD OF ANALYSIS

Presented herein are the methods employed in calculating the mode shapes and frequencies of the fuselage and wing structure of the 5 V/STOL configurations. The analysis was conducted utilizing matrix iteration methods in an IBM digital computer program. The following discussion describes the procedures used in arriving at the solution.

After determining the panel point mass distribution (Ref. Section II and Appendix III, Table 15, 16) the mass matrix $[M]$ can be formed. Since the fuselage bending and torsional rigidities are known (Ref. Section II and Figs. 11, 12, 13, 14, 15) the influence coefficients for the previously mentioned panel points can be calculated.

The fuselage absolute coordinates are now written in terms of relative coordinates since the system must be transformed to a common energy plane. Introducing dummy or ignorable coordinates, which are taken at the junction of the fuselage and wing root, the transformation matrix $[A]$ is formed. The ignorable or rigid body coordinates are found in the last row of this matrix. The following diagram defines some of the terms and the sign convention used in this analysis.

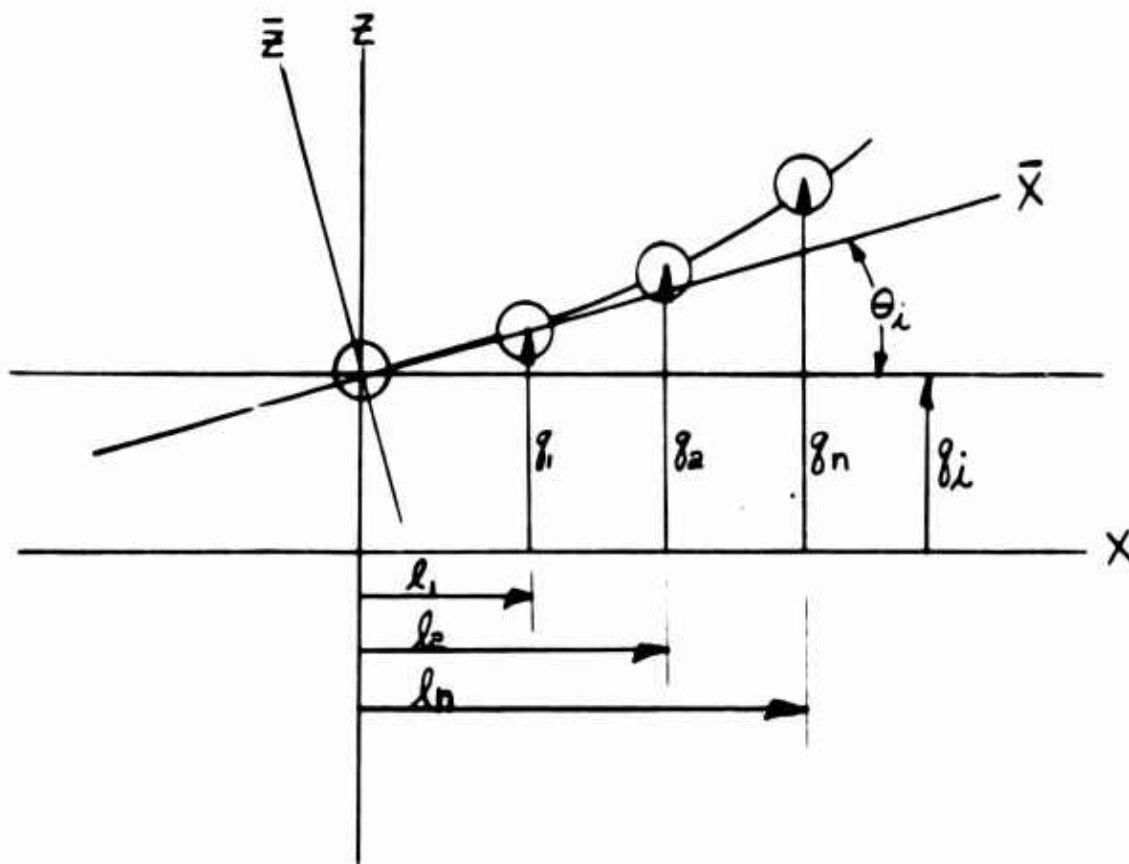


Figure 7.3 - Schematic of Fuselage Panel Points

BLANK PAGE

The equations for the kinetic and potential energy and the equations describing the panel point motions are as follows:

$$2KE = [\dot{g}][M]\{\dot{g}\} \quad (204)$$

$$2PE = [\bar{g}][K]\{\bar{g}\} \quad (205)$$

$$\begin{aligned} g_1 &= \bar{g}_1 + \bar{\theta}_1 l_1 + \bar{g}_1 \\ g_2 &= \bar{g}_2 + \bar{\theta}_2 l_2 + \bar{g}_2 \\ g_3 &= \bar{g}_3 + \bar{\theta}_3 l_3 + \bar{g}_3 \\ &\vdots \\ g_{n-1} &= \bar{g}_{n-1} + \bar{\theta}_{n-1} l_{n-1} + \bar{g}_{n-1} \\ g_n &= \bar{g}_n + \bar{\theta}_n l_n + \bar{g}_n \end{aligned} \quad (206)$$

where

$\bar{g}_i = \bar{g}_i$ fuselage ignorable coordinate.

$\bar{\theta}_i = \bar{\theta}_i$ fuselage ignorable coordinate.

$g_{1,2,3,\dots,n}$ = absolute fuselage coordinates.

$\bar{g}_{1,2,3,\dots,n}$ = relative fuselage coordinates.

$M_{1,2,3,\dots,n}$ = lumped masses assigned to fuselage stations.

$K_{1,2,3,\dots,n}$ = spring constants assigned to fuselage stations.

In matrix form:

g_1	1	0	0	0	0	1	l_1	\bar{g}_1
g_2	0	1	0	0	0	1	l_2	\bar{g}_2
g_3	0	0	1	0	0	1	l_3	\bar{g}_3
\vdots	\vdots	\vdots	\vdots	\vdots	\vdots	\vdots	\vdots	\vdots	\vdots	\vdots
g_{n-1}	0	0	0	1	0	1	l_{n-1}	\bar{g}_{n-1}
g_n	0	0	0	0	1	1	l_n	\bar{g}_n
\bar{g}_i	0	0	0	0	0	1	0	\bar{g}_i
$\bar{\theta}_i$	0	0	0	0	0	0	1	$\bar{\theta}_i$

or this can be written as:

$$\{g\} = [\mu]\{\bar{g}\} \quad (207)$$

and

$$\{\dot{g}\} = [\mu]\{\dot{\bar{g}}\} \quad (208)$$

also

$$[\dot{g}] = [\bar{g}][\mu]' \quad (209)$$

from which

$$2KE = [\dot{\bar{g}}][\mu][M][\mu]\{\ddot{\bar{g}}\} \quad (210)$$

The generalized mass matrix is determined by carrying out the matrix multiplication $[\mu][M][\mu]$ which yields the $[\bar{M}]$ matrix.

Let

$$[\mu][M][\mu] = [\bar{M}] \quad (211)$$

then

$$2KE = [\dot{\bar{g}}][\bar{M}]\{\ddot{\bar{g}}\} \quad (212)$$

Applying Lagrange's equation

$$\frac{d}{dt} \left(\frac{\partial KE}{\partial \dot{\bar{g}}} \right) - \frac{\partial KE}{\partial \bar{g}} + \frac{\partial PE}{\partial \bar{g}} = 0 \quad (213)$$

$$[\bar{M}]\{\ddot{\bar{g}}\} + [K]\{\bar{g}\} = 0 \quad (214)$$

Assume

$$\{\bar{g}\} = \{\bar{Q}\} e^{i\omega t} \quad (215)$$

then

$$-\omega^2 [\bar{M}]\{\bar{Q}\} + [K]\{\bar{Q}\} = 0 \quad (216)$$

The problem now existing is that the generalized mass matrix is not compatible with the $[K^{-1}]$ matrix, being larger by rows and columns equal to the number of ignorable coordinates. The coordinates are separated by partitioning the matrices so as to separate those portions that contain ignorable coordinates.

(217)

$$-\omega^2 \begin{bmatrix} \alpha & \beta \\ \beta^T & \delta \end{bmatrix} \begin{bmatrix} \bar{Q}_1 \\ \bar{Q}_2 \end{bmatrix} + \begin{bmatrix} K & 0 \\ 0 & 0 \end{bmatrix} \begin{bmatrix} \bar{Q}_1 \\ \bar{Q}_2 \end{bmatrix} = 0$$

Solving the simultaneously equations for \bar{Q}_1 only:

$$\begin{aligned} -\omega^2 [\alpha \{\bar{Q}_1\} + \beta \{\bar{Q}_2\}] + [\kappa] \{\bar{Q}_1\} &= 0 \\ [\beta' \{\bar{Q}_1\} + \delta \{\bar{Q}_2\}] &= 0 \\ \{\bar{Q}_2\} &= -\beta' \{\bar{Q}_1\} \delta^{-1} \\ -\omega^2 [\alpha \{\bar{Q}_1\} - \beta \delta^{-1} \beta' \{\bar{Q}_1\}] + \kappa \{\bar{Q}_1\} &= 0 \\ -\omega^2 [\alpha - \beta \delta^{-1} \beta' \{\bar{Q}_1\}] + \kappa \{\bar{Q}_1\} &= 0 \end{aligned}$$

After reduction of the generalized mass matrix, equation 218 is obtained.

$$\frac{1}{\omega^2} \{\bar{Q}_1\} = [\bar{\kappa}'] [\bar{M}] \{\bar{Q}_1\} \quad (216)$$

where $[\bar{M}]$ is the reduced generalized mass matrix.

A mode shape $\{\bar{Q}_1\}$ is assumed and the multiplication $[\bar{\kappa}'] [\bar{M}] \{\bar{Q}_1\}$ is performed. Normalizing the resulting column matrix gives a new mode $\{\bar{Q}_1\}$. The operation is repeated until the normalized mode converges on its previous value. The fundamental frequency is also obtained at convergence of the mode. Higher modes are extracted by application of the orthogonality principle as each successive mode is solved.

The results of this analysis are shown in Table 19 where the modes and frequencies are given for the wing cantilever and free aircraft. Figs. 71 - 73 show plots of the first three model shapes of the wing and fuselage for the free aircraft and Fig. 79 shows the bending-torsion mode shapes of the wing and fuselage for the cantilever wing.

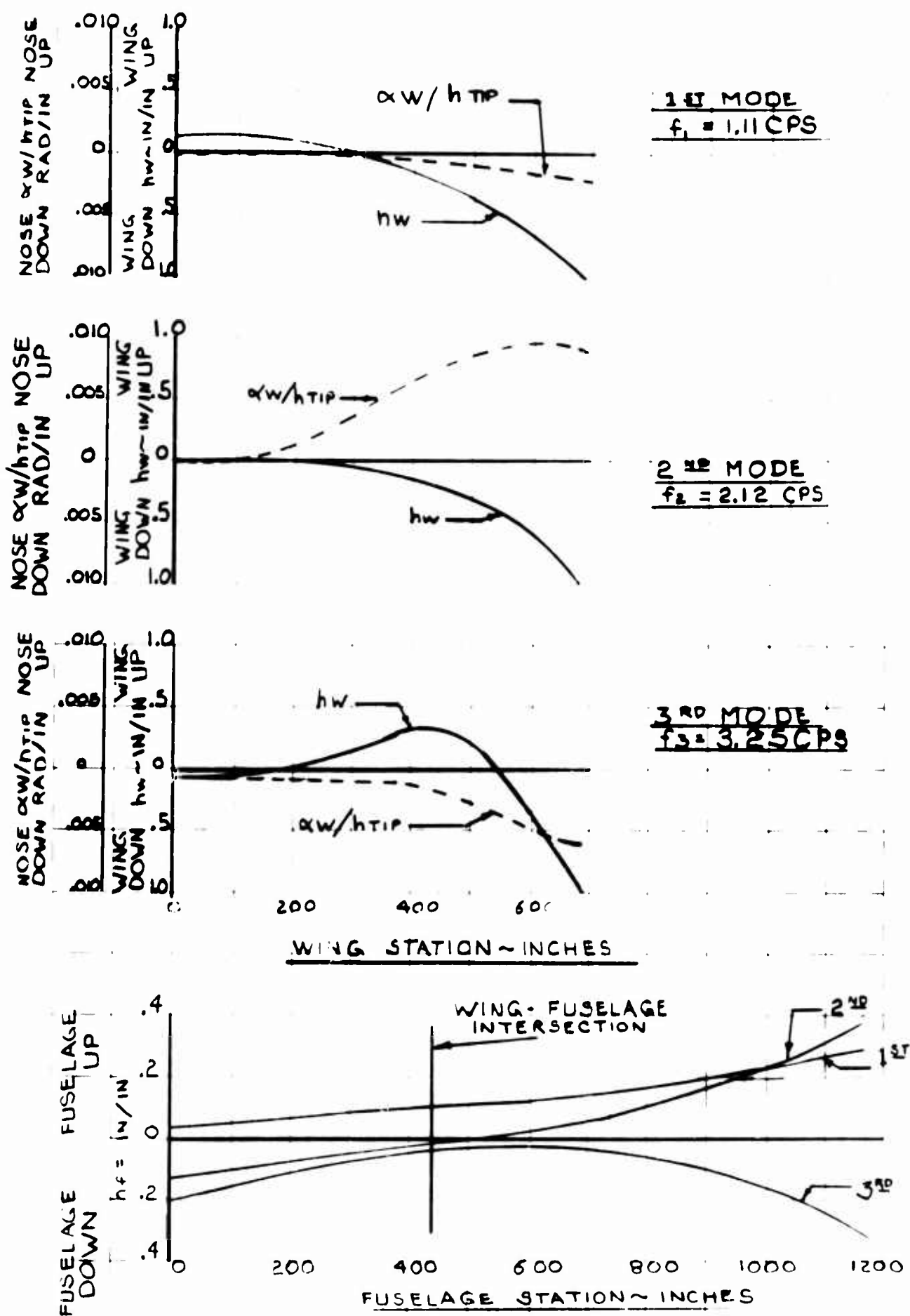


Figure 74 - 1st Three Modes, Symmetrical Fuselage, Coupled Wing Bending-Torsion: Fixed Jet

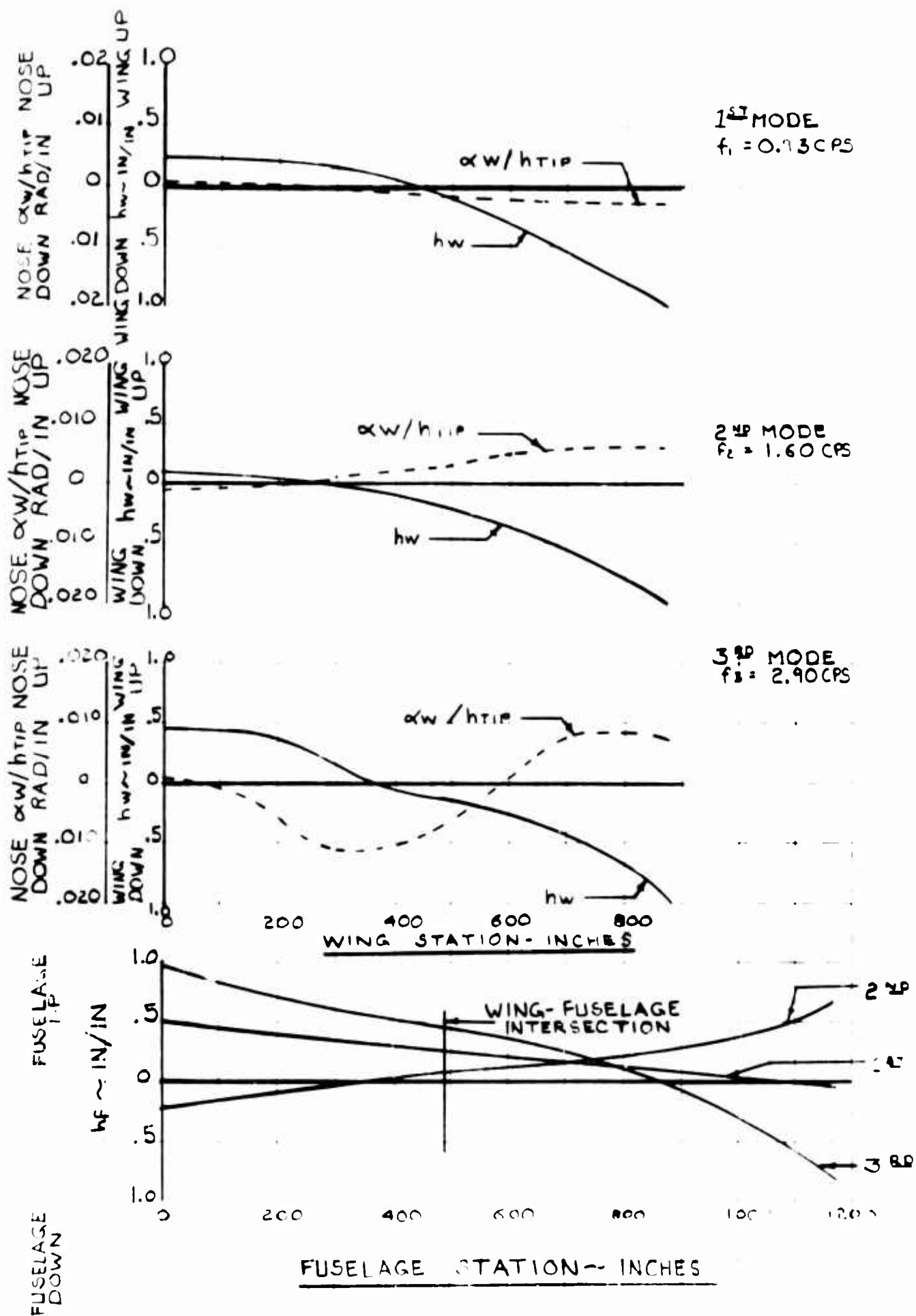


Figure 75 - 1st Three Modes, Geometrical Fuselage, Coupled Wing Bend-Torsion, Tilt Wing

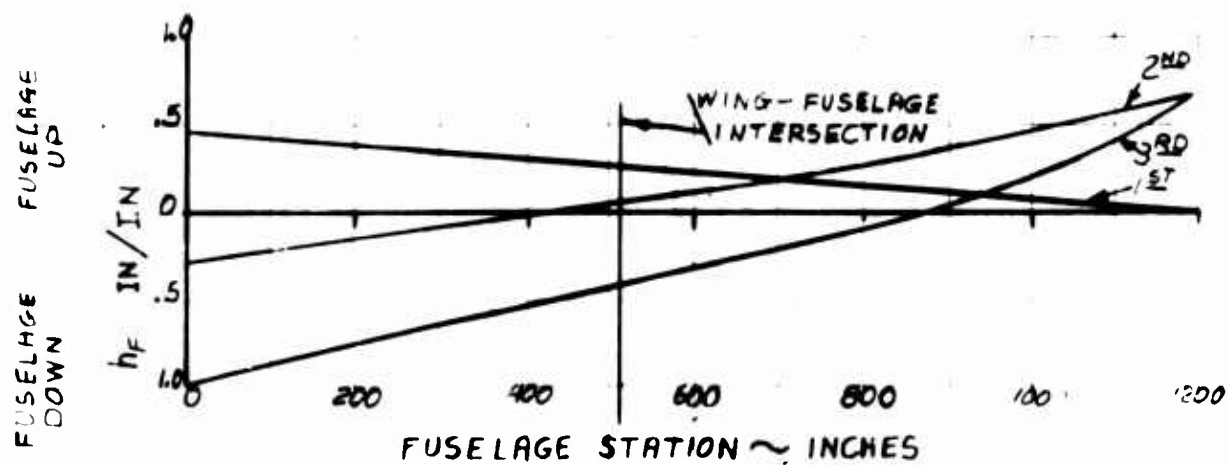
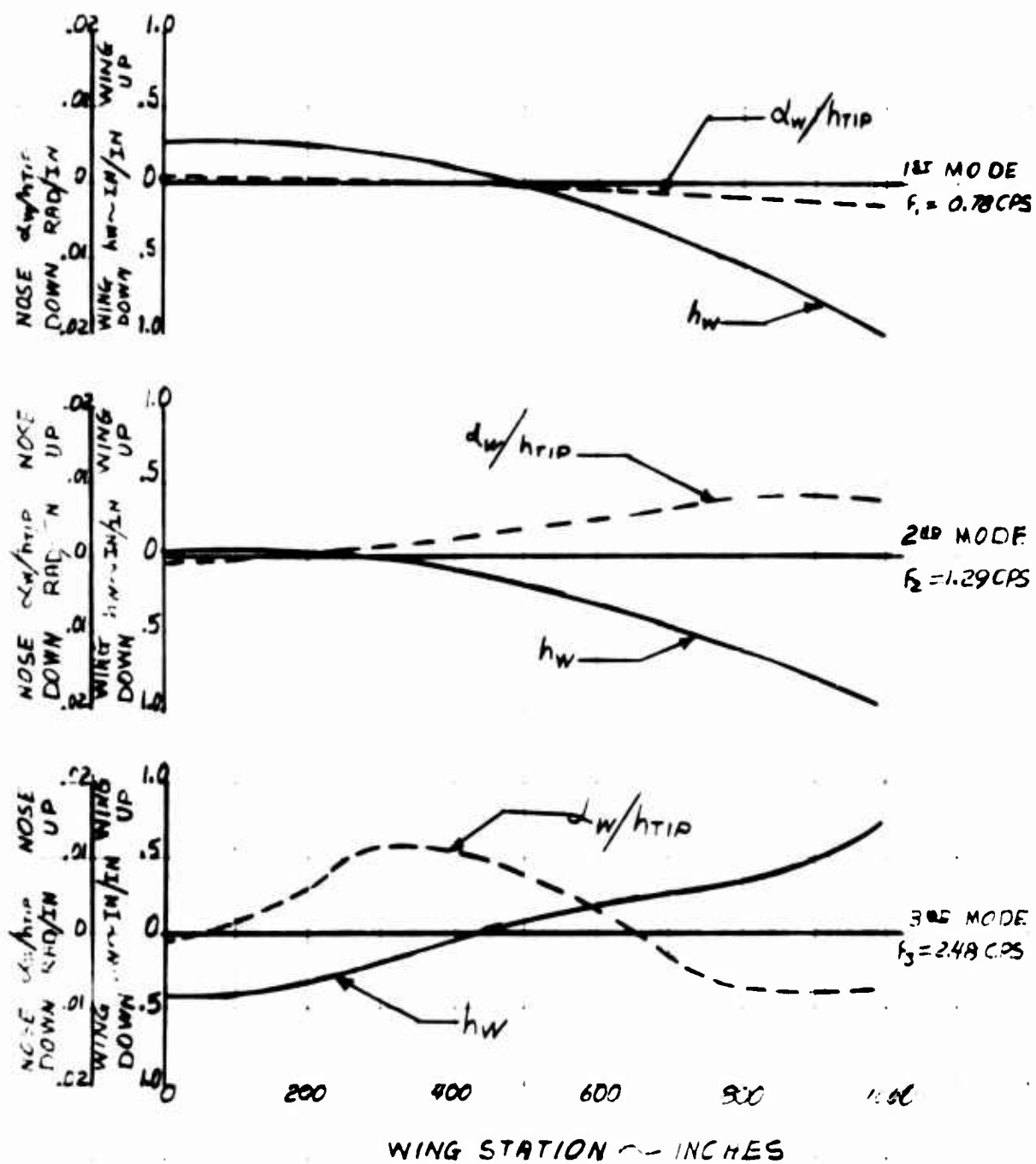


Figure 76 - 1st Three Modes , Symmetrical Fuselage,
Coupled Wing Bending-Torsion: Extended Flap

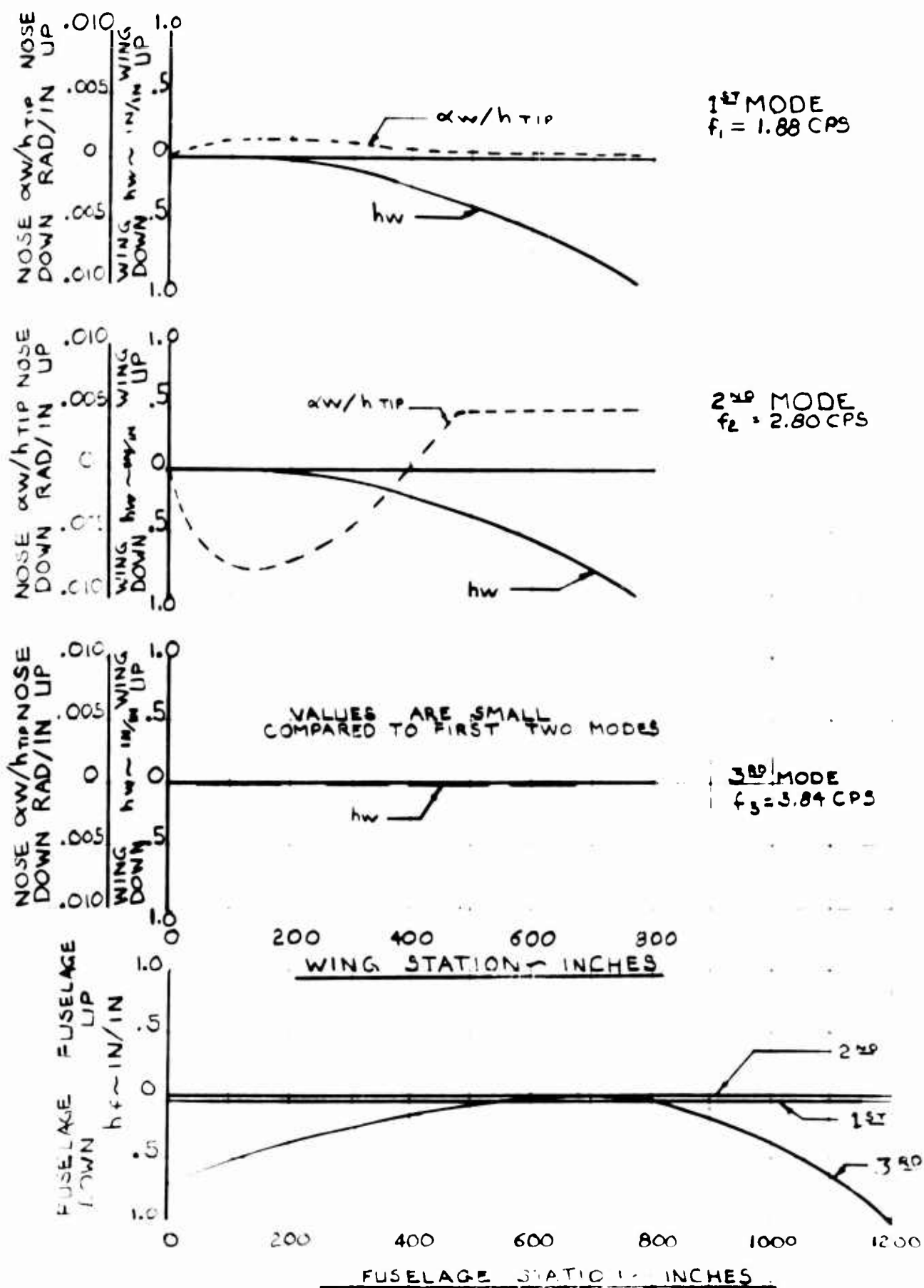
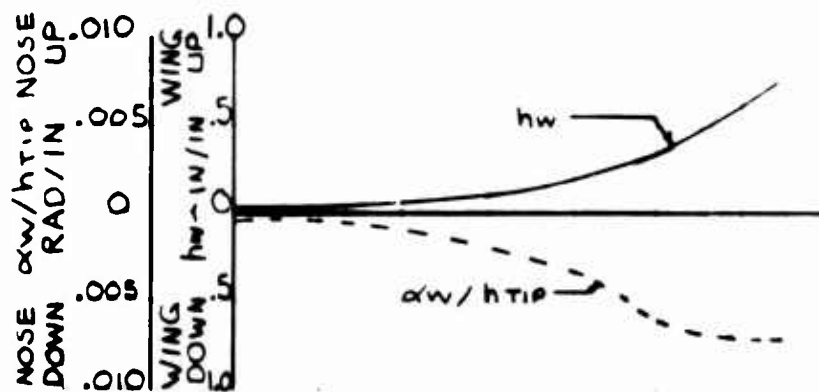


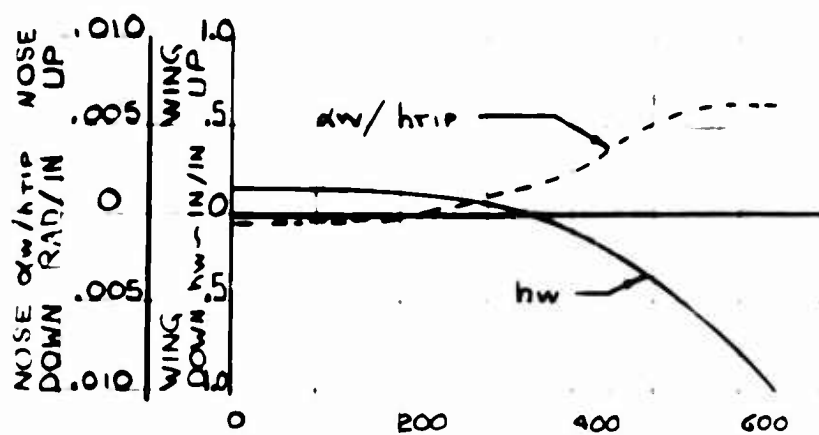
Figure 77 - 1st Three Modes, Symmetrical Fuselage, Coupled Wing Bending - 1st Mode



1st MODE
f₁ = 2.29 CPS



2nd MODE
f₂ = 3.5 CPS



3rd MODE
f₃ = 4.2 CPS

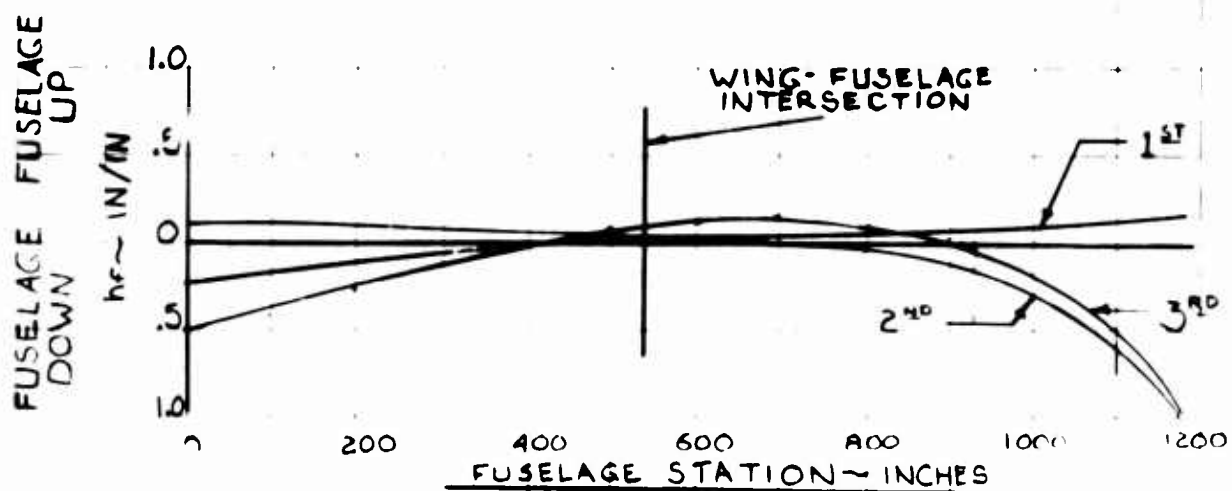


Figure 78 - 1st Three Modes, Symmetrical Fuselage, Coupled Wing Bending-Torsion: Buried Fan

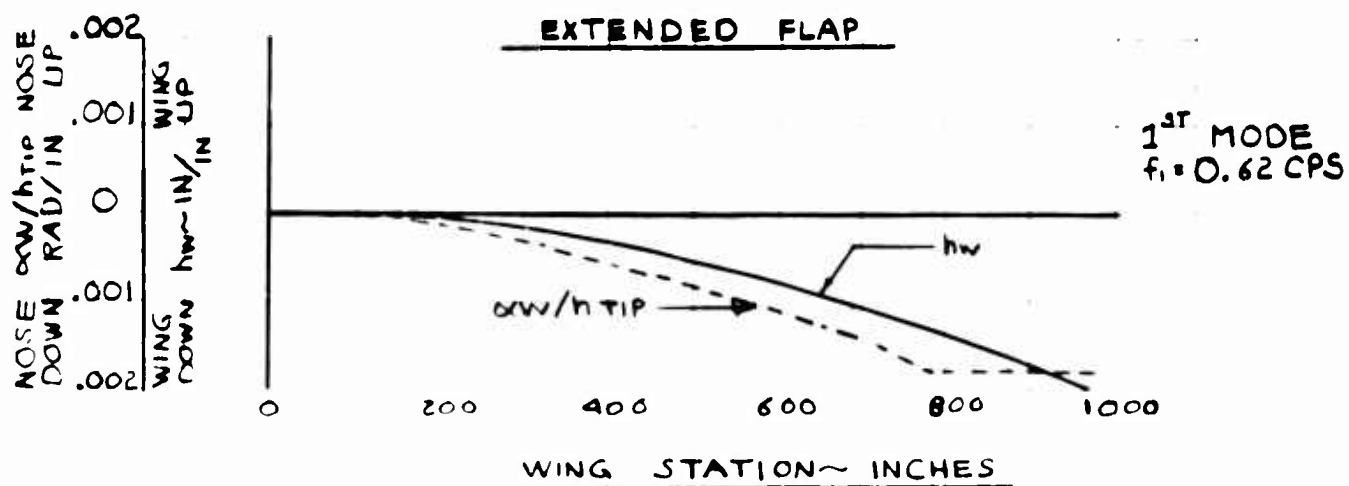
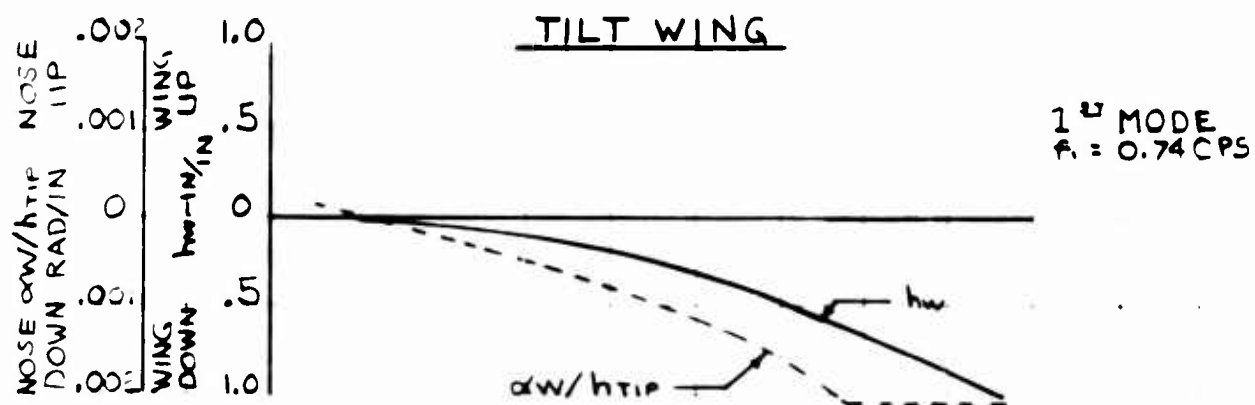
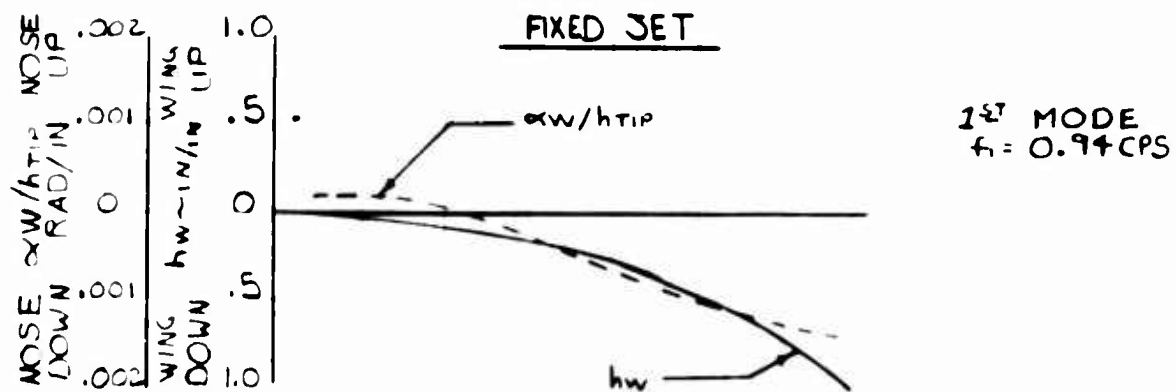
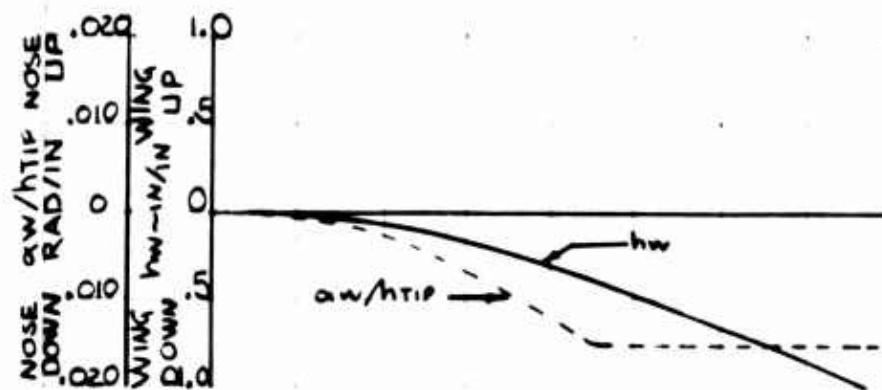


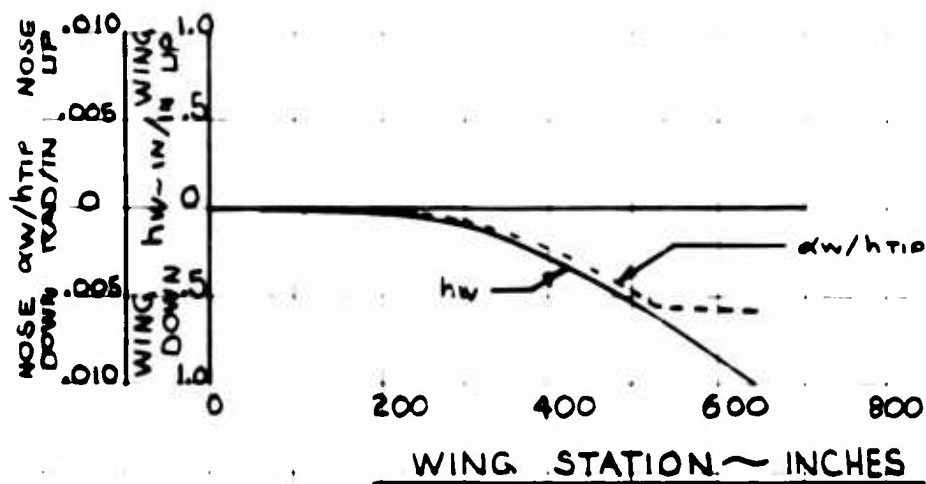
Figure 79 - Cantilever Fundamental Wing Bending-Torsion Modes

TILT PROP



1st MODE
 $f_1 = 1.16 \text{ CPS}$

BURIED FAN



1st MODE
 $f_1 = 2.16 \text{ CPS}$

(continued)

Figure 79 - Cantilever Fundamental Wing Bending-Torsion Modes

BLANK PAGE

Table 19 - Summary of Vibration Data

Aircraft Configuration (VTOL)	Analysis Condition	Aircraft Mode and Frequency - GPM				
		1st Wing Bending	1st Wing Torsion	2nd Wing Bending	2nd Wing Torsion	1st Fuselage Bending
Fixed Jet G.W. = 172,000 lbs.	Wing Cantilever	0.94	1.85	3.04	Not Required	Not Applicable
	Free Aircraft	1.11	2.12	3.25	*	4.50
Tilt Prop G.W. = 223,000 lbs.	Wing Cantilever	0.74	1.51	**	2.58	Not Applicable
	Free Aircraft	0.93	1.60	*	2.90	4.10
Extended Flap G.W. = 263,000 lbs.	Wing Cantilever	0.62	1.22	3.23	2.23	Not Applicable
	Free Aircraft	0.78	1.29	3.39	2.48	4.31
Tilt Prop G.W. = 300,000 lbs.	Wing Cantilever	2.02	1.16	5.13	Not Required	Not Applicable
	Free Aircraft	1.88	2.80	6.48	*	3.84
Buried Fan G.W. = 253,000 lbs.	Wing Cantilever	2.16	3.66	**	5.30	Not Applicable
	Free Aircraft	2.29	3.50	*	5.37	4.20

Notes: * Mode does not appear in the first four natural frequencies and therefore is omitted.
 ** Mode does not appear in the first three natural frequencies and therefore is omitted.

REFERENCES

1. Abbott, I.R., vonDoenhoff, A.E., Stivers, L.S., Jr., Summary of Airfoil Data NACA TR-824.
2. Airplane Strength and Rigidity. Landplane and Ground Handling Loads, MIL-A-8862 (ASG).
3. Allen, F.C., Mosby, L.B., An Analytical Investigation of Aircraft Loads Induced by Rough Terrain Landings, Douglas Aircraft, CAL/TRECON Symposium, Buffalo, New York, 1963.
4. Bislinghoff, Ashley & Halfman, Aeroelasticity, Addison-Wesley Publishing Company, Cambridge, Massachusetts, 1955.
5. Corning, G., Airplane Design, Edwards Brothers Inc., Ann Arbor, Michigan, 1953.
6. Crommwell, C.H., Payne, H.E., A Stability Analysis of Tilt Wing Aircraft (Analytical), Report No. 477, Princeton University, May 1960.
7. Harris, T.H., Recant, I.G., Wind Tunnel Investigation of NACA 23012, 23021 and 23030 Airfoils Equipped with 40-percent-Chord Double Slotted Flaps, NACA TR-723.
8. Jacobson and Ayre, Engineering Vibrations, McGraw Hill Book Co., Inc. New York, 1958.
9. Kuhn, R.E., Review of Basic Principles of V/STOL Aerodynamics, NASA Conference on V/STOL Aircraft, Compilation of Papers Presented, Langley Research Center, November 17-18, 1960.
10. Kuhn, R.E., Draper, J.W., Investigation of Effectiveness of Large-Chord Slotted Flaps in Deflecting Propeller Slipstreams Downward for Vertical Take-Off and Low Speed Flight, NACA TM-3362, January 1955.
11. Perkins, C.D., Hage, R.E., Airplane Performance Stability and Control, Wiley & Sons, New York, 1949.
12. Pratt, P.W., Smith, C.B., Slaiby, T.G., Silverman, B.B., A Generalized Study of Propulsion Systems for VTOL Aircraft, United Aircraft Corporation, January, 1960.
13. Research on Dynamic Response of V/STOL Vehicles Study, Contract No. AF33(657)-8452, BPSN 2(6199-750A-137008).
14. Sardanowsky, W., Sikorsky Engineering Memo No. 4645, October 24, 1963.
15. Templin, R.J., Note on the Minimum Power Required for Flight at Low Speeds, National Research Laboratories Report LR-245 (Canada), May 21, 1959.

16. Menzinger, C.F., Harris, T.A., Wind-Tunnel Investigation of
NACA 23012, 23021, 23030 Airfoils with Various Sizes of Split
Flap, NACA TR-468, 1939.
17. Struss, A., Kennedy, R.L. HSF-2 Tail Wheel Drop Test, Sikorsky
Engineering Report No. 561, January 26, 1959.
18. Rich, M.J., An Energy Absorption Safety Alighting Gear for
Helicopter and VTOL Aircraft, IAS Paper No. 62-16, January 1962.